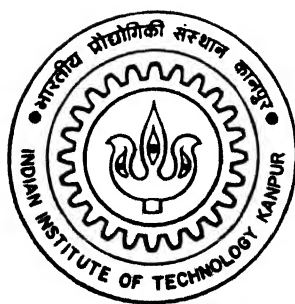


POSITRON ANNIHILATION LIFETIME STUDIES OF SOME POLYMER ELECTROLYTES, POLYMERS AND METAL MATRIX COMPOSITES

by

BIDYUT HALDAR



PHY
1996
D
HAL
POS
TH
PHY/1996/D
H1294

DEPARTMENT OF PHYSICS

INDIAN INSTITUTE OF TECHNOLOGY KANPUR

May, 1996

POSITRON ANNIHILATION LIFETIME STUDIES OF SO
POLYMER ELECTROLYTES, POLYMERS AND
METAL MATRIX COMPOSITES

*A Thesis Submitted in
Partial Fulfilment of the Requirements
for the Degree of
DOCTOR OF PHILOSOPHY*

by

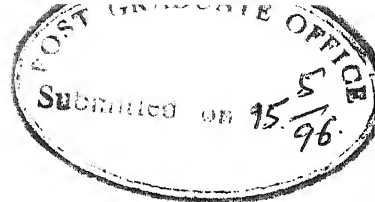
BIDYUT HALDAR

to the

DEPARTMENT OF PHYSICS
INDIAN INSTITUTE OF TECHNOLOGY KANPUR
May, 1996

25 AUG 1997
CENTRAL LIBRARY
I.I.T. KANPUR


Vol. No. A 1236.44



C E R T I F I C A T E

It is certified that the work contained in the thesis entitled " POSITRON ANNIHILATION LIFETIME STUDIES OF SOME POLYMER ELECTROLYTES, POLYMERS AND METAL MATRIX COMPOSITES " by Bidyut Haldar has been carried out under my supervision. This work has not been submitted elsewhere for a degree.

May, 1996


(R. M. Singru)
Professor
Department of Physics
I I T Kanpur, INDIA

dedicated to my wife

A C K N O W L E D G E M E N T S

At first I would like to express my deep sense of gratitude to Professor R. M. Singru for the most inspiring and valuable guidance, constant encouragement and help throughout the course of this research. His invaluable advice from time-to-time at crucial stages has helped me to overcome the hurdles that I came across. I am also grateful to him for introducing me to this exciting field of positron annihilation technique.

I am also grateful to Professor Suresh Chandra, Department of Physics, Banaras Hindu University, Varanasi, India, for providing me with samples of polymer electrolytes and data for various electrical measurements on these polymer electrolytes which have been used in the present thesis. I am also thankful to him for extending a warm hospitality during my stay at Banaras Hindu University. I also want to thank him for spending his most valuable time for some fruitful discussion that has improved my present understanding of polymer electrolytes.

I am also thankful to Professor B.D. Agarwal and Professor N.N.Kishore of Department of Mechanical Engineering, I.I.T. Kanpur for allowing me to use the raw materials for preparing the epoxy and polyester samples. I also express my sincere thanks to Dr. S. Balasubramaniam of Department of Materials and Metallurgical Engineering, I. I. T. Kanpur for providing me with samples of metal matrix composites and for helping me to charge them with hydrogen.

v

I also wish to thank Professor Y.C. Jean, Professor R.B. Gregory and Professor M. Eldrup for their help in making available the computer programs, CONTIN and PATFIT, used for the analysis of positron lifetime spectra.

I am also grateful to Professor V. N. Kulkarni and Professor R. Prasad for giving me valuable suggestions during the course of this thesis work. I take this opportunity to express my thanks to Professor Y.R. Waghmare and Dr. H.C. Verma for the constant encouragement and moral support rendered to me. I am also thankful to Professor A.K.Majumdar and Professor R.K.Thareja for allowing us to use the xerox and laser printing facilities of the department that has saved us valuable time and money.

I express my sincere thanks to Dr. K.K.Maurya, Department of Physics, B.H.U., Varanasi, for the help he has extended to me during my stay at B.H.U. and spending his valuable time in explaining me the method of sample preparation and the working of various instruments being used for the electrical characterizations of polymer electrolyte samples.

My special thanks go to Dr. U.C.Johri for introducing me to the various instruments in our laboratory and helping me to learn their operation during the initial stages of my work.

I also take this opportunity to thank Dr. Nobin Banerjee, Dr. Rita Singhal, Dr. S.S.Rajput, Dr. S.S.A Razee, Debashis, Tapabroto, Sankar and others for creating a lively atmosphere in the laboratory and some happy moment they have shared with me. Special thanks goes to Guptaaji, Masoodji, Rajputji, Anilji and Shivprakashji but for their help, this work could not have been

possible.

Thanks are also due to Mr. H. K. Panda, Mr. L.S. Rathore and Mr. A.K. Srivastava of Physics Department and Mr. Ram Singh, Mr. Bahadur Singh, Mr. Ram Mangal Singh and others in the Physics workshop for their all time cooperation.

I thank Mr. V.K.Jain and Mr. A.K.Ganguli for providing me with some good figure drawings that have been used in the present thesis. I would also like to acknowledge the homely environment provided by all my friends and colleagues including Gautam, Sudhansu, Swapan, Abir, Alok Sharan, Ajay wasan and many more during my stay at I.I.T. Kanpur.

The constant encouragement, excellent understanding and abundant affection provided to me by my parents and relatives for boosting my morale throughout my research career culminating in this thesis are always to be remembered.

Last but not the least, I would like to express my deep feelings for my wife, Debasree for patiently bearing my gloominess, providing mental support during critical periods, managing the house all alone, and never complaining of my regular absence for long hours away from home.

BIDYUT HALDAR

SYNOPSIS

POSITRON ANNIHILATION LIFETIME STUDIES OF SOME POLYMER ELECTROLYTES, POLYMERS AND METAL MATRIX COMPOSITES

Bidyut Haldar
Department of Physics
Indian Institute of Technology, Kanpur, India
May 1996

Over the past thirty years positron annihilation technique has been used in various studies involving metals, alloys, molecular solids and other technologically important materials. In particular the technique of positron annihilation lifetime spectroscopy has been applied to study different types of polymeric materials. It is now well recognised that the annihilation characteristics of ortho-positronium (o-Ps) are sensitive to the free volume in polymers. A loose definition of free volume is the volume within a polymer that is unoccupied by molecules. Many physical properties of the polymer are influenced by the free volume. Hence in recent years positron annihilation lifetime spectroscopy is being widely used to characterize free volume in polymers.

In the present work we report positron lifetime measurements in some polymer electrolytes, polymers and metal matrix composites. Each of the above type of materials has found useful applications in technology and industry. Ion-conducting polymer electrolytes are the materials of current interest because of their possible applications in modern electrochemical devices,|

mostly as high-energy density solid state batteries and sensors. High-temperature resistant glassy polymers such as cured epoxy and polyester resins are also technologically important materials because of their wide range of applications as adhesives, fillers, host matrices for composite materials etc. The third kind of materials i.e. the metal matrix composites are the most recently developed materials that have attracted considerable attention because of their excellent mechanical properties.

In view of the above technological importance of these materials, we found it interesting to investigate them by positron annihilation lifetime spectroscopy.

The present thesis is divided into seven Chapters. The first chapter provides a brief introduction to the phenomenon of positron annihilation. It describes the two-photon and three-photon annihilation processes and the characteristic lifetimes for these decays. Factors governing the formation and decay of positronium (Ps) atom are discussed and a very brief introduction to the Ore-model and spur-model is given. The phenomenon of quenching of Ps from the ortho- to the para- state are discussed. A relation between the positron annihilation lifetimes with the properties of free-volume holes of polymers is discussed outlining the existing model for the spherical holes.

The experimental methods for the study of positron annihilation are briefly reviewed in Chapter 2. The techniques for studying the Doppler-broadening of annihilation radiation lineshape and angular correlation of annihilation radiation are described briefly while the technique of positron annihilation

lifetime measurements is discussed in some detail. The details of the present lifetime spectrometer and the methods used for analyzing positron lifetime spectra are also discussed. Experimental procedures involved in the preparation of positron source and in checking the time calibration etc. are described.

Since the major part of the present work deals with the study of polymer electrolytes, a brief introduction to the structural and physical properties of these new technological materials is given in Chapter 3. The free-volume model and its application to the mechanism of ion-transport in polymer electrolytes is also outlined. Some specific polymer electrolyte materials and their typical industrial applications are briefly described.

The present studies of the temperature dependence of positron annihilation lifetime, free volume, conductivity, ionic-mobility and number of charge carriers in the proton-conducting polymer electrolyte, polyethylene oxide (PEO) complexed with ammonium perchlorate (NH_4ClO_4) are described in Chapter 4. The above physical properties have been studied in the temperature range 300-370 K. The positron lifetime spectra were analyzed in two ways: (i) determination of three lifetimes and their intensities using the computer program PATFIT and (ii) determination of the annihilation rate probability distribution function using the computer program CONTIN. Such analysis provided valuable results for the free-volume parameters in this material. The free volume and conductivity show sudden increase at the melting temperature $T \sim T_m$ (~ 333 K). It appears that the increase in the free volume arises out of the increase in the size of the holes rather than an

increase in their number. Although the free volume shows an increase around T_m , the measured ionic mobility does not show similar behaviour. The increase in the conductivity at T_m is, therefore, ascribed to an increase in the number of charge carriers at $\sim T_m$. A suitable dissociation model involving the dielectric constant is proposed to explain this increase. The value of the dissociation energy for $\text{PEO:NH}_4\text{ClO}_4$ has been determined to be 2.4 eV.

In Chapter 5 we have presented the positron annihilation lifetime studies of free volume in polymer electrolyte polyethylene oxide (PEO) complexed with ammonium iodide (NH_4I). Temperature variation of o-Ps lifetime and intensity studied in the temperature range 298-353 K showed different behaviour during the heating and cooling cycles. A relative free-volume fraction has been calculated from the measured o-Ps lifetime parameters. The measured positron lifetime spectra have been analyzed into continuous lifetime distributions using Laplace's inversion technique, and the free-volume hole volume distributions were obtained at different temperatures. An attempt made to explain the observed variation in o-Ps lifetime and intensity is described at the end of this chapter.

The present studies of the positron annihilation lifetimes in two polymers, cured epoxy and polyester resins are described in Chapter 6. The effect of temperature, physical aging and moisture on positron lifetimes and intensities in these two polymers is measured. The temperature dependence was studied in the range 295-473 K during the heating and cooling cycles. The study of

physical aging was carried out at room temperature for samples quenched at different rates. Moisture absorption in both these polymers was studied at room temperature and at 371 K. Attempts was made to explain the observed behaviour in terms of free-volume properties.

In the last chapter we have described positron lifetime studies in the Al-Al₂O₃ metal matrix composites, containing 0%, 2%, 4% and 8 wt. % Al₂O₃ particulates. Metal matrix composites are not polymers, but they are also technologically important materials having excellent mechanical properties. Positron lifetime measurements were performed for the as-cast samples, samples charged with hydrogen and samples annealed (after hydrogen charging) for all the above compositions. An attempt has been made to explain the observed variation in the mean positron lifetimes with composition in terms of trapping behaviour of hydrogen by the defects.

It is hoped that the present studies carried out in the polymer electrolytes PEO+NH₄ClO₄ and PEO+NH₄I, cured epoxy and polyester resin polymers and in the Al+Al₂O₃ metal matrix composites using positron lifetime measurements and other characterization techniques have helped to extend our present understanding of these systems.

CONTENT

	Page No.
LIST OF FIGURES	xviii
LIST OF TABLES	xxviii
CHAPTER 1 : INTRODUCTION	1
1.1 Positron and positron annihilation	1
1.2 Properties of positrons	4
1.3 Interaction with matter	4
1.4 Direct annihilation	5
1.5 Bound-state/positronium annihilation	7
1.6 Lifetimes for 2-photon and 3-photon annihilation processes	8
1.6.1 2-photon annihilation process	8
1.6.2 3-photon annihilation process	9
1.7 Factors controlling the positronium formation and decay	10
1.8 Quenching	14
1.9 Positron annihilation in metals	17
1.10 Positronium and molecular substances	20
1.10.1 Existing model - spherical holes	23
1.11 Free volume and positron annihilation in polymers	27
1.11.1 Ps-hole theory in polymers	33
1.12 Scope of the present study	35
References	38

CHAPTER 2 :	EXPERIMENTAL METHODS FOR POSITRON ANNIHILATION STUDIES	43
2.1	Introduction	43
2.2	Methods for measuring positron lifetimes.	44
2.2.1	Positron source	44
2.2.2	Source preparation	47
2.2.3	Source strength	47
2.2.4	Sample thickness	48
2.2.4	Positron lifetime spectrometer	48
2.3	Doppler broadening and angular correlation measurements of annihilating radiations	55
2.4	Present positron spectrometer	61
2.4.1	Positron source	61
2.4.2	Present lifetime setup	63
2.4.3	Resolution and performance of our positron lifetime spectrometer	68
2.4.4	Calibration of the TPHC	70
2.5	Analysis of positron annihilation lifetime spectra	71
2.5.1	Finite-term lifetime analysis	74
2.5.2	Continuous lifetime analysis	77
2.6	Summary	79
	References	81
CHAPTER 3 :	POLYMER ELECTROLYTES - A REVIEW	85
3.1	Introduction	85

3.1.1	Framework crystalline materials	88
3.1.2	Composite or dispersed phase solid electrolytes	89
3.1.3	Ion-conducting glasses	89
3.2	Polymer electrolytes	90
3.2.1	Introduction	90
3.2.2	Solvent-swollen polymers	94
3.2.3	Polyelectrolytes	94
3.2.4	Solvent-free polymer-salt complexes	95
3.2.5	Formation of polymer-salt complex	96
3.3	Structure of polymer electrolytes	97
3.3.1	Structure of poly(ethylene oxide)	98
3.4	Phase diagram	99
3.5	Ion-transport mechanism in polymer electrolytes	100
3.5.1	Introduction	100
3.5.2	Observed conductivity dependence on temperature	102
3.6	Free-volume model	106
3.6.1	Introduction	106
3.6.2	Concept of free volume in liquids and solids	106
3.6.3	Free-volume theory of ion-transport	111
3.7	Configurational entropy model	114
3.8	Dynamic bond percolation model	115
3.9	Specific polymer electrolytes	116
3.9.1	Alkali-metals ion-conducting polymers	116

3.9.2	Silver and copper-based polymer electrolytes	117
3.9.3	Divalent/transition metal salt based polymers	117
3.9.4	Proton-conducting polymer electrolytes	118
3.10	Applications of polymer electrolytes	121
	References	124
CHAPTER 4 :	TEMPERATURE DEPENDENCE OF POSITRON LIFETIME, FREE VOLUME, CONDUCTIVITY, IONIC MOBILITY AND NUMBER OF CHARGE CARRIERS IN A POLYMER ELECTROLYTE PEO COMPLEXED WITH NH_4ClO_4	136
4.1	Introduction	136
4.2	Experimental	143
4.3	Results and discussions	150
4.3.1	Positron lifetimes, free volume and related distribution functions	151
4.3.2	Conductivity, mobility, number of charge carriers and free volume	171
4.4	Conclusions	178
	References	180
CHAPTER 5 :	POSITRON ANNIHILATION LIFETIME STUDIES OF FREE VOLUME IN A POLYMER ELECTROLYTE PEO COMPLEXED WITH NH_4I	183
5.1	Introduction	183
5.2	Experimental	185
5.3	Results and discussions	187

5.3.1	Analysis of lifetime spectra using PATFIT program	188
5.3.1	Analysis of lifetime spectra using CONTIN program	202
5.4	Conclusions	211
	References	214
CHAPTER 6	TEMPERATURE DEPENDENCE, PHYSICAL AGING AND MOISTURE ABSORPTION STUDIES IN CURED EPOXY AND POLYESTER RESIN POLYMERS USING POSITRON LIFETIME SPECTROSCOPY	216
6.1	Introduction	216
6.1.1	Free volume and physical aging	221
6.1.2	Effect of moisture on glassy polymers	223
6.2	Experimental	226
6.2	Results and discussions	232
6.3.1	Temperature dependence of positron lifetime spectra in epoxy and poly- ester resin polymers	233
6.3.2	Study of structural relaxation and physical aging	254
6.3.3	Water absorption studies	259
6.4	Summary and conclusions	262
	References	264
CHAPTER 7 :	POSITRON ANNIHILATION LIFETIME STUDY OF HYDROGEN-CHARGED $\text{Al-Al}_2\text{O}_3$	268
7.1	Introduction	268

7.2	Experimental	272
7.3	Results and discussions	274
7.4	Conclusions	280
	References	282

LIST OF FIGURES

	Page No.
Fig. 1.1 The 'hole' theory.	2
Fig. 1.2 Hypothetical dependence of Ps formation probability in Argon gas as a function of positron energy.	12
Fig. 1.3 Flow diagram of positron annihilation.	18
Fig. 1.4 Schematic diagram of Ps distribution according to the Brandt-Berko-Walker free-volume model of Ps decay in molecular substances.	26
Fig. 1.5 A schematic diagram for a semi-empirical quantum model for Ps localized in a spherical box with radius R .	26
Fig. 1.6 Correlation curve of o -Ps lifetime as a function of free-volume hole size, assuming spherical hole.	31
Fig. 1.7 Cross-sectional view of the Ps localized in the free-volume holes in a polymeric material.	31
Fig. 2.1 Decay scheme of ^{22}Na .	46
Fig. 2.2 Block diagram of positron lifetime spectrometer using slow-fast coincidence technique.	50
Fig. 2.3 A typical positron lifetime spectrum.	52
Fig. 2.4 Vector diagram of momentum conservation in the 2γ -annihilation process, (a) $\vec{p} = 0$, (b) $\vec{p} \neq 0$.	57
Fig. 2.5 Schematic diagram of a Doppler broadening measurement system.	57
Fig. 2.6 Energy spectrum for Doppler broadened	58

annihilation radiation compared with the intrinsic energy resolution of the spectrometer.

- Fig. 2.7** Schematic diagram of the apparatus to study 1D angular correlation of annihilating radiation. 60
- Fig. 2.8** General outline of the geometry of the 2D ACAR apparatus. Two sets of detectors lie on the (y_1, z_1) and (y_2, z_2) planes. 62
- Fig. 2.9** Block diagram of the lifetime spectrometer, based on fast-fast coincidence technique, used in the present work. 64
- Fig. 2.10** Method of time pick-off used in a typical constant fraction timing unit. 67
- Fig. 2.11** (a) Decay scheme of ^{60}Co . (b) Prompt spectrum of ^{60}Co . 69
- Fig. 2.12** (a) Time spectrum recorded using time calibrator. (b) Calibration curve for the present lifetime spectrometer. 72
- Fig. 2.13** Schematic representation of the interaction between programs, files and output devices, using POSITRONFIT as an example. 73
- Fig. 3.1** Electrochemical devices based on solid electrolytes. 86
- Fig. 3.2** Molecular models of PEO conformations. (A) and (B): conformation of crystalline PEO $(T_2G)_7$; (C) and (D): PEO in a new $T_2GT_2\bar{G}$ conformation as proposed for complexation to sodium cations. 101
- Fig. 3.3** Phase diagram of a polymer electrolyte PEO complexed to NH_4ClO_4 salt (C=crystalline, CC=crystalline complex and L = liquidus). 101
- Fig. 3.4** Conductivity vs $1/T$ plots for a series of polymer-salt complexes (1) $\text{P}(\text{EO}_{12}\text{LiClO}_4)$; (2) cross-linked $\text{PEO}_8\text{LiClO}_4$; (3) $\text{P}(\text{PO}_9\text{LiSO}_2\text{CF}_3)$; (4) $\text{poly}[(\text{ethylene adipate})_4\text{LiSO}_3\text{CF}_3]$ (5) 104

poly(ethylene succinate)₆LiBF₄; (6) poly{[bis(methoxyethoxyethoxy)phosphazene]₄LiSO₃CF}
and (7) poly[(N-methylaziridine)₈LiClO₄.

- Fig. 3.5** A schematic illustration of the free volume and their expansivities in the glassy and liquid states. The shaded area represent the available free volume (V_f). 108
- Fig. 3.6.** (a) The thin film design of an all-solid-state battery and two typical configurations of a solid polymer battery (b) Bi-polar structure (c) Swiss-roll configuration. 123
- Fig. 4.1** Temperature dependence of conductivity for polyethylene oxide complexed with different (a) ammonium salts [A] PEO:(NH₄)₂SO₄ [B] PEO:NH₄ClO₄; [C] PEO:NH₄HSO₄ and [D] PEO:NH₄I. (b) lithium salts [E] PEO:LiH₂PO₄; [F] PEO:LiSCN and [G] PEO:LiClO₄. The position indicated by the vertical arrow corresponds to the melting temperature ($T_m \sim 338$ K) for pure crystalline PEO. 142
- Fig. 4.2** Experimental arrangement for electrical conductivity measurements. 145
- Fig. 4.3** (a) Experimental arrangement for transient ionic current technique for mobility measurement (b) A typical transient ionic current vs time plot of PEO:NH₄ClO₄ system. 147
- Fig. 4.4** Experimental arrangement for temperature dependence of positron lifetime measurements. 149
- Fig. 4.5** Positron lifetime spectra at two different temperatures in PEO:NH₄ClO₄ (80:20 wt %). 152
- Fig. 4.6** Temperature variation of positron lifetime parameters τ_2 , I_1 and I_2 in PEO:NH₄ClO₄ (80:20 wt %). Open symbols describe the data for increasing temperature, while solid symbols describe the data for decreasing 155

temperature.

- Fig. 4.7** Temperature dependence of o-Ps lifetime, τ_3 , in polyethylene oxide complexed with ammonium perchlorate (PEO:NH₄ClO₄) (80:20 wt %). Positions indicated by the arrows 1 and 2 correspond to the melting temperatures of uncomplexed PEO ($T_{m1} \sim 339$ K) and crystalline complexed material ($T_{m2} \sim 239$ K). Open symbols describe the data for increasing temperature, while solid symbols describe the data for decreasing temperature. 156
- Fig. 4.8** Same as Fig. 4.7, but for the temperature dependence of o-Ps lifetime intensity, I_3 . 157
- Fig. 4.9** Temperature dependence of relative fractional free volume F_r in PEO:NH₄ClO₄ (80:20 wt %). Positions indicated by 1 and 2 correspond to melting temperatures of uncomplexed PEO ($T_{m1} \sim 339$ K) and crystalline complexed material ($T_{m2} \sim 239$ K). Open symbols are for increasing temperature, closed symbols for decreasing temperature. 160
- Fig. 4.10** Positron lifetime distribution functions in PEO : NH₄ClO₄ (80:20 wt %) at some representative temperatures during the (a) increasing and (b) decreasing temperature obtained from CONTIN analysis. The positions corresponding to the lifetime values τ_1 , τ_2 and τ_3 obtained from PATFIT analysis are shown by arrows. 163
- Fig. 4.11** o-Ps lifetime distribution functions in PEO:NH₄ClO₄ (80:20 wt %) at different temperatures for (a) increasing and (b) decreasing temperature. The data correspond to the right hand peaks in Fig. 4.10 (a) and (b) respectively. 166
- Fig. 4.12** Free-volume hole radius distribution 168

functions $f(R)$ in PEO:NH₄ClO₄ (80:20 wt %) at different temperatures corresponding to the o-Ps lifetime distribution shown in Fig. 4.11 for (a) increasing and (b) decreasing temperature.

- Fig. 4.13** Free-volume hole volume distribution functions $g(V)$ in PEO:NH₄ClO₄ (80:20 wt %) at different temperatures for (a) increasing and (b) decreasing temperature. 170
- Fig. 4.14** Temperature dependence of cationic (μ^+) and anionic (μ^-) mobilities along with the conductivity (σ) for PEO:NH₄ClO₄ (80:20 wt %) at different temperatures. Positions indicated by 1 and 2 correspond to the melting temperatures of uncomplexed PEO ($T_{m1} \sim 339$ K) and crystalline complexed material ($T_{m2} \sim 239$ K). 172
- Fig. 4.15** Variation of number of mobile cations (n^+) and anions (n^-) with temperature for PEO:NH₄ClO₄ (80:20 wt %). Positions indicated by 1 and 2 correspond to the melting temperatures of uncomplexed PEO ($T_{m1} \sim 339$ K) and crystalline complexed material ($T_{m2} \sim 239$ K). 174
- Fig. 4.16** The dielectric constant at different temperature for PEO:NH₄ClO₄ (80:20 wt %). Positions indicated by 1 and 2 correspond to the melting temperatures of uncomplexed PEO ($T_{m1} \sim 339$ K) and crystalline complexed material ($T_{m2} \sim 239$ K). 176
- Fig. 4.17** Variation of number of mobile charge carriers (a) cations (n^+) and (b) anions (n^-) with $1/\epsilon T$ for PEO:NH₄ClO₄ (80:20 wt %) . 177
- Fig. 5.1** DTA curve for the present sample polyethylene oxide complexed with ammonium iodide NH₄I (PEO:NH₄I with NH₄⁺/EO ≈ 0.076). 189

- Fig. 5.2** Temperature variation of positron lifetime parameters τ_1 , τ_2 , I_1 and I_2 in PEO:NH₄I (NH₄⁺/EO \approx 0.076). Open symbols describe the data for increasing temperature, while solid symbols describe the data for decreasing temperature. 194
- Fig. 5.3** Temperature dependence of o-Ps lifetime, τ_3 , in PEO:NH₄I (NH₄⁺/EO \approx 0.076). Positions indicated by the arrow corresponds to the melting temperature of uncomplexed PEO ($T_m \sim 329$ K). Open symbols describe the data for increasing temperature, while solid symbols describe the data for decreasing temperature. 195
- Fig. 5.4** Same as Fig. 5.3, but for the temperature dependence of o-Ps lifetime intensity, I_3 . 196
- Fig. 5.5** Temperature dependence of I_3V_f in PEO:NH₄I (NH₄⁺/EO \approx 0.076). Positions indicated by the arrow corresponds to the melting temperature of uncomplexed PEO ($T_m \sim 328$ K). Open symbols describe the data for increasing temperature, while solid symbols describe the data for decreasing temperature. 203
- Fig. 5.6** Positron lifetime distributions in PEO:NH₄I (NH₄⁺/EO \approx 0.076) at some representative temperatures during the (a) heating and the (b) cooling cycle, obtained from CONTIN analysis. The positions corresponding to the lifetime values τ_1 , τ_2 and τ_3 obtained from PATFIT analysis are shown by arrows. 204
- Fig. 5.7** o-Ps lifetime distribution in PEO:NH₄I ((NH₄⁺/EO \approx 0.076) at different temperatures during the (a) heating and (b) cooling cycle. The data were taken from right hand peaks in Fig. 5.6 (a and b). The continuous lines are drawn through the data points for visual guidance. 208

- Fig. 5.8** Free-volume hole radius distribution functions $f(R)$ in PEO:NH₄I (NH₄⁺/EO \approx 0.076) at different temperatures corresponding to o-Ps lifetime distribution function in Fig.5.7 ((a) and (b)) during the (a)heating and (b)cooling cycle.The continuous lines are drawn through the data points for visual guidance. 210
- Fig. 5.9** Free-volume hole volume distribution functions $g(V)$ in PEO:NH₄I (NH₄⁺/EO \approx 0.076) at different temperatures during the (a) heating and (b) cooling cycle. The continuous lines are drawn through the data points for visual guidance. 212
- Fig. 6.1** Origin of physical aging from free volume concept. In the figure T_g is the glass transition temperature and T_1 is any temperature below T_g . Downward arrow represent the isothermal free-volume contraction. 222
- Fig. 6.2.** Chemical structure of resins and hardener used for sample preparations (a) Diglycidyl ether of Bisphenol A (DGEBA). (b) Triethylene tetramine and (c) Unsaturated polyester resin. 228
- Fig. 6.3.** DTA spectrum for the epoxy sample used in the present work. 230
- Fig. 6.4.** Typical positron lifetime spectra at two different temperatures (293 K and 473 K) in (a) epoxy and (b) polyester samples used in the present work. 234
- Fig. 6.5.** Temperature variation of positron lifetime parameters τ_1 , τ_2 , I_1 and I_2 in epoxy polymer. Open symbols describe the data for the heating cycle, while solid symbols describe the data for the cooling cycle. Typical error associated with the data points 238

are shown separately in each case by the vertical error bars.

- Fig. 6.6.** Temperature dependence of (a) o-Ps lifetime, τ_3 , and (b) o-Ps intensity, I_3 in epoxy polymer. Open symbols describe the data for the heating cycle, while solid symbols describe the data for the cooling cycle. Positions corresponding to the various transitions are indicated by vertical arrows. Typical error associated with the data points are shown separately by the vertical error bars. Best fit curves to the observed data points are given by the dotted lines. 239
- Fig. 6.7** Temperature variation of positron lifetime parameters τ_1 , τ_2 , I_1 and I_2 in polyester polymer. Open symbols describe the data for the heating cycle, while solid symbols describe the data for the cooling cycle. Typical error associated with the data points are shown separately in each case by the vertical error bars. 244
- Fig. 6.8** Temperature dependence of (a) o-Ps lifetime, τ_3 , and (b) o-Ps intensity, I_3 in polyester polymer. Open symbols describe the data for the heating cycle, while solid symbols describe the data for the cooling cycle. Position indicated by the arrow corresponds to a possible phase transition. 246
- Fig. 6.9** Temperature dependence of relative free-volume fraction $F_r (=I_3 V_f)$ in (a) epoxy and (b) polyester samples. Open symbols describe the data for the heating cycle, while solid symbols describe the data for the cooling cycle. Positions indicated by the arrows correspond to various transitions observed for our samples. Best fit curves to 249

the observed data points are given by the dotted lines.

- Fig. 6.10** Positron lifetime distributions in epoxy polymer at some representative temperatures during the heating cycle, obtained from CONTIN analysis. The positions corresponding to the lifetimes values τ_1 , τ_2 and τ_3 obtained from PATFIT (Table 6.1(a)) analysis are shown by arrows. 250
- Fig. 6.11** o-Ps lifetime distribution in epoxy polymer at different temperatures during the heating cycle. The data were taken from right hand peaks in Fig. 6.10. The continuous lines are drawn through the data points for visual guidance. 253
- Fig. 6.12** The free-volume (a) hole radius distribution functions $f(R)$ and (b) volume distribution functions $g(V)$ in epoxy polymer at different temperatures corresponding to o-Ps lifetime distribution functions in Fig.6.11 during the heating cycle. The continuous lines are drawn through the data points for visual guidance. 255
- Fig. 6.13** Effect of physical aging on (a) τ_3 and (b) I_3 as a function of time for epoxy samples cooled at different rates. Typical error associated with the data points are shown separately by the vertical error bars. 257
- Fig. 6.14** Effect of physical aging on (a) τ_3 and (b) I_3 as a function of time for polyester samples cooled at different rates. Typical error associated with the data points are shown separately by the vertical error bars. 258
- Fig. 6.15** Effect of moisture/water absorption on (a) τ_3 and (b) I_3 for various time of absorption in epoxy sample. Typical error associated with the data points are shown separately by the 260

the vertical error bars.

- Fig. 6.16** Effect of moisture/water absorption on (a) τ_3 and (b) I_3 for various time of absorption in polyester sample. Typical error associated with the data points are shown separately by the vertical error bars. 261
- Fig. 7.1** Schematic representation of particle cracking in (a) Al-2%Al₂O₃ and (b) Al-8% Al₂O₃. 271
- Fig. 7.2** Variation of positron lifetime parameters with percentage composition of Al₂O₃, (a) τ_1 , (b) I_1 , (c) τ_2 , and (d) I_2 for (A) as-prepared (as-cast) samples, (B) charged with hydrogen for 12h and (C) annealed (after hydrogen charging) at 573 K for 1h. Lines are drawn through the data points for visual guidance. 276
- Fig. 7.3** Variation in mean lifetime τ_m with different percentage composition of Al₂O₃ particulates for (A) as-cast samples, (B) samples charged with hydrogen for 12h and (C) annealed (after hydrogen charging) at 573 K for 1h. Lines are drawn through the data points for visual guidance. 278

LIST OF TABLES

	Page No.
Table 2.1 Resolution function of the spectrometer used in the present work.	76
Table 3.1 Solid electrolyte materials	91
Table 3.2 Some polymer electrolyte materials	119
Table 4.1 Temperature dependence of positron lifetime parameters in polymer electrolyte PEO:NH ₄ ClO ₄ (80:20 wt. %) obtained from PATFIT analysis.	154
Table 4.2 Temperature dependence of positron lifetime parameters in polymer electrolyte PEO:NH ₄ ClO ₄ (80:20 wt. %) obtained from CONTIN analysis.	165
Table 5.1 Temperature dependence of positron lifetime parameters in polymer electrolyte PEO:NH ₄ I (NH ₄ ⁺ \EO ≈ 0.076) obtained from PATFIT analysis.	191
Table 5.2 Temperature dependence of positron lifetime parameters in polymer electrolyte PEO:NH ₄ I (NH ₄ ⁺ \EO ≈ 0.076) obtained from CONTIN analysis.	207
Table 6.1(a) Temperature dependence of positron lifetime parameters in epoxy polymer (DGEBA+TETA) during the heating cycle obtained from PATFIT analysis.	235
Table 6.1(b) Temperature dependence of positron lifetime parameters in epoxy polymer (DGEBA+TETA) during the cooling cycle obtained from PATFIT analysis.	236
Table 6.2 Temperature dependence of positron lifetime parameters in an unsaturated polyester (cured by MEKP and cobalt octate) obtained from PATFIT analysis.	243
Table 6.3 Temperature dependence of mean positron	252

lifetime parameters in epoxy polymer (DGEBA+TETA) during the heating cycle obtained from CONTIN analysis.

Table 7.1 Positron lifetime parameters in Al-Al₂O₃ composites containing different weight percentage of Al₂O₃ particles in the matrix

275

CHAPTER 1

INTRODUCTION

1.1 Positron and positron annihilation

The most thoroughly characterized antiparticle is the antielectron, i.e., the positron. The existence of positron was theoretically predicted by Dirac [1] in 1930 from the solution of a relativistic wave equation for an electron. The relativistic wave equation for an electron with total energy E has two permissible solutions $E = \pm (p^2 c^2 + m^2 c^4)^{1/2}$ where p is the momentum of the electron, m the rest mass of the electron and c is the velocity of light. Therefore in the absence of any external field electrons may have energies of $\pm mc^2$ to $\pm \infty$. His theory, therefore, predicts that both positive and negative energy states are admissible for electrons. He proposed that all negative energy states are normally occupied by electrons and all positive energy states are empty (Fig. 1.1). Any transition from the positive energy state to the sea of negative energy state is forbidden in order to satisfy the Pauli's exclusion principle. The negative and the positive energy states are separated by an energy gap of $2mc^2$. Therefore, it is possible to excite an electron from the negative energy state to the positive energy state by imparting an energy $E > 2mc^2$ to the electron. When such an electron is excited to the positive energy state, a 'hole' is left in the midst of the occupied negative energy states. This 'hole' behaves as a particle with mass equal to that of electron and charge $+e$.

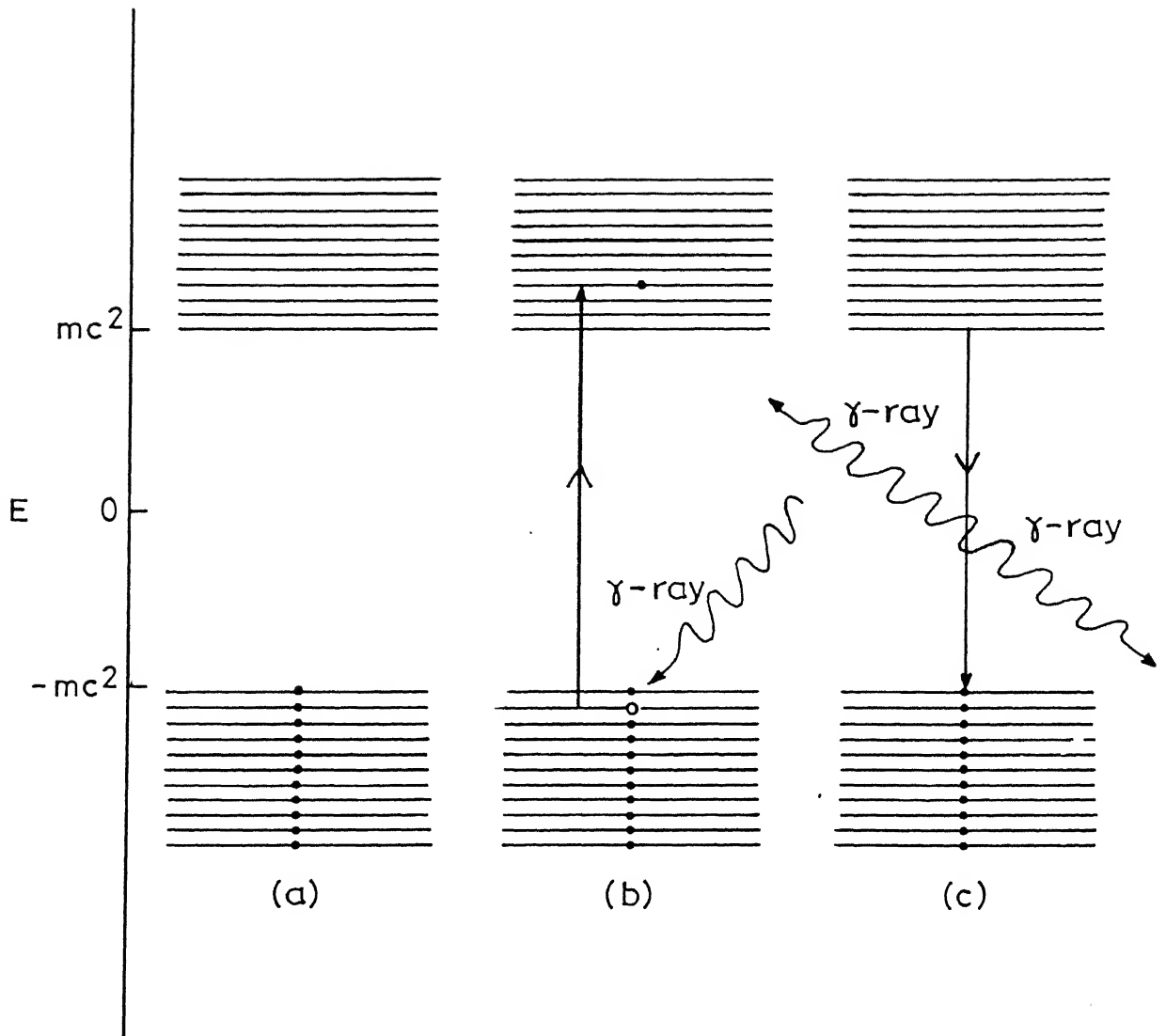


Fig. 1.1

The 'hole' theory.

- (a) All negative energy states are occupied
- (b) Incident γ -ray causes a transition from negative to positive energy states and leaves back a hole (pair production)
- (c) The positive energy electron falls back into the hole releasing energy $2mc^2$ in the form of γ -photons (annihilation)

Similarly if there is a hole in the negative energy sea of electrons, an electron from the positive energy state could fall into the vacant negative energy state and then both the electron and the hole will disappear (annihilate) and an equivalent amount of energy $\sim 2mc^2$ of the electron-hole pair will appear in the form of electromagnetic radiation (gamma rays). Based on this theory, Dirac in 1930 predicted the existence of a particle, which could either be interpreted as an electron with positive energy or as positively charged particle, with mass equivalent to that of an electron.

In 1933, Carl Anderson [2-4] observed a new particle for the first time in a cloud chamber photograph of cosmic ray showers having the same mass as that of electron but with opposite charge. This particle (equivalent to that of hole in Dirac's theory) was called 'positron'. The discovery of this new particle was soon confirmed by Blackett and Occhialini [5]. It was subsequently shown by Thibaud [6] that the electron and positron masses are exactly equal. Annihilation of the positron with an electron with resultant conversion of the mass of the two particle into electromagnetic energy was found soon after the discovery of positron [7-9]. It was later found that positrons were also emitted by radioactive nuclei in β^+ decay. After the discovery of positron, early experimental work was mainly devoted to test the basic laws of quantum electrodynamics governing the electron-positron interactions and consequently annihilation of positrons.

One of the well-known conversion of electromagnetic energy to

mass is pair production. Pair production is conversion of high-energy photon into a pair of a positron and an electron by interaction with the electric field of a nucleus. For pair production to occur the photon must have an energy of at least as great as the mass equivalent of a positron and electron, $2mc^2 = 1.02 \text{ MeV}$. Any excess energy is carried away by the positron and the electron.

1.2 Properties of positron

Positron is an antiparticle of electron with mass equal to that of electron but with a positive charge $+e$. A positron is stable in vacuum. Upon entering matter positron may annihilate with an electron and produce electromagnetic radiation. When a positron collides with an electron, the electron has a high probability for making a radiative transition to the negative energy level. This transition results predominantly [10,11] in the conversion of mass of the electron and the positron into electromagnetic radiation of total energy $E_\gamma = 2mc^2 + E_+ + E_-$ where E_+ and E_- are the kinetic energies of positron and the electron respectively.

1.3 Interaction with matter

Although positrons are quite stable in vacuum, they have very short lifetimes in matter. Upon entering matter, the positron can cause excitation, ionization etc. similar to the electron using

most of its kinetic energy in undergoing collision with the atoms of the matter. It has been shown theoretically that in material medium positron is quickly thermalized as a result of collisions with atoms, and slows down to thermal energy in a very short time of the order of a few ps (10^{-12} s) [10,11]. After living in thermal equilibrium, positron finally annihilates with electrons from the surrounding medium within a very short time ($\sim 10^{-10}$ s). However this time is quite long compared to the atomic response time, and hence they are used as probe particles for understanding atomic phenomena. The annihilation results in the emission of one, two, three or more photons, with net energy equal to sum of the rest mass energy of the electron-positron pair and their kinetic energies before annihilation.

1.4 Direct annihilation

The positron may annihilate with an electron either directly or may form a bound state before annihilation. The process where a positron annihilates with an electron without any intermediate step, is known as the direct annihilation of the free positron. Distinct selection rules, based on the invariance properties of quantum electrodynamics, govern the number of photons or quanta, that can be emitted in the annihilation of a free positron with an electron [12]. One photon (1γ) annihilation occurs only when there is an interaction of the positron-electron ($e^+ - e^-$) pair with some nucleus or electrons which can absorb the recoil momentum. Most common way of annihilation is into two (2γ) or three (3γ) photons.

The properties and the number of emitted photons depend on the relative spins of the $e^+ - e^-$ pair. In order to conserve momentum, energy, parity and other symmetries of the annihilating particles, two or even number of photons are emitted when the relative spins between the annihilating particles are antiparallel (i.e. in singlet state (1S_0)) and three or odd number of photons are emitted when the relative spins between the annihilating particles are parallel, (i.e. in triplet state (3S_1)). The total energy of the annihilating particles is shared by the radiation photons. The cross-section for the three-photon annihilation is more than two orders of magnitude smaller than that for the two-photon process i.e. smaller by factor of α^2 , where α ($= 1/137$) is the fine structure constant. The probability of multiple-photon annihilation decrease sharply with increasing multiples.

Two-photon annihilation is the most common annihilation process. The relative number of $2\gamma:3\gamma$ photon annihilations depends on the singlet-to-triplet interactions and their annihilation rates. The singlet state has a total angular momentum $J = 0$, hence the z-component of angular momentum m , is 0. The triplet state has a total angular momentum $J = 1$ and hence $m = 0, \pm 1$. Thus statistical ratio of the singlet to the triplet interaction is 1:3.

A free positron may interact on the average with more than one electron depending on the electron density of the medium. The free annihilation lifetime is generally between 1 to 5×10^{-10} s i.e. 100 to 500 ps.

1.5 Bound-state/positronium annihilation

In molecular substances (solids and liquids), positron may form a relatively stable (bound) state 'atom' with an electron. This ($e^+ - e^-$) bound state, which is very much like a hydrogen atom with a positron replacing the proton, is called "positronium or Ps". Ps is a metastable state and may decay with a lifetime as large as 1.4×10^{-7} s. Positronium atom has the following properties:

- (i) the Bohr radius is about twice the corresponding Bohr radius of hydrogen atom i.e. 1.06 \AA ,
- (ii) the reduced mass is $m/2$, where m is the rest mass of the electron,
- (iii) the ionization potential is 6.8 eV,
- (iv) the first excited state has an energy equal to 5.1 eV, and
- (v) the wavelength of Lyman α -line is 2430 \AA .

Ps exists in two ground states, the singlet state (1S_0) or para-Ps (p-Ps) with relative spin orientations of the $e^+ - e^-$ pair antiparallel ($\uparrow\downarrow$) and the triplet state (S_1^3) or ortho-Ps (o-Ps) with parallel spin orientation ($\uparrow\uparrow$). The p-Ps decays into two photons, whereas the o-Ps decays into three photons. In the ground state, Ps is an admixture of the ortho (3S_1) and para (1S_0) states in the ratio 3:1 or

$$Ps = \frac{3}{4} (\text{o-Ps}) + \frac{1}{4} (\text{p-Ps}) \quad (1.1)$$

where Ps on the left hand side stands for the total number of Ps atoms formed.

When positronium is formed in excited state ($l > 0$) it decays to the ground state ($l=0$) by optical de-excitation and then annihilates into two or three photons.

1.6 Lifetimes for 2-photon and 3-photon annihilation process

1.6.1 2-photon annihilation process

Dirac [1] calculated the cross-section for 2-photon annihilation in the limit $v \ll c$ (it has been found that positrons are always thermalized and come to room temperature energy before annihilation) to be

$$\sigma = \frac{\pi r_0^2 c}{v} \quad (1.2)$$

where r_0 ($= e^2/mc^2$) is the classical electron radius, m and v are the mass and velocity of the positron respectively and c is the velocity of light in vacuum.

Normally the rate of free annihilation depends on the cross-section σ as well as number of electrons (n) in the surrounding medium. If n is the number of electrons per cm^3 , then the rate of positron annihilation λ is given by

$$\lambda = \sigma n v = \pi r_0^2 n c \quad (1.3)$$

or

$$\lambda = 4.5 \times 10^9 (Zd/A) \text{ s}^{-1} \quad (1.4)$$

where d , Z and A are the density, atomic number and atomic weight of the medium. The mean lifetime for such a annihilation process

in metals is therefore

$$\tau = \frac{1}{\lambda} = 1.25 \times 10^{-10} \text{ s} \quad (1.5)$$

1.6.2 3-photon annihilation process

The ratio of mean lifetimes for 3-photon annihilation to the 2-photon annihilation process was found by Ore and Powell [13] to be

$$\frac{\tau(2\gamma)}{\tau(3\gamma)} = \frac{4}{9\pi} (\pi^2 - 9) \alpha \quad (1.6)$$

where $\alpha (= \frac{1}{137})$ is the fine structure constant and $\tau(2\gamma) = 1.25 \times 10^{-10} \text{ s}$. Hence the mean positron lifetime in the 3-photon annihilation process comes out to be

$$\tau(3\gamma) = 1.4 \times 10^{-7} \text{ s} \quad (1.7)$$

Thus the ratio of the 2γ (singlet) to 3γ (triplet) annihilation rate [14] is approximately 1115:1. Since, the statistical ratio of the singlet to triplet interaction is 1:3, the ratio of probability of two-photon (singlet) to three-photon (triplet) annihilation resulting from free-positron interaction with electron is 1115:3 or 372:1.

Because of many factors e.g. Coulomb attraction between e^- and e^+ , nuclear repulsion, Pauli's exclusion principle and other effects [15], it is difficult to calculate the effect of electron density on free-annihilation rate. But it is obvious from eq.(1.2) that greater the electron density, greater will be the annihilation rate and shorter will be the mean lifetime of free

positron annihilation.

1.7 Factors controlling the positronium formation and decay

Positronium formation in a medium is governed by many factors e.g. electron density, space available for positronium to be accommodated etc. It has been found experimentally that positronium formation is more favourable in molecular solids, liquids, amorphous solids and polymers, disordered solids and gases, whereas positronium formation is unfavourable in metals and ionic crystals. The large electron density available in metals render direct annihilation as the most probable process. In ionic crystals, positronium formation is energetically not possible. In the case of molecular substances, liquids, amorphous and disordered solids, positronium formation is possible due to the availability of empty space (free volume). A detailed discussion of positronium formation and its subsequent annihilation in molecular substances has been reported by Tao [16].

Several models were proposed for the positronium formation in molecular solids, liquids and gases including the "Ore-model" [17] of Ps formation in gases, the "spur-model" of Ps formation in liquids and molecular solids [18] and the quantum mechanical model of Ps decay rate in porous and polymeric materials [16,19].

The energy of positron also plays a vital role in deciding whether positronium formation in a substance would be possible or not. Ore [17] in his model has discussed the energetics of positronium formation in gases. In order to form positronium (Ps)

in gases, the positrons emitted by radioactive decays, should possess certain threshold energy which is just enough to extract an electron from the molecule of a gas, after losing most of its initial kinetic energy ($\sim 10 - 100$ KeV) through different collision processes with matter. If I_p is the ionization potential of the molecule of the gas, then the energy range in which Ps formation may occur is between I_p to $(I_p - 6.8)$ eV (Fig. 1.2), where 6.8 eV is the binding energy of the $e^+ - e^-$ pair released during Ps formation. However, presence of an excitation level, E , within the energy interval I_p and $(I_p - 6.8)$ eV increases the excitation cross-section resulting in lesser formation of Ps, thus setting an upper limit on the energy of positron to form Ps. Therefore, those positrons whose energies lie within the interval between $(I_p - 6.8)$ to E eV (Fig. 1.2) are expected to form positronium. This energy gap between $(I_p - 6.8)$ eV to E eV, is called the 'Ore gap'. The probability, P , of Ps formation in gases, therefore, is given by

$$\frac{6.8}{I_p} > P > \frac{E_p - (I_p - 6.8)}{E} \quad (1.8)$$

The probability of Ps formation remains practically constant in the range $(I_p - 6.8) - E$ eV. There has been some success achieved for the above model in gases [20].

This picture of Ore gap is somewhat modified for the case of condensed matter because of changes in the parameters of the Ore-gap due to the different unknown affinities of the medium for electrons, positrons and the positronium atoms in the crystal

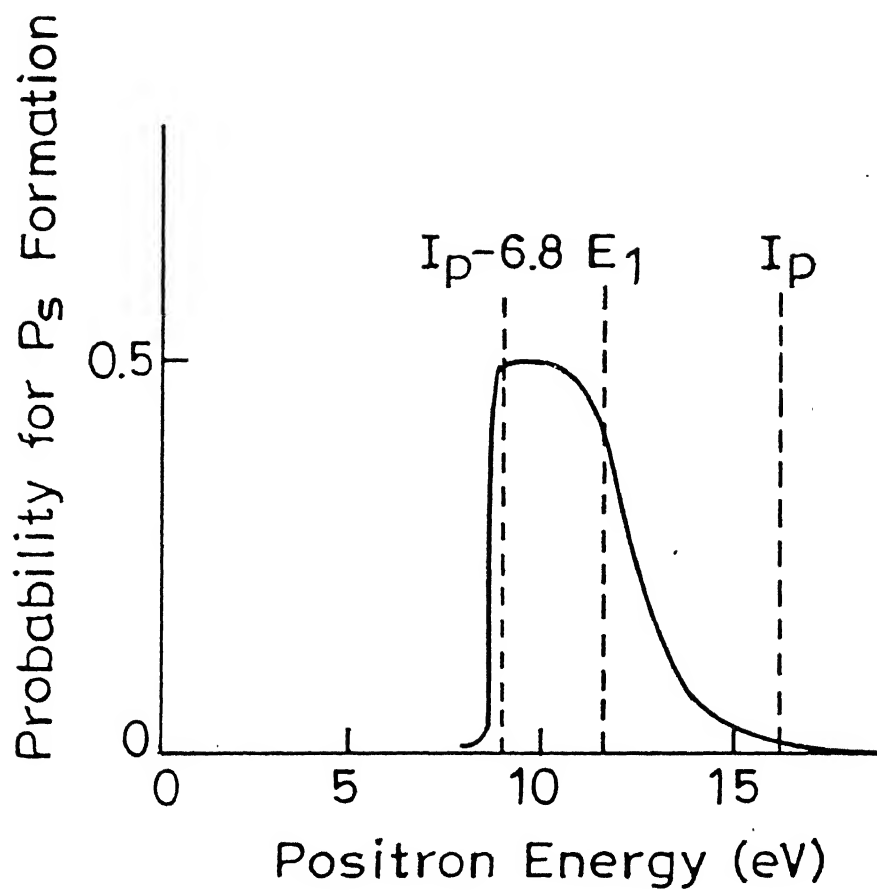


Fig. 1.2 Hypothetical dependence of P_s formation probability in Argon gas as a function of positron energy [taken from Ref. 14].

lattice. Solute or solvent molecules may decrease the probability, P , owing to positron capture processes and inelastic processes, which remove the positron from the above-mentioned energy interval, the so-called Ore gap. Ferrel [15] thus modified this Ore model to find the probability of positronium formation in condensed media by including in his model the affinities of the positrons and of positronium to molecules in condensed medium.

In the "spur model", as proposed by Mogensen [18], it is assumed that Ps is formed as a result of a spur reaction between the positron and a secondary electron in the positron spur. The concept of spur came from radiation chemistry. Upon entering the matter, the positron will lose the last 50-200 eV of its kinetic energy in creating a spur of excess electrons plus the corresponding positive ions. A spur can, therefore, be defined as a group of reactive intermediates (positron, excess electrons, positive ions, etc.) which are so close together that there is a significant probability of their reacting with each other before diffusion into the bulk medium. The electrons will lose their initial of 10-50 eV by travelling a distance of the order of the spur size constant b . Similarly the positron will also lose its last 10-50 eV by travelling over the same distance b . Ps is formed when such a thermalized positron is under the Coulombic attraction of an electron in the radiation spur created by the positron so that they move together. However the process must compete with the recombination of electrons and the positive ions and also with the diffusion of electrons out of the spur. Reactions in the spur of the electrons or of positrons with the solvent molecules or with

scavengers will also decrease the Ps formation. Chemical reactions in the spur will also modify the Ps formation. The model indicated a correlation between the positronium formation probabilities and the properties of excess electrons studied in radiation chemistry [21,22].

The properties of the spur have attracted much attention in radiation chemistry. This model also explained the fact that the fractions of Ps formation in simple liquid hydrocarbons are much higher than the simple Ore Gap theory. However its usefulness is somewhat qualitative. A modified spur model was also proposed in order to bridge the gap between the Ore Gap and spur models [23], details of which are beyond the scope of this thesis.

The quantum-mechanical model of Ps annihilation in molecular solids and liquids will be discussed in Sec.1.10.1.

1.8 Quenching

Quenching refers to any means by which the Ps lifetime is shortened from its self-annihilation lifetime. As already discussed, the decay rate for the 3γ -annihilation is very slow as compared to the 2γ -annihilation by a factor of 1115 in free space. However in condensed matter the state of the positronium atom can change from ortho-to-para state as a result of collision with the surrounding medium, resulting in a faster decay by the 2γ -annihilation. All processes which bring about such conversion from ortho-to-para state are termed as quenching processes. The

four important processes which can induce quenching are

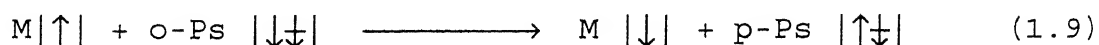
- (i) Spin-flip quenching
- (ii) Pick-off quenching
- (iii) Paramagnetic quenching
- (iv) Magnetic quenching

(i) Spin-flip quenching : Spin-flip quenching [24] refers to those processes in which there is a spin reversal of electron with respect to positron in o-Ps because of scattering with the molecules of the medium. As a result of spin reversal, the o-Ps changes to p-Ps. Since decay rate of p-Ps is much faster than o-Ps, the lifetime gets shortened (some p-Ps may get converted into o-Ps, but relatively small para-to-ortho conversion can occur due to greater annihilation rate of p-Ps). Statistically the probability for such spin-flip is very small and hence quenching does not occur very frequently.

(ii) Pick-off quenching : During collision of o-Ps (with parallel spin) with another atom or molecule, the positron may interact with an electron of the antiparallel spin (with sufficient overlap of positron wavefunction in Ps with the external electron) and may annihilate with the external electron with a rate approaching that of the p-Ps [25]. Hence the positron in positronium "picks off" an electron from the surrounding medium. The phenomenon reduces the lifetime of o-Ps from 140 ns to a few ns or less in the condensed phase, depending upon the molar density of the medium. Green and Lee [14] have calculated this pick-off annihilation rate, λ_{pickoff} to be equal to $2 \times 10^9 \text{ s}^{-1}$ i.e. the mean

lifetime is of the order of 10^{-9} s. Pick-off quenching becomes less prevalent as the free volume in a system increases, thus temperature and phase changes that result in a higher free volume will result in a lower rate of pick-off and a relatively longer o-Ps lifetime [26]. Pick-off quenching occurs to some extent in all substances, but it is more prevalent in the solids and the liquids which lack unpaired electrons. Therefore the study of lifetime ($1/\lambda_{\text{pickoff}}$) and the fraction of such process is of great significance in understanding the mechanism of positron annihilation in condensed matter.

(iii) Paramagnetic quenching : Paramagnetic systems e.g. NO, NO₂ and O₂ and most of the transition-metal cations and complexes have unpaired electrons. The unpaired electron of the paramagnetic molecule can replace the electron of the o-Ps such that it decays via p-Ps [27]. This process is illustrated by the following equation,



The symbol (\uparrow) refers to the direction of electron spin and (\downarrow) to the direction of positron spin. M is the paramagnetic molecules having an unpaired electron. The effect of conversion quenching is to yield an o-Ps lifetime less than 140 ns.

(iv) Magnetic quenching : It has been observed [28] that the presence of external magnetic field enhances the two-photon

annihilation. By the presence of a magnetic field the $S=1$ state of o-Ps splits up into three substates with $m=0, \pm 1$. The state $S=1, m=0$ of o-Ps is mixed during part of its lifetime with the $S=0, m=0$ (p-Ps) state. This causes an equality between the singlet and one-third of the triplet states. Hence one-third of the o-Ps can decay by two-photon emission at the same rate as p-Ps with magnetic field absorbing the unbalanced momentum. A radio frequency signal corresponding to the magnetic substate splitting in the magnetic field enhances this type of quenching [29].

Processes other than the four mentioned above can also induce quenching or alter the quenching rate of Ps-atom. They may be either due to the application of external electric field [15,28,30,31] or may be due to chemical reaction between Ps and one of the active species in the matter [32]. In some cases, the application of external electric field may enhance the Ps formation [28], while in others this may reduce the Ps formation [30].

Out of all types of quenching processes discussed above, pick-off quenching is the most important process. Other processes are not very common and they are effective only under certain conditions. The positron annihilation processes discussed in the previous pages can be illustrated with the help of the flow-diagram shown in Fig. 1.3.

1.9 Positron annihilation in metals

In metals, the presence of large density of free conduction

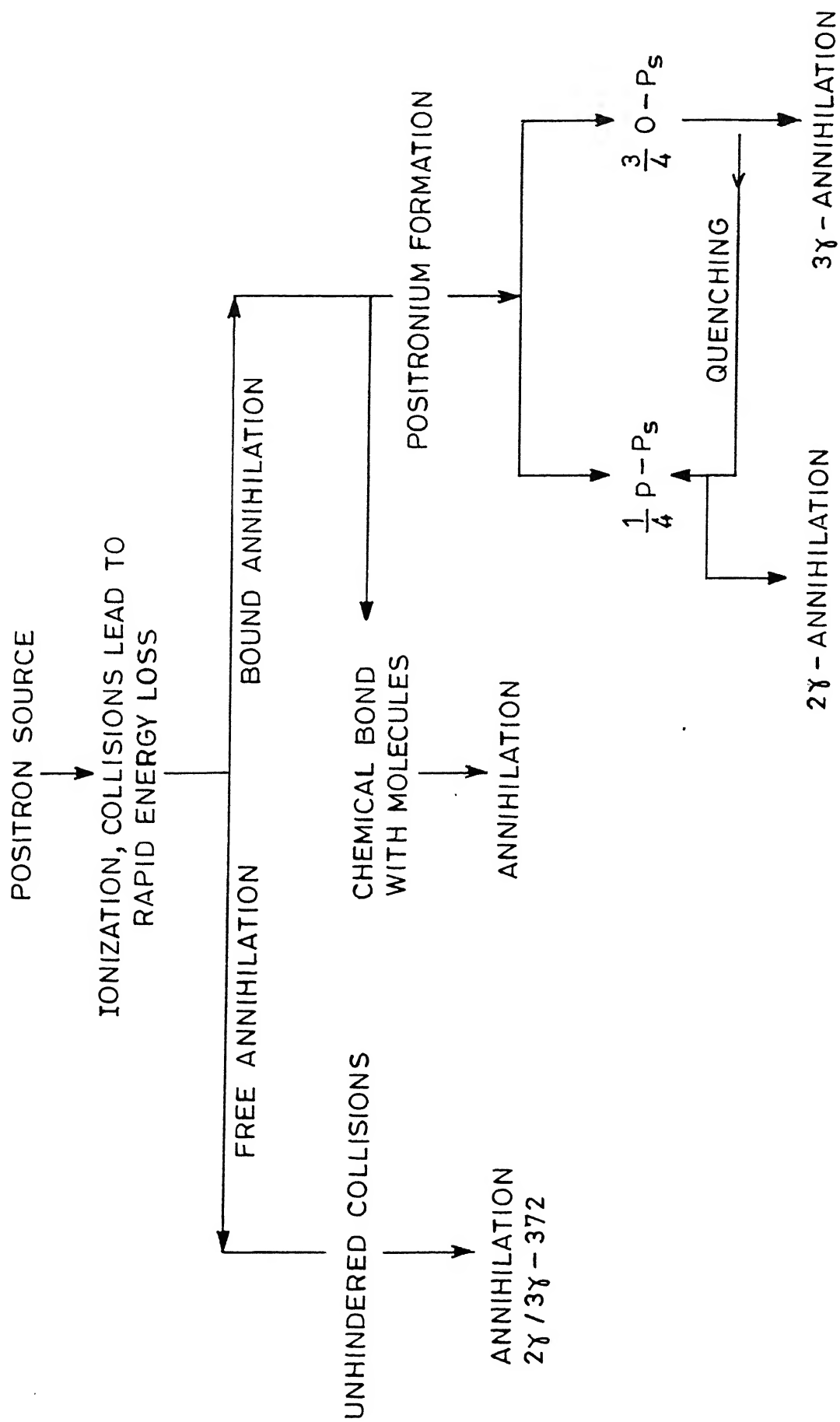


Fig. 1.3

Flow diagram of positron annihilation.

electrons renders the direct annihilation as the most probable process. The lifetime is determined by the average density of electrons at the site of the positron in the ground state of the one-positron many-electron system. Because of its charge, positrons are repelled from the positive ions at the lattice sites; thus it mainly annihilates with the electrons in the conduction band and, to a lesser extent, with core electrons. However open-volume defects (such as monovacancies and larger vacancy clusters), voids and dislocations present in metals, can alter the lifetime of positrons from that of the free annihilation rates depending on the types of defects present. This is because of the trapping of positrons in the defects. The trapping of positrons in defects depend on the nature of the defects and the resulting positron annihilation spectra have been explained by the so-called "trapping model" [33,34].

If the defects are of a void type, the average electron density of the surrounding electron cloud sensed by the "trapped" positron will be less than that for the "free" positron resulting in an increase in the average lifetime. If the defects are of electron-carrier type, the average electron density of the surrounding electron cloud sensed by the "trapped" positron may be higher than that for the "free" positrons resulting in the decrease in the average lifetime. If the positrons are deeply trapped and the trapping is the only major alternative in addition to the annihilation of "free" positrons, then the processes can be mathematically represented by the rate equations [35] (for only one type of defect in the sample) as

$$\frac{dn_f}{dt} = -\lambda_f n_f - \nu C_t n_f \quad (1.10)$$

$$\frac{dn_t}{dt} = -\lambda_t n_t + \nu C_t n_f$$

where n_f and n_t are the number of positrons annihilating with rates λ_f and λ_t from free and trapped states respectively, C_t is the concentration of the trapping defects and ν is the trapping rate of positrons by the defects. By solving the rate equations, one can find the defect concentration from the observed positron annihilation lifetimes in metals.

1.10 Positronium and molecular substances

In polymers and other molecular substances, positron annihilation takes place both due to the direct annihilation of positrons with electrons as well as through the formation of positronium atom. As already stated, positronium formation is favoured in these substances due to the presence of free or empty spaces. In general, lifetime spectra in such materials consist of three or four lifetime components, arising due to different modes of positron annihilation processes. In case of three-component lifetime spectra, it is generally believed [36] that the three lifetimes correspond to the three positron and positronium states existing in the material. The longest lifetime component ($\sim 1-10$ ns) is believed to be due to the pick-off annihilation of o-Ps. The shortest lifetime of the order of 100-200 ps arises due to the p-Ps annihilation and the intermediate lifetime of the order

200-500 ps is due to free(unbound)/direct annihilation of positron with electrons of the matter [36]. Some researchers usually describe the lifetime spectra into four lifetime components. In this case the shortest lifetime component is assigned to the annihilation of p-Ps and free positron respectively. The largest lifetime component (\sim ns) arises from the pick-off annihilation of o-Ps. Exact physical significance of the third lifetime is still a matter of debate. Recent work of Consolati [37] and Consolati and Quosso [38] indicates that this component is a quasi-positronium (q-Ps) species i.e. it is a correlated electron-positron pair 'swollen' with respect to o-Ps.

Attempts have been made to understand the pick-off behaviour of the positronium in the molecular substances. Story [39] suggested a correlation between the o-Ps in a number of plastics to their dielectric constant. Khan [40] suggested a correlation between the lifetime of o-Ps in a number of polymers with molecular cohesive energy density. Gray et al. [41] found that the quenching cross-sections of the o-Ps in the n-alkanes correlate directly with the electron polarizability of the molecules. Measurements of other classes of organic liquids have shown a similar relationship of positronium pick-off in molecular solids.

In 1960, Brandt et al. [26] proposed a theory to explain the observed positron lifetimes and their variation with temperature in molecular solids and polymers. The concept underlying their theory was based on the solid-state cell model which assumed the Bloch state of Ps to be distributed in the interstitial regions of the molecular lattice or polymer arrays. They called this

interstitial region as the "free volume", which was defined as the cell volume minus the excluded volume. The wavefunction of the positron in the field of electron was replaced by the wavefunction of the positronium atom. The annihilation lifetime is determined by the overlap between the Ps and the electron wavefunctions. Since the electron wavefunctions could not be calculated at that time, they adopted a Wigner-Seitz cell model approximation and calculated the wavefunctions for Ps for different lattice structure. This model is expressed schematically in Fig. 1.4. This theoretical model is also called the 'free volume' model since free volume (as described in their theory) was used as one of the parameters in the calculation.

Although the Brandt-Berko-Walker theory of Ps/free volume is very different from the general concept of free-volume holes and of 'free volume moving' spaces in polymers, it gave a very important and general guideline for positron annihilation in molecular systems, and laid the foundation for the development of positron annihilation research in polymers and other molecular solids. In polymers, one considers the free volumes to be fast-moving holes, which was considered to be a static interstitial space in Brandt's theory. However the important result derived from Brandt's theory is that a larger volume gives a longer Ps lifetime. A direct connection between the bulk volume and the expansion of free volume holes was also predicted. Therefore this theoretical prediction of Ps lifetime in relation to volume changes is quantitatively correct. For nearly thirty years, this theory has been the foundation for the interpretation

of all positron annihilation data in polymers.

The present model of Ps annihilation in molecular, polymeric and other similar porous materials based on the theory proposed by Tao [16] and others [42,43], will be discussed in the next section.

1.10.1 Existing model - spherical holes

In a system composed of neutral atoms or molecules, if ϕ_+ is the positron wavefunction in the electron field to which it is bound as o-Ps, and ϕ_- is the wavefunction of all electrons in the medium, then the observed positron annihilation lifetime, τ , is the reciprocal of the integral of the positron and electron densities, $|\phi_+|^2$ and $|\phi_-|^2$ respectively at the site where the annihilation takes place [26] and

$$\lambda = \frac{1}{\tau} = \pi r_0^2 c \int \phi_+^*(r) \phi_-^*(r) \phi_+(r) \phi_-(r) dr \quad (1.11)$$

where c is the speed of light and r_0 is the classical radius of the electron. In order to understand the experimental o-Ps lifetimes, one must relate the electron and the positron densities with the molecular dimensions. The exact solution of ϕ_+ and ϕ_- pose a difficult intractable quantum-mechanical problem. At this moment, only an approximate approach is feasible.

Using a zero-velocity approximation and neglecting the polarization between Ps and the lattice electrons, one can replace $\phi_+(r)$ in eq. (1.11) by $\phi_{Ps}(r_0)$, where $\phi_{Ps}(r_0)$ is the wavefunction of the Ps atom at the center of mass. Therefore eq. (1.11) can be

written as

$$\lambda = \pi r_o^2 c \int \phi_{Ps}^*(r) \phi_-^*(r) \phi_{Ps}(r) \phi_-(r) dr \quad (1.12)$$

If the wavefunction $\phi_-(r)$ arises from an average electron density of ρ_- , one can further simplify the above eq. (1.12) as

$$\tau = \frac{1}{\lambda} = \left(\pi r_o^2 c \rho_- \int \phi_{Ps}^*(r) \phi_{Ps}(r) dr \right)^{-1} \quad (1.13)$$

Therefore one can obtain the value of τ in eq. (1.13) by solving explicitly for ϕ_{Ps} for a suitable potential (usually a square well or spherical well type of potential) with proper boundary conditions which will appropriately represent the molecular forces involved. Tao [16] thus considered a simple model in which a Ps particle resides in a spherical well with radius R_o , having an infinite potential barrier. The radial part of the Schrödinger equation for the center-of-mass motion of Ps in the ground state for such a spherical well potential is given by

$$\begin{aligned} \Phi_{Ps} &= \frac{(2\pi R_o)^{-1/2}}{r} \sin \left(\frac{\pi r}{R_o} \right) \quad \text{for } 0 \leq r \leq R_o \\ &= 0 \quad \text{elsewhere} \end{aligned} \quad (1.14)$$

The calculation of the annihilation rate will, therefore, require the electron density ρ_- . Instead of pursuing a calculation of ρ_- for electrons, Tao [16] and Eldrup et al. [42] used a semi-empirical approach and assumed that the positronium annihilate in a homogeneous electron layer of thickness $\Delta R = R_o - R$

inside the well surrounding the region. The probability, P , that the o-Ps in the ground state is located inside the electron layer is thus given by

$$P = \int_R^\alpha |\phi_{Ps}|^2 r^2 dr / \int_0^\alpha |\phi_{Ps}|^2 r^2 dr \quad (1.15)$$

$$= 1 - \frac{R}{R_o} + (2\pi)^{-1} \sin \left(\frac{2\pi R}{R_o} \right) \quad (1.16)$$

This simple quantum-mechanical model of Ps confined in a spherical box is schematically shown in Fig. 1.5. Following Eldrup et al. [42] in assuming the annihilation rate of o-Ps inside the electron layer as 2 ns^{-1} (i.e. the spin averaged annihilation rate of p-Ps and o-Ps), which is very close to the annihilation rate of Ps^- [44], the o-Ps annihilation lifetime, τ , as a function of hole radius, R , is then given by [43]

$$\tau = (2P)^{-1} = 0.5 \left[1 - \frac{R}{R_o} + \frac{1}{2\pi} \left\{ \sin \left(\frac{2\pi R}{R_o} \right) \right\} \right]^{-1} \quad (1.17)$$

where R and τ are expressed in \AA and ns. In eq. (1.17), $R_o = R + \Delta R$, where ΔR is an empirical parameter. Nakanishi et al. [43] determined ΔR by fitting the observed τ with the known cavity sizes in molecular substrate. The best-fitted value of ΔR for all known data was determined to be 1.656 \AA [43]. A correlation between τ of o-Ps and cavity size (spherical) [45] is shown in Fig. 1.6. In recent years, eq. (1.17) has been extensively used to correlate the observed o-Ps lifetimes with the radius of the spherical holes in polymers, zeolites and other molecular

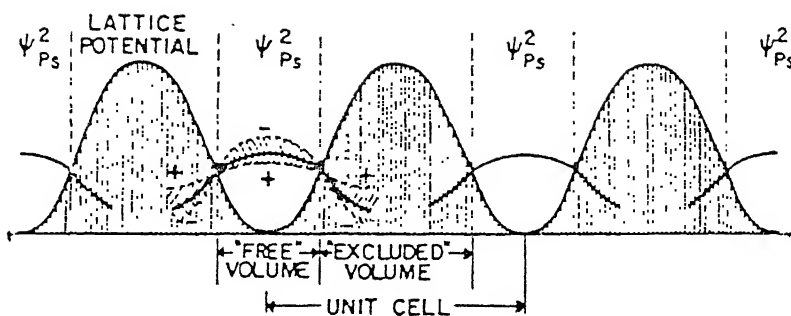


Fig. 1.4 Schematic diagram of Ps distribution according to the Brandt-Berko-Walker free-volume model of Ps decay in molecular substances [taken from Ref. 26].

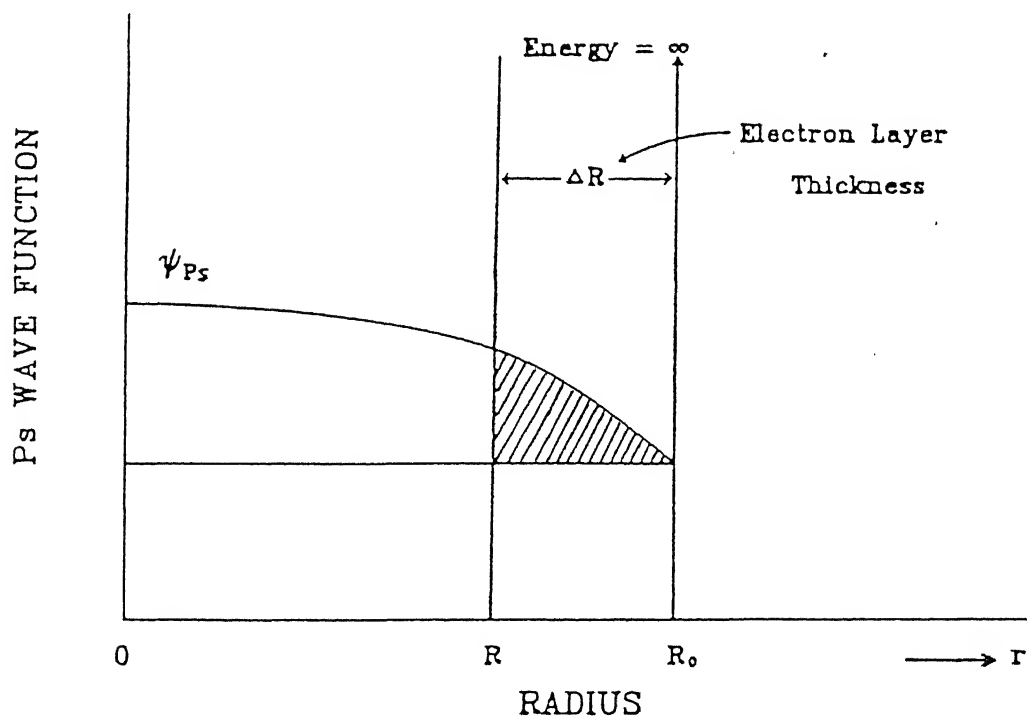


Fig. 1.5 A schematic diagram for a semi-empirical quantum model for Ps localized in a spherical box with radius R_0 [taken from Ref. 45].

substrates [44,46]. Further developments by including a finite potential depth instead of infinite potential in the above model has been made by Nakanishi and Jean [47], which gave almost similar results.

1.11 Free volume and positron annihilation in polymers

The existence of free volume in polymers has been postulated for more than four decades [48]. The explanation of viscoelastic properties in polymeric materials has been based on the free-volume theory [49] which describes the kinetic and dynamical behaviour of polymeric molecules and free volume in the matrix. More details on free-volume properties in polymeric materials is discussed in Chapter 3.

The study of open spaces can offer investigation of many properties which the study of bulk cannot. One of the special advantages of utilizing polymeric materials in industries is their mechanical flexibility in engineering processing. And this special property in polymeric materials was thought to be due to the free volume present in polymers [50,51]. In 1959, Cohen and Turnbull [52] used the concept of free-volume holes to explain the diffusion in liquids as a function of temperature and pressure and defined the free volume to be the volume difference between the space of the molecular cage made by the surrounding molecules and the Van der Waal volume of the molecules in the cage. Therefore a free volume in a polymer is a moving open space in a molecular matrix. The existence of free volume in a polymer is crucial

because it allows a polymer to relax under external forces.

Although the concept of free volume in polymers has been known for nearly a century, the experimental determination was not possible for a long time due to two facts

- (i) the size of the free volume is very small, of the order of \AA , and
- (ii) the time involving the motion is very small of the order of 10^{-13} s or larger.

Consequently in the early stages [52] the free volume was merely thought to be a theoretical concept which could not be measured experimentally. It could only be deduced from other indirect measurements such as specific volume experiments, or model calculations, such as the Van der Waal dimensions of molecules [53]. Polymer scientists therefore often describe any unexplained phenomenon as an effect of the free volume.

In spite of great deal of research done in the past decade to understand the physical properties of free volume, only limited information about the hole size, concentration, and shape were available. In fact reports of direct experimental observations of these parameters are essentially non-existent. But it is now possible to probe such small sizes, moving free spaces or free volumes using probes such as,

- (i) photochromic and fluorescent spectroscopy,
- (ii) small angle X-ray diffraction and neutron diffraction, and
- (iii) positron annihilation spectroscopy (PAS).

Photochromic labelling technique by site-specific probe was developed to monitor the rate of photoisomerizations of

characterized probe and determination of free-volume distributions [54-56]. Similarly, small angle X-ray diffraction and neutron diffraction techniques were also used to determine the density fluctuations in polymers from which free-volume sizes were calculated [57,58]. However, X-ray and neutron diffraction methods become very difficult for hole sizes below 10 Å, whereas the photochromic and fluorescent method induces additional perturbation by incorporating a sizeable probe into the holes, thus the extracted information about the hole size can only be considered as roughly estimated values. Other important probes, such as scanning tunneling microscopy and atomic force microscopy are sensitive to Å sizes but are limited to a static hole on the surface. Scanning electron microscopy and transmission electron microscopy are more sensitive to static holes at a size of ten Å or larger.

In this regard, positron annihilation is an ideal nano-probe which has been developed to directly determine and measure local free-volume hole properties in polymeric materials [59]. Positron annihilation is uniquely sensitive in probing the free volume in polymers and other molecular substance. The unique sensitivity of positron annihilation in probing the free-volume properties in polymers and similar molecular solids is mainly due to the fact that Ps is found to be preferentially localized in the free-volume regions of polymeric materials. Also because of the relatively small size of Ps probe (1.06 Å) compared with other probes, PAS is particularly sensitive to small holes and free volumes of Å size, and within a time of molecular motion from 10^{-10} s and larger.

Contrary to other probes PAS is capable of determining the holes and free volumes in polymers without any significant interference by the bulk.

Unlike conventional probes such as neutron, photon and electron, the positron is a strongly interacting probe. The process of $e^+ - e^-$ annihilation is governed by interaction at the zero range i.e. the overlap between the positron and electron at the same position. In this technique [59], one employs the positron as a probe and monitors the lifetimes of the positron and positronium (Ps- bound state of $e^- - e^+$) in the polymeric material under study. Because of the positively-charged nature of the positrons, the positron and Ps are repelled by the positive ion-cores of polymers and are trapped in open spaces, such as holes, the free volumes and voids (Fig. 1.7). In other words, the positron will naturally favour those regions which the electron does not, i.e. open spaces. Thus the study of positron annihilation becomes meaningful because of localization (or trapping) of the positron in the open spaces and free volume in polymers. Further these Ps atoms are unstable and they annihilate within the free volume region and hence the annihilating photons that come from these open spaces carry information about the free volume.

In molecular systems, a large fraction of Ps formation is observed in the free-volume regions. The long lifetime of o-Ps gives us a great advantage of quantifying the lifetime results. Since Ps is localised in the free-volume holes, one expects to correlate the hole dimension with the measured lifetimes.

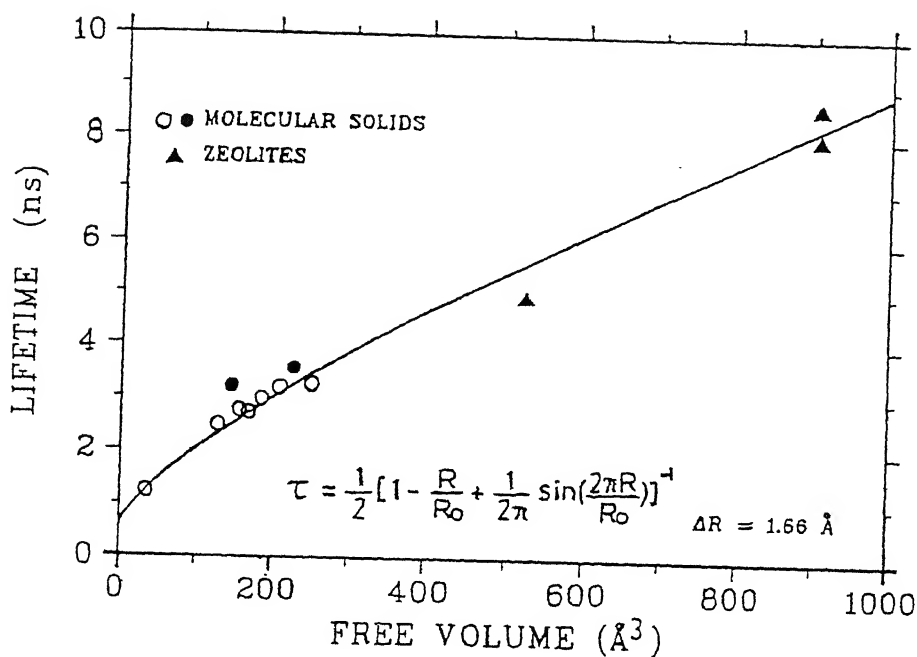


Fig. 1.6 Correlation curve of *o*-Ps lifetime as a function of free-volume hole size, assuming spherical hole [taken from Ref. 45].

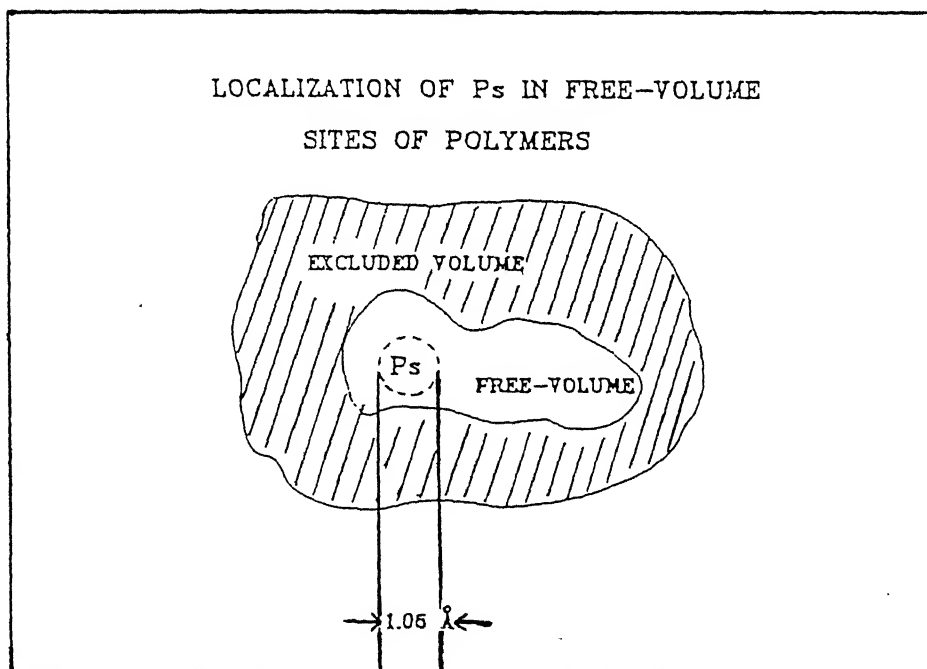


Fig. 1.7 Cross-sectional view of the *Ps* localized in the free-volume holes in a polymeric material [taken from Ref. 45].

Therefore measuring the positron lifetimes in these materials not only gives information about the size and fraction of free-volume holes, but gives the free-volume hole size distribution in the range 1-10 Å also. This has become possible due to recent development of Laplace's inversion technique [60] incorporated into a computer program [60,61] for the analysis of the measured lifetime spectra in terms of continuous lifetime distribution. Further these positron lifetime distributions can be converted into free-volume hole radii and volume distributions. In this manner one can experimentally study the free-volume properties of polymers using positron lifetime technique and such experimental studies, specifically measuring the variation of free volume with temperature [62,63], pressure [64-66], physical aging and structural relaxation [67,68], stress-induced structural deformations [69], degree of crystallinity [70] etc. have been reported in the literature.

Theoretical treatment using molecular dynamics simulation and kinetic theory [71,72] has predicted that the radii and the hole-volumes of the free volume in a polymer exist as a distribution. Experimentally the dependence of these distribution on pressure [64,65] and temperature [62] have been determined with positron lifetime techniques, combined with the Laplace's inversion technique [60,61] for data analysis. Interestingly, the range of values for the hole radii distributions obtained from positron annihilation agrees fairly well with theoretically calculated values for known polymers. All these results provide evidence that the Ps are usually localised in the pre-existing

local holes and free-volume holes in polymers.

1.11.1 Ps-hole theory in polymers

Two types of holes must be considered in positron annihilation studies. They are either static and pre-existing or dynamic and transient. The former is considered as defect type volume and the latter is the free volume in polymers. The origin of free volume in polymers is a composite result from molecular relaxation among chains and terminal ends. Creation time for the holes can be as short as 10^{-13} s and larger ; i.e. the vibration and rotations of bond. Since positron lifetime is of the order of 10^{-10} s, the majority of free volumes can be probed by positron annihilation. Both "static" and "dynamic" holes (longer than 10^{-10} s) are favourable trapping sites for Ps and positrons.

Another important aspect of Ps-hole theory is the hole size required to trap Ps. The simple spherical hole model (i.e. Ps resides in a spherical hole radius R_0 having an infinite potential barrier) described in sec. 1.10.1 gave a relatively good correlation between the hole radius and the o-Ps lifetime in known polymers. In reality, the shape of a free-volume hole is known to be non-spherical. Jean and Shi [73] presented a newly developed relationship between the o-Ps lifetime and the anisotropic hole dimensions for an ellipsoidal free-volume hole, present in polymers which are either deformed or anisotropic in nature. However under normal circumstances, polymers are mostly isotropic and the Ps-hole model based on spherical hole dimensions is adequate for that matter.

Shortly after the positron annihilation lifetime technique was established , positron annihilation was applied to polymeric systems. However, only a few studies were made in the early years [74]. This was due to the lack of any understanding about the nature of interaction of positrons with such materials and the information thus obtained from such studies. Most of the earlier studies were confined to the study of temperature dependence of positron annihilation lifetimes in polymers such as polystyrene, polyvinyl chloride, etc. [74]. The field of polymer studies using positron annihilation spectroscopy has been revived only recently [46,75] and has again attracted considerable interest in the scientific community. This is due to the new role that positron annihilation can play in understanding the physical, mechanical and electrical properties in polymers, which are becoming technologically more important materials in industries [75,76] . Applications of this new method of PAS to study practical materials and to solve some of the mechanical properties appears to be possible and promising. However, as it happens with all other newly emerging techniques, there are still many unsettled problems which need to be looked into. Some of these are addressed by Jean [46] and others [77,78]. Therefore application of PAS for the study of polymers and polymeric materials requires further intense and systematic effort before PAS can become a routine and reliable tool in the scientific and engineering applications.

1.12 Scope of the present study

As already discussed in the previous section, routine application of PAS technique to study polymers and polymeric materials require further research in this field. Physics of polymers and polymeric materials is still little understood, and further research using PAS in this field can help us to understand their physical and mechanical properties.

Ion-conducting polymer electrolytes is an area of recent theoretical and experimental interest due to their possible applications in various electrochemical devices [79] e.g. as high-energy density batteries, fuel cells, electrochromic devices etc. Mechanism of ionic conductivity and their dependence on temperature, pressure and degree of crystallization in such polymer electrolytes is not properly understood yet. An explanation based on the free-volume theory has also been proposed for the temperature dependence of electrical conductivity of these ion-conducting polymers [79]. However, the experimental results to support such explanation are very few [80] and also highly unsatisfactory as far as their ion transport properties are concerned. Positron annihilation spectroscopy with its unique ability to probe free-volume properties in polymers can help in understanding some of the basic questions related to the mechanism of ion-transport in polymer electrolytes. We have, therefore, carried out positron lifetime studies in polyethylene oxide (PEO) based polymer electrolytes doped with two different ammonium salts (i.e. $\text{PEO} + \text{NH}_4\text{ClO}_4$ and $\text{PEO} + \text{NH}_4\text{I}$) as a function of temperature.

Some of the technologically important polymers include epoxy and polyester resins, because of their wide range of applications as adhesives, fillers, host matrices for composite materials etc. Although they are being used in industries for the last three decades, their microstructure is still unclear. Study of their microstructure down to the atomic scale can help us to understand their mechanical behaviour and failure during loading. Keeping these aspects in mind, we have also performed positron lifetime studies in two different high-temperature resistant glassy polymers (i.e. epoxy and polyester resin polymers) as a function of temperature, physical aging and moisture absorption.

The main aim of the present work was, therefore, to study various polymers and polymer electrolytes with an objective to (i) understand the free volume properties and their dependence on different external conditions of temperature, time and environmental effects in the case of epoxy and polyester resin polymers, and (ii) the role of free-volume in determining the ion transport mechanism and hence the large ionic conductivity observed in the polymer electrolytes. In the last part of this thesis we have presented our positron lifetime studies in certain aluminium-alumina composites and tried to investigate the nature of hydrogen trapping that can possibly explain the hydrogen embrittlement observed in these composites.

The present thesis is divided into seven chapters. Following the present chapter is Chapter 2 providing a brief review of the experimental methods used for the study of positron annihilation. Since the major part of the present work deals with the study of

polymer electrolytes, a brief introduction to the structural and physical properties of these new technological materials is given in Chapter 3. The present studies of the temperature dependence of positron annihilation lifetime, free volume, conductivity, ionic-mobility and number of charge carriers in the proton-conducting polymer electrolyte, polyethylene oxide (PEO) complexed with ammonium perchlorate (NH_4ClO_4) are described in Chapter 4. In Chapter 5 we have presented the positron annihilation lifetime studies of free volume in polymer electrolyte polyethylene oxide (PEO) complexed with ammonium iodide (NH_4I). The present studies of the positron annihilation lifetimes in two polymers, cured epoxy and polyester resins are described in Chapter 6. In the last chapter we have described positron lifetime studies in the $\text{Al-Al}_2\text{O}_3$ metal matrix composites, containing 0%, 2%, 4% and 8 wt. % Al_2O_3 particulates. We feel that a systematic investigation of some of the technologically important materials using positron annihilation lifetime technique has been carried out in the present work. It is hoped that the present studies carried out in the polymer electrolytes $\text{PEO}+\text{NH}_4\text{ClO}_4$ and $\text{PEO}+\text{NH}_4\text{I}$, cured epoxy and polyester resin polymers and in the $\text{Al}+\text{Al}_2\text{O}_3$ metal matrix composites using positron lifetime measurements and other characterization techniques have helped to extend our present understanding of these systems.

References

1. P.M.A. Dirac, Proc. Cambridge Phil. Soc. 26, 361 (1930).
2. C.D. Anderson, Phys. Rev. 41 , 405 (1932).
3. C.D. Anderson, Phys. Rev. 43 , 491 (1933).
4. C.D. Anderson, Phys. Rev. 44 , 406 (1933).
5. P.M.S. Blackett and G.P.S. Occhialini, Proc. Roy. Soc. A 139, 699 (1933).
6. J. Thibaud, Compt. Rend. 197, 1629 (1933).
7. J. Thibaud, Phys. Rev. 45, 781 (1934).
8. F. Joliot , Compt. Rend. 197, 1622 (1933).
9. F. Joliot , Compt. Rend. 198, 81 (1934).
10. R.L. Garwin, Phys. Rev. 91, 1571 (1953).
11. G.E. Lee-Whiting, Phys. Rev. 97, 1157 (1955).
12. C.N. Yang, Phys. Rev. 77, 242 (1950).
13. A. Ore and J.L. Powell, Phys. Rev. 75, 7696 (1949).
14. J. Green and J. Lee, "Positronium Chemistry" (Academic Press, New York, 1964).
15. R.A. Ferrel, Rev. Mod. Phys. 28, 308 (1956).
16. S.J. Tao, J. Chem. Phys. 56, 5499 (1972).
17. A. Ore, Univ.Bergen Arbok, Naturvidenskap Rekke, No. 9, 1-16 (1949).
18. O.E. Mogensen, J. Chem. Phys. 60, 998 (1974).
19. M. Eldrup, D. Lightbody and J.N. Sherwood, Chem. Phys. 63, 51 (1981).
20. F. Rohrlich and B.C. Carlson, Phys. Rev. 93, 38 (1954).
21. W.F. Schmidt and A.O. Allen, J. Chem. Phys. 52, 2345 (1970).

22. G. Czapski and E. Peled, J. Chem. Phys. 77, 893 (1973).
23. A.K. Pikaev, "Solvated Electron in Radiation Chemistry" (Nauka, Moscow, 1969).
24. R.E. Bell and R.L. Graham, Phys. Rev. 90, 644 (1953).
25. R.L. Garwin, Phys. Rev. 91, 1571 (1953).
26. W. Brandt, S. Berko, and W.W. Walker, Phys. Rev. 120, 1289 (1960).
27. R.A. Ferrel, Phys. Rev. 110, 1355 (1958).
28. M. Deutsch and E. Dulit, Phys. Rev. 84, 601 (1951).
29. M. Deutsch and S.C. Brown, Phys. Rev. 85, 1047 (1952).
30. A. Bisi, F. Bisi, A. Fasana and L. Zappa, Phys. Rev. 122, 1709 (1961).
31. A. Bisi, A. Fasana and L. Zappa, Phys. Rev. 124, 454 (1968).
32. S.J. Tao and J.H. Green, J. Chem. Soc. A2, 408 (1968).
33. M.A. Bertolaccini, A. Bisi, G. Gambarini, and L. Zappa, J. Phys. C4, 734 (1971).
34. W. Brandt, Appl. Phys. 5, 1 (1974).
35. M.J. Puska and R.M. Nieminen, Rev. Mod. Phys. 66, 841 (1994).
36. "Positron Solid State Physics", edited by W. Brandt and A. Dupasquier (Amsterdam, North Holland, 1983)
37. G. Consolati, in "Positron and Positronium Chemistry", edited by Y.C. Jean (World Scientific, Singapore, 1990) p. 62.
38. G. Consolati and F. Quasso, Appl. Phys. 50, 43 (1990).
39. E.J. Story, M.S. Thesis, Vanderbilt University, 1960.
40. M.N.G.A. Khan, Ph.D. Thesis, University of New South Wales, 1968.
41. P.R. Grey, C.F. Cook and G.P. Starm, J. Chem. Phys. 48, 1145

(1968).

42. M. Eldrup, D. Lightbody and J.N. Sherwood, Chem. Phys. 63, 51 (1981).
43. H. Nakanishi, S.J. Wang and Y.C. Jean, in "Positron Annihilation Studies in Fluids", edited by S.C.Sharma (World Scientific, Singapore, 1988) p. 292.
44. A. P. Mills Jr., Phys. Rev. Lett. 46, 717 (1981).
45. Y.C. Jean, in "Positron and Positronium Chemistry", edited by Y.C. Jean (World Scientific, Singapore, 1990) p. 1.
46. Y.C. Jean, Mater. Sci. Forum 175-178, 59 (1995).
47. H. Nakanishi and Y.C. Jean, in "Positron and Positronium Chemistry", edited by D.M. Schrader and Y.C. Jean (Elsevier, Amsterdam, 1988) ch. 5.
48. A.K. Doolittle, J. Appl. Phys. 22, 1471 (1951).
49. M.L. Williams, R.F. Landel and J.D. Ferry, J. Am. Chem. Soc. 77, 3701 (1955)
50. T.G. Fox and P.J. Flory, J. Phys. Chem. 55, 211 (1951).
51. T.G. Fox and P.J. Flory, J. Appl. Phys. 21, 21 (1951).
52. M.H. Cohen and D. Turnbull, J. Chem. Phys. 31, 1164 (1959).
53. J.D. Ferry, "Viscoelastic Properties of Polymers" 3rd Edition (John Wiley & Sons, New York, 1980).
54. J.S. Royal, J.G. Victor and J.M. Torkelson, Macromolecules 25, 4792 (1992).
55. W.C. Yu and C.S.P. Sung, Macromolecules 21, 365 (1988).
56. Y. Tanabe, N Muller and E.W. Fischer, Polym. J. 16, 1445 (1984).
57. S. Nojima, R.J. Roe, D. Rigby and C.C. Han, Macromolecules 23,

- 4305 (1990).
58. W.C. Yu, C.S.P. Sung and R.W. Robertson, *Macromolecules* 21, 355 (1988).
 59. "Positron and Positronium Chemistry", edited by D.M. Schrader and Y.C. Jean (Elsevier, Amsterdam, 1988).
 60. S.W. Provencher, *Comput. Phys. Commun.* 27, 213 (1982) ; *ibid*, 27, 229 (1982).
 61. R.B. Gregory and Y. Zhu, *Nucl. Instrum. Methods A* 290, 172 (1990); R.B. Gregory, *Nucl. Instrum. Methods A* 302, 496 (1991).
 62. Q. Deng, F. Zandiehnam, and Y.C. Jean, *Macromolecules* 25, 1090 (1992).
 63. Y.C. Jean, T.C. Sandreczki and D.P. Adams, *J. Polym. Sci. Polym. Phys. Ed.* 24, 1247 (1986).
 64. Q. Deng and Y.C. Jean, *Macromolecules* 26, 30 (1993).
 65. Y.C. Jean and Q. Deng 1992 *J. Polym. Sci. Polym. Phys. Ed.* 30, 1359 (1992).
 66. Q. Deng, C.S. Sunder and Y.C. Jean, *J. Phys. Chem.* 96, 492 (1992).
 67. K.J. Heater and P.L. Jones, *Nucl. Instrum. Methods B* 56/57, 610 (1991).
 68. Y. Kobayashi, W. Zheng, E.F. Meyer, J. D. McGervy, A. M. Jamieson and R. Simha, *Macromolecules* 22, 2303 (1989).
 69. C.L. Wang, B. Wang, S.Q. Li, and S.J. Wang, *J. Phys. : Condens. Matter* 5, 7515 (1993).
 70. H. Nakanishi, Y.C. Jean, E.G. Smith and T.C. Sandreczki, *J. Polym. Sci. Polym. Phys. Ed.* 27, 1419 (1989).

71. D. Rigby and R.J. Roe, *Macromolecules* 23, 5312 (1990).
72. R.E. Robertson, R. Simha, and J.G. Curro, *Macromolecules* 18, 2239 (1985).
73. Y.C. Jean and H. Shi, *J. Non-Cryst. Solids* 172-174, 806 (1994).
74. A.E. Hamielec, M. Eldrup, O. Mogensen, and P. Jansen, *J. Macromol. Sci. Rev. Macromol. Chem.* C9, 305 (1973).
75. Y.C. Jean, *Microchemical J.* 42, 72 (1990).
76. J.R. Stevens in "Probe and Label Techniques in Methods of Experimental Physics" edited by R.A. Fava (Academic Press, London, 1980) p. 371.
77. Y. Ito, *Mater. Sci. Forum* 175-178, 627 (1995).
78. J.D. McGervey, Zhibin Yu, A.M. Jamieson and R. Simha, *Mater. Sci. Forum* 175-178, 727 (1995).
79. "Polymer Electrolyte Reviews 1" edited by J.R. MacCallum and C.A. Vincent (Elsevier Applied Science, London, 1987) ;
"Polymer Electrolyte Reviews 2" edited by J.R. MacCallum and C.A. Vincent (Elsevier Applied Science, London, 1989) ;
80. Z.L. Peng, B. Wang, S.Q. Li, S.J. Wang, H. Liu and H.Q. Xie, *Phys. Lett. A* 194, 228 (1994).

CHAPTER 2

EXPERIMENTAL METHODS FOR POSITRON ANNIHILATION STUDIES

2.1 Introduction

In the present work, positron annihilation and other characterization techniques have been applied for the study of polymeric materials and metal-composites. In the last two decades positron annihilation technique has emerged as a powerful non-destructive technique for investigating condensed matter. Several books and reviews have been published on this subject [1-18] and in addition the proceedings of the various International Conferences on Positron Annihilation (ICPA's) have been published regularly [19-27]. One recent and interesting application of positron annihilation technique has been for studying free-volume properties in polymers and polymeric materials [15,25,27]. Such studies can help us to understand the role that free volume plays in determining the various physical, mechanical and electrical properties in these materials.

Generally, positron annihilation studies are performed by using three different methods involving different experimental observables and setups. They are

- (1) Positron lifetime measurements,
- (2) Angular Correlation between the annihilation radiation, and
- (3) Doppler broadening of the annihilation radiation.

Out of the above-mentioned methods, the most commonly employed measurement techniques are the first two. In the present

work, only the first method of measurement has been used. In subsequent sections, positron lifetime technique and related apparatus used for such measurement will be discussed along with a brief outline of the other measurement techniques including the angular correlation and Doppler broadening measurements.

2.2 Methods for measuring positron lifetimes

The mean lifetime of positrons in gases was first measured by Deutsch [28]. In condensed media, such measurements were first made by De Benedetti and Richings [29]. Bell and Graham [30] first applied the technique of delayed coincidence to measure positron lifetimes in condensed matter. Since then positron lifetimes are measured by using this standard delayed coincidence technique [31,32]. The technique of measuring the lifetimes of positrons in a medium is termed as 'Positron lifetime spectroscopy'. There are some review articles describing this subject [32-35]. Different types of organic and inorganic scintillators with fast decay time along with fast photomultipliers and improved version of electronic time derivation devices are now available. Together they can provide a very good instrumental time resolution suitable for making positron lifetime measurements in a given medium. Apart from the advances made in the electronics with very good resolution of the system, good computer programs for data analysis have also been developed over the years [36-40].

Positron annihilation lifetime measurements involve measurement of lifetimes in the range 0.1 to 100 ns. Therefore the

method employed for measuring such short lifetimes is very similar to those employed in nuclear spectroscopy. Present state-of-the-art positron lifetime spectroscopy has resolution as good as 145 ps [41].

2.2.1 Positron sources

The most commonly used laboratory sources of positrons are radioactive isotopes such as ^{22}Na (sodium-22), ^{64}Cu , ^{58}Co and ^{68}Ge . Out of these ^{22}Na is normally used as a source of positrons for lifetime measurements. Accelerator-based positron beams are also used for studying positron lifetimes.

A detailed decay scheme of ^{22}Na is shown in Fig. 2.1. This radioactive isotope ($t_{1/2} = 2.7$ years), can be obtained from most suppliers of radioisotope as sodium chloride in carrier-free aqueous solution. The decay of ^{22}Na to ^{22}Ne produces positrons with continuous energy distribution having a maximum energy of 542 keV and average energy of about 120 keV. The emission of a positron from ^{22}Na leads to an excited state of ^{22}Ne . The half-life of the excited state of ^{22}Ne is $\sim 10^{-12}$ s and decays to the ground state of ^{22}Ne with an emission of a 1.276 MeV γ -ray. The emission of the positron can, therefore, be taken to be simultaneous with the emission of the γ -ray within the finite time resolution of the instrument. Detection of this essentially simultaneous emission of the 1.276 MeV γ -ray provides a convenient timing signal that marks the birth of the positron. Some of the advantages of using ^{22}Na used as a positron source for positron lifetime measurements include

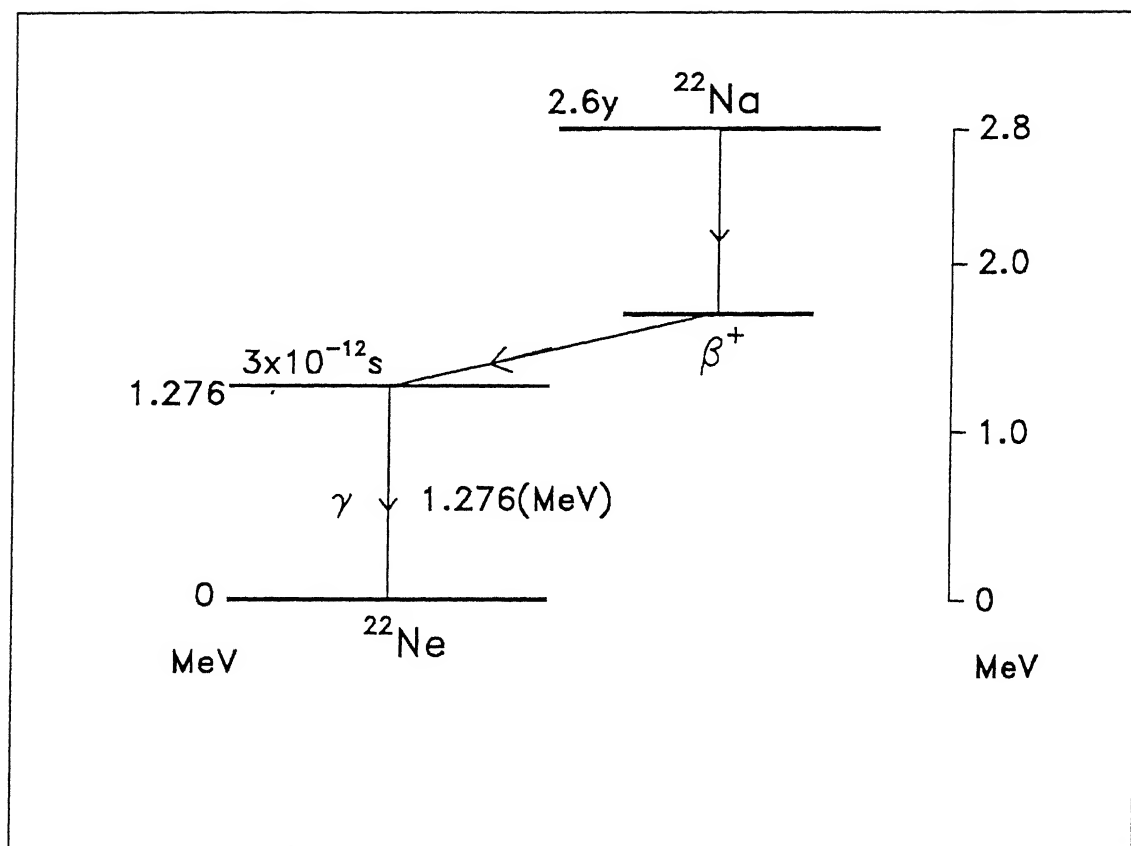


Fig. 2.1 Decay scheme of ^{22}Na .

- (i) its long half-life ($\tau_{1/2} \approx 2.7$ years) , which allows for a relatively constant strength of the source over a prolonged period of measurement,
- (ii) almost simultaneous emission of a γ -ray and a positron, which is important for measuring the lifetime of the positron, and
- (iii) the separation in energy of the γ -ray (1.276 MeV) and the annihilation photons (0.511 MeV), which provide an easy discrimination between their energies in the energy spectrum.

2.2.2. Source preparation

A typical ^{22}Na source is prepared by depositing drops of carrier-free solution onto aluminium, nickel or mica foil having a thickness of about 5-10 μm . Upon evaporation the host material is then folded and sealed in a leakproof "sandwich". The host material should be structurally as thin as possible to ensure that a maximum fraction of positrons interacts with the sample under study rather than getting absorbed in the holder. On the other hand, the holder should be strong enough to withstand handling (during the measurement) and any corrosive action of the sample or the $^{22}\text{NaCl}$.

2.2.3. Source strength

The ideal source activity is dictated by the type of investigation and apparatus used. In lifetime measurements the radioactivity is a function of the maximum allowable random coincidence. In practice, a source strength of 2-25 μCi are commonly used for positron lifetime measurements.

2.2.4. Sample thickness

The thickness of material under study should be chosen to allow absorption of all positrons that escape the source holder. The maximum penetration of positrons in a sample can be calculated in the same manner as that for negative β -particles. However, because of its opposite charge, the positron has a range in some material upto 80% greater than an electron of the same energy. In condensed materials a thickness of 200 mg/cm^2 is adequate for stopping positrons emitted from ^{22}Na .

2.2.5. Positron lifetime spectrometer

In most media, the singlet state annihilation of positron with electrons leads to the emission of two gamma quanta of energy 0.511 MeV each. As already described above, the detection of 1.276 MeV γ -ray marks the birth of the positron. Detection of one of the annihilation γ -ray of 0.511 MeV marks the death of the positron. Therefore, a measurement of the time interval between the emission of 1.276 MeV and one of the annihilation γ -ray (0.511 MeV) can yield information about the positron lifetimes in the medium. Some of the first measurements involved the method of delayed coincidence in which a start pulse generated by the detection of the 1.28 MeV γ -ray was delayed for various times and routed to a fast coincidence circuit that received a stop pulse arising from the detection of 0.511 MeV γ -rays. A plot of coincidence rate vs time delay was analyzed to yield the average positron lifetime [28]. Although this method was improved with the development of fast circuitry, accurate results were not easy to obtain.

With the invention of the time-to-pulse-height converters (TPHC) [42,43] and other nuclear electronic instruments, the determination of positron lifetimes became relatively easy. Present-day positron lifetime spectrometers, based on TPHC technology, involve the use of either slow-fast or a fast-fast coincidence technique. A block diagram giving the schematic arrangement of a typical positron lifetime spectrometer involving slow-fast coincidence is shown in Fig. 2.2. The setup basically consists of (i) radiation detectors (ii) time derivation devices (iii) time-to-pulse height converter (TPHC) or time-to-amplitude converter (TAC) and (iv) a data acquisition system or a multi-channel analyzer (MCA).

The ^{22}Na source is sandwiched between two identical specimens of the sample under study. This source-sample assembly is kept between two detectors. The detectors consist of fast scintillators coupled to fast photomultipliers (PM). Each of the photomultipliers can give two output pulses, one from the anode and the other from one of the dynode stages, usually the last dynode. The timings of the pulses corresponding to the 1.276 MeV and 0.511 MeV have to be determined carefully so that their time difference is known precisely. Since anode pulses are relatively faster pulses, having short risetimes (~ 4 ns), these are used for timing purposes. The anode pulses from each of the two photomultipliers are fed to two time derivation devices, usually a fast discriminator (FD) or constant fraction discriminators (CFD), which accept fast pulses at adjusted discriminating level. This level is usually fixed such that the photomultiplier noise is

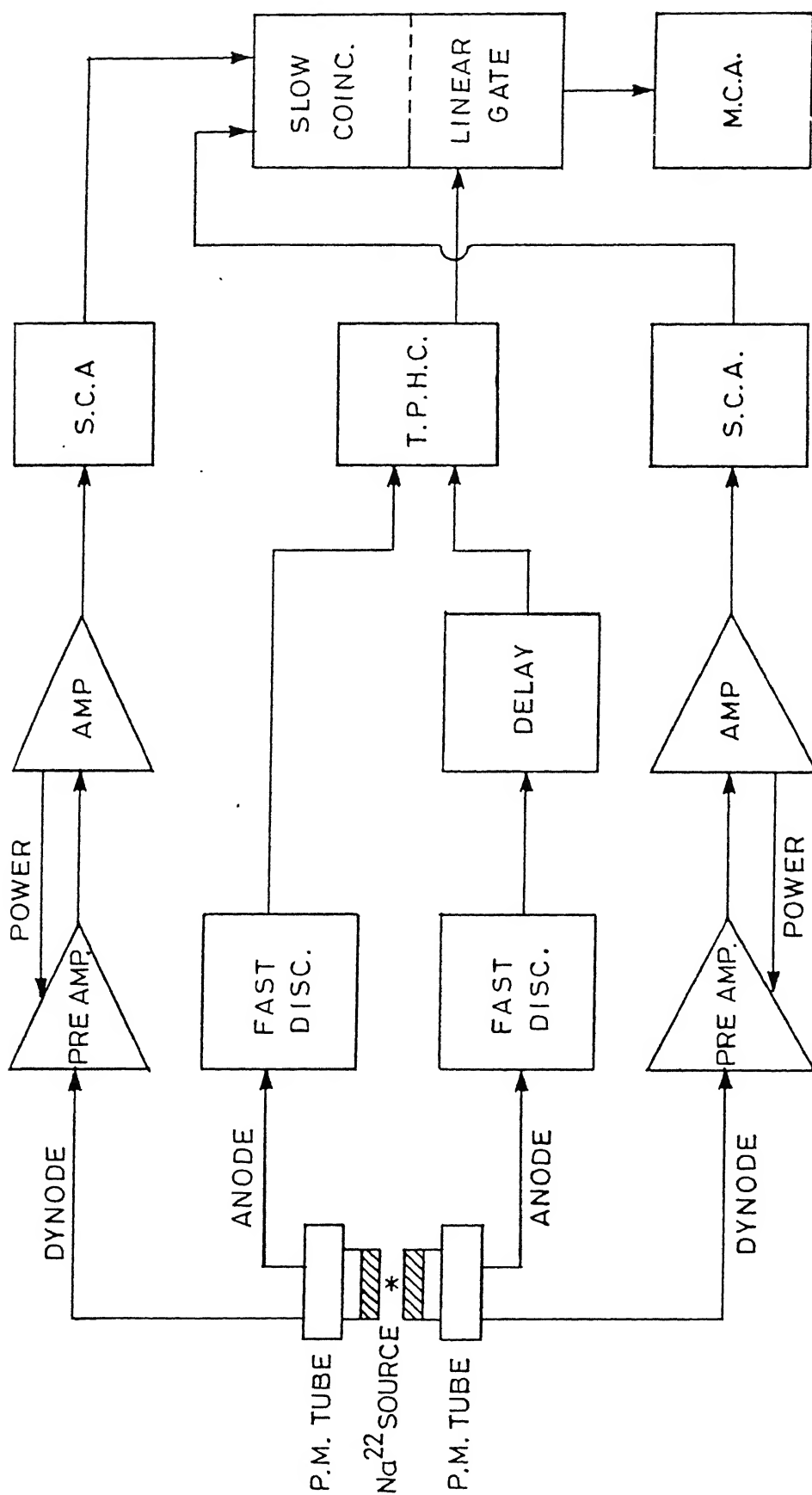


Fig. 2.2 Block diagram of positron lifetime spectrometer using slow-fast coincidence technique.

discriminated out. Each of the discriminators provide a well defined and discriminated timing output. The detection of a photon on the start side triggers the TPHC to begin building a pulse until a stop signal is received. The amplitude of the TPHC output is proportional to the time difference between the two signals. The start signal must arrive prior to the stop signal in the TPHC.

In positron lifetime measurements, the TPHC output is gated with a coincidence circuit output pulse, so that the gate will open only when a coincidence signal, corresponding to the coincidence of the photons of energies 1.276 and 0.511 MeV is received from the coincidence circuit. The slow pulses from one of the dynodes of the photomultipliers are more suited for the purpose of energy selection, and they are used for energy analysis. The pulses taken from the dynode of the photomultipliers are fed to a preamplifier and then to an amplifier. These amplified pulses are then processed by a single channel analyzer (SCA). The start-side SCA is set to emit a signal when it receives a 1.276 MeV photon and the stop-side SCA emits a signal upon receiving a 0.511 MeV photon. The output pulses from the SCA are then fed to a slow coincidence which gives an output only when these two pulses arrive there within a short time known as the resolving time, typically about one μsec . The slow coincidence output provides the gating signal for the TPHC, whose output is then routed to a multi-channel analyzer (MCA), where it is stored in a channel corresponding to the amplitude of the TPHC output. The resultant spectrum stored in the MCA gives a typical lifetime spectrum shown in Fig. 2.3. Subsequent analysis of this lifetime

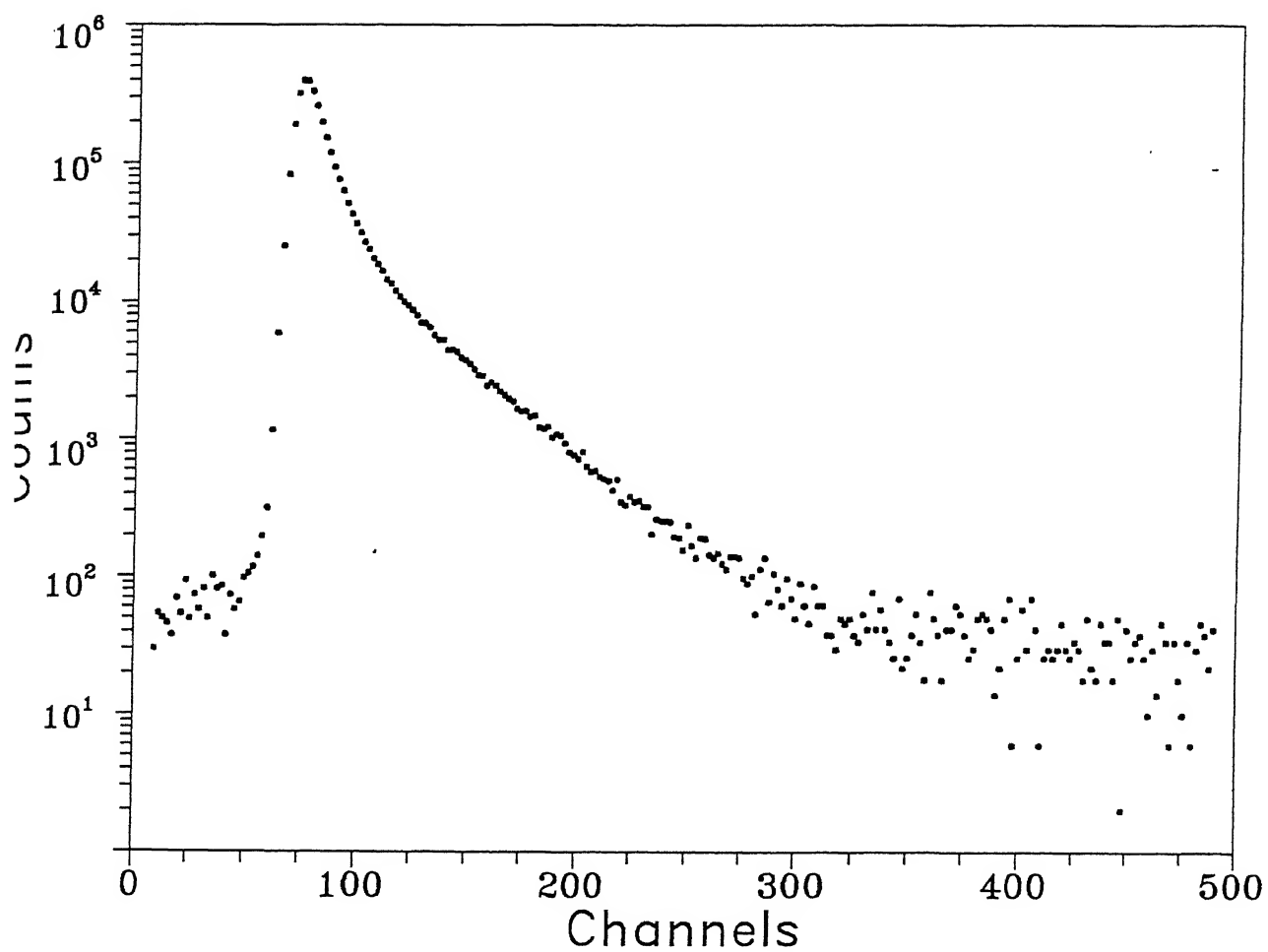


Fig. 2.3 A typical positron lifetime spectrum.

spectrum yields the lifetimes of positrons in condensed matter. This technique of slow-fast coincidence has been used to measure the positron lifetimes in condensed matter for the last two decades.

A typical fast-fast coincidence spectrometer employing a TPHC requires only one signal from the detector. Energy selection and time derivation are achieved simultaneously in a single unit, using the technique of fast zero crossover [44] or constant fraction discriminator (CFD) timings [45], which then triggers the TPHC. When the energy requirements are met and the start and the stop pulses arrive at the TPHC within the selected time range, the TPHC sends a signal to the MCA. This system has some advantage over the slow-fast coincidence spectrometer. Our present setup of positron lifetime spectrometer is based on the fast-fast coincidence technique, details of which are presented in section 2.4 of this chapter.

Recently, fast timing with photomultiplier dynode pulses (bipolar pulses), BaF_2 scintillators and the method of internal shaping were used by Radiation Technology group at TU Delft to develop a positron lifetime spectrometer having a high timing resolution [41]. Later part of our present work was done using this type of positron lifetime spectrometer.

The requirements of the various components in a timing spectrometer are treated in several publications [32,33,45-48]. In all these measurements, the determination of timing resolution of the system is necessary. In positron lifetime measurements, this can be done by measuring either a prompt spectrum from ^{60}Co or by

measuring the positron lifetime parameters from lifetime spectrum in a sample having a well known single lifetime component e.g. properly annealed high purity copper or aluminium. Major factors that affect the time resolution are (i) decay time of the scintillators (ii) risetime of the PM tubes and (iii) method of time pick-off. The timing jitter due to the introduction of noise in the timing signals in present-day positron spectrometer is a minor factor in currently available PM's, timing discriminators, and TPHCs. A time resolution of 300ps (full width at half maximum (FWHM) in case of ^{60}Co spectrum) is typically obtained with a commercially available setup. However for improved and better time resolution, proper choice of the scintillators and the PMTs is needed. The best time resolution reported in the literature is perhaps 125ps [48].

A positron in condensed matter annihilates from different states resulting in a multi-exponential time spectrum. The positron lifetime spectrum measured is then analyzed into different lifetime components (τ_i) having respective intensities I_i (where $i=1,2,3..$ etc.) using computer programs [36-40]. Usually the shortest to longest lifetime components are denoted in the order $\tau_1, \tau_2, \tau_3, \tau_4..$ The lifetimes are actually the inverse of the slopes of the best-fit straight lines through the data points after subtraction of the background. In general, the physical interpretation of lifetime data is difficult and therefore the numerical data analysis should be done very carefully.

The details of the experimental setup, used in the present work, and its calibration and methods of data analysis are

discussed in sections 2.4 and 2.5 of this chapter.

2.3 Doppler broadening and angular correlation measurements of annihilating radiation

The total linear momentum \vec{p} of the annihilating ($e^+ - e^-$) pair is conserved during the annihilation process. The distribution of \vec{p} (in momentum space) is experimentally observed by measuring the momentum distribution of annihilation photons. Let us consider only the 2γ mode (singlet state) of $e^+ - e^-$ annihilation since the cross-section for the 3γ (triplet state) mode is smaller by a factor 372. If the photon momenta are written as \vec{q}_1 and \vec{q}_2 , the laws of conservation of momentum and energy give

$$\vec{q}_1 + \vec{q}_2 = \vec{p} \quad (2.1)$$

$$q_1 c + q_2 c = \frac{p^2}{2m} + 2mc^2 \quad (2.2)$$

respectively, where c is the speed of light and m is the mass of the electron. In the first approximation, we may neglect the kinetic energy, and momentum of the annihilating pair (in comparison with the energy and momentum of the photon) and put $\vec{p} = 0$, $p = 0$, to obtain $\vec{q}_1 = -\vec{q}_2$ and $q_1 = q_2 = mc = 137$ a.u. This approximation leads to the picture shown in Fig. 2.4 (a), indicating that the two annihilation photons are emitted in exactly opposite directions (along the x-axis) and each photon has an energy of $mc^2 = 0.511$ MeV.

In a real solid, the ($e^+ - e^-$) pair momentum \vec{p} has finite

value with components (p_x , p_y , and p_z). If the x-axis is assumed to lie along the approximate direction of emission of the photons, the longitudinal components p_x give rise to a Doppler energy shift $\pm p_x c/2$ [12-18]. The transverse (p_y, p_z) components of finite \vec{p} cause the direction of emission of the two photons to deviate from collinearity by an angle $\vartheta \approx (p_y^2 + p_z^2)^{1/2}/mc$ (Fig. 2.4(b)) [12-18]. These two effects thus lead to two different measurement techniques: (i) Doppler broadening of annihilation radiation lineshape (or DBARL) and (ii) angular correlation of positron annihilation radiation (or ACAR).

The experimental method of DBARL has been well reviewed by Mackenzie [49]. Such studies are performed with the help of a high-resolution solid state detector (typically a Ge(Li) or a HPGe detector having an energy resolution of about 1.1-1.4 keV at 511 keV) coupled to a stable energy analysis system as shown in Fig. 2.5. A typical Doppler broadening of the annihilation line is characterised by a FWHM of about 2-3 keV (Fig. 2.6) and hence the resolution of the DBARL spectrometer is insufficient for studying the momentum distributions. Nevertheless clever use of deconvolution procedure and lineshape parameters [12-18,49] allows one to interpret relative changes in the so-called 'lineshape parameters' in terms of the states of $e^+ - e^-$ annihilation etc.

The measurement of the angular correlation of the annihilation radiation can be carried out using one-dimensional (1D) or two-dimensional (2D) geometry for the gamma-ray detectors. In the early days people used the 1D geometry involving two long NaI scintillator detectors placed parallel to each other (say in

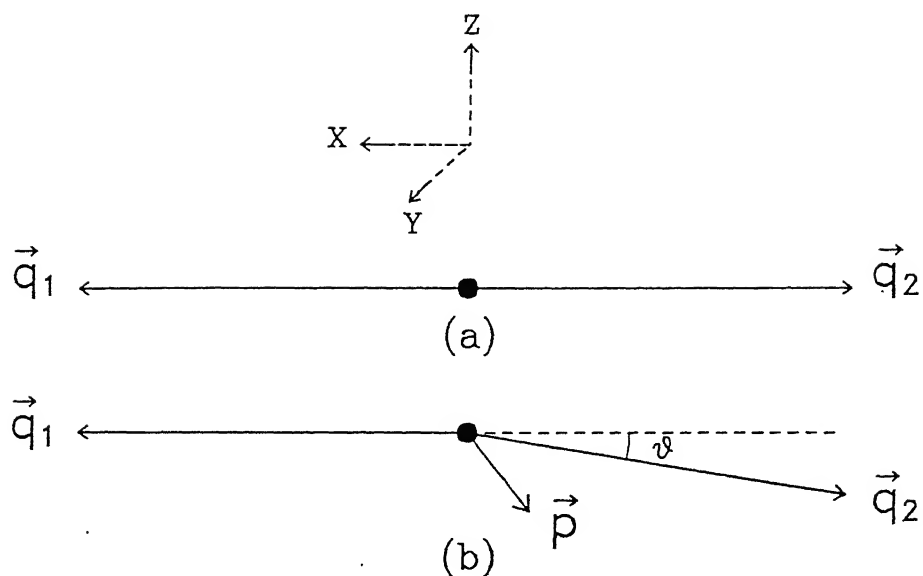


Fig. 2.4 Vector diagram of momentum conservation in the γ -annihilation process, (a) $\vec{p} = 0$, (b) $\vec{p} \neq 0$.

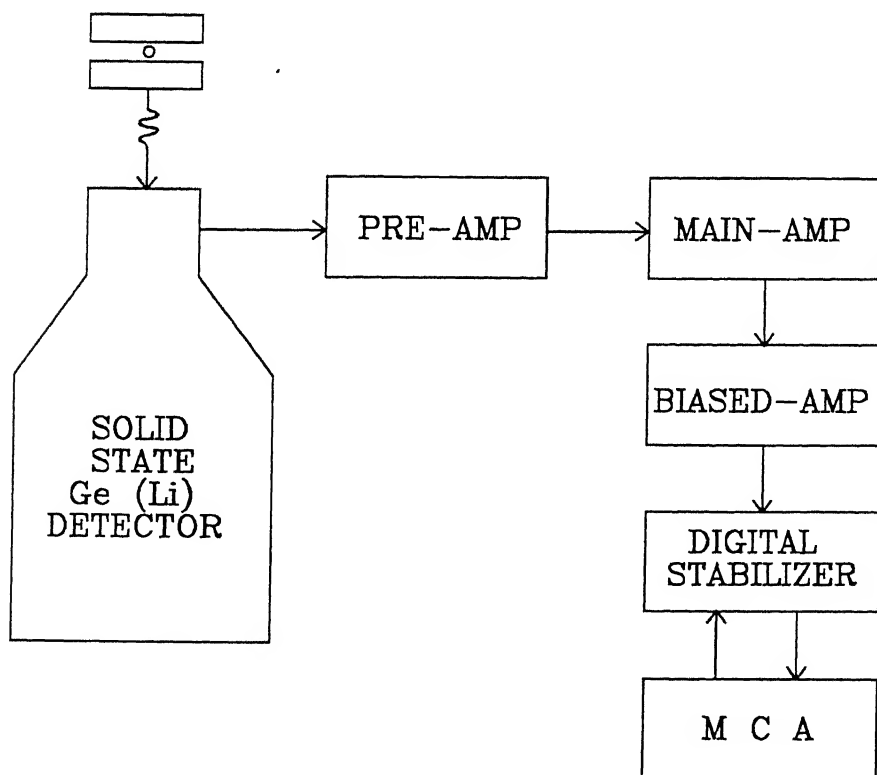


Fig. 2.5 Schematic diagram of a Doppler broadening measurement system.

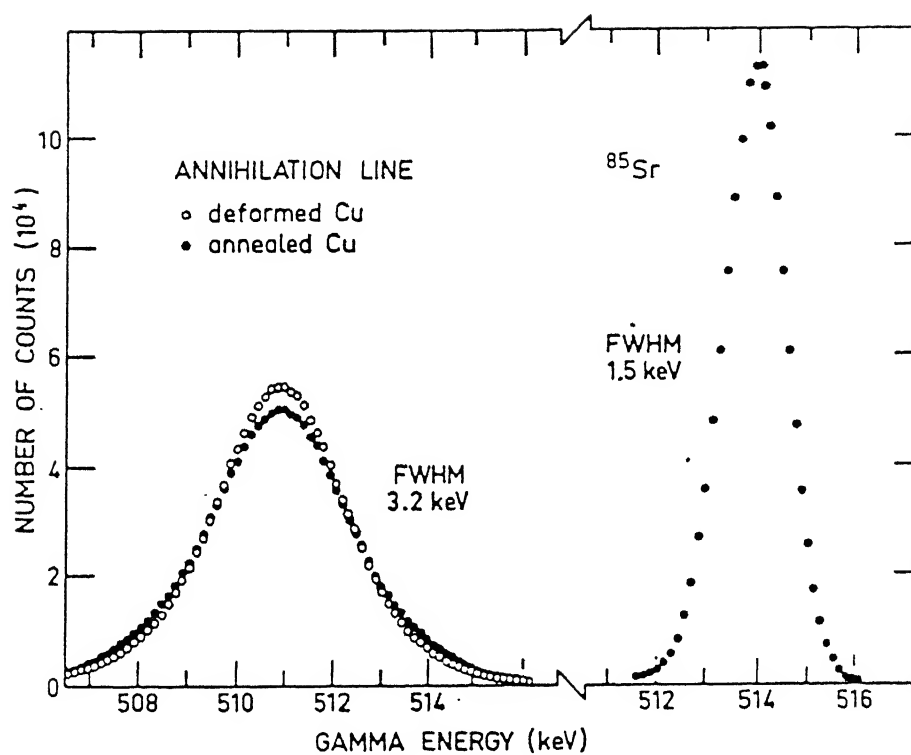


Fig. 2.6 Energy spectrum for Doppler broadened annihilation radiation compared with the intrinsic energy resolution of the spectrometer [taken from Ref. 17].

the y-direction) on either side of the source+sample assembly (Fig. 2.7). One of the detectors was held stationary while the other detector was moved to scan the z-direction. Lead collimators were placed in front of each detector to obtain high angular resolution. Kubica and Stewart [50] designed a 1D ACAR apparatus having a slit-width of 0.1 mrad with the equivalent momentum resolution of 0.0137 a.u. Most commonly used 1D ACAR instruments had momentum resolution in the range 0.05 - 0.15 a.u. The angular correlation measurement consisted in measuring the counting rate $N(\vartheta_z)$ between the two detectors as a function of ϑ_z . In such a measurements $\vartheta_z \rightarrow p_z$ and the momentum distribution of the two annihilation photons, $\rho_{2\gamma}(\vec{p})$, is integrated along the p_x and p_y directions. The measured 1D ACAR spectra is therefore expressed as a distribution

$$N(p_z) = \text{const.} \iint \rho_{2\gamma}(\vec{p}) dp_x dp_y \quad (2.3)$$

Considerable technological progress has been made during the last two decades to develop 2D ACAR spectrometers such that both the transverse components (p_y, p_z) of the momentum could be determined. These instruments involve a bank of point detectors, or multiwire proportional chambers or Anger cameras and their design and performance has been reviewed in the literature [16-18,51]. The 2D ACAR measurements yield the 2D distributions

$$N(p_y, p_z) = \text{const.} \int \rho_{2\gamma}(\vec{p}) dp_x \quad (2.4)$$

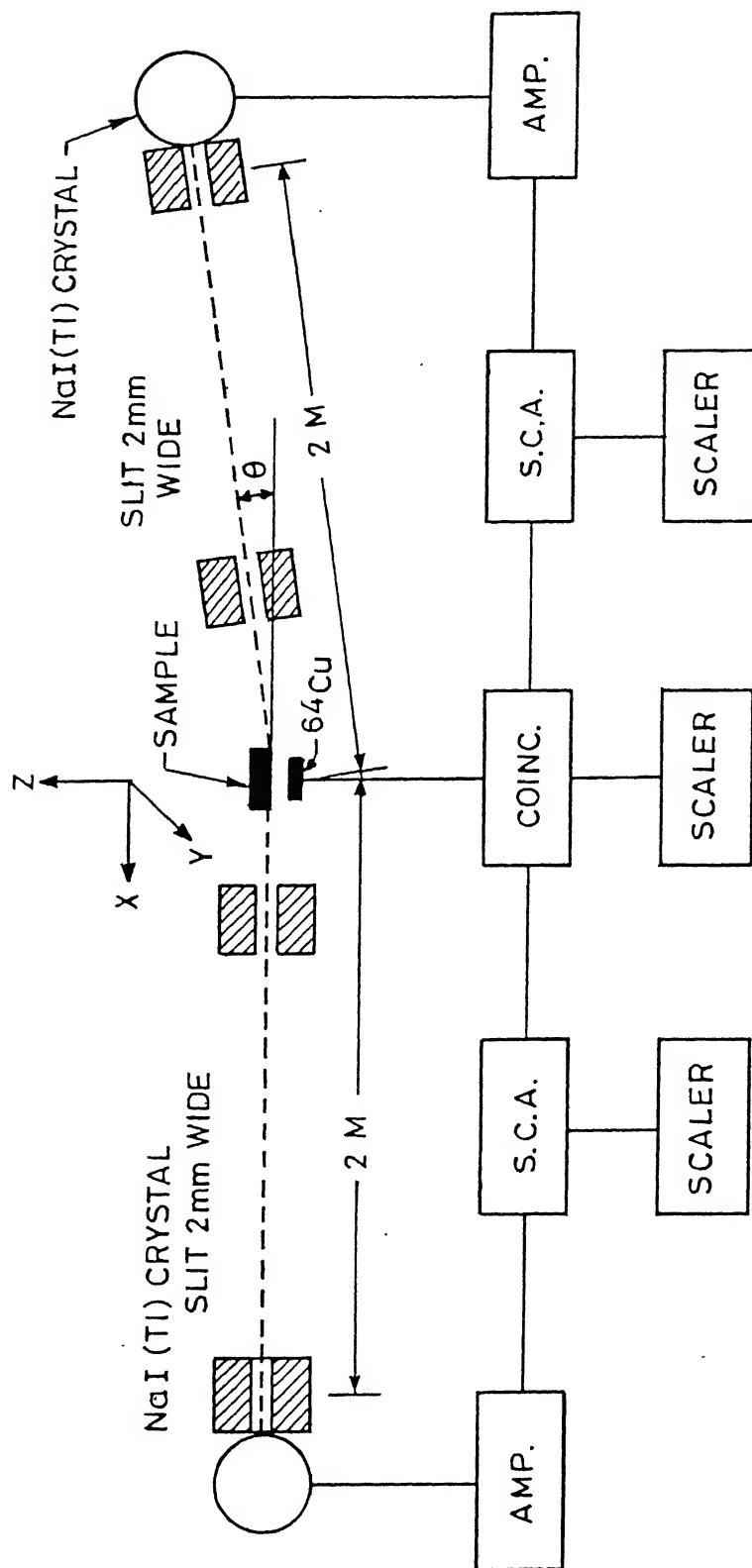


Fig. 2.7 Schematic diagram of the apparatus to study 1D angular correlation of annihilating radiation.

where

$$\frac{p_y}{mc} = \frac{Y_1}{L_1} + \frac{Y_2}{L_2} \quad (2.5)$$

$$\frac{p_z}{mc} = \frac{Z_1}{L_1} + \frac{Z_2}{L_2} \quad (2.6)$$

and where the coordinates and distances are explained in Fig. 2.8.

The measurement of 2D ACAR is more useful with metals and alloys for which valuable information about the Fermi surface and band structure is obtained from the 2D distributions [16-25,52,53].

2.4 Present positron lifetime spectrometer

The methods used in positron annihilation lifetime spectroscopy (PAL) have already been discussed in Section 2.2. In this section we shall briefly discuss the actual positron lifetime setup used in the present work along with the calibration, performance and the methods of data analysis performed by us.

2.4.1 Positron source

The radioisotope used as positron source in the present work was ^{22}Na in the form of aqueous solution ($^{22}\text{NaCl}$ from Amersham International, U.K.). A few drops of the aqueous solution containing ^{22}Na was deposited at the center of a very thin ($2.5\text{ }\mu\text{m}$ thick) nickel foil of the size $6\text{mm} \times 6\text{mm}$, and then folded in the middle and soldered at the edge so that the source was at the

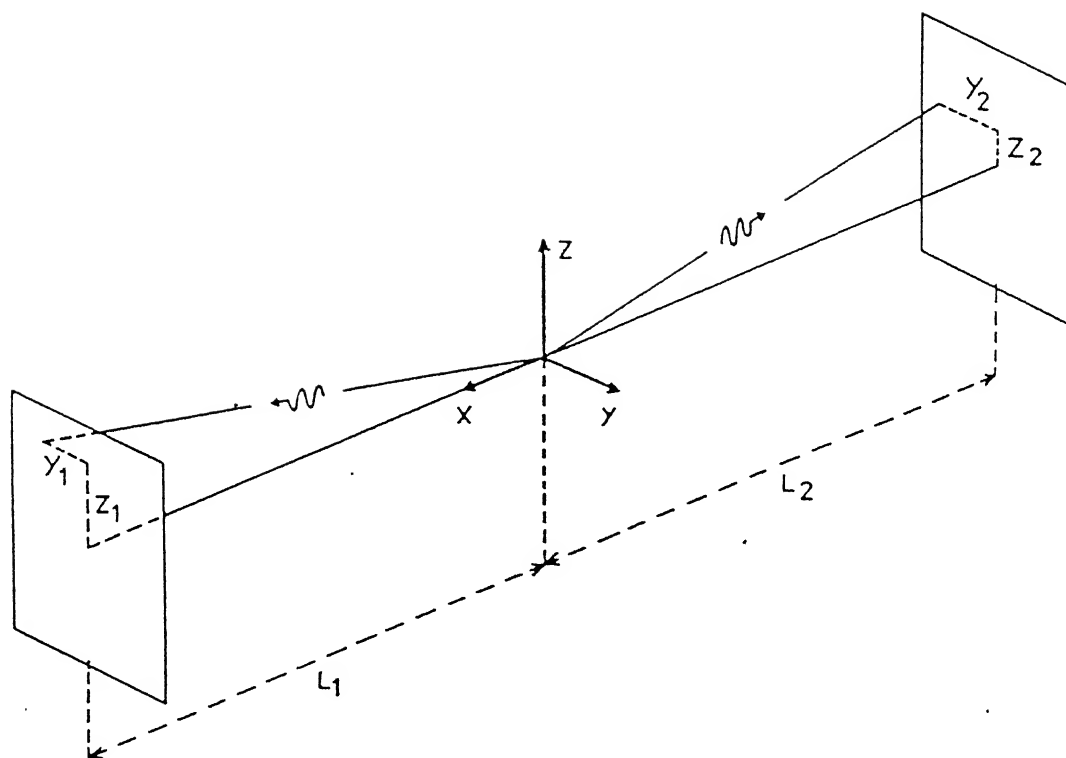


Fig. 2.8 General outline of the geometry of the 2D ACAR apparatus. Two sets of detectors lie on the (y_1, z_1) and (y_2, z_2) planes.

center of the folded foil. Several such sources were prepared, each with a strength of about 15 μCi . This source of positrons was then sandwiched between two identical specimens of the sample to be studied.

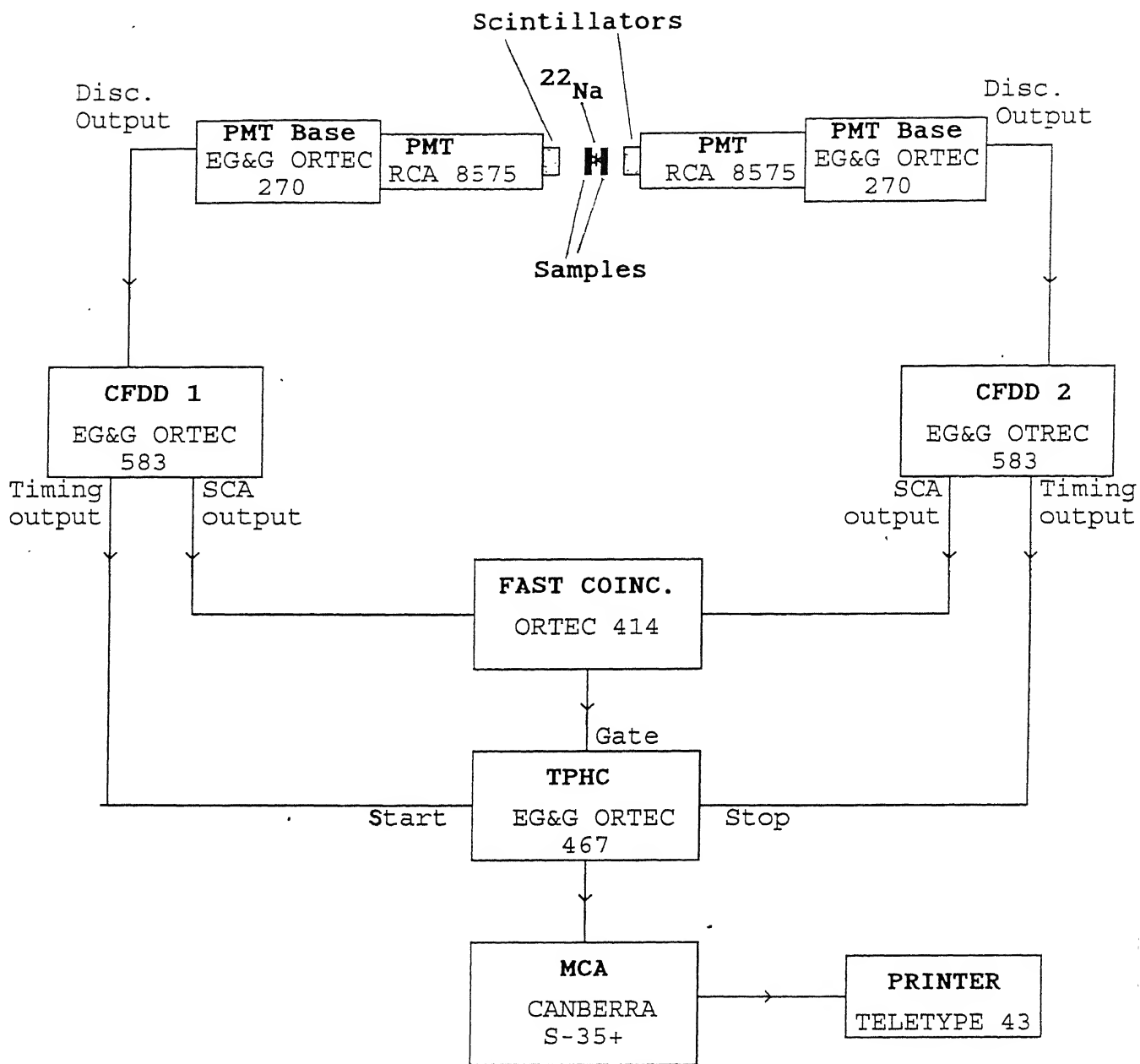
2.4.2 Present lifetime setup

A block diagram of the actual positron lifetime setup, based on fast-fast coincidence technique, used in the present work is given in Fig. 2.9. The source-sample assembly was kept between the two γ -ray detectors. The performance of such a system, its resolution and long term stability depends on the choice of scintillators, photomultipliers and the time derivation devices [31-32,41,47,54-57]. In this section we shall briefly describe the various important parts of our timing spectrometer.

(A) Scintillators and photomultipliers

Scintillators and photomultiplier tubes (PMTs) constitute the most vital parts of a timing spectrometer since the time resolution of such a spectrometer is directly related to the decay time of the scintillator, the number of photoelectrons produced as a result of the scintillations and the transit time of electrons in the PMT. For better time resolution, the scintillator should have a very fast decay time and a high efficiency for light output. Also the photomultiplier tube should have small transit time for the electrons and a short rise time of the anode pulses.

In our spectrometer, we have used cylindrical ultra-fast NE 111 plastic scintillators of size 1" (diameter) x 3/4" (thickness)



PMT ≡ Photomultiplier Tube

CFDD ≡ Constant Fraction Differential Discriminator

TPHC ≡ Time-to-Pulse Height Converter

MCA ≡ Multi-channel Analyzer

Fig. 2.9 Block diagram of the lifetime spectrometer, based on fast-fast coincidence technique, used in the present work.

with a decay time of ~ 1.2 ns and a pulse height of 40% that of anthracene. To improve the light collection efficiency, the scintillators were wrapped in teflon. These scintillators were then optically coupled to RCA-8575 PMTs using optical coupling grease from REXON Inc., USA. RCA-8575 is a 12 stage PMT (with bialkali photocathode), having a rise time of about 1.2 ns with a total gain of $\sim 3.6 \times 10^7$ and a transit time of 32 ns. The PMTs were fixed to a pair of EG&G Ortec 270 constant timing photomultiplier bases. The EG&G Ortec 270 base consists of a resistive voltage divider network with appropriate capacitive decoupling for the operation of the RCA 8575 PMTs. A constant fraction of pulse height trigger (CFPHT) [45,57] is also included in the base to provide the optimum time resolution and a dynamic range of 100:1 of the anode pulse height. EG&G Ortec 270 PMT base produces two outputs at the same time, the discriminator output and the monitor output. Discriminator output pulses are fast logic signals of width 6 ns and rise time < 2.5 ns. These are ideally suited for the timing purpose, and was therefore used by us for timing measurements. The monitor output can be used to monitor the anode signals. Magnetic shields were also put over the PMTs to reduce the effect of the external magnetic fields. Both the detectors were operated at -1850 volts, supplied by a EG&G Ortec 556 high voltage power supply.

(B) Time derivative device

Next important part of a timing apparatus is the time derivation device, used to derive the timing information from the

detector pulse. The detector pulse in general have long risetime ($t_r = 2.0$ ns) and they also vary in amplitude. Therefore these pulses must be processed by using a time derivative device to produce standard shape pulses of constant amplitude and fast rise-time for further analysis.

In the present setup, a pair of EG&G Ortec 583 constant fraction differential discriminators (CFDD) based on the principle of constant fraction (CF) timings [45,57], were used for precise time and energy information. In a CFDD, each input signal (discriminator outputs from PMT bases) is inverted and delayed, and at the same time a fraction (~ 0.2) of the undelayed pulse is added to the delayed pulse using a built-in CF timing circuit. As a result a bipolar signal is generated, whose zero-cross-over is used to trigger the timing output pulses (Fig. 2.10). Moreover, these units can be operated either in the integral mode or as a single channel analyser (SCA) in the differential mode. We have operated both the CFDDs in the differential mode, one to detect the 1.276 MeV photons (therefore acting as a start channel) and the other to detect the 0.511 MeV annihilation photons (thus acting as a stop channel). The window settings in the two discriminators were set to accept 50% of the Compton distribution corresponding to 1.276 MeV and 0.511 MeV γ -rays. Thus for each input signal satisfying the energy criteria, this unit generates two decoupled fast negative outputs (or the timing outputs) of about 5 ns in width and a slow positive pulse (or the SCA output).

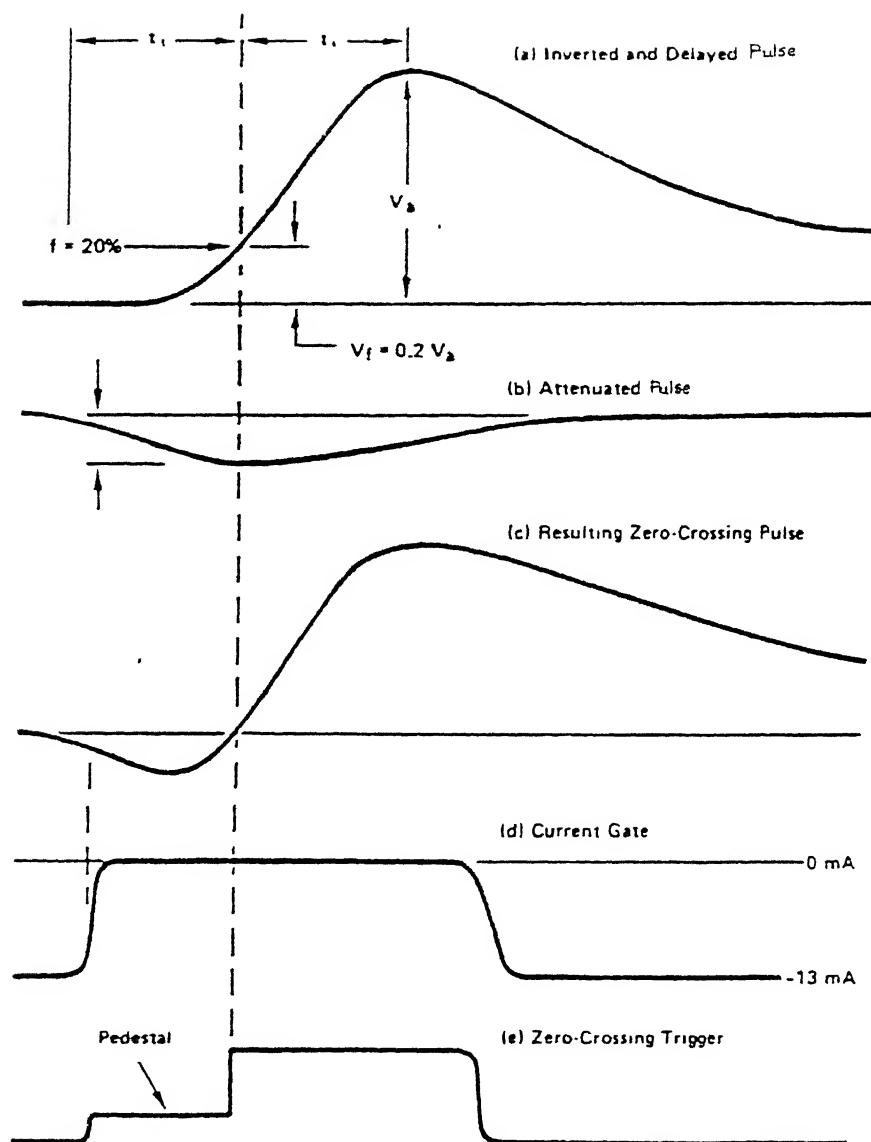


Fig. 2.10 Method of time pick-off used in a typical constant fraction timing unit [taken from Ref. 45].

(C) Time-to-pulse height conversion

The last part of the timing process is the conversion of the time interval between the timing pulses into a voltage amplitude pulse. This was done using a EG&G Ortec 467 TPHC/SCA unit, which measures the time interval between the leading edge of the timing output pulses from the two CFDDs furnished to its start and the stop inputs, to generate an analog output pulse whose height is proportional to the time difference between the start and the stop pulses. The pulses from the timing outputs of the two CFDDs were further shaped using long cables and 50 Ω terminators at the TPHC end for this purpose. The TPHC output was gated to a Fast Coincidence (ORTEC 414) circuit which uses the two SCA outputs from the CFDDs. The TPHC output was then fed to the ADC input of the multi-channel analyzer Canberra S-35 plus, to acquire the positron lifetime spectrum. Printouts of the spectral data were taken using a TELETYPE 43 serial port printer, which were then fed to the computer for further data analysis.

2.4.3 Resolution and performance of our positron lifetime spectrometer

Resolution of our positron lifetime spectrometer was determined by recording the 'prompt' spectrum arising from ^{60}Co gamma-rays. Radioactive isotope ^{60}Co emits two gamma rays (Fig. 2.11(a)) of energies 1.17 and 1.33 MeV with the intermediate state having a lifetime of 8×10^{-13} s. Since this lifetime is much less compared to the resolution of the spectrometer, the time distribution of these gamma-rays is known as the 'prompt' spectrum of ^{60}Co (Fig. 2.11(b)) having a shape which can be approximated to

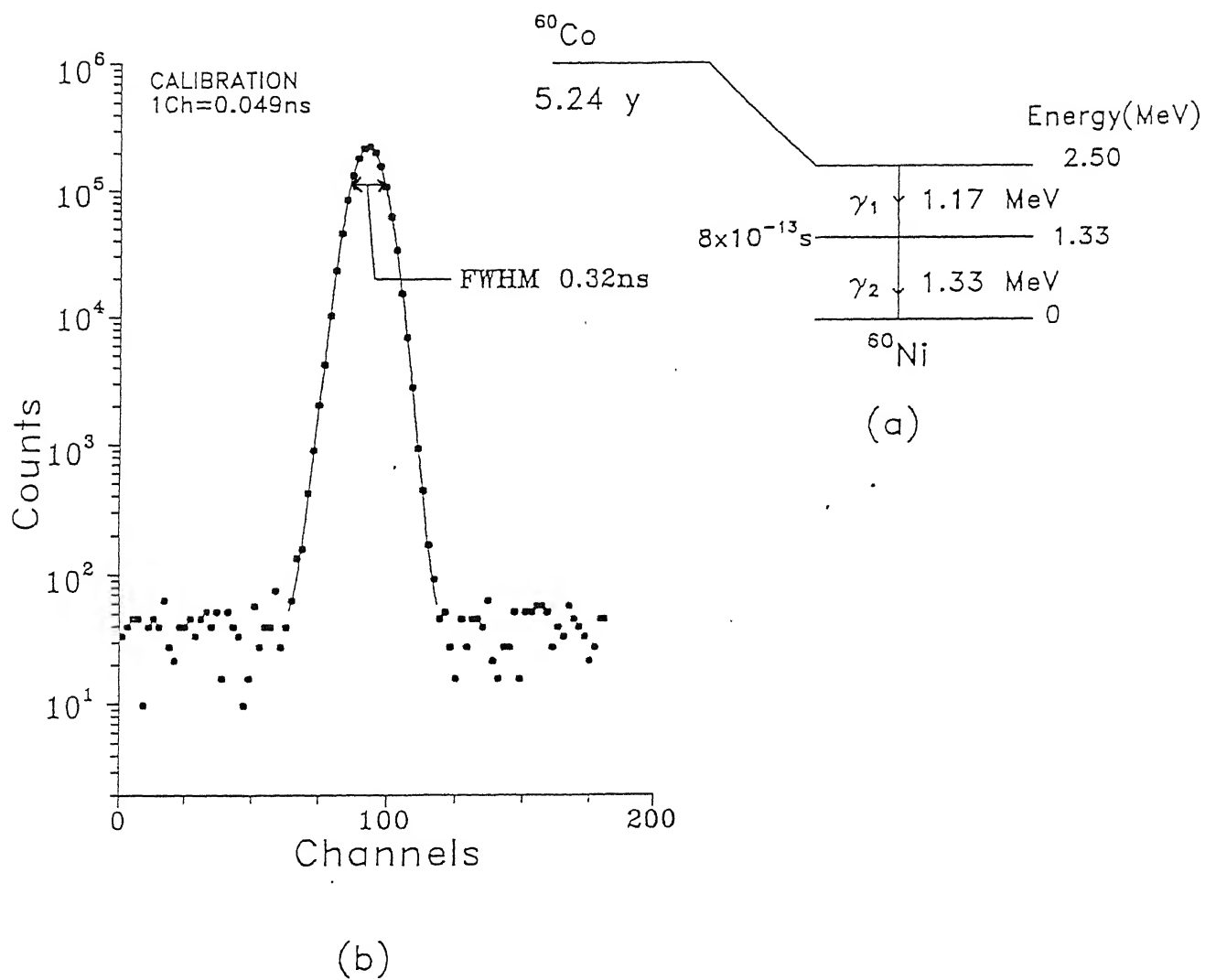


Fig. 2.11 (a) Decay scheme of ^{60}Co .
 (b) Prompt spectrum of ^{60}Co .

a gaussian. Time resolution of our spectrometer was, therefore, determined from the 'full width at half-maximum' (FWHM) of this prompt spectrum. During most of our work, this time resolution for our instrument was found to be 0.32 ns (FWHM) using the energy window setting for ^{22}Na . Such prompt spectra were taken by us regularly to monitor the stability of our spectrometer. The slope of the prompt spectrum gives the limiting lifetime resolution of the instrument.

The performance of our positron lifetime spectrometer was tested by comparing the observed lifetime parameters in different samples (e.g., in well-annealed and high-purity Ni, Cu, Al and Teflon) with that of the reported values in the literatures. Our results for the lifetime parameters were found to be in good agreement with the reported values for the different samples.

2.4.4 Calibration of the TPHC

The TPHC was calibrated by using a EG&G Ortec 462 time calibrator (TC). The TC generates logic signals at precise time intervals suitable to calibrate a TPHC. Each output from the TC consists of a pair of start and stop pulses which are fed to the start and the stop inputs of the TPHC. A time spectrum is then collected in a MCA using the TPHC output (with same settings used during actual lifetime measurements). This time spectrum consists of a series of sharp peaks at intervals equal to the time period chosen in the TC (Fig. 2.12(a)). Time calibration per channel was therefore calculated from the ratio of the time intervals between the various peaks and the corresponding difference between the

channel numbers of the peaks or from the slope of the curve given in Fig. 2.12(b). The average time calibration obtained in this way for our spectrometer was 48.78ps/channel, which was also verified by introducing variable nanosecond delays in the stop channel.

2.5. Analysis of positron annihilation lifetime spectra

As stated earlier, a positron annihilation lifetime (PAL) spectra is composed of a superposition of several decaying exponentials, which may be either finite (2 to 5) or may consist of a continuous distribution of decaying exponentials, depending on the nature of the sample. In most metals and ionic solids, the lifetime spectrum is relatively simple and consists of two or three lifetime components. The lifetime spectrum in most molecular materials is complex, where several positron states can exist. The measured positron lifetime spectra were, therefore, analysed by us using the following two different methods:

- (i) finite-term lifetime analysis and
- (ii) continuous lifetime analysis

Finite-term lifetime analysis were performed using the computer program PATFIT [37] consisting of the fitting programs, POSITRONFIT and RESOLUTIONFIT, along with two more programs, RESEDIT and POSEDIT, to generate control input data files for the fitting programs (Fig. 2.13). It also contains one graphics program, PATGRAPH, to generate graphics of the fitted spectra. The continuous lifetime analysis was performed by using the modified version [38] of the original computer program CONTIN [58]

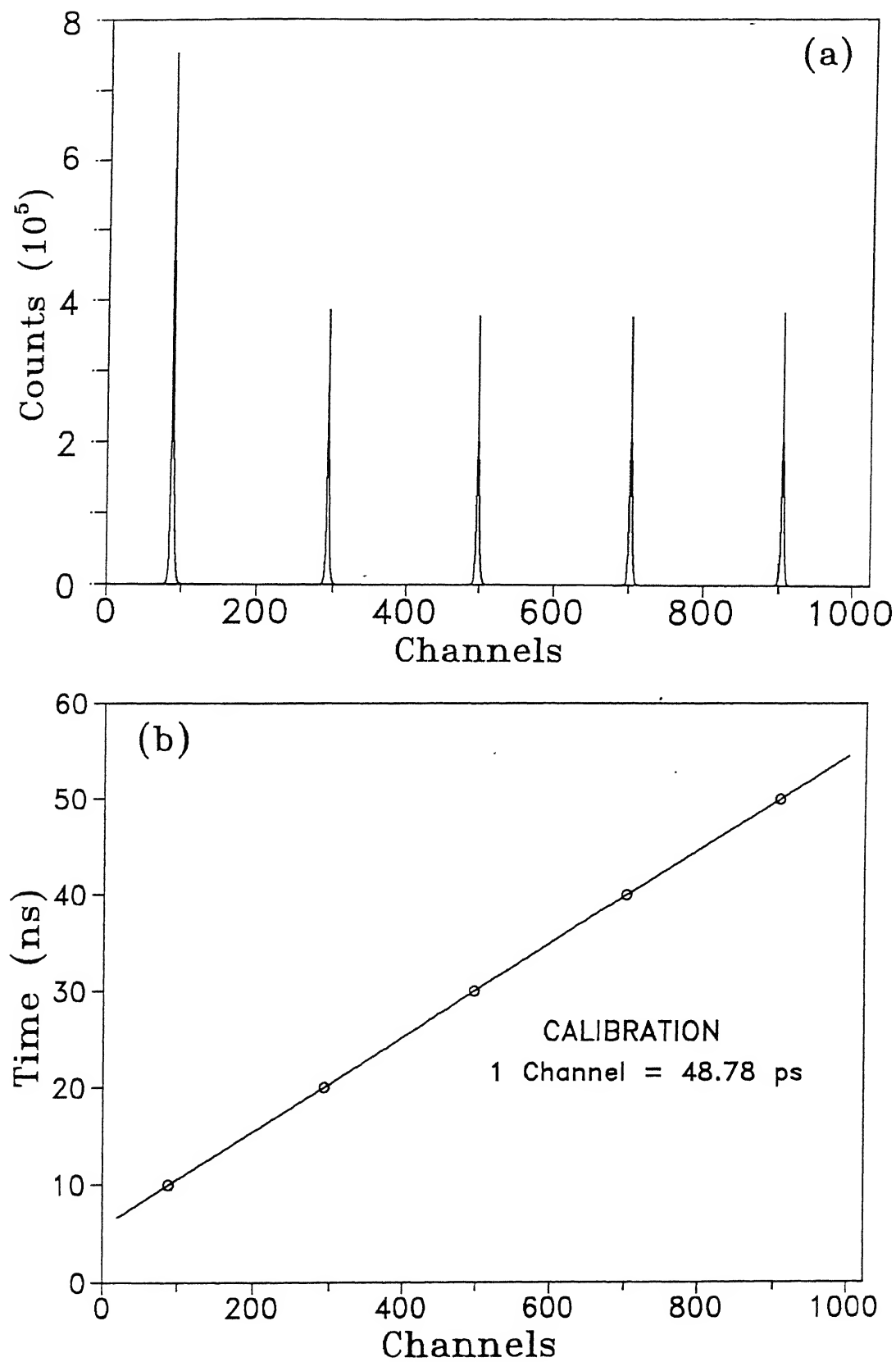


Fig. 2.12 (a) Time spectrum recorded using time calibrator.

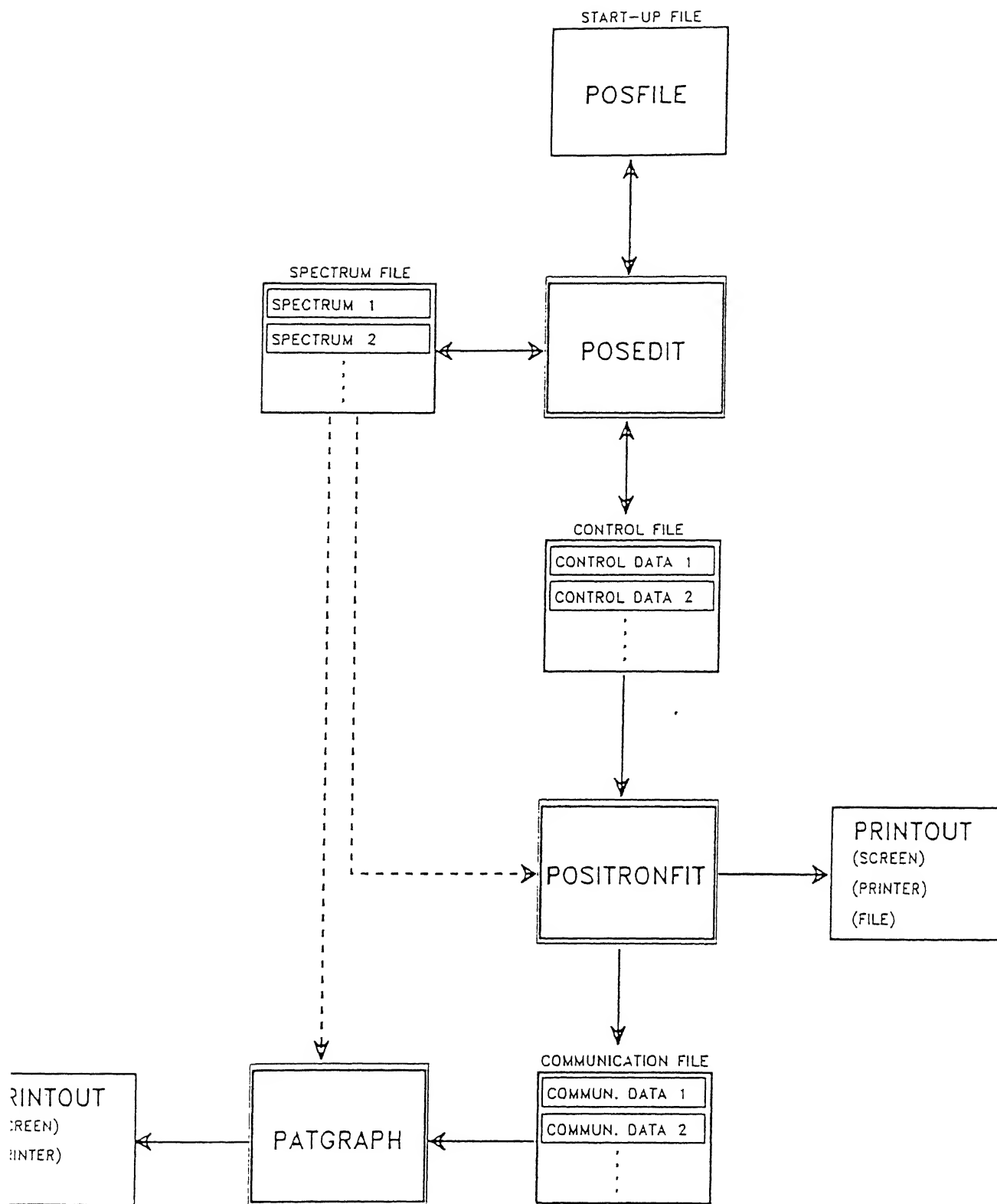


Fig. 2.13 Schematic representation of the interaction between programs, files and output devices, using POSITRONFIT as an example.

developed by Provencher. Both the methods of data analysis were done on a HP-9000 Series-800 main-frame computer.

2.5.1 Finite-term lifetime analysis

The finite-term lifetime analysis decomposes a PAL spectrum into a finite number (n) of lifetime components. However, due to the finite time resolution of the lifetime spectrometer, an experimental positron lifetime spectrum is always convoluted with the resolution function of the instrument. Therefore, a PAL spectrum is mathematically represented by a convoluted expression (denoted by $*$) of the instrumental resolution function and a superposition of a finite number (n) of negative exponentials expressed as

$$Y(t) = R(t) * (N_s \sum_{i=1}^n \alpha_i \lambda_i e^{-\lambda_i t} + B) \quad (2.7)$$

where $Y(t)$ is the experimental raw data, $R(t)$ is the instrumental resolution function, N_s is the total number of counts observed, λ_i and α_i are the annihilation rate (inverse of the lifetime τ) of the i th lifetime component and the fraction of positrons annihilating with natural lifetime τ_i respectively, and B is the background counts. The number of resolvable terms (n) is usually limited to 2-5 due to the unknown resolution function of the instrument, whose exact form is rather difficult to obtain. In practice the form of the resolution function is taken approximately as the linear combination of Gaussian type functions (GTF). The experimental raw data $Y(t)$ is then least-square fitted

to the above expression (eq. 2.7) with finite number of terms ($i=2-5$) to obtain the lifetimes $\tau_i (= \frac{1}{\lambda_i})$ and their corresponding intensities $\alpha_i \lambda_i$, for the best fitted curve.

The actual fitting of the raw experimental data were performed by using the computer program POSITRONFIT [37] to extract the lifetimes and their intensities. Since, the time resolution function measured by using the ^{60}Co prompt spectrum (already discussed in sec. 2.5.3) is quite different from the actual instrument resolution function when a lifetime spectrum is collected by using a ^{22}Na positron source, the actual form of the resolution function used in the present analysis was determined by least-square fitting the lifetime spectrum arising from a well-annealed and high purity (99.99+ %) nickel, having lifetime $\tau = 110\text{ns}$ (kept fixed during the fitting), using the computer program RESOLUTIONFIT [37]. The best fit (with $\chi^2 < 1.0$) corresponds to a linear combination of three gaussians for the resolution function (Table 2.1). The form of the resolution function thus obtained (Table 2.1) was subsequently used to find the positron lifetimes in our samples. Details about the mathematical treatment and the fitting procedures used by the computer programs POSITRONFIT and RESOLUTIONFIT can be found elsewhere [37,59].

In the polymers studied by us, we found that a 3-lifetime fit gave the best χ^2 (< 1.1) and most acceptable standard deviations. Measured lifetime spectra were corrected for the contribution arising from positron annihilation in the source. We have analysed all our spectra using this method of analysis. In some of the cases, we have also analysed our lifetime spectra in terms of

TABLE 2.1

Resolution function of the spectrometer used in the present work.

	Gaussian 1	Gaussian 2	Gaussian 3
FWHM (ns)	0.3189	0.2460	1.0639
Relative Intensities (%)	87.0	10.0	3.0
Shifts (ns)	0.000	-0.0521	0.6327

continuous lifetime distributions.

2.5.2. Continuous lifetime analysis

In molecular systems e.g. polymers, composites, porous media, and other such materials, the heterogeneity of the local molecular environment in which annihilation takes place is expected to generate distribution of lifetimes. Therefore, finite-term lifetime analysis of the PAL spectrum in polymers gives a value which is only an average effect of the actual lifetime distribution, arising from positron annihilating at free-volume holes which exist more in the form of a distribution. In such cases a continuous lifetime analysis can give us a more complete picture. The above expression (eq.2.7) should, therefore, be expressed in the continuous form instead of a discrete summation, as originally suggested by Schrader [60]

$$Y(t) = R(t) * (N_s(t) \int_0^{\infty} \alpha(\lambda) \lambda e^{-\lambda t} + B) \quad (2.8)$$

In the above expression, the annihilation decay integral function is simply a Laplace transform of the decay probability density function (PDF) $\lambda \cdot \alpha(\lambda)$. However, the exact mathematical solution to the above eq. (2.8), for $\alpha(\lambda)$ and λ , is difficult to obtain. This is more due to the convolution of the actual spectrum with the instrumental resolution function $R(t)$, whose exact form is somewhat difficult to get. However, an indirect method to get rid of this problem is to measure a reference spectrum $Y_r(t)$ for a sample, which has a single known positron annihilation rate (λ_r).

The reference spectrum $Y_r(t)$ can be expressed as

$$Y_r(t) = R(t) * N_r \lambda_r e^{-\lambda_r t} \quad (2.9)$$

where, N_r is the normalised total count for the reference spectrum, which can then be used to deconvolute the positron spectrum $Y(t)$. For this purpose, ultra-high purity, defect-free metals can be chosen as the reference sample. The data used for the reference must be measured under the same experimental configuration as kept during the actual sample measurements. The deconvolution procedure performed by a Laplace inversion technique is now available in the form of a computer code named CONTIN [58] for a numerical solution to the above integral (eq. 2.8), which was later modified by Gregory [38] for the analysis of PAL spectra.

We have, therefore, used the modified version of the computer program CONTIN [38], for analysis of some of the PAL spectra, to determine the annihilation rate probability distribution function $\lambda \cdot \alpha(\lambda)$ versus λ (annihilation rate). In the present analysis using this program, we have used the reference spectrum arising from well-annealed and high-purity (99.99+ %) nickel with annihilation rate $\lambda = 9.1 \text{ ns}^{-1}$. A total of 85 grid points over the range $0.25 \text{ ns}^{-1} < \lambda < 13 \text{ ns}^{-1}$ were used to obtain the lifetime distributions $\lambda^2 \cdot \alpha(\lambda)$ versus τ ($=1/\lambda$). The lifetime distributions were later used to determine the distribution functions for other physical parameters such as free-volume hole radius and volume distribution.

Analysis using CONTIN has to be done very carefully, because

temperature, pressure, electric and magnetic fields, etc. Measurements using Doppler broadening technique are also used to determine the nature of defects and defects concentration in metals. ACAR measurements are mostly done to determine the Fermi surface and energy band structures in metals and alloys. DBARL and ACAR measurements in polymeric and molecular substances are relatively few. In the last part of this chapter, we have briefly outlined the positron lifetime setup and the methods of analysis of the PAL spectra used by us in the present work.

References

1. M. Deutsch, Prog. Nucl. Phys. 3, 131 (1953).
2. S. De Benedetti and H.C. Corben, Ann. Rev. Nucl. Sci. 4, 191 (1954).
3. S. Berko and F.L. Hereford, Rev. Mod. Phys. 28, 299 (1956).
4. R.A. Ferrell, Rev. Mod. Phys. 28, 308 (1956).
5. P.R. Wallace, Adv. Solid State Phys. 10, 1 (1960).
6. J.H. Green and J. Lee, "Positronium Chemistry" (Academic Press, Inc., New York-London, 1964).
7. V.I. Goldanskii, At. Energy Rev. 6, 3 (1968).
8. B.G. Hogg and G.M. Laidlaw, At. Energy Rev. 6, 149 (1968).
9. P. A. Fraser, Adv. At. Mol. Phys. 4, 63 (1968).
10. J.A. Merrigan, J.H. Green, and S.J. Tao, "Physical Methods of Chemistry" edited by A. Weissberger and B.W. Rossiter (John Wiley, New York, 1972), Vol. I, Part III D.
11. A.E. Hamielec, M. Eldrup, O. Mogensen, and P. Jansen, J. Macromol. Sci. Rev. Macromol. Chem. C9, 305 (1973).
12. R.N. West, Adv. Phys. 22, 263 (1973).
13. I.Ya. Dekhtyar, Phys. Lett. 9C, 243 (1974).
14. R.M. Singru, Phys. Status Solidi A 30, 11 (1975).
15. "Positronium and Muonium Chemistry", edited by H.J. Ache, (Advances in Chemistry Series 175, American Chemical Society, Washington D.C., 1979).
16. S. Berko in "Compton Scattering", edited by B. Williams (McGraw-Hill Book Co., London, 1977), p. 273.
17. "Positrons in Solids", edited by P. Hautojarvi (Springer-Verlag,

Berlin, 1979).

18. "Positron Solid State Physics", edited by W. Brandt and A. Dupasquier (North-Holland Publishing Co., Amsterdam, 1983).
19. "Positron annihilation", edited by A.T. Stewart and L.O.Roellig (Academic Press, New York, 1967).
20. "Positron Annihilation", edited by R.R.Hasiguti and K. Fujiwara (Japan Institute of Metals, Sendai, 1979).
21. "Positron Annihilation", edited by P.G.Coleman, S.C.Sharma and L.M.Diana (North-Holland, Amsterdam, 1982).
22. "Positron Annihilation", edited by P.C.Jain, R.M.Singru and K.P.Gopinathan (World Scientific, Singapore, 1985).
23. "Positron Annihilation", edited by L. Dorikens-Vanpraet, M. Dorikens and D. Segers (World Scientific, Singapore, 1989).
24. "Positron Annihilation", edited by Zs. Kajcsos and Cs. Szeles, Materials Science Forum, 105-110, Parts 1,2 and 3 (1992).
25. "Positron Annihilation", edited by Yuan-Jin He, Bi-song Cao and Y.C.Jean, Materials Science Forum, 175-178 Parts 1 and 2 (1992).
26. "Positron Annihilation Studies of Fluids", edited by S.C. Sharma (World Scientific, Singapore, 1988).
27. "Positron and Positronium Chemistry", edited by Y.C. Jean (World Scientific, Singapore, 1990).
28. M. Deutsch, Phys. Rev., 82, 455 (1951).
29. S. DeBenedetti and H.J. Richings, Phys Rev. 90, 644 (1953).
30. R.E.Bell and R.L.Graham, Phys. Rev. 90, 644 (1953).
31. R.E. Bell, in "Alpha, Beta and Gamma Ray Spectroscopy", edited by K. Siegbahn (North-Holland, Amsterdam, 1965) 2, 905.

32. A. Schwarzschild, Nucl. Instrum. Methods. 21, 1 (1963).
33. A. Ogata, S.J. Tao and J.H. Green, Nucl. Instrum. Methods 92, 403 (1971).
34. R.D. Carton and S.J. Wadden, Nucl. Instrum. Methods
35. N.P. Valuev and A.N. Zikharev, Inst. Exp. Teck. 29, 1 (1986).
36. P. Kirkegaard and M. Eldrup, Comput. Phys. Commun. 7, 401 (1974).
37. P. Kirkegaard, M Eldrup, O.E. Mogensen and N.J. Pedersen, Comput. Phys. Commun. 23, 307 (1981) ; PATFIT package, Riso National Laboratory, Roskilde, Denmark (1989).
38. R.B.Gregory and Y.Zhu, Nucl. Instrum. Methods A 290, 172 (1990); R.B.Gregory, Nucl. Instrum. Methods A 302, 496 (1991).
39. A. Shukla, M. Peter and L. Hoffmann, Nucl. Instrum. Methods A 335, 310 (1993); L. Hoffmann, A. Shukla, M. Peter, B. Barbiellini and A.A. Manuel, *ibid* A 335, 276 (1993).
40. H. Sormann, P. Kindl and W. Puff, Nucl. Instrum. Methods 206, 203 (1983).
41. J.De Vries and F.E.T. Kelling, Nucl. Instrum. Methods A 262, 385 (1987).
42. J.H. Green and R.E. Bell, Nucl. Instrum. 3, 127 (1958).
43. G.C.Neilson and D.B. James, Rev. Sci. Inst. 26, 1018 (1955).
44. C.W. Williams, Private communication, ORTEC, Oak Ridge, Tennessee (1967).
45. D.A. Gedcke and W.J. McDonald, Nucl. Instrum. Methods 58, 253 (1968).
46. G. Present et al., Nucl. Instrum. Methods 31, 71 (1964).
47. A. Schwarzschild and K.E.Warburton, Ann. Rev. Nuc. Sci, 18,

265 (1968).

48. K. Rytsola, in [21], p. 886.
49. I. K. MacKenzie, in [18], p. 196.
50. P. Kubica and A.T. Stewart, Phys. Rev. Lett. 34, 852 (1975).
51. R.N. West, J. Mayers and P.A. Walters, J. Phys. E14, 478 (1981).
52. R.M. Singru in "Positron Annihilation and Compton Scattering",
edited by B.K.Sharma, P.C. Jain and R.M. Singru (Omega
Scientific Publishers, New Delhi, 1990), p. 1.
53. R.M. Singru, Mater. Science Forum 175-178, 843 (1995).
54. J. De Vries, A. Zeeca, R.S. Brusa, R.G. Grisenti, S. Oss and
A. Van Veen, in [23], p. 654.
55. D.A. Gedcke and C.W. Williams, Ortec News, Aug. 1968.
56. W. Meiling and F. Stary, "Nanosecond Pulse Technique (Gordon
and Breach, New York, 1968).
57. D.A. Gedcke and W.J. McDonald, Nucl. Instrum. Methods 55, 377
(1967).
58. S.W. Provencher, Comput. Phys. Commun. 27, 213 (1982);
S.W. Provencher, ibid 229.
59. P. Kirkegaard and M. Eldrup, Comput. Phys. Commun. 3, 240
(1972); P. Kirkegaard and M. Eldrup, Comput. Phys. Commun. 7,
401 (1974).
60. D.M. Schrader, in [21], p. 912.
61. Y.C. Jean and G.H. Dai, Nucl. Instrum. Methods B79, 356 (1993).
62. J.D. McGervey, Zhibin Yu, A.M. Jamieson and R. Simha, in [25],
p. 727.

CHAPTER 3

POLYMER ELECTROLYTES - A REVIEW

3.1 Introduction

In the past few decades a large number of solids with high ionic conductivity have been developed. These solids are termed as solid electrolytes or fast-ion conductors, or more commonly as superionic solids [1,2]. Ionic conductivity (σ) in such solid electrolytes is far higher than that of a typical ionic solid such as NaCl which has $\sigma = 10^{-18} \text{ S.cm}^{-1}$. The conductivity of solid electrolytes lies within a range ($10^{-6} \leq \sigma \leq 10^{-1} \text{ S.cm}^{-1}$) which are of the same order of magnitude as those of liquid electrolytes [3]. Technologically, solid electrolytes are gaining more importance because of their potential applications in modern electrochemical devices (Fig. 3.1) such as high-energy-density batteries, gas sensors, electrochromic display devices etc. [4-6]. Solid electrolytes cover a wide range of materials including refractory covalent solids such as β -alumina, soft ionic crystals like AgI, glasses and more recently developed species, the polymer electrolytes.

Some of the basic characteristics of the solid electrolytes are

- (i) crystal binding is generally ionic in nature ,
- (ii) electrical conductivity is high (10^{-1} - $10^{-5} \text{ S.cm}^{-1}$) with a low activation energy,
- (iii) principal charge carriers are ions i.e. the ionic

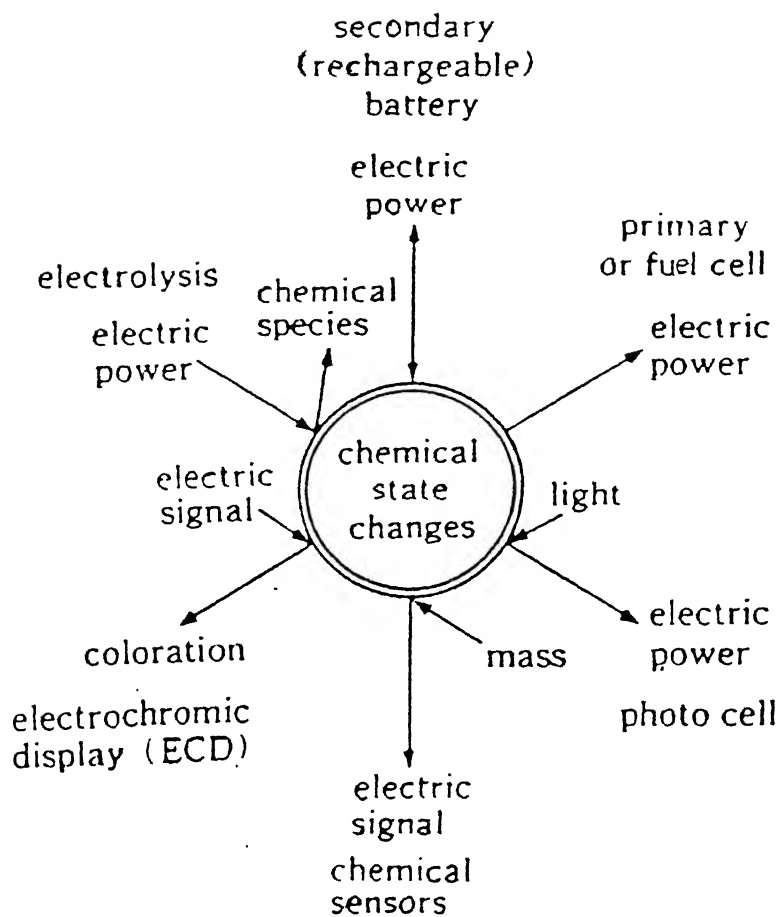


Fig. 3.1 Electrochemical devices based on solid electrolytes [taken from Ref. 4].

transference number is almost equal to one ($t_{\text{ions}} \approx 1$) and the electronic transference number is less than 10^{-4} , and

(v) the lattice contains large number of vacant sites for ions to hop from one site to another.

In the past two decades, various new materials have been identified as potential solid electrolytes specially for high-energy-density batteries. This is an important development, as the existing batteries mostly employ aqueous electrolytes and they suffer from various inherent disadvantages such as - limited shelf-life, low specific energy density, and limited temperature range of operation etc. The electrolytes based on solid state not only eliminate a container otherwise required for liquid electrolytes but also make handling convenient. These electrolytes also have high-energy and power-carrying capacity. The solid electrolytes can, in fact, be practical substitutes for aqueous electrolytes and this was first demonstrated by Takahashi and Yamamoto [7] using Ag_3SI i.e. $[\text{Ag}:\text{Ag}_3\text{SI}; \text{I}_2, \text{C}]$.

On the basis of the microstructure and the physical properties, solid electrolyte materials are broadly classified into four categories,

- (a) crystalline framework materials,
- (b) dispersed phase composite materials,
- (c) ion-conducting glasses, and
- (d) polymer electrolytes

In the following subsections, a brief overview of the first three groups of materials used as solid electrolytes are given. The subject of polymer electrolytes, being the subject matter

covering the major part of the present thesis, is reviewed in greater detail.

3.1.1 Framework crystalline materials

Superionic solids developed in the earlier years belong to this group of materials. They generally consist of mobile ions in a rigid crystalline framework. These materials are further sub-divided into the following two subgroups.

(a) Soft framework crystals

(b) Hard framework crystals

Soft framework crystals are characterized by ionic bonding, heavy polarizable ions, low Debye temperature and a sharp order-disorder transition. Some of the soft framework crystals are AgI, CuI, Ag_2HgI_2 etc. Among these, extraordinary high ionic conductivity is found in α -AgI [3,8], which was the first "superionic conductor" to be discovered.

The hard framework crystalline materials have predominantly covalent bonding, low polarizability of mobile ions, high Debye temperature and generally less sharp order-disorder phase transition. NASICONs, or Na super ionic conductors, $(\text{Na}_{1+x}\text{Zr}_2(\text{SiO}_2)_x(\text{PO}_4)_{3-x})$ for $0 \leq x \leq 3$ [9,10] and β -alumina (ideally, $(\text{Na}_2\text{O})_2 \cdot 11\text{Al}_2\text{O}_3$) [11] are two important hard framework crystals with high Na^+ ion conduction. At present, sodium sulfur batteries using this kind of solid electrolytes are being developed all over the world. Framework crystalline materials also consist of a large number of proton-conducting solids [12-15]. Some of the common framework crystalline materials are given in

Table 3.1.

3.1.2 Composite or dispersed phase solid electrolytes

The composite electrolytes are obtained by mixing different ionic conductors with fine particles of Al_2O_3 , SiO_2 , Fe_2O_3 etc. Liang [16] was the first to observe a remarkable enhancement in the conductivity (10^2 - 10^3 times) of Li^+ in $\text{LiI-Al}_2\text{O}_3$ systems. Since then a lot of work has been done in this field [17-20]. Some of the common composite solid electrolytes are given in Table 3.1.

3.1.3 Ion-conducting glasses

Usually the ionic conductivity in glasses is low (about 10^{-7} $(\Omega \text{ cm})^{-1}$) at room temperature, which is not suitable for majority of applications as electrolytes. Kunze [21] was the first to find the high ionic conductivity in glasses. Since then a number of ions like Li^+ , Na^+ , Ag^+ , Cu^+ , F^- etc. are found to have high values of conductivities in the glassy materials [22,23]. These highly conducting glasses are known as 'ion-conducting glasses' or 'superionic glasses' and they are technologically important materials for manufacturing devices. Unlike crystalline materials and ceramics, they do not suffer from problems of grain boundaries and therefore have ionic conductivity which is isotropic. They are also easy to fabricate (with wide range of chemical compositions) into different shapes and sizes and in the form of thin films with uniform properties and good electrode-electrolyte contacts in batteries and other electrochemical devices.

Superionic glasses ($\text{A}_x\text{O}_y\text{-M}_2\text{O-MX}$) are mostly prepared by either slow cooling or moderate to rapid quenching of a molten

mixture of a glass-former (A_xO_y), e.g. B_2O_3 , P_2O_5 , SiO_2 , MoO_3 , GeO_3 etc., a metal oxide (M_2O) as glass network modifier and a dopant salt (MX) (usually a metal halide). They are also prepared by laser glazing, sol-gel method and by condensation from the gas phase. Some of the important ion-conducting glasses are listed in Table 3.1.

3.2 Polymer electrolytes

3.2.1 Introduction

The polymer electrolytes are the materials of current interest because along with their high ionic conductivity they possess unique physical and chemical properties [24] viz. chemical stability, thin film-forming properties, good processability, flexibility, light weight, elasticity (plasticity) and transparency with a wide potential window in the solid state. As a result the polymer electrolytes can be fabricated into thin films of desirable shapes and sizes with excellent electrode-electrolyte contacts in different electrochemical devices. Moreover their ability to accommodate volume changes minimizes the problems generally associated with all solid-state secondary batteries arising from deformation and deterioration of the interfaces during charge/discharge cycles. Also polymer electrolytes based on simple polyethers have a wide electrochemical stability. Some of these properties cannot be attained by hard organic solid electrolytes and thus have been exploited to bridge a gap between fluid electrolyte solutions and hard inorganic solid electrolytes. All these favourable aspects have led to extensive research and

TABLE 3.1

SOLID ELECTROLYTE MATERIALS

(References given in the last column are shown separately at the end of this chapter).

Type of Electrolyte	Max. σ ($\Omega^{-1}\text{cm}^{-1}$)	Temp. (K)	Referenc
Soft framework crystalline material			
α -AgI	1.31	≥ 419	[1]
β -AgI	10^{-4}	≤ 419	[1]
RbAg_4I_5	0.27	300	[2]
Ag_3SBr	2×10^{-3}	300	[3]
$\text{P}_{\text{y}}\text{Ag}_5\text{I}_6$	0.77	300	[4]
α -CuHgI ₄			[5]
Hard framework crystalline materials			
$\text{Na}_{1+x}\text{Zr}_2\text{P}_{3-x}\text{Si}_x\text{O}_{12}$ (x=2.0)	200×10^{-1}	300	[6]
NASICON - doped with Mg^{2+} , V^{5+} , Nb^{5+} and Ta^{5+}	1.1-1.6 $\times 10^{-1}$	300	[7]
$\text{Na}_{2.8}\text{Zr}_{1.7}\text{Nd}_{0.3}\text{P}_{1.5}\text{O}_{12}$	1.9×10^{-4}	300	[8]
$\text{Na}_3\text{Sc}_2\text{P}_3\text{O}_{12}$	2.7×10^{-4}	300	[9]
$\text{Li}_2\text{M}_2(\text{PO}_4)_3$	2.5×10^{-2}		[10]
Na- β -Alumina	10^{-3} - 10^{-2}		[11]
Proton conducting crystal- line framework materials			
$\text{H}_2\text{UO}_2\text{PO}_4 \cdot 4\text{H}_2\text{O}$ (HUP)	4×10^{-6}	300	[12]
$\text{H}_2\text{UO}_3\text{AsO}_4 \cdot 4\text{H}_2\text{O}$ (HUAs)	6×10^{-3}	300	[12]
$\text{NH}_4^+ / \text{H}_3\text{O}^+$ - β -Alumina			
H^+ - Montmorillonite clay	1.4×10^{-4}	300	[13]
NAFION (Hydrated)	$\sim 10^{-2}$	300	[14]
$\text{N}_2\text{H}_6\text{SO}_4$	10^{-4}	473	[15]
$\text{Nb}_2\text{O}_5 \cdot 3.20\text{H}_2\text{O}$	1×10^{-4}	-	[16]
$\text{Ta}_2\text{O}_5 \cdot 3.9\text{H}_2\text{O}$	3×10^{-4}	-	[16]

(Continued on the next page)

TABLE 3.1 - Continued

Composite or dispersed solid electrolyte			
LiI + Al ₂ O ₃ (40 mol%)	100	300	[17]
AgI + Al ₂ O ₃ (0.06μ, 10mol%)	50	300	[18]
AgI + SiO ₂ (0.007μ, 10mol%)	45	300	[18]
AgCl+Al ₂ O ₃ (fibers, 3.0μ, 4vol%)	15 - 200nS/cm	300	[19]
SrCl ₂ + Al ₂ O ₃ (2.6μ, 30%)	5x10 ⁻⁴	773	[20]
Ionically conducting Glasses			
75AgI.25Ag ₂ SO ₄	6x10 ⁻²	293	[21]
50Na ₂ S.50SiS ₂	1x10 ⁻⁷	293	[21]
M ₂ O:B ₂ O ₃ :P ₂ O ₅ (M = Li, Ag)			[22]
50AgBr.25Ag 0.25B O	2.7x10 ⁻³	298	[23]
LiW ₂ O ₇	1.17x10 ⁻⁵	333	[24]
Li ₂ Mo ₂ O ₇	1.0x10 ⁻⁵	333	[24]

development in the field of polymer electrolytes.

Both electronically conducting polymers and polymeric electrolytes have been prepared and studied in a large number of laboratories. The dominant class of polymer electrolytes comprises of neutral polar polymers complexed with alkali metals (i.e. Li^+ , Na^+ , etc) /divalents/transition metals (i.e. Pb^{2+} , Zn^{2+} , Ni^{2+} , Co^{2+} , Hg^{2+} etc)/ ammonium salts and ions. Some acids also form complexes with some polymers to give a good electrolyte.

Although it was recognised in the mid-1960's that potassium salts form complexes with polyethylene oxide (PEO) [25] and polypropylene oxide (PPO) [26], it was only in the seventies that these materials (i.e. polymer-salt complexes) were found to exhibit appreciable ionic conductivity [27,28]. The technological importance of these polymer electrolytes was first pointed out by Armand [29]. Since then, the subject of polymer electrolytes is hotly pursued. There are some good review articles [24,30-34] on polymer electrolytes. Since the early studies on PEO, a wide variety of PEO- and PPO- based salt complexes have been prepared and characterized [31,35-40]. Some of the well-known solvating polymers include polyethylene oxide (PEO) [25], polyethylene succinate (PESc) [41], polyethylene imine (PEI) [42], polyethylene sulphide [35], polyethylene adipate [43], poly(β -propiolactone) [44], polyphosphazenes [45] etc. which can form complexes with different alkali-metal salts, silver and copper salts, ammonium salts, acids etc. to form polymer electrolytes. Addition of high-dielectric and low-viscosity solvents [46] to these complexes increase their conductivity. Recently solvent-free polymer-salt

complexes were also prepared with optimized conductivity and mechanical properties [47-49].

The polymer electrolyte materials are broadly classified as

[a] solvent-swollen polymers,

[b] polyelectrolytes and

[c] solvent-free polymer-salt complexes.

and their brief description is given below.

3.2.2 Solvent-swollen polymers

Addition of some solvent (aqueous /non-aqueous) to the basic polymer (e.g. poly-vinyl alcohol (PVA) or poly-vinyl pyrrolidone (PVP)) usually swell the basic polymer host. As a result the dopant ionic solute like H_3PO_4 are accommodated in the swollen lattice which permit the ionic motion in the solvent swollen region of the polymer host. These materials are in general unstable and their conductivity depends on the type and concentration of the solvent in the swollen region of the polymer and on other ambient conditions like temperature, relative humidity and the history of the sample pre-treatment.

3.2.3 Polyelectrolytes

A completely different type of conducting matrix is formed by the dissolution of an ionic polymer in an aqueous medium to give a 'polyelectrolyte'. Polyelectrolytes have self ion-generating groups (or ion-centers) responsible for ionic conductivity, attached with the main chain of the polymer [50]. These

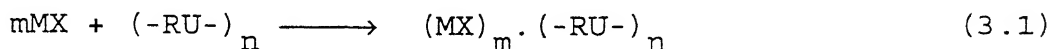
ion-centers may be either positively or negatively charged, giving rise to 'polyacids' (e.g. poly(acrylic acid), poly(vinylsulphonic acid), etc.) and 'polybases' (e.g. poly(vinyl-trimethylammonium chloride), poly(*N*-methylvinylpyridium chloride) etc.). Polymers which contain both acidic and basic groups on the same chain are termed as 'polyampholytes'. In general, small counterions such as H^+ , Na^+ , OH^- , or Cl^- are associated with the ionic centers to maintain electroneutrality.

The ionic conductivity in polyelectrolytes is a function of the water content and increases dramatically on exposure to moisture, which make these materials ideal for humidity sensors [51]. Two important polyelectrolytes include polystyrene sulphonate (used as ion exchange resin) and perfluorinated Nafion (used as membrane for brine electrolysis and in devices like fuel cells). Systems with water as solvent and poly(vinyl alcohol) (PVA) as the host matrix are used as battery separator [52] and hydrogen sensors [53]. In spite of this, polyelectrolytes so far have not been seriously considered as ion conductors.

3.2.4 Solvent-free polymer-salt complexes

These are the most common and extensively studied materials. They are prepared, in general, in the form of thin films, by solution-cast technique in which the solution of polymers (common solvents used are acetonitrile, methanol, water etc.) and salts of monovalent alkali metals/divalent/transition metals and ammonium salts are mixed. The mixture is stirred thoroughly and cast into teflon/polypropylene dishes. This solution is then

slowly evaporated followed by vacuum-drying and heating. The final film is 'solvent-free' and is essentially an ion-complexed polymer. The complex-forming reaction can be written as



where $(-RU-)$ denotes the polymer repeat unit, MX is the salt and n gives the relative stoichiometry of the repeating unit to salt. The kinetics for the above reaction (3.1) in most cases is unfavourable even when the complex is stable.

3.2.5 Formation of polymer-salt complex

The formation of a polymer-salt complex will be possible if reaction (3.1) is thermodynamically favourable and the Gibbs energy of solvation of the salt by the polymer is large enough to overcome the lattice energy of the salt. In addition to this, there are also some other criteria that determine the possibility of forming complexes. Some of them include,

(i) the polymer should have a high concentration of polar (basic) groups (e.g. O, N, or S) in the chain.

(ii) the polymer chain should be flexible and the value of glass transition temperature (T_g) should be low, and

(iii) the cohesive energy density of the polymer in addition to the lattice energy of the salt should be low to facilitate the dissociation of the salt. Therefore the salts having large anions such as I^- , SCN^- , ClO_4^- , $CF_3SO_3^-$, CH_3COO^- , $H_2PO_4^-$, BF_4^- etc. are most suitable.

By far the most common method for preparing the solvent-free polymer electrolytes in either bulk/thin film form is the solution cast technique stated above. Care must be taken to purify the starting material and to exclude water. For polymers which are insoluble, as in the case of cross-linked network, complexes can be produced by dipping a film of the polymer into a solution containing the appropriate amount of salt. Recently experiments were reported in which $P(\text{EO}_n\text{LiSO}_3\text{CF}_3)$ was heated in vacuum and deposited from the vapour state onto a surface [54].

3.3 Structure of polymer electrolytes

Our understanding of polymer-salt complexes and its formation and the mechanism of ion-transport would be greatly improved if detailed structural studies are made on them. Although a large number of such complexes have been studied for their electrical properties, the structural studies are rather few. Till now most of the structural studies have been performed on high molecular weight PEO-based polymer-salt complexes. Relatively little structural data are available for polymer-salt complexes other than PEO.

Structural characterizations of polymer-salt complexes are mostly done using optical microscopy, X-ray diffraction, electron microscopy and neutron diffraction techniques along with spectroscopic methods such as infrared (IR), Raman, nuclear magnetic resonance (NMR) and extended x-ray fine structure (EXAFS). Recently, very useful information on the structure and

dynamics of polymer electrolytes have been obtained. by NMR spectroscopy e.g. pulsed gradient NMR studies provide detailed information on the diffusion coefficient for NMR-active nuclei [55,56]. Since our present work deals with PEO-based polymer-salt complexes, a brief overview of the structure of PEO and its polymer-salt complex is given below.

3.3.1 Structure of poly(ethylene oxide)

Pure poly(ethylene oxide) or $(\text{CH}_2\text{CH}_2\text{O})_n$ is a semicrystalline material with 60-70% of the bulk being crystalline at room temperature and the remaining present as dispersed amorphous phase. This phenomenon of partial crystallinity carries over to many of the polymer-salt-complexes. Upon addition of a complexing salt, an amorphous polymer-salt complex is formed until the saturation of the amorphous phase occurs. At this point a crystalline complex is also formed. The morphology of PEO-based salt complexes varies depending on whether the complex is cast from solution or from melt [57]. Molecular weight of commercially available PEO can vary from very low value (~ 400) to a very high value (5×10^6).

Poly(ethylene oxide) is a linear polymer with helical configuration (Fig. 3.2) [58] and the regularity of the unit allows a high degree of crystallinity. The melting point of the crystalline phase is $T_m = 65^\circ \text{C}$ and the glass transition temperature of the amorphous phase is $T_g \sim -60^\circ \text{C}$. The density of the polymer determined from X-rays is 1.2 and 1.15 for the $\sim 80\%$ crystalline high molecular weight material and the dielectric

constant is low (~ 5). The polymer is chemically quite stable. However, in air, peroxide formation and UV chain cleavage are responsible for the slow decrease in the molecular weight with time. The morphology of the crystalline phase can be observed with an optical microscope. For both PEO and PEO complexes, the form of the polycrystalline phase is often dendritic or spherulitic [57,59]. Small ions like Li^+ , Na^+ are suggested to lie inside the helical structure of PEO [41,48] whereas large-sized cations like Rb^+ and Cs^+ lie outside the helix as suggested by different structural studies [60,61].

3.4 Phase diagram

It is not so easy to determine the phase diagrams for the polymer electrolytes because the kinetics of crystallization can be very slow and also a certain amount of randomness is inevitable in many polymers. These complications lead to apparent violations of Gibbs phase rule and to experimental problems in determining the liquidus and solidus boundaries. In spite of this it has been possible to obtain useful phase diagrams for several PEO salt complexes [62-64]. For most polymer-salt complexes, several phases may coexist, such as crystalline polymer, amorphous polymer, crystalline complex, amorphous complex and crystalline salt etc. A variety of techniques including DSC/DTA [65,66], X-ray studies [60,62], optical microscopy [63], NMR [67,68] and EXAFS [61] have been successfully employed to determine the phase diagrams and formulas for polymer-salt complexes. The properties

are sometimes found to be dependent on the thermal history and the rates of crystallization of the system. Phase diagram for PEO complexed with NH_4ClO_4 is shown in Fig. 3.3, where several phases are existing at the same time.

3.5 Ion-transport mechanism in polymer electrolytes

3.5.1 Introduction

The conductivity (σ) of any material can be expressed in terms of the mobility by the relationship

$$\sigma = \sum_i n_i \mu_i q_i \quad (3.2)$$

where n_i and μ_i are respectively the number density and mobility of the i th type of charge carriers and q_i the charge of the i th species. The polymer electrolytes are mainly ionically conducting and have negligible electronic conductivities. In the above eq. (3.2) both cations and anions can contribute towards the total conductivity in polymer electrolytes.

Most pure organic polymers are non-conducting but after complexing with salts, the ionic conductivity is introduced. Ion-transport in such materials occurs through the amorphous phase above its glass transition temperatures, T_g . Spin lattice relaxation data provided the first conclusive demonstration in this respect [65,66,68]. Further the ionic conductivity in the polymer electrolytes is strongly temperature-dependent above their T_g . Many theoretical models have been proposed to explain the observed ion-transport mechanism in the polymer electrolytes.

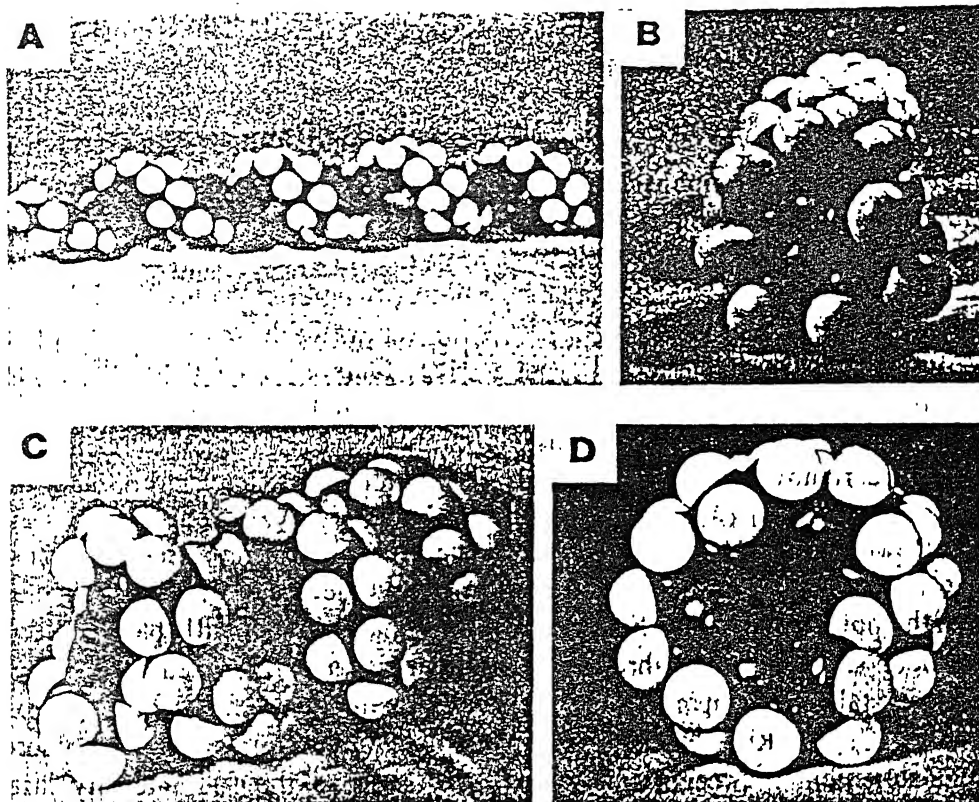


Fig. 3.2 Molecular models of PEO conformations. (A) and (B): conformation of crystalline PEO (T_2G)₇; (C) and (D): PEO in a new T_2GT_2G conformation as proposed for complexation to sodium cations [taken from Ref. 58].

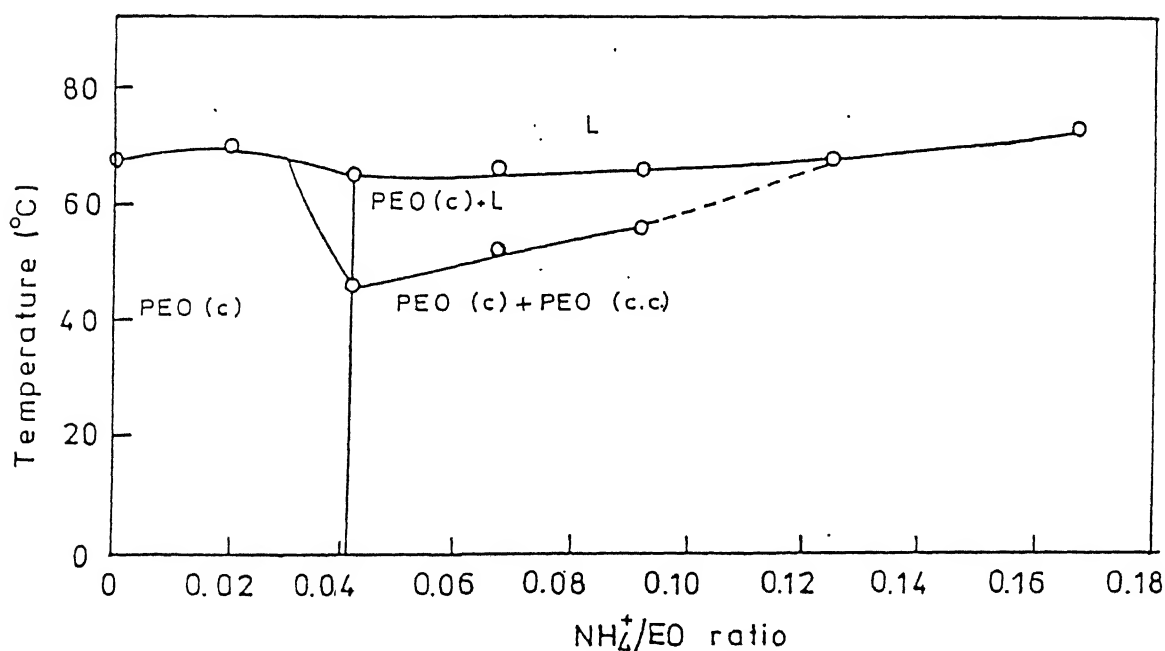


Fig. 3.3 Phase diagram of a polymer electrolyte PEO complexed to NH_4ClO_4 salt (C=crystalline, CC=crystalline complex and L= liquidus) [taken from Ref. 69].

Experimentally, ionic-conductivity, the nature and concentration of ion-transport and other related measurements in polymer electrolytes are performed by using the following measurement techniques,

- (i) d.c. conductivity,
- (ii) a.c. conductivity by complex impedance spectroscopy,
- (iii) transport number measurements by Wigner's polarization method and Tabandt's method (coulometry), and
- (iv) number of ionic species and their mobilities by transient ionic current (TIC) technique.

The experimental details of the above-mentioned techniques can be found elsewhere [24,69].

3.5.2 Observed conductivity dependence on temperature

The temperature dependence of ionic conductivity in polymer electrolytes is an activated process and the observed conductivity data can be represented by an Arrhenius type of equation

$$\sigma = \sigma_0 \exp \left(\frac{-E_a}{k_b T} \right) \quad (3.3)$$

where E_a is activation energy and σ_0 is a constant. Therefore a plot of $\ln \sigma$ vs $1/T$ should give a linear plot. However in most cases the $\ln \sigma$ vs $1/T$ plots have a curved nature. An abrupt change in the slope of this curve may arise due to a change of phase. Observed $\ln \sigma$ vs $1/T$ plots are usually fitted to the following empirical relation

$$\sigma = A T^{-1/2} \exp \left(\frac{-E_a}{k_b(T - T_o)} \right) \quad (3.4)$$

where A is a constant proportional to the carrier concentration and T_o is a reference temperature usually associated with the ideal glass transition temperature at which "free" volume disappears or the temperature at which the configurational entropy becomes zero. The above eq.(3.4) is also known as the Vogel-Tamman-Fulcher (VTF) equation [70]. In general T_o is 50K lower than actual glass transition temperature T_g .

Watanabe et al. [71] later found that the temperature dependence of ionic conductivity for the various PEO-alkali metal-salts complexes in rubbery and amorphous state can be fitted to the following equation involving $\sigma(T)$

$$\log \frac{\sigma(T)}{\sigma(T_g)} = \frac{C_1 (T - T_g)}{C_2 + (T - T_g)} \quad (3.5)$$

where C_1 and C_2 are universal constants empirically determined for a wide range of polymers. The above equation (eq. 3.5) is also known as the "Williams-Landel-Ferry" (WLF) equation [72]. Eq. (3.5) with corresponding WLF parameters for C_1 and C_2 provided a good fit to the observed temperature dependence of ionic conductivity data in polymer electrolytes. Temperature dependence of ionic conductivity in some of the common polymer salt complexes are shown in Fig. 3.4.

To a good first approximation, the VTF and WLF equations hold

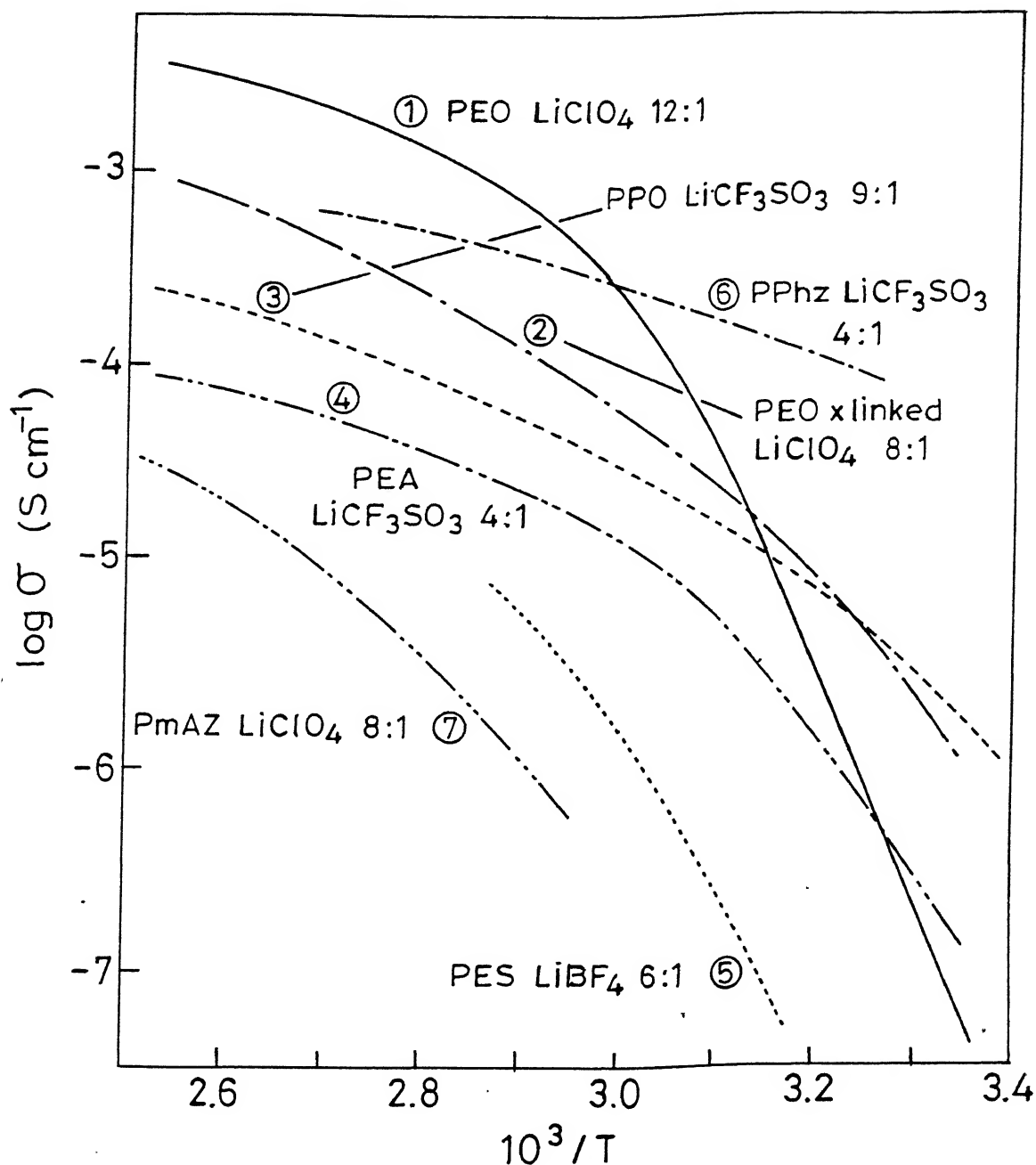


Fig. 3.4 Conductivity vs $1/T$ plots for a series of polymer-salt complexes

(1) $\text{P}(\text{EO}_{12}\text{LiClO}_4)$; (2) cross-linked $\text{PEO}_8\text{LiClO}_4$; (3) $\text{P}(\text{PO}_9\text{LiSO}_2\text{CF}_3)$; (4) $\text{poly}[(\text{ethyleneadipate})_4\text{LiSO}_3\text{CF}_3]$; (5) $\text{poly}(\text{ethylene succinate})_6\text{LiBF}_4$; (6) $\text{poly}\{[\text{bis}(\text{methoxyethoxyethoxy})\text{phosphazene}]_4\text{LiSO}_3\text{CF}\}$ and (7) $\text{poly}[(\text{N-methylaziridine})_8\text{LiClO}_4]$ [taken from Ref. 33].

quite well for a series of polymer electrolytes. Attempts were made to explain the observed transport properties and conductivity mechanisms in polymer electrolytes using theories and models originally developed to deal with pure polymers and molten salts [73-75] with some success. Almost all these theories and models, involve either the glass transition temperature, T_g , or the "equilibrium" glass transition temperature, T_o . The concept of equilibrium glass transition temperature, T_o , becomes meaningful due to the kinetic feature of T_g i.e. depending on the rates of cooling, different glass transition temperatures are observed.

The theoretical scheme which treats T_o in terms of volume is called the free-volume theory [73], and that which treats it in terms of entropies is called the excess entropy or configurational entropy model [74,75]. Both the above models are quasi-thermodynamical models. Models based on microscopic behaviour such as transport properties as a function of molecular weight, dielectric relaxation etc. were also proposed. One of them is the "Dynamic Bond Percolation Model" proposed by Druger et al. [78-80]. Since the main objective in the present work is connected with the temperature dependence of free-volume and ionic conductivity in certain polymer-salt complex $\text{PEO:NH}_4\text{ClO}_4$, the model based on free-volume theory will be discussed in some detail along with a very brief introduction to other theoretical models.

3.6 Free-volume model

3.6.1 Introduction

Before we go on to discuss the free-volume model and its application to mechanism of ion-transport in polymer electrolytes, a brief introduction to the concept of free volume in polymers and other amorphous solids and liquids will be given. This will not only help us to understand the mechanism of ion-transport in polymer electrolytes based on free volume but also help us to interpret positron lifetime results in polymers and polymer electrolytes

3.6.2 Concept of free volume in liquids and solids

Liquids, or for that matter many solids, have their volume partly occupied by molecules while the remaining part consists of 'unoccupied' or "free" volume. This unoccupied volume is supposed to consist of "holes" of molecular dimensions or imperfections in the packing order of molecules which arises from their random array. Moreover these holes have varying shapes and sizes and therefore exist as a distribution. It is into this unoccupied volume that the molecules must be able to move in order to adjust from one configurational state to another [81]. It was Doolittle [82] who used the idea of free volume to explain the fluidity of certain hydrocarbon liquids. William-Landel-Ferry [72] developed the idea further to characterise the relaxation processes in polymers and other glass-forming liquids. Cohen and Turnbull [73] later gave a clear-cut formulation for the free-volume theory to

explain phenomenon of diffusion, viscosity, etc.

Doolittle [82] defined the 'free volume' V_F for liquids in terms of the expansion volume ($V_T - V_0$) where V_T and V_0 represent the volumes at any temperature T and at 0 K respectively. This free volume was regarded by Fox and Flory [83,84] as being essential prerequisite for molecular motion by rotation or translation to occur. A minimum level for the free volume in reality will fix the point at which a glass structure will be frozen into the matrix. Therefore for any polymer, there is a temperature at which the "free volume" reaches a critical value below which there is insufficient room for any molecular maneuver. This temperature is known as the "glass-transition temperature" (T_g).

In the glassy state the free volume will be frozen in and will remain at a constant value and the "hole" size and distribution of free volume within the glass will similarly remain fixed below the glass-transition temperature. The glass will, however, contract or expand with decreasing or increasing temperature due to the normal expansion process of all molecules which result from the changing vibrational amplitudes of bond distance. Above the glass transition, in addition to the normal expansion process there will be an expansion of the free volume itself which will result in a larger expansion of the rubber than of the glass. This situation is represented in Fig. 3.5. If V_0 is the occupied volume of the glass at the absolute zero and V_g is

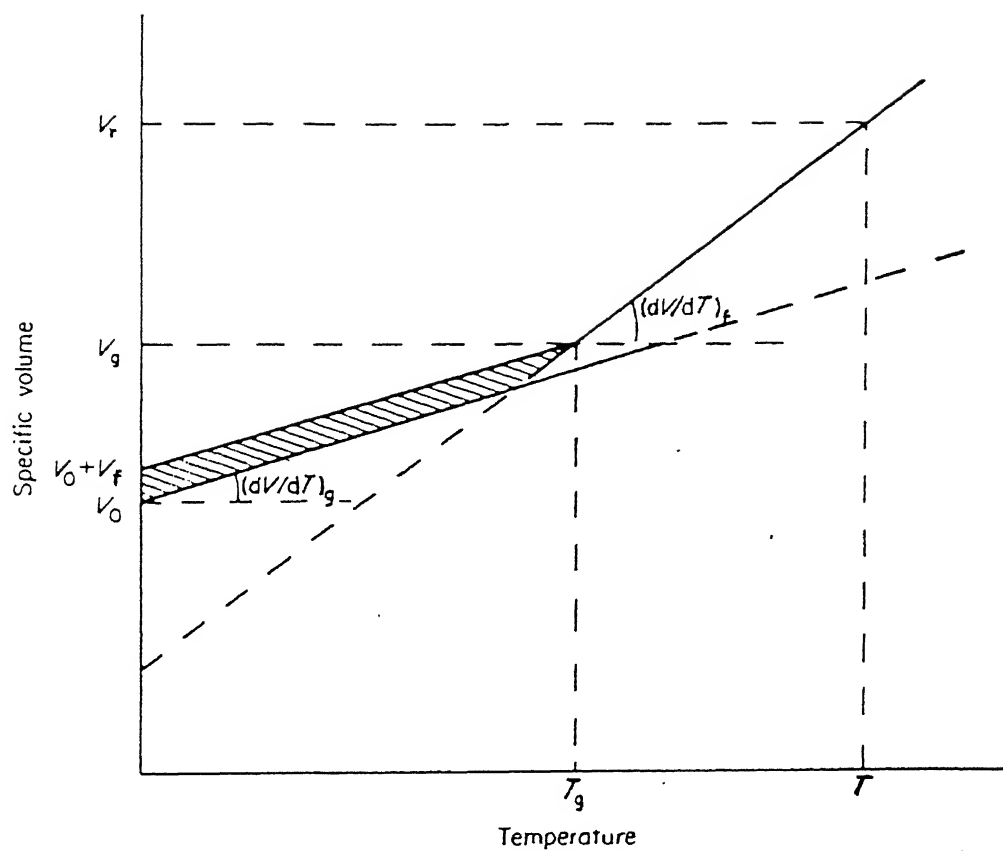


Fig. 3.5 A schematic illustration of the free volume and their expansivities in the glassy and liquid states. The shaded area represent the available free volume (V_f) [taken from Ref. 81].

the total volume at T_g , then

$$V_g = V_f + V_o + \left(\frac{dV}{dT} \right)_g T_g \quad (3.6)$$

where V_f is the frozen-in excess volume due to molecular immobility in the glass state. Similarly at a temperature above the glass transition ($T > T_g$), the volume V_r in the liquid (or rubbery) state is given as

$$V_r = V_g + \left(\frac{dV}{dT} \right)_r (T - T_g) \quad (3.7)$$

The expansion of free-volume alone is represented by the difference in the expansivities of the liquid and glassy state i.e. $\left(\frac{dV}{dT} \right)_r - \left(\frac{dV}{dT} \right)_g$. Hence if the volume expansion coefficient at any temperature T_r and at the glass-transition temperature T_g are α_r and α_g respectively, then $\alpha_r - \alpha_g = \Delta\alpha$ may be used to represent the volume expansion of free volume close to T_g .

Various authors have used different definition of the free volume and there is still some confusion about its definition and measurement. According to Simha and Boyer [85], free volume of the glass at $T=0$ is the difference between the occupied volume of the glass and the extrapolated value of the liquid volume at $T=0$. An alternative and perhaps more widely used definition of the free volume of a polymeric glass arises from the work of Williams et al. [72]. This work by Williams et al. [72] helped empirical correlations to be obtained between the mechanical and electrical

relaxation times at a temperature T to a standard reference temperature (usually T_g) for a series of polymers. It has also enabled us to rationalize the viscoelastic and time-dependent mechanical and physical behaviour of polymeric materials close to their transition temperature. They defined a mechanical shift factor a_T , to be the ratio of any relaxation process (say viscosity η , diffusion D , etc.) at a temperature T to its value at some reference temperature T_s , analytically expressed by the so-called WLF equation

$$\ln a_T = \frac{C_1 (T - T_s)}{C_2 + (T - T_s)} = \ln \left[\frac{\eta(T)}{\eta(T_s)} \right] \quad (3.8)$$

where C_1 and C_2 are universal constants empirically determined for a wide range of polymers to be $C_1 = -8.9$ and $C_2 = 102K$. An appropriate choice of T_s yields a universal plot of $\log(a_T)$ as a function of $(T - T_g)$. The above eq. (3.8) can be replaced by following expression involving T_g ,

$$\ln a_T = \frac{-17.44 (T - T_g)}{51.6 + (T - T_g)} \quad (3.9)$$

where the numerical constants are obtained from experiments. Although there is no single definition of free volume, the basic concepts of the free volume in liquids and molecular solids in its qualitative form is well established. Bondi [86] has compiled the various definitions of the different possible concepts of free volume in amorphous materials (also see ref. [81]).

3.6.3 Free-volume theory of ion-transport

In practice, the application of the free-volume concept to polymer electrolytes consists largely of using the WLF relationship (eq. 3.8) for the physical properties (viscosity, storage modulus, diffusivity) and the VTF form (eq.3.4) for conductivity although the WLF and VTF equations are empirical and do not depend on free-volume theory for their derivation. The free-volume theory is simple and has been widely discussed as a theoretical framework for understanding conductivity in polymer electrolytes [24]. According to the free-volume theory of ionic conductivity, the increase in temperature results in the expansivity of the material and produces local empty space or free volume, into which ionic carriers, solvated molecules, or polymer segments themselves can move. Therefore the overall mobility of the material, then, is determined by the amount of empty space or free volume present in the material.

According to the free-volume theory of Cohen and Turnbull [72], diffusion (inverse of the viscosity) is not an activated process and molecular transport processes occur by the movement of molecules into the voids/holes formed by the redistribution of the free volume. However, diffusion can take place only through those voids which have a size greater than a critical volume V^* , to permit molecules to jump into it. They used straightforward statistical mechanics (calculating the most probable distribution) to derive a probability distribution for void volume of various sizes by considering a liquid of hard sphere and obtained the following expression for the diffusion constant D [24]

$$D = gaU \exp \left(\frac{-\gamma V^*}{V_f} \right) \quad (3.10)$$

where g is a geometrical factor, U is the thermal velocity of the molecules, a is roughly the molecular diameter, γ is a constant nearly equal to unity and V_f is the total free volume available. Upon expanding, V_f can be written by the following expression around the temperature at which the free volume disappears;

$$V_f = \alpha \bar{V}_m (T - T_o) \quad (3.11)$$

where \bar{V}_m is the mean molecular volume over the temperature range (T, T_o) and α is the thermal expansion coefficient over the same range. One can also expand the above eq.(3.11) around the glass transition temperature T_g so that

$$V_f = V_g [f_g + \alpha (T - T_g)] \quad (3.12)$$

where V_g is the molar volume at T_g and f_g is the free volume fraction at T_g . Eqs. (3.11) and (3.12) will be equivalent if

$$T_o = T_g - f_g/\alpha \quad (3.13)$$

Upon substituting eq.(3.11) into eq.(3.10), the expression for diffusion coefficient takes the form

$$D = gau \exp \left(\frac{-\gamma V^*}{\alpha \bar{V}_m (T - T_o)} \right) \quad (3.14)$$

In polymer electrolytes, the moving particles which contribute to the ionic conductivity are the carrier ions and the ionic conductivity is expressed by eq. (3.2). The ionic mobility μ is related to the ionic diffusion coefficient D by the Nernst-Einstein equation

$$\mu = \frac{qD}{k_b T} \quad (3.15)$$

One can arrive at eq. (3.8) involving $\eta(T)$ or eq. (3.5) involving $\sigma(T)$ using eqs. (3.2), (3.14) and (3.15), (provided we neglect the temperature dependence of the number of charge carriers) with

$$\begin{aligned} C_1 &= \gamma V_i^* / 2.303 V_g T_g \\ C_2 &= f_g / \alpha_f \end{aligned}$$

Further from equipartition theory $u \sim T^{1/2}$ and eq.(3.15), the free-volume theory yields the relationship same as that of VTF type

$$\sigma = \sigma_o \exp \left(\frac{-B}{(T - T_o)} \right) \quad (3.16)$$

where the parameter B can be correlated with the C_1 and C_2 parameters through

$$B = 2.303 C_1 C_2 = \gamma V_i^* / \alpha V_g \quad (3.17)$$

One can, therefore, arrive at the VTF and WLF relations for ionic conductivity from the free-volume theory. Although the

free-volume model of ionic conduction in polymers is simple to understand, this model has been subjected to criticism when it is used to explain the temperature dependence of ion-transport mechanism. This is so because $\sigma(T)$ for different polymer electrolytes do not merely follow the VFT behaviour, and the reasons for this are

- (i) free-volume theory considers only the motion of the polymer host (and not the ionic hopping in the polymer-salt complexes),
- (ii) the theory has been derived for rigid molecules which is not true in reality, and
- (iii) it does not take into account the temperature dependence of number of charge carriers.

A more detailed discussion in this respect have been given by Ratner [87]. The polymer electrolytes which involve strong ion-polymer and ion-ion interactions present a much greater degree of complexity than the hard-sphere liquid of Cohen and Turnbull [72].

The observed pressure dependence of ionic conductivity in polymer electrolytes is also interpreted by free-volume type concepts. However in some cases free-volume models gave incorrect quantitative prediction of the pressure dependence of transport properties [76].

3.7 Configurational entropy model

There are some basic conceptual problems in the application of the free-volume model for ion transport in polymer

electrolytes. In some cases, the free-volume model gave a wrong estimate of the activation energy for ionic conductivity [32]. A more energetically accepted model is that of the polymer and associated ions undergoing cooperative fluctuations which lead to ion transport [32,,88]. Gibbs and co-workers [74,75,89] have put forward a configurational entropy model for polymer properties. They gave an argument based on statistical mechanics to relate the relaxation properties of glass-forming liquids to their quasistatic-properties, characterized by the glass transition temperature T_g , the specific heats of the glass and the equilibrium melt. In their model the transition probabilities for glass-forming liquids are expressed in terms of the equilibrium distribution of an isothermal-isobaric ensemble of small systems of the size of the cooperatively rearranging region. The cooperatively rearranging region is defined as the smallest region that can undergo a transition to a new configuration without a requisite simultaneous configurational change on and outside its boundary. Adam and Gibbs [75] have, therefore, shown that the WLF functional dependence of polymer properties can be derived from configurational entropy model. Detailed mathematical formulation of this theory can be found elsewhere [24].

3.8 Dynamic bond percolation model

The well-known experimentally observed property that the crystalline phase has no conductivity and amorphous phase is responsible for the ionic conduction in polymer electrolytes, has

been explained on the basis of static bond percolation model. But in the polymer electrolytes above the glass transition temperature ($T > T_g$) the ionic motion is due to the combination of ionic translation motion/hopping and dynamic segmental motion of the polymer host which assists the ionic motion. Druger et al [78-80] gave a generalised 'dynamic percolation model' in which the segmental mobility has also been included along with the ionic motion. In this generalised model, the bonds which are closed or open change with characteristic rate λ or characteristic renewal time τ_r ($\lambda = 1/\tau_r$). This change or renewal event is related to the segmental motion which either permits the ions to hop from one site to another site or give a pathway for ions to move. In other words, the segmental movement of the polymer facilitates the translational ionic motion. Thus the dynamic percolation model has been used to describe the various physical properties of polymer electrolytes such as dependence of conductivity on chain length of the polymers, molecular weight, applied pressure, effect of host polymer change, variation of stoichiometry, plasticization, frequency dependence of conductivity and dielectric relaxation etc.

3.9 Specific polymer electrolytes

3.9.1 Alkali-metals ion-conducting polymers

Most of the alkali-metal ion-conducting polymer electrolytes are mainly Li- and Na-based (very few are based on K, Rb). Conductivity is mainly due to Li^+ and Na^+ ions which have small

conductors. Some of them are listed in Table 3.2. Polyether-transition metal salt systems are particularly interesting, because, in many cases distinct ionic species can be identified and quantified using visible spectroscopy [94,95].

3.9.4 Proton-conducting polymer electrolytes

The term "proton-conducting polymer electrolyte" refers in general to the materials in which the charge transport is primarily due to H^+ , NH_4^+ etc. Solvent-swollen polyelectrolytes have long been recognised as excellent protonic conductors [94]. Armand and co-workers [95] have focussed on rigorously anhydrous PEO- H_3PO_4 material, cast in thin-film form from tetrahydrofuran/acetonitrile solution. Armand group has also investigated polyamide electrolytes, including nylon 6 and acrylamide, complexed with H_3PO_4 and cast into films from methanol [96]. with $\sigma = 10^{-4} \text{ S.cm}^{-1}$ and proton transport number t_H^+ roughly equal to 0.9 at room temperature.

However only few reports on the study of proton-conducting polymer electrolytes exist in the literature prior to 1990 [97,98]. Most of the proton-conducting polymers studied are based on PEO, PEI, PAA, PVA etc. complexed with some ammonium salts/acids (Table 3.2). Some proton-conducting polymer electrolytes based on PEO complexed with ammonium salts such as NH_4ClO_4 , NH_4I , $(NH_4)_2SO_4$ and NH_4HSO_4 have been developed [99-102] and these show anionic conduction apart from predominantly cationic (or H^+) conduction.

Although there exist a large number of polymers which act as

TABLE 3.2

SOME POLYMER ELECTROLYTE MATERIALS
(References given in the last column
are shown separately at the end of this chapter)

Type of Electrolyte	Conductivity	Temp.	References
Alkali-metal based polymer electrolyte	($\Omega^{-1} \text{ cm}^{-1}$)	(K)	
(PEO)-LiClO ₄	$\sim 10^{-6}$	300	[1]
(PEO)-LiCF ₃ SO ₃	$10^{-4} - 10^{-3}$	373	[2]
(PVAc)-LiSCN	$\sim 10^{-6}$	300	[3]
(PVAc)-LiCF ₃ SO ₃	$\sim 10^{-9}$	313	[3]
(PESc) ₃ -LiClO ₄	$\sim 10^{-5}$	363	[4]
(PEO) ₈ -NaI	$\sim 10^{-5}$	318	[5]
(PPO) ₈ -NaI	$\sim 10^{-8}$	300	[6]
(PPO)-LiBr	$\sim 10^{-5}$	408	[7]
(PPO)-LiI	$\sim 10^{-5}$	338	[7]
(PEO)-LiSCN	$\sim 1.4 \times 10^{-6}$	330	[8]
(PEO)-LiI	1×10^{-7}	329	[8]
(PPO)-LiClO ₄	$\sim 10^{-5}$	343	[9]
Copper and silver based polymer electrolyte			
(PEO) ₆ Cu(CF ₃ SO ₃) ₂	5×10^{-7}	313	[10]
(PEO) ₆ Cu(ClO ₄) ₂	$\sim 10^{-6}$	300	[11]
(PEO)CuSCN	1.3×10^{-3}	300	[12]
(PEO)CuI	1.25×10^{-3}	300	[12]
(PEO) ₄ AgClO ₄	1.3×10^{-3}	300	[13]
(PEO)-AgNO ₃	4×10^{-7}	300	[14]
Divalent/transition salt based polymer electrolyt			
(PEO) ₁₆ ZnI ₂	3.6×10^{-4}	413	[15]
(PEO) ₂₄ PbI ₂	$\sim 10^{-6}$	473	[15]
(PEO)NiBr ₂	$\sim 10^{-3}$	423	[16]
(PEO) ₈ ZnCl ₂	$\sim 10^{-4}$	393	[17]
(PEO) ₂₀ La(ClO ₄) ₂	$\sim 10^{-5}$	353	[18]

(Continued on the next page)

Table 3.2 - Continued

(PEO) ₁₀ RbBF ₄	7.5×10^{-9}	303	[19]
(PEO) ₁₀ -CsCF ₃ SO ₃	4.1×10^{-5}	303	[19]
Proton conducting polymer electrolytes			
(PVA)-H ₃ PO ₄	$\sim 10^{-5}$	300	[20]
(PVA)-NH ₄ HSO ₄	2.4×10^{-5}	300	[21]
(PEI)-H ₃ PO ₄	5.0×10^{-6}	300	[22]
(PEO)-H ₃ PO ₄	$\sim 10^{-5}$	-	[23]
(PEO)-NH ₄ SCN	$\sim 10^{-8}$	300	[24]
(PEO)-NH ₄ ClO ₄	1.05×10^{-5}	300	[25]
(PEO)-NH ₄ I	$\sim 10^{-5}$	300	[26]
(PEO)-(NH ₄) ₂ SO ₄	$\sim 10^{-7}$	300	[21]
(PEO)-NH ₄ HSO ₄	2×10^{-4}	290	[27]

host matrices for dissolution of salts to form solvent-free polymer electrolytes, most of them tend to have high T_g or substantial crystallinity, which makes the complexes poor ionic conductors in the temperature range of interest. Following approaches were made to modify the polymer electrolytes with an aim of enhancing their ionic-conductivity by

- (i) addition of another polymer to lower the T_g [103] and synthesis of flexible polymer backbone [71,100,103].
- (ii) addition of low molecular weight to provide flexibility of polymers and polymer electrolytes, and
- (iii) making the host polymer mechanically stable by addition of ceramic fillers like α -alumina, β -alumina etc. during casting [103].

Recently, approaches has been made to suppress the crystallinity of PEO, by randomly interrupting the OC_2H_4 repeat unit of PEO with OCH_2 unit and good conductivity has been achieved at room temperature [105].

3.10 Applications of polymer electrolytes

The properties of polymer electrolytes such as their high compliance, good adherence to electrodes, and the possibility of fabricating the polymers into thin films are attractive not only for batteries but for many other electrochemical devices also. Some of the potential areas of application are briefly described below

- (a) High-energy-density batteries : The current research in high-energy-density batteries has been motivated towards

alkali-metal based ion-conducting electrolytes, particularly batteries based on polymer electrolytes doped with various lithium salts. The reasons to choose polymer electrolytes in batteries are (i) ease of formation of thin films of larger area which reduce the internal resistance of the battery thus improving the current density (ii) proper contact with the electrodes is possible, and (iii) it eliminates the use of inert porous separator existing in commercial batteries. Hooper et al. [106] and Gauthier and coworkers [107] have shown the validity of a film (50-200 μm) cell concept as shown in Fig. 3.6.

(b) Fuel cells :- Efforts have been devoted to fabricate fuel cells based on high temperature oxide-ion-conductive solid electrolyte most advantageous for power generation because of their structural simplicity [4].

(c) Gas sensors :- There are a number of reports on gas sensitive electrochemical devices using solid polymers as electrolytes [4]. Shimuzi et al. [108] reported a CO_2 potentiometric sensor based on K_2CO_3 - polyethylene glycol (PEG) system supported on porous ceramics. Similar sensors based on polymer electrolytes for O_2 [109] and H_2 [110] sensing have also been reported.

(d) Electrochromic display (ECD) devices:- Another important application of the polymeric electrolytes is their use in electrochromic display devices [4]. ECDs are based on colour changes of certain kinds of materials due to electrochemical reduction or oxidation. Electrochromic displays, belonging to flat panel type, compete with liquid crystal displays (LCD) because both are passive type of displays.

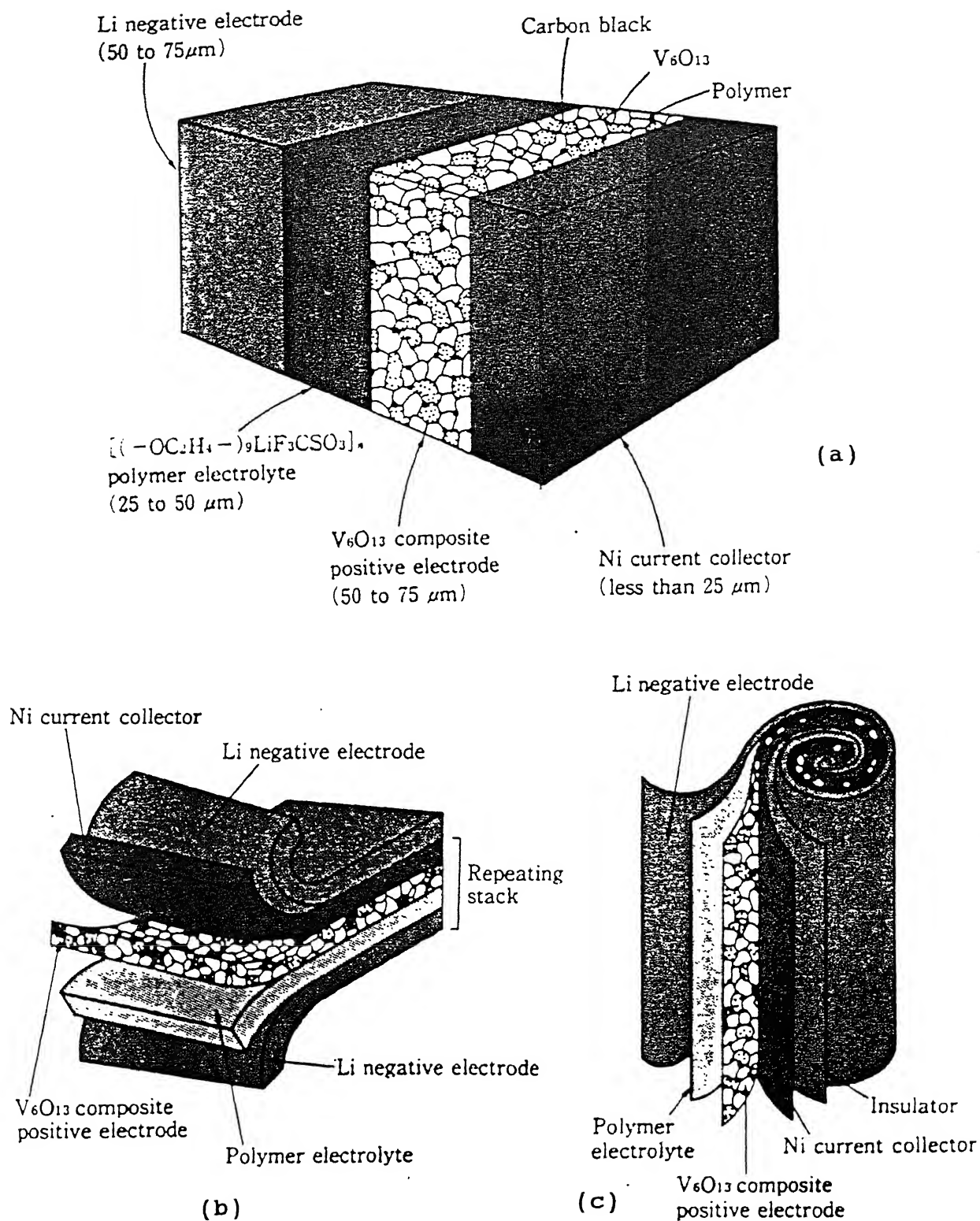


Fig. 3.6 (a) The thin film design of an all-solid-state battery and two typical configurations of a solid polymer battery (b) Bi-polar structure (c) Swiss-roll configuration [taken from Ref. 4].

References

1. S. Chandra, "Superionic Solids - Principles and Applications" (North Holland, Amsterdam, 1981).
2. "Superionic Solids and Solid Electrolytes - Recent Trends", edited by A.L. Laskar and S.Chandra (Academic press, New York, 1989).
3. C. Tabandt, Z. anorg. allgem. Chem. 115 , 105 (1921).
4. T. Kudo and K. Fueki, "Solid State Ionics" (VCH Publishers, New York, 1990).
5. O. Tillement, Solid State Ionics 68, 9 (1994).
6. Q. Liu, in "Solid State Ionic Devices" edited B.V.R. Chowdari and S. Radhakrishna (World Scientific, Singapore, 1988).
7. T. Takahashi and O. Yamamoto, Electrochem. Acta 11, 779 (1966); T. Takahashi and O. Yamamoto, *ibid*, 11, 911 (1966).
8. C. Tabandt, H. Reinhold, Z. Electrochem. 29, 313 (1923).
9. H.Y.-P. Hong, Mater. Res. Bull. 11 , 173 (1976).
10. J.B. Goodenough, H.Y.-P. Hong and J.A. Kafalas, Mater. Res. Bull. 11 , 203 (1976).
11. Y.F.Y. Yao and J.T. Kummer, J. Inorg. Nucl. Chem. 29, 2553 (1967)
12. A.M. Glass and K. Nassau, J. Appl. Phys. 51, 3756 (1980).
13. F.W. Poulsen, in "High Conductivity Solid Ionic Conductors - Recent Trends and Applications", edited by T. Takahashi (World Scientific, Singapore, 1989), p. 166.
14. S. Chandra, in Ref [2] p. 185.
15. R.C.T. Slade, "Solid State Protonic Conductors IV" (North-

Holland, Amsterdam, 1989).

16. C.C. Liang, J. Electrochem. Soc. 120, 1289 (1973).
17. J. Maier, Mater. Res. Bull 20, 383 (1985).
18. K. Shahi and J.B. Wagner Jr., J. Solid State Chem. 42, 107 (1982).
19. K. Shahi and J.B. Wagner Jr., J. Phys. Chem. Solids 43, 713 (1982).
20. M.R.W. Chang, K. Shahi and J.B. Wagner Jr., J. Electrochem. Soc. 131, 1213 (1984).
21. D. Kunze, in "Fast Ion Transport in Solids - Solid State Batteries and Devices", edited by W. Van Gool (North-Holland, Amsterdam, 1973), p. 403.
22. F.A. Fusco and H.I. Tuller, in Ref. [20] p. 215.
23. T. Minami, J. Non-cryst. Solids. 73, 273 (1985).
24. "Polymer Electrolyte Reviews 1", edited by J.R. MacCallum and C.A. Vincent (Elsevier, London, 1987); "Polymer Electrolyte Reviews 2", edited by J.R. MacCallum and C.A. Vincent (Elsevier, London, 1989).
25. A.A. Blumberg, S.S. Pollack and C.A.J. Hoeve, J. Polym. Sci. A 2, 2499 (1964).
26. J. Moacanin and E.F. Cuddihy, J. Polym. Sci. C 14, 313 (1966).
27. P.V. Wright, Br. Polym. J. 7, 319 (1975).
28. B.E. Fanton, J.M. Parker and P.V. Wright., Polymer 14, 589 (1973).
29. M.B. Armand, J.M. Chabagno and M.J. Duclot, in "Fast Ion Transport in Solids" edited by P. Vashishta, J.N. Mundy and G.K. Shenoy (North-Holland, Amsterdam, 1979), p. 131.

30. M.A. Ratner and D.F. Shriver, Chem. Rev. 88, 109 (1988).
31. M.B. Armand, Ann. Rev. Mater. Sci. 16, 245 (1986).
32. B.L. Papke, M.A. Ratner and D.F. Shriver, J. Electrochem. Soc. 129, 1694 (1982).
33. J.S. Tonge and D.F. Shriver, in "Polymers for Electronic Applications", edited by J.H. Lai (CRC Press, Florida, 1989), p. 157.
34. S. Chandra, in "Proceedings of the Fifth Asia-Pacific Physics Conference"; (World Scientific, Singapore, 1992), p. 704.
35. D.F.Shriver, B.L.Papke, M.A.Ratner, R.Dupon, T.Wong, and M.Brodwin, Solid State Ionics 5, 83 (1981).
36. E.A.Rietman, M.L.Kaplan and R.J.Cava, Solid State Ionics 17, 67 (1985).
37. J.J.Fontaneila, M.C.Wintergill, J.P.Calame and C.G.Andeen, J. Polym. Sci. Polym. Phys. Ed. 23, 113 (1985).
38. M. Stainer, L.C.Hardy, D.H.Whitmore and D.F.Shriver, J. Electrochem. Soc. 131, 784 (1984).
39. M. Watanabe, M. Rikukawa, K. Sanui, N. Ogata, H. Kato, T. Kobayashi and Z.Ohataki, Macromol. 17, 2902 (1984).
40. M. Watanabe, K. Sanui, N. Ogata, F. Inoue, T. Kobayashi and Z.Ohataki, Polym. J. 17, 549 (1985).
41. R. Dupon, B.L. Papke, M.A.Ratner and D.F.Shriver J. Electrochem. Soc. 131, 586 (1984).
42. G.T.Davis, C.K.Chaing and C.A.Harding, Solid State Ionics 18/19, 321 (1986).
43. R.D.Amgstrong and M.D.Clarke, Electrochem. Acta 29, 1443 (1984).

44. M. Watanabe, M. Togo, N. Ogata, T. Kobayashi and T. Ohtaki, *Macromolecules* 17, 2908 (1984).
45. P.M.Blonski and D.F.Shriver, *J. Am. Chem. Soc.* 106, 6854 (1984).
46. J.E.Weston and B.C.H. Steele, *Solid State Ionics* 7, 81 (1992).
47. P.M.Blonski, D.F.Shriver, P. Austin and H.R.Allcock, *J. Am. Chem. Soc.* 106, 6854 (1984).
48. D. Fish, I.M. Khan and J.Smid, *Polym. Prepr.* 27, 325 (1986).
49. A. Killis, J.F.LeNest, A.Gandini and H.Cheradame, *J. Polym. Sci. Polym. Phys. Ed.* 19, 1073 (1981).
50. R.C.T. Slade, A. Hardwide and P.G.Dickens, *Solid State Ionics* 9/10, 1053 (1983).
51. J.L. Crowley, R.A. Wallace and R.H. Babe, *J. Polym. Sci. Polym. Phys. Ed.* 14, 1769 (1976).
52. M.G. Dodin, *Polymer* 22, 788 (1981).
53. A.J. Polak, S. Petty-weeks and A.J. Beuhler, *Sensors and Actuators* 9, 1 (1986).
54. Y. Ito, K. Syakushire, M. Hiratani, K. Miyachi and T. Kudo, *Solid State Ionics* 18/19, 277 (1986).
55. N. Bodel, S.A. Lwng and I.M. Ward, *Solid State Ionics* 45, 261 (1991).
56. S. Arumugam, J. Shi, D.P. Tunstall and C.A. Vincent, *J. Phys.: Condens. Matter* 5, 153 (1993).
57. P.V. Wright and C.C. Lee, *Polymer* 23, 681 (1982).
58. B.L. Papke, M.A. Ratner and D.F. Shriver, *J. Phys. Chem. Solids* 42, 493 (1981).
59. R. Neat, M. Glasse, R. Linford and A. Hooper, *Solid State*

- Ionics 18/19, 1088 (1986).
60. T. Hibma., Solid State Ionics 9/10, 1101 (1983).
61. S. Okamura and Y. Chatani, Polymer 28, 1815 (1987).
62. C.P.Robitaille and D. Fauteux, J. Electrochem. Soc. 133, 315 (1986).
63. Y.L.Lee and B.Crist, J. Appl. Phys. 60, 2683 (1986).
64. M. Stainer, L.C. Hardy, D.H. Whitmore and D.F. Shriver J. Electrochem. Soc. 131, 784 (1984).
65. M.Minier, C. Berthier and W.Gorecki, Solid State Ionics 9/10, 1125 (1983).
66. D. Fauteux, M.D. Lupien and C.P. Robitaille, J. Electrochem. Soc. 134, 2761 (1987).
67. M.Minier, C. Berthier and W.Gorecki, J. Phys. 45, 739 (1984).
68. C. Berthier, W.Gorecki, M.Minier, M.B.Armand, J.M. Chabagno and P. Rigaud, Solid State Ionics 11, 91 (1983).
69. K.K. Maurya, Ph.D. Thesis, Banaras Hindu, University, Varanasi, India, (1993) unpublished.
70. H.Vogel, Phys. Z. 22, 645 (1921); G. Thammann and W. Hesse, Z. Anorg. Allg. Chem. 156, 245 (1926); G.S. Fulcher, J. Am. Ceram. Soc. 8, 339 (1925).
71. M. Watanabe, M. Itoh, K. Sanui and N.Ogata, Macromolecules 20, 569 (1987).
72. M.I. Williams, R.F. Landel and J.D.Ferry, J. Am. Chem. Soc. 77 3701 (1955).
73. M.H. Cohen and D. Turnbull, J. Chem. Phys. 31, 1164 (1959).
74. J.H. Gibbs and E.A.DiMarzio, J. Chem. Phys. 28, 373 (1958).
75. G.Adams and J.H.Gibbs, J. Chem. Phys. 43, 139 (1965).

76. M. Goldstein, J. Phys. Chem. 77, 667 (1973).
77. C.A.Angell and W.Sichina, Ann. N.Y. Acad. Sci. 279, 53 (1976).
78. S.D.Druger, A. Nitzan and M.A.Ratner, J. Chem. Phys. 79, 3133 (1983).
79. S.D.Druger, A. Nitzan, and M.A.Ratner, Solid State Ionics 9/10, 1115 (1983).
80. S.D.Druger, M.A.Ratner and A. Nitzan, Phys. Rev. B. 31, 3939 (1985).
81. "The Physics of Glassy Polymers", edited by R.N.Haward (Applied Science Publishers, London, 1973).
82. A.K. Doolittle, J. Appl. Phys. 22, 577 (1951).
83. T.G. Fox and P.J. Flory, J. Am. Chem. Soc. 70, 2384 (1948).
84. T.G. Fox and P.J. Flory, J. Appl. Phys. 21, 581 (1950).
85. R. Simha and R.F. Boyer, J. Chem. Phys. 37, 1003 (1962).
86. A. Bondi, J. Phys. Chem. 58, 929 (1954).
87. M.A.Ratner, in Ref [42] p. 173.
88. C.A.Angell, in "Solid State Ionics", edited by M. Kleitz, B. Sapoval and D. Ravine (North-Holland, Amsterdam, 1983), p. 3.
89. J.H. Gibbs, "Modern Aspects of the Vitreous State", (Butterworths, London, 1965) Ch. 7.
90. S.Chandra, S.A.Hashmi, M.Saleem, and R.C.Agarwal, Solid State Ionics 67, 1 (1993).
91. T.M.A. Abrantes, L.J.Alcacer and C.A.C.Sequeira, Solid State Ionics 18/19, 315 (1986).
92. K.J.Ademic, S.G.Greenbaum, M.C.Wintergill and J.J.Fontanella, J. Appl. Phys. 60, 1342 (1986).
93. M.Watanabe, S.Nagano, K.Sanui, and N.Ogata, J. Power Sources

- 20, 327 (1987).
94. R.C.T. Slade, A. Hardwrick, P.G.Dickens, Solid State Ionics 9/10, 1053 (1983).
 95. P.Donoso, W.Gorecki, C.Berthier, F.Defendini, C.Poinsignon and M.B.Armand, Solid State Ionics 20/30, 969 (1988).
 96. M.B. Armand, "Abstracts -First International Symposium on Polymer Electrolytes", St. Andrews, Scotland, 1987.
 97. R.D. Armstrong and M.D. Clarke, Electrochem. Acta 29, 1443 (1984).
 98. J. Plocharski, W. Wieczorek, J. Przyluski and K. Such, Appl. Phys. A 49, 55 (1981).
 99. S.A.Hashmi, Ajay Kumar, K.K.Maurya, and S.Chandra, J. Phys. D: Appl. Phys. 23, 1307 (1990).
 100. K.K.Maurya, S.A.Hashmi, and S.Chandra, J. Phys. Soc. Jpn. 61, 1709 (1992).
 101. K.K.Maurya, B.Bhattacharya and S.Chandra. Phys. Stat. Sol. (a) 147, 347 (1995).
 102. K.K.Maurya, Neelam Srivastava, S.A.Hashmi and S.Chandra, J. Mat. Sci. 27, 6357 (1992).
 103. P.G. Hall, G.R. Davies, J.E. McIntire, I.M. Ward, D.J. Bannister and K.M.F. LeBrocq, Polym. Commun. 27, 98 (1986).
 104. T.A. Skotheim, S.W.Feldberg and M.B. Armand, J. de. Physique C 3, 44 (1983).
 105. J.R. Craven, R.H. Mobbs and A. Booth, Macromol. Chem. Rapid. Commun. 7, 81 (1986).
 106. A.Hooper and J.M. North, Solid State Ionics 9/10, 1161 (1983).
 107. M.Gauthier, D.Fauteux, G.Vassort, A.Belanger, M.Duval,

- P.Ricoux, J.M.Chabagno, D.Muller, P.Rigaud, M.B.Armand and D.Deroo, J. Electrochem. Soc. 132, 1333 (1985).
108. Y.Shimizu, K. Komori and M. Egashira, J. Electrochem. Soc. 136, 2256 (1989).
109. S. Kuwata, H. Miura and N. Yamazoe, Chem. Lett. 68, 1197 (1988).
110. A.J.Polak, S.Petty-Weeks and A.J.Beuhler, Sensors and Actuators 9, 1 (1986).

Bibliography exclusively for TABLE 3.1

1. C. Tubandt and E. Lorenz, Z. Physik. Chem. 87, 512 (1914).
2. B.B. Owens and G.R. Argue, Science 157, 308 (1967).
3. C. Berthier, V.Chabre and M.Minier, in "Proc. 2nd International on Meet Solid Electrolytes", St.Andrew (1978), p. 7.41.
4. S. Geller and B.B. Owens, J. Phys. Chem. Solids 33, 1241 (1972).
5. J.A.A. Ketlaar, Trans. Farad. Soc. 34, 874 (1938).
6. J.B. Goodenough, H.Y.-P Hong and J.A. Kafalas, Mater. Res. Bull. 11, 293 (1976).
7. T. Takahashi, K. Kuwabara and M. Shibata, Solid State Ionics 1, 163 (1980).
8. W. Wang, S. Wang, L. Rao, Z. Lu and X. Yi, Solid State Ionics 28-30, 424 (1988).
9. L. Boehm, C.J. Delbecq, E. Huchison and S. Susman, Solid State Ionics 5, 311 (1981).
10. G.A. Genkina, L.N. Dem'yanets, A.K. Ivanov-shits, B.A.Maksimov, O.K. Mel'nikov and V.I. Simonov, J.E.T.P. Lett. 38, 305 (1983).
11. Y.F.Y. Yao and J.T. Kummer, J. Inorg. Nucl. Chem. 29, 2453 (1967).
12. A.T. Howe, S.H. Sheffield, P.E.Childs, and M.G. Shilton, Thin Solid Films 67, 365 (1980).
13. S.H. Sheffield and A.T. Howe, Mater. Res. Bull. 14, 929 (1976).
14. R.T.C Slade, A. Hardwick and P.G. Dickens, Solid State Ionics 9/10, 1093 (1983).
15. S. Chandra and N. Singh, J. Phys. C: Solid State Phys. 16, 185 (1983).
16. R.C.T. Slade, J.Barker and T.K.Halstead, Solid State Ionics 24, 147 (1987).
17. C.C. Liang, J. Electrochem. Soc. 120, 1289 (1973).
18. K. Shahi and J.B. Wagner, J. Electrochem. Soc. 128, 6 (1981a).
19. S. Fujitsu, K. Koumoto and H. Yanagida, Solid State Ionics 18/19, 1146 (1986).

20. D. Kunze, in "Fast Ion Transport in Solids - Solid State Batteries and Devices", edited by W. Van Gool (North-Holland, Amsterdam, 1972), p. 403
21. M. Andeen, D. Ravaina and J.L. Souquet, C. R. Acad. Sci. Paris, Sec C 282, 499 (1976).
22. L.M. Torell, J. Chem. Phys. 76, 3467 (1982)..
23. Y. Minami, T. Shimizu and M. Tanaka, Solid State Ionics 9/10, 577 (1983).
24. K. Nassau, A.M. Glass, M. Grasso and D.H. Olson, J. Non-cryst. Solids 46, 45 (1981).

Bibliography exclusively for TABLE 3.2

1. W. Gorecki, R. Andreani, C. Berthier, M.B. Armand, M. Mali, J. Roos and D. Brinkman, *Solid State Ionics* 18/19, 295 (1986).
2. R. R. Sorensen and T. Jacobson, *Polym. Bull.* 9, 47 (1988).
3. M.C. Wintersgill, J.J. Fontanella, J.P. Calme, M.K. Smith, T.B. Jones, S.G. Greenbaum, K.K. Ademic, A.N. Shetty and G. Andein, *Solid State Ionics* 18/19, 326 (1986).
4. M. Watanabe, M. Rikukawa, K. Sanui, N. Ogata, H. Kato, T. Kobayashi and Z. Ohtaki, *Macromolecules* 17, 2907 (1984).
5. D. Fauteux, M.D. Lupien and C. D. Robitaille, *J. Electrochem. Soc.* 134, 2761 (1987).
6. M.C. Wintersgill, J.J. Fontanella, S.G. Greenbaum, and K.K. Ademic, *Br. Polym. J.* 20, 195 (1988).
7. M. Watanabe and N. Ogata, in "Polymer Electrolyte Reviews 1", edited by J.R. MacCallum and C.A. Vincent (Elsevier, London, 1992), p. 149.
8. E.A. Rietman, M.L. Kaplan and R.J. Cava, *Solid State Ionics* 17, 67 (1985).
9. M. Watanabe, K. Sanui, N. Ogata, T. Kobayashi and Z. Ohtaki, *J. Appl. Phys.* 57, 123 (1985).
10. F. Bonino, S. Pantaloni, S. Passerini and B. Scrosati, *J. Electrochem. Soc.* 135, 1961 (1986).
11. A. Magistris, G. Chiodelli, K. Singh and P. Ferloni, *Solid State Ionics* 38, 235 (1990).
12. K.S. Sidhu, S.S. Sekhon, S.A. Hashmi and S. Chandra, *J. Mater. Sci. Lett.* 12, 346 (1993).
13. T.M.A. Abrantes, L.T. Alcacer and C.A.C. Sequeira, *Solid State Ionics*, 28-30, 315 (1986).
14. S. Chandra, S.A. Hashmi, M. Sallem and R.C. Agarwal, *Solid State Ionics* 67, 1 (1993).
15. G.C. Farrington and R.G. Linford, in "Polymer Electrolyte Reviews 2" edited by J.R. MacCallum and C.A. Vincent (Elsevier, London, 1989), p. 395.
16. R. Haq and G.C. Farrington, *Solid State Ionics* 28/30, 990

(1988).

17. M.D. Glasse, R.G. Linford and M. Schlidwein, in " Second International Symposium on Polymer Electrolytes" edited by B. Scrosati, p. 203, 1989.
18. F.M. Grey, C.A. Vincent, P.C. Bruce and J. Nowinshi, in "Polymer Electrolyte Reviews 2" adited by J.R.MacCallum and C.A. Vincent (Elsevier, London, 1989), p. 299.
19. E.A. Reitman, M.L. Kaplan and R.J. Cava, Solid State Ionics, 25, 41 (1987).
20. A.J. Polak, S. Petty-Weeks and A.J. Beuhler, Sensors and Actuators 9, 1 (1980).
21. M.F.Daniel, B. Desbal, J.C. Lassegues, Solid State Ionics 28/30, 632 (1988).
22. M.F.Daniel, B. Desbal, F. Cruege, O. Trinquel and J.C. Lassegues, Solid State Ionics 28/30, 639 (1988).
23. P. Donoso, W. Goreki, C. Berthier, F. Defendini, C. Poinsignon and M. Armand, Solid State Ionics 28/30, 966 (1988).
24. M. Stanier, L.C. Hardy, D.H. Whitmore and D.F. Shriver, J. Electrochem. Soc. 131, 784 (1984).
25. S.A. Hashmi, A. Kumar, K.K. Maurya and S. Chandra, J. Phys. D. Appl. Phys. 23, 1307 (1990).
26. K.K. Maurya, N. Srivastava, S.A. Hashmi and S. Chandra, J. Mat. Sci. 27, 6357 (1992).
27. K.K. Maurya, S.A. Hashmi and S. Chandra, J. Phys. Soc. Jpn. 61, 1709 (1992).

CHAPTER 4

TEMPERATURE DEPENDENCE OF POSITRON LIFETIME, FREE VOLUME, CONDUCTIVITY, IONIC MOBILITY AND NUMBER OF CHARGE CARRIERS IN A POLYMER ELECTROLYTE PEO COMPLEXED WITH NH_4ClO_4

4.1 Introduction

In the previous chapter we have briefly introduced the topic of polymer electrolytes and outlined their structure and physical properties, ionic conductivity and their temperature dependence etc. along with a discussion on the free-volume model and its possible application to the mechanism of ion-transport in polymer electrolytes. In this chapter we are going to discuss the various physical properties of a proton conducting polymer "polyethylene oxide (PEO) complexed with ammonium perchlorate (NH_4ClO_4)" studied by us in the temperature range 300-370 K. These properties include free volume by positron lifetime spectroscopy, ionic conductivity by impedance spectroscopy, ionic mobility by transient ionic current technique, number of charge carriers, dielectric constant etc. The present sample ($\text{PEO}+\text{NH}_4\text{ClO}_4$ with 80:20 weight percentage composition) is essentially a solvent-free polymer-salt complex recently developed by Hashmi et al. [1] with high ionic-conductivity ($\sigma \sim 10^{-5} \text{ S.cm}^{-1}$) at room temperature which is nearly 10^4 times greater than pure PEO. This sample is dominantly a proton or H^+ ion (cation) conductor with a part of the conductivity coming from ClO_4^- (anion) transport in the bulk. The ion transference numbers for H^+ and ClO_4^- ions are ~ 0.085 and \sim

0.08 respectively [1].

Although polymer electrolytes have been subjected to extensive studies, the mechanism of ion-transport in these materials is not yet clearly understood because of the involvement of many factors [2] like the degree of crystallization, relative values of the glass transition temperature (T_g) and the melting temperature (T_m), intrinsic motion of elastomeric phase, degree of dissociation of salts in the complex which controls the number of charge carriers, interfacial effects, ion pair formation etc. It is also known that most of the visco-elastic transport properties of polymers depend strongly on temperature. Efforts have been made to study the temperature dependence of various experimentally accessible parameters e.g. ionic-conductivity, viscosity, ion-diffusion and structural and ionic relaxation rates etc. as a function of temperature to understand the conduction mechanism. The temperature dependence of observed ionic conductivity are mostly described in terms of various empirical expressions including the VTF (eq. 3.4) and WLF (eq. 3.5) relations which we have already discussed in Chapter 3. The simplest is the Arrhenius form which is most appropriate for the thermally activated ionic motions (eq. 3.3).

Attempts were therefore made to understand theoretically the VTF or the WLF relationships and its success in fitting the temperature dependence of ionic-conductivity data [3,4], although very little is known about the underlying microscopic conduction mechanism in the polymer electrolytes. Several models were proposed to explain the temperature dependence of ionic

conductivity for variety of amorphous polymeric electrolytes [2,5,6]. Further, the concept of free volume [7] has been widely used over the last three decades for explaining some of the observed results in polymeric materials [8]. The observed temperature dependence of the electrical conductivity of ion-conducting polymers were also explained in terms of the free-volume theory [2], about which we have already discussed in Chapter 3. Most studies have concluded that ionic transport, which occurs in the amorphous regions of the polymers, is the result of a coupling between the ions and segmental motions of polymer chains given sufficient "free volume" [9-11].

Therefore an explanation [2] for the behaviour of ionic-conductivity (σ) with $1/T$ has been accepted in terms of the somewhat vague statement that the amorphicity (and hence the free volume) increases with temperature and that this leads to an increase in the mobility and hence in the conductivity. It may be pointed out that such an explanation has been accepted even in the absence of any reported (in literature) direct measurement of number of charge carriers n and the mobility μ over a wide temperature range on any specific materials for which the measurements of free volume (usually a difficult measurement) has also been carried out.

In Chapter 1, we have already discussed the usefulness of positron annihilation spectroscopy for studying the free-volume properties of polymeric materials. Although such positron lifetime studies have been performed for a large number of polymers as a function of temperature, pressure, time etc. [12-16], very few are

reported for polymer electrolytes. Peng et al. [17] recently investigated the ionic conductivity of a polymer electrolyte based on poly(ether urethane) networks using positron lifetime studies and obtained a correlation between the fractional free volume present in the material and the observed temperature dependence of conductivity (σ) above the glass transition temperature (T_g). According to them [17], the ionic transport takes place by segmental motion of the polymer chains with associated carrier ions and an increase in the free-volume with temperature will increase the mobility of the carrier ions due to an increase in the segmental motion of the polymer chain. However such correlation cannot be taken for granted due to the absence of any temperature dependence of mobility data in support of their explanation. Therefore, the theoretical explanation of the measured ion transport properties is still not satisfactory.

The electrical conductivity σ in an conducting polymers is expressed in terms of the mobility μ by eq. (3.2). In the eq. (3.2) both cations and anions can contribute towards the total conductivity in polymer electrolytes. Further, n_i and μ_i are found to be temperature (T) dependent. Therefore, in order to understand the behaviour of σ with $1/T$ we have to know:

- (a) variation of n with T ,
- (b) mechanism of generation of mobile carriers,
- (c) variation of μ with T ,
- (d) mechanism of temperature dependence of μ and
- (e) whether the variation in n or μ is the controlling factor ?

In the present work we have tried to address ourselves to

some of these vital questions by choosing the polymer electrolyte polyethylene oxide complexed with NH_4ClO_4 (or $\text{PEO:NH}_4\text{ClO}_4$) on which systematic studies could be performed. The ion transport in this proton conducting polymer electrolyte $\text{PEO:NH}_4\text{ClO}_4$ have already been characterised [1] using optical spectroscopy, XRD, DTA, IR, coulometry, transient ionic current and electrical conductivity studies. In the present chapter we will discuss the results of the following systematic studies on $\text{PEO:NH}_4\text{ClO}_4$ and analyze them to obtain partial answers to some of the vital questions raised above :

- (i) temperature dependence of the bulk electrical conductivity using impedance spectroscopy technique,
- (ii) temperature dependence of mobilities using transient ionic current technique,
- (iii) temperature dependence of the number of mobile charge carriers from the knowledge of the respective values of σ and μ ,
- (iv) temperature dependence of the mean free volume and also their probability density function by positron annihilation technique.

We have carried out all the measurements (i) to (iv) listed above, both above ($T > T_m$) and below ($T < T_m$) the melting temperature T_m because most of the properties are expected to change significantly at T_m . Secondly the choice of the material to be studied had to be guided by the criteria that significantly large changes in the physical properties like σ , n or μ , free volume etc. should be observed. We have shown in Figs. 4.1(a) and (b) the observed behaviour of σ vs $1/T$ reported by various workers

[1,2,18-20] for some H^+ and Li^+ ion-conducting PEO based polymers. It is observed that these polymers (or for that matter all other known ion-conducting polymers) show one of the following types of temperature dependence of σ near T_m : (i) sharp increase in σ at T_m and an Arrhenius-like behaviour above and below T_m as shown by curves A,B,C (Fig. 4.1(a)) and E (Fig.4.1(b)), (ii) no sudden increase in σ at T_m i.e. a curved σ vs $1/T$ plot as shown by curve D (Fig. 4.1(a)) and F (Fig.4.1(b)). Such variation in the ionic conductivities of the polymer electrolytes are generally described by the so called Vogel-Tamman-Fulcher (VTF) and Williams-Landel-Ferry (WLF) equations already discussed in Chapter 3, and (iii) high (but not so sudden) increase in σ at T_m spread over a relatively larger temperature range as shown by curve G (Fig. 4.1(b)). Since our aim was to study the mechanism of the ionic conductivity in the polymer electrolytes and its correlation with the number of charge carriers (n), mobility (μ), free-volume etc., we found it important to choose a system in which distinct and large change in σ with temperature (especially around T_m) is observed. The data collected in Figs. 4.1 (a) and (b) indicate that the system PEO: NH_4ClO_4 (curve B in Fig. 4.1(a)) fulfills this criterion best and hence this material has been chosen for the present study. Further, this polymer electrolyte has already been studied in detail by Hashmi et al. [1]. Their studies of the composition dependence of conductivity [1] have also shown that the 80:20 weight percentage composition of PEO: NH_4ClO_4 has the highest conductivity at room temperature and hence this composition was chosen for the present work.

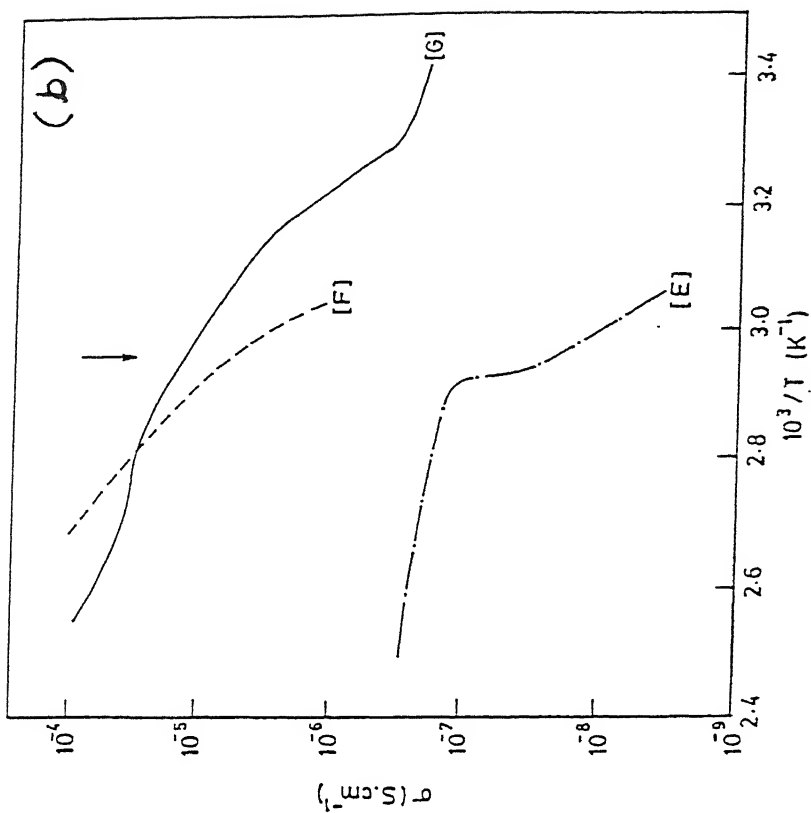
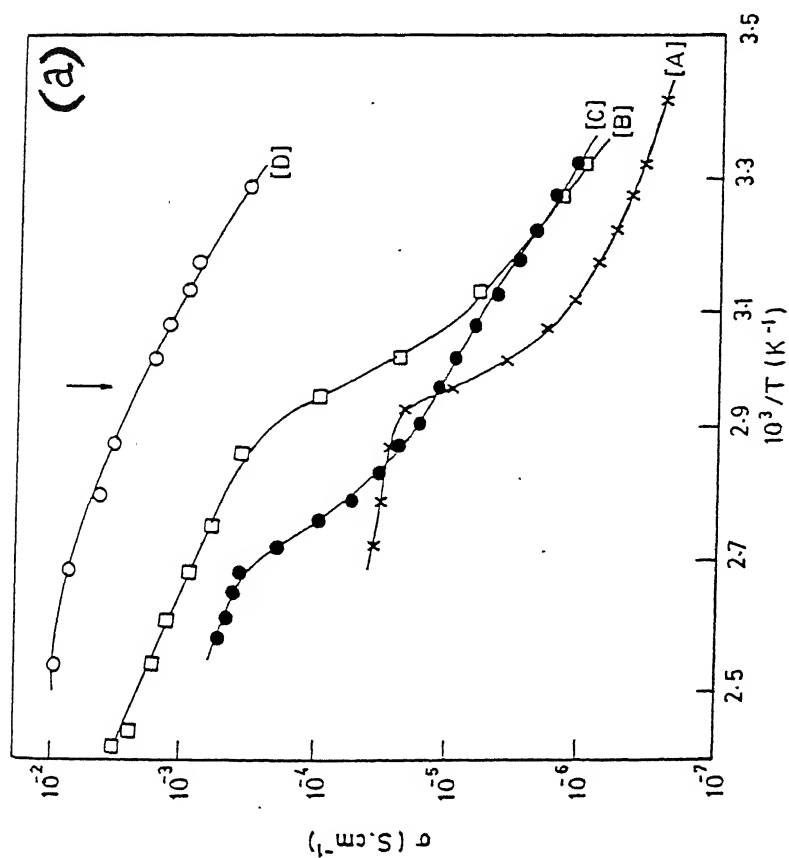


Fig. 4.1 Temperature dependence of conductivity for polyethylene oxide complexed with different

(a) ammonium salts [A] $\text{PEO}:(\text{NH}_4)_2\text{SO}_4$ [Ref. 18]; [B] $\text{PEO}:\text{NH}_4\text{ClO}_4$ [Ref. 11]; [C] $\text{PEO}:\text{NH}_4\text{HSO}_4$ [Ref. 19] and [D] $\text{PEO}:\text{NH}_4\text{I}$ [Ref. 20].
 (b) lithium salts [Ref. 2] [E] $\text{PEO}:\text{LiH}_2\text{PO}_4$; [F] $\text{PEO}:\text{LiSCN}$ and [G] $\text{PEO}:\text{LiClO}_4$. The position indicated by the vertical arrow corresponds to the melting temperature ($T_m \sim 338 \text{ K}$) for pure crystalline PEO.

The results of the present work are described below. The most significant result obtained by us for the present material is that both σ and free volume show rapid increase at $T \approx T_m$. However the increase in the free volume is not associated with an increase in the ionic mobility. In view of this, the changes in the mobility cannot be the primary cause for the variation of σ . On the other hand, the number density n is found to change rapidly at T_m and a suitable dissociation model has been proposed by us to account for this increase in n at T_m . The positron lifetime data have been analyzed to provide a detailed discussion of the free volume and its distribution, hole size etc.

4.2 Experimental

The sample of polyethylene oxide (PEO) complexed with ammonium perchlorate (NH_4ClO_4) under study was prepared in the laboratory of the Department of Physics, Banaras Hindu University, Varanasi, India [1] and the other related characterizations and measurements (except positron lifetime measurements, which were studied by us at Indian Institute of Technology, Kanpur, India) for the samples were also carried out in their laboratory [1,21,22]. However, for the sake of completeness, we will briefly describe the method of sample preparation and the apparatus/methods used for studying the temperature dependence of ionic-conductivity, mobility, dielectric constant etc. which are directly related to the interpretation of our results in the present work.

The sample $\text{PEO:NH}_4\text{ClO}_4$ (80:20 wt. %) was prepared by solution cast technique. Desired amount of PEO ($\text{MW} \sim 6 \times 10^5$) procured from Aldrich and NH_4ClO_4 (obtained from VEB Laborchemie Apolda, Germany) were dissolved in dehydrated methanol and stirred thoroughly. Resulting solution of polymer-salt was poured into polypropylene dishes for casting the films by slow evaporation. Finally, the films were dried under vacuum to eliminate all traces of the solvent. Resulting film ($\sim 300 \mu\text{m}$ thick) was essentially a solvent-free polymer-salt complex of $\text{PEO:NH}_4\text{ClO}_4$.

The experimental arrangement for temperature dependence of conductivity measurement is shown in Fig. 4.2. The temperature of the furnace was monitored by a temperature controller/indicator model-806 (Century Instrument Pvt. Ltd., Chandigarh, India). The electrical conductivity of the $\text{PEO:NH}_4\text{ClO}_4$ sample was measured in the temperature range 300 K to 400 K using vacuum-coated silver electrodes. The complex impedance/admittance plots were obtained using computer-controlled Schlumberger Solartron (1250) frequency response analyzer coupled with a Solartron (1286) electrochemical interface. The temperature dependence of the electrical conductivity was evaluated using the complex impedance/admittance plots [23,24].

The transient ionic current (TIC) measurement technique was used to detect number of different types of mobile ionic species in the bulk and to evaluate their respective mobilities. This technique has been extensively applied by Chandra et al. [23] to proton conductors for similar studies. In this method, the sample was kept between two blocking electrodes and then polarized by

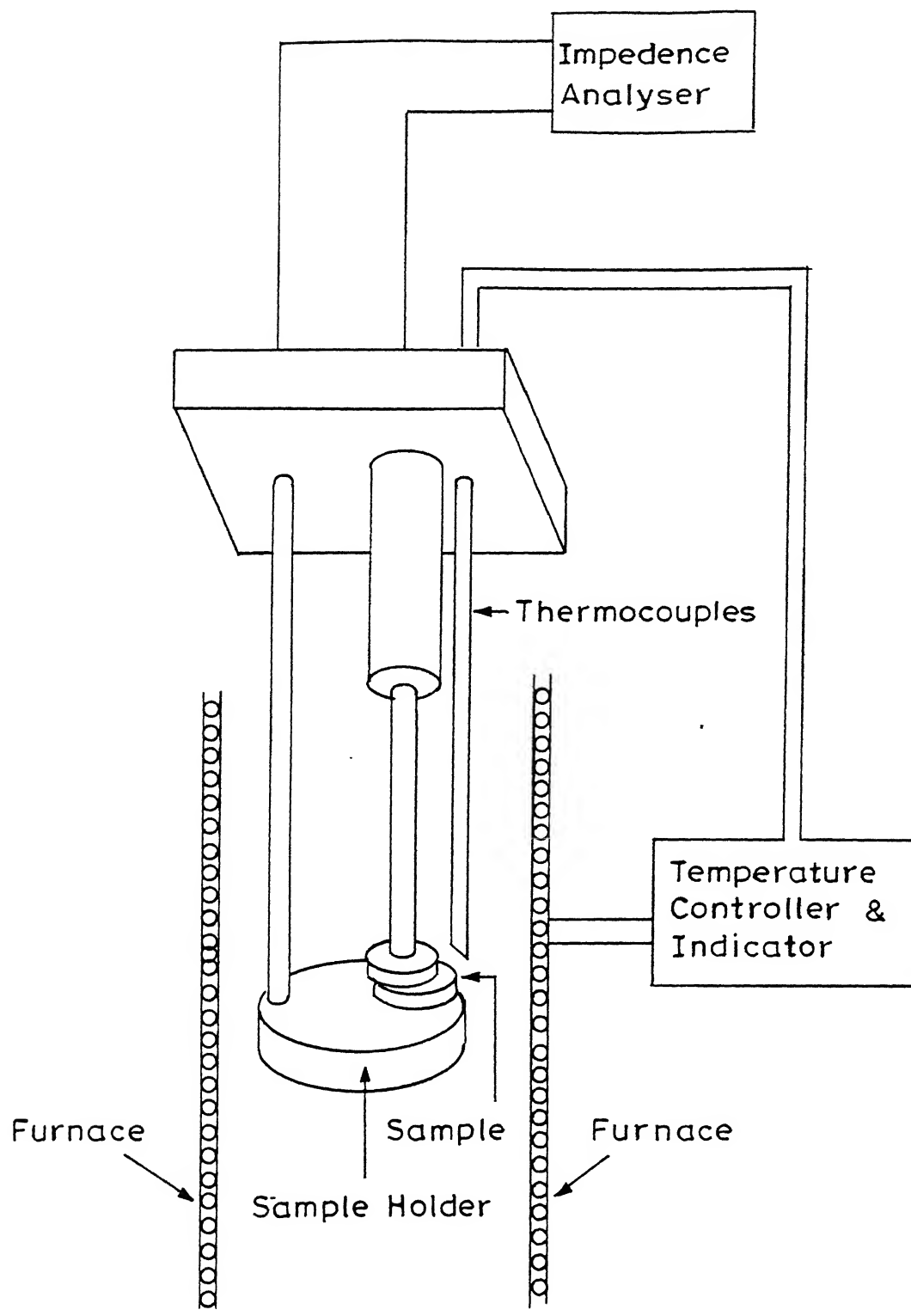


Fig. 4.2 Experimental arrangement for electrical conductivity measurements [taken from Ref. 21].

applying a dc electric field with Ag electrodes as shown in Fig. 4.3 (a). The polarity of the field was then reversed after a certain period of polarization. On reversing the polarity of the applied field, these ionic species start to move in the reverse directions. The transient ionic current was monitored as a function of time after reversing the polarity of the polarising voltage using a X-Y-t recorder (Riken Denshi Model D-BF). Since the different ions have different mobilities, they will reach their counter electrodes at different times giving peaks in the current vs time plots as shown in Fig. 4.3(b). The number of peaks corresponds to the number of mobile ionic species. The mobility, μ , of mobile ionic species was calculated using the formula [21]

$$\mu = \frac{d^2}{t.V} \quad (4.1)$$

where d is the thickness of the sample, V is the voltage applied and t is time of flight corresponding to the current maxima.

The variation of dielectric constant of the sample with temperature was also measured. These data were needed for the interpretation of some of the results described later in this chapter. The dielectric constant was calculated from the ratio of the measured capacitance with and without dielectric (polymeric film). The capacitance was measured by using a capacitance meter (Boonton Electronics, Model 72B). The frequency of 1MHz was chosen to avoid relaxation effects of double layer or electrode-electrolyte interface.

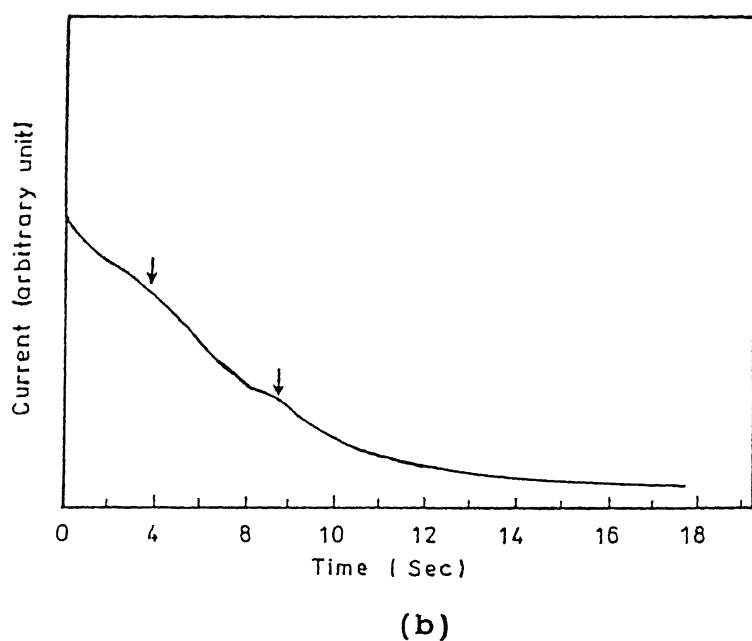
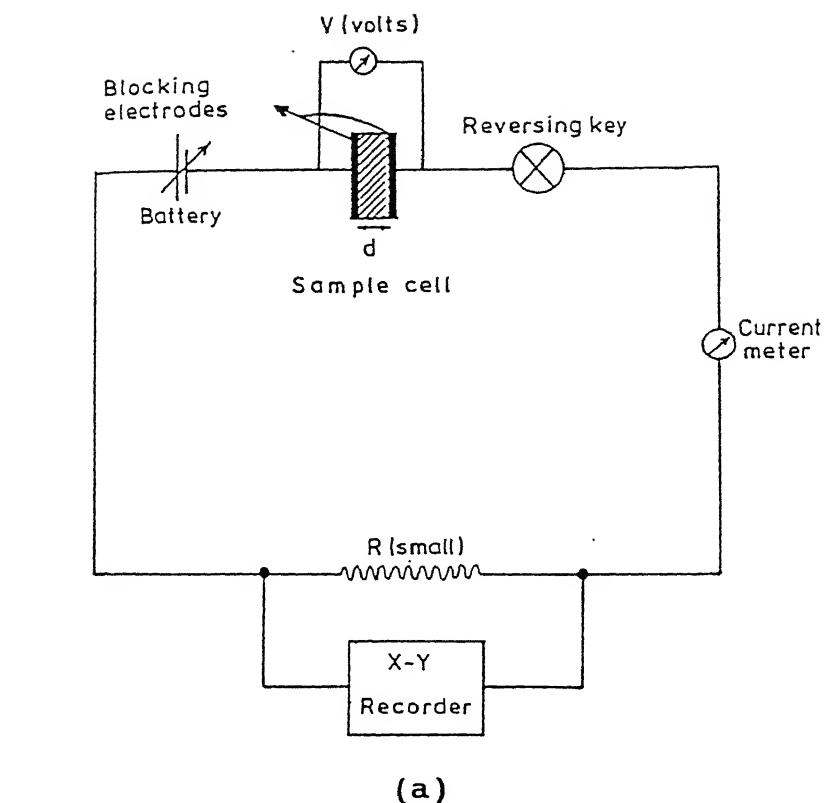


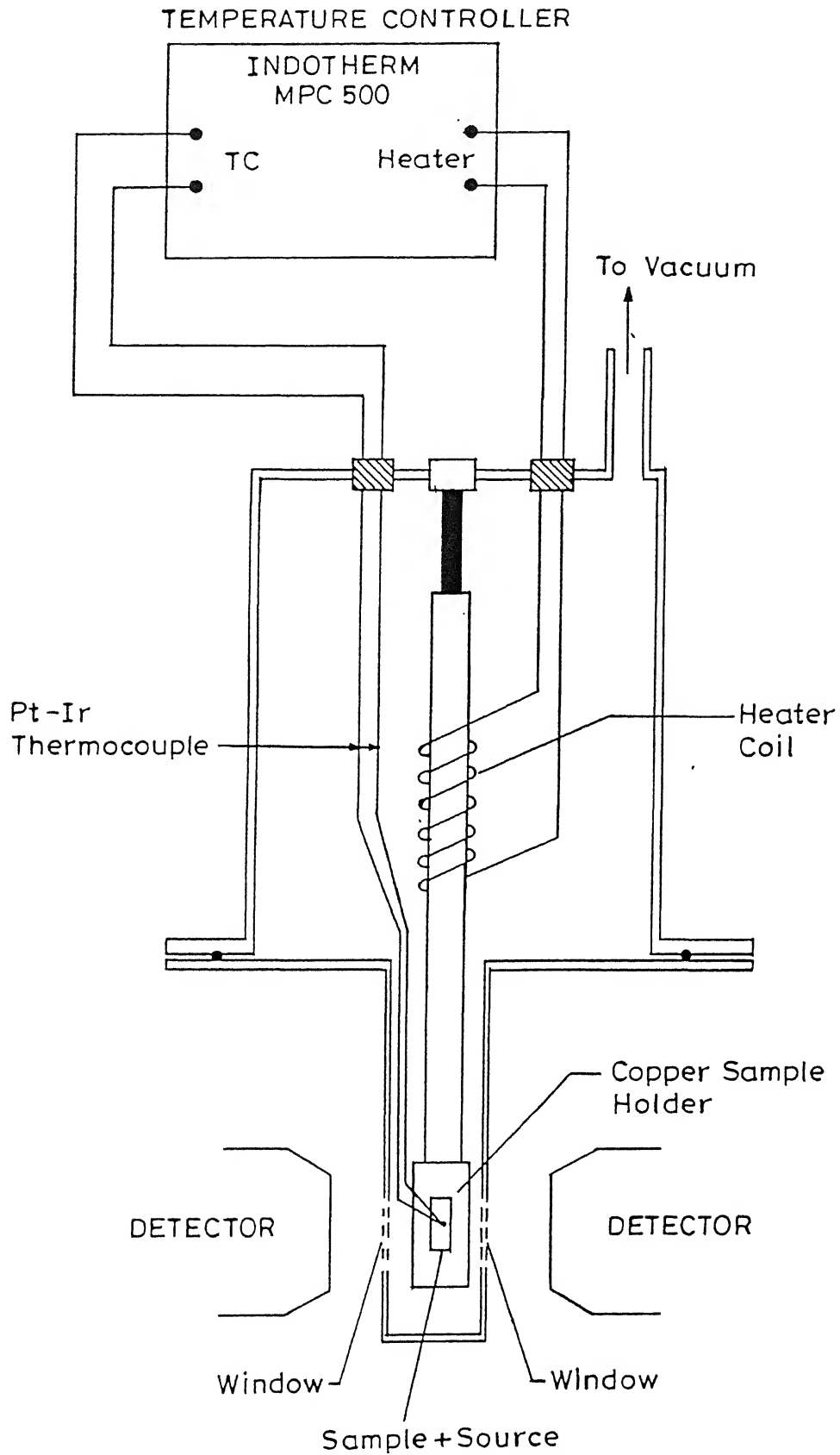
Fig. 4.3 (a) Experimental arrangement for transient ionic current technique for mobility measurement. (b) A typical transient ionic current vs time plot of PEO: NH_4ClO_4 system [taken from Ref. 21].

Positron lifetime measurements were carried out in our laboratory at Indian Institute of Technology, Kanpur at room temperature using a conventional fast-fast coincidence spectrometer already discussed in Chapter 2. The source of positron (about $15\mu\text{Ci}$ of $^{22}\text{NaCl}$) was sandwiched between two identical specimens of the sample. Polymer electrolyte films were stacked to prepare specimens of about 1 mm thickness. The typical time resolution of our spectrometer was 0.32 ns (FWHM) as measured by the prompt spectrum from ^{60}Co source. For measuring the temperature dependence of positron lifetime spectra, the source-sample assembly was placed inside a specially designed cell (Fig. 4.4) and the temperature of the cell were controlled using a microprocessor-based programmable temperature controller (Indotherm MPC 500) with an accuracy of ± 1 K. The lifetime spectra were measured in the temperature range 298 K to 353 K in steps of about 5K both during the heating and the cooling cycle. A total of about 5×10^6 counts were recorded under each lifetime spectrum. Prompt spectra were taken regularly to monitor the instrumental stability.

The measured lifetime spectra were analyzed in two ways. In the first method the lifetime spectra were subjected to a least-squares fitting procedure using the computer program PATFIT (see chapter 2). Our analysis showed that best $\chi^2 (< 1.1)$ and most acceptable standard deviations were obtained when each spectrum is fitted in terms of three lifetime components. In our analysis we have constrained τ_1 to 0.13 ns in order to obtain a result for τ_2 , I_1 and I_2 [26]. It may be mentioned that we have also carried out

Positron lifetime measurements were carried out in our laboratory at Indian Institute of Technology, Kanpur at room temperature using a conventional fast-fast coincidence spectrometer already discussed in Chapter 2. The source of positron (about $15\mu\text{Ci}$ of $^{22}\text{NaCl}$) was sandwiched between two identical specimens of the sample. Polymer electrolyte films were stacked to prepare specimens of about 1 mm thickness. The typical time resolution of our spectrometer was 0.32 ns (FWHM) as measured by the prompt spectrum from ^{60}Co source. For measuring the temperature dependence of positron lifetime spectra, the source-sample assembly was placed inside a specially designed cell (Fig. 4.4) and the temperature of the cell were controlled using a microprocessor-based programmable temperature controller (Indotherm MPC 500) with an accuracy of ± 1 K. The lifetime spectra were measured in the temperature range 298 K to 353 K in steps of about 5K both during the heating and the cooling cycle. A total of about 5×10^6 counts were recorded under each lifetime spectrum. Prompt spectra were taken regularly to monitor the instrumental stability.

The measured lifetime spectra were analyzed in two ways. In the first method the lifetime spectra were subjected to a least-squares fitting procedure using the computer program PATFIT (see chapter 2). Our analysis showed that best $\chi^2 (< 1.1)$ and most acceptable standard deviations were obtained when each spectrum is fitted in terms of three lifetime components. In our analysis we have constrained τ_1 to 0.13 ns in order to obtain a result for τ_2 , I_1 and I_2 [26]. It may be mentioned that we have also carried out



ig. 4.4 Experimental arrangement for temperature dependence of ositron lifetime measurements.

an analysis by removing the constraint on the value of τ_1 . This analysis yielded a value of τ_1 in the range $\tau_1 = 0.10-0.14$ ns while the values of τ_3 (lifetime of present interest) and I_3 showed a typical deviation that was less than 5% from the values obtained by fixing $\tau_1 = 0.13$ ns. The accompanying effect on the free-volume hole radius (see next section) was also found to be less than 5%. In view of this we have constrained τ_1 to 0.13 ns.

Our second method of analysis involved determination of the annihilation rate probability distribution function (PDF) $\lambda\alpha(\lambda)$ versus λ (annihilation rate) using the computer program CONTIN already discussed in Chapter 2. In the present analysis using the CONTIN program we used the annihilation rate $\lambda = 9.1 \text{ ns}^{-1}$ from well-annealed and high-purity (99.99+ %) nickel as a reference while a total of 85 grid points over the range $0.25 < \lambda < 13 \text{ ns}^{-1}$ were used.

4.3 Results and discussions

As mentioned earlier, the sample $\text{PEO:NH}_4\text{ClO}_4$ has already been characterized and studied in detail by Hashmi et al. [1] for different percentage composition of NH_4ClO_4 . A tentative phase diagram [21] based upon the DTA studies is shown in Fig. 3.3. From the figure, it is obvious that apart from $(\text{PEO})_{\text{crystalline}}$ and $(\text{PEO})_{\text{amorphous}}$ phases, there are also phases related to $(\text{PEO})_{\text{crystalline complex}}$ and its melting. For the present sample $(\text{PEO:NH}_4\text{ClO}_4$ with 80:20 wt. % composition) two endothermic peaks at $T_{m_1} = 339 \text{ K}$ and $T_{m_2} = 329 \text{ K}$ were observed in the measured

differential thermal analysis spectrum [24] corresponding to the melting temperature of the pure crystalline PEO and crystalline complex material respectively.

4.3.1 Positron lifetimes, free volume and related distribution functions

We shall first present our results obtained from the positron lifetime spectroscopy. Typical positron lifetime spectra at two different temperatures measured by us for the present sample is shown in Fig. 4.5. The positron lifetime spectra measured for the PEO:NH₄ClO₄ (80:20 wt %) at room temperature were first analysed by the PATFIT computer program and each of the lifetime spectrum measured in the temperature range 298 - 353 K showed the presence of three lifetimes: $\tau_1 = 0.13$ ns, ($I_1 = 39 - 44$ %), $\tau_2 = 0.41 - 0.44$ ns ($I_2 = 44 - 50$ %) and $\tau_3 = 1.6 - 2.4$ ns (10 - 12%) where the range of values of the intensities (I) is given in brackets. It is generally believed that the lifetime $\tau_1 = 0.13$ ns arises mostly due to the annihilation of singlet Ps (or p-Ps) while the second lifetime $\tau_2 = 0.41 - 0.44$ ns arises from the free (or unbound) annihilation of positrons. The longest or the third lifetime $\tau_3 = 1.6 - 2.4$ ns is due to triplet Ps (or o-Ps) annihilation. In the case of present results I_1 is much larger than $I_3/3$ and this suggests that the I_1 component receives contributions from p-Ps as well as other modes of annihilation.

Following earlier approach [27-29], and assuming spherical shapes for the free volumes holes we make use of the semiempirical relationship given by eq. (1.17) to determine the free volume hole radius R from the observed lifetime τ_3 (for details see

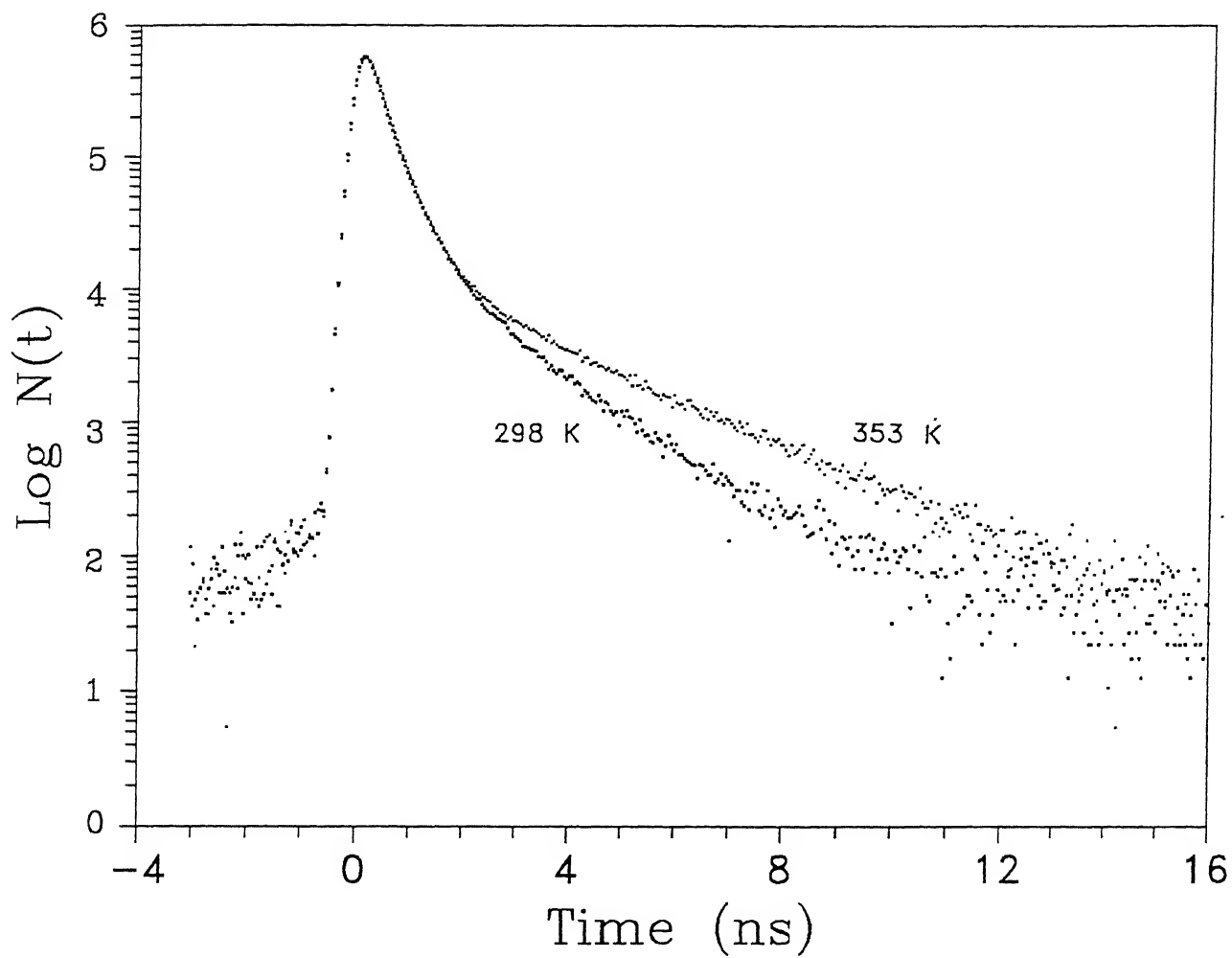


Fig. 4.5 Positron lifetime spectra at two different temperatures in $\text{PEO:NH}_4\text{ClO}_4$ (80:20 wt %).

Chapter 1). The values of τ_3 evaluated by the PATFIT program and the values of R calculated from eq. (1.17) are shown in Table 4.1 along with τ_2 and the values of intensities (I_i , $i = 1, 2, 3$ and $I_1 + I_2 + I_3 = 100$). The temperature dependence of τ_2 , I_1 and I_2 are plotted in Fig. 4.6. The temperature dependence of τ_3 and I_3 are plotted separately in Figs. 4.7 and 4.8 respectively, where the variation with $1/T$ is plotted because other physical properties of polymer electrolytes are usually described as a function of $(1/T)$. The values of R calculated from τ_3 were also used to obtain the hole volume $V_f = 4\pi R^3/3$, and the variation in the value of V_f (see right axis) is also shown in Fig. 4.7.

From the Fig. 4.6, we find that τ_2 as well as I_1 and I_2 do not show any significant variation over the temperature range 298 - 339 K. Above the melting temperature (T_{m2}) of crystalline PEO the values of τ_2 and I_2 drops slightly and the value of I_2 changed (increased in this case) by almost the same amount as that of I_1 . It may be noted that intensities are connected by $I_1 + I_2 + I_3 = 100\%$ and hence change in any of the intensities is also going to affect the others. Small changes that occur in the values of τ_2 , I_1 and I_2 above T_{m2} is due to the change in the physical state of the material (i.e. semicrystalline state changes to amorphous state above T_{m2}) in which the positrons are annihilating. Since our main interest lies in the study of free volume properties related to the values of τ_3 and I_3 for the present sample, we are not going to discuss the lifetime parameters τ_2 , I_1 and I_2 and their temperature variations any further.

Our results of τ_3 versus $1/T$ (Fig. 4.7 and Table 4.1) show an

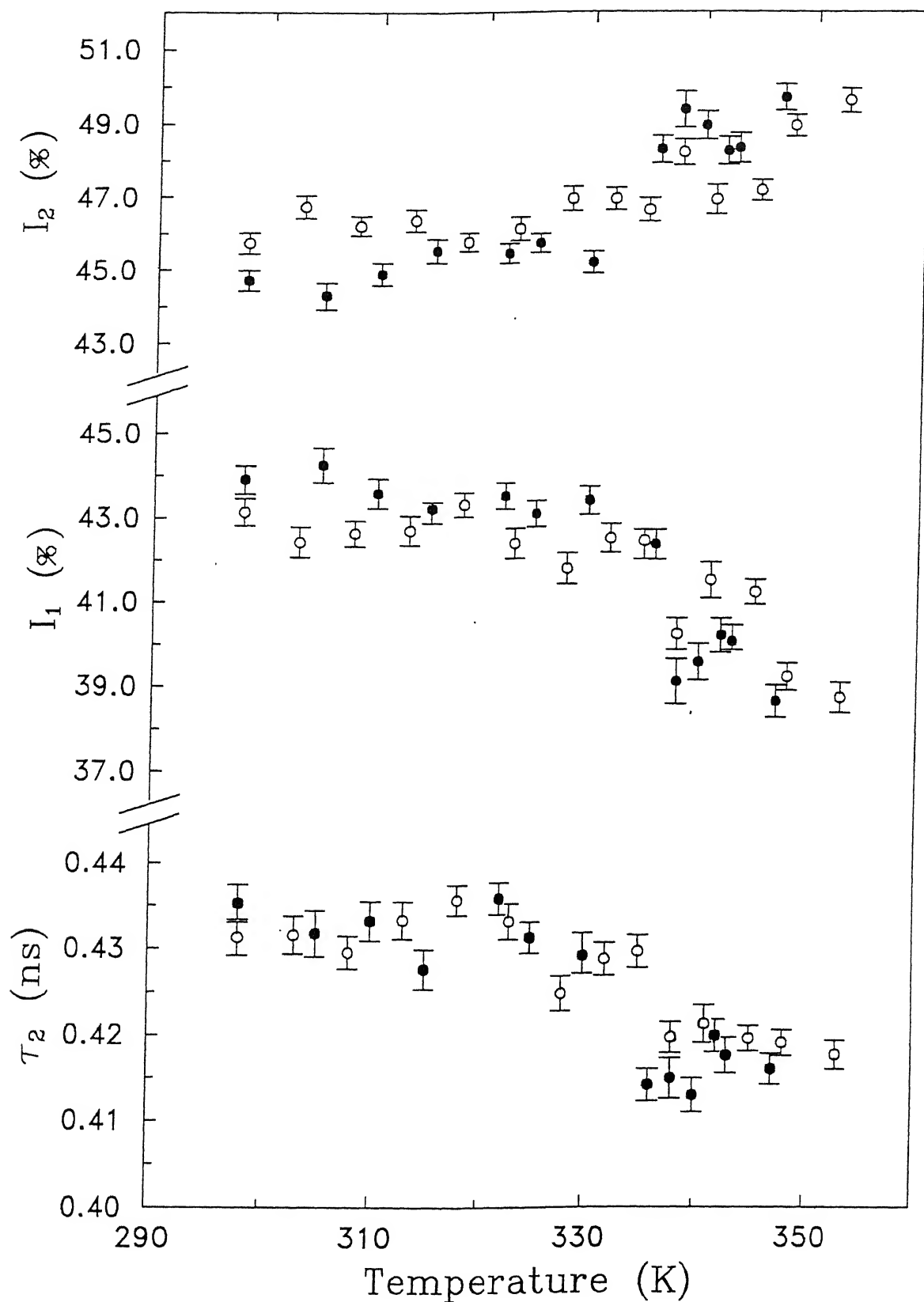


Fig. 4.6 Temperature variation of positron lifetime parameters τ_2 , I_1 and I_2 in PEO:NH₄ClO₄ (80:20 wt %). Open symbols describe the data for increasing temperature, while solid symbols

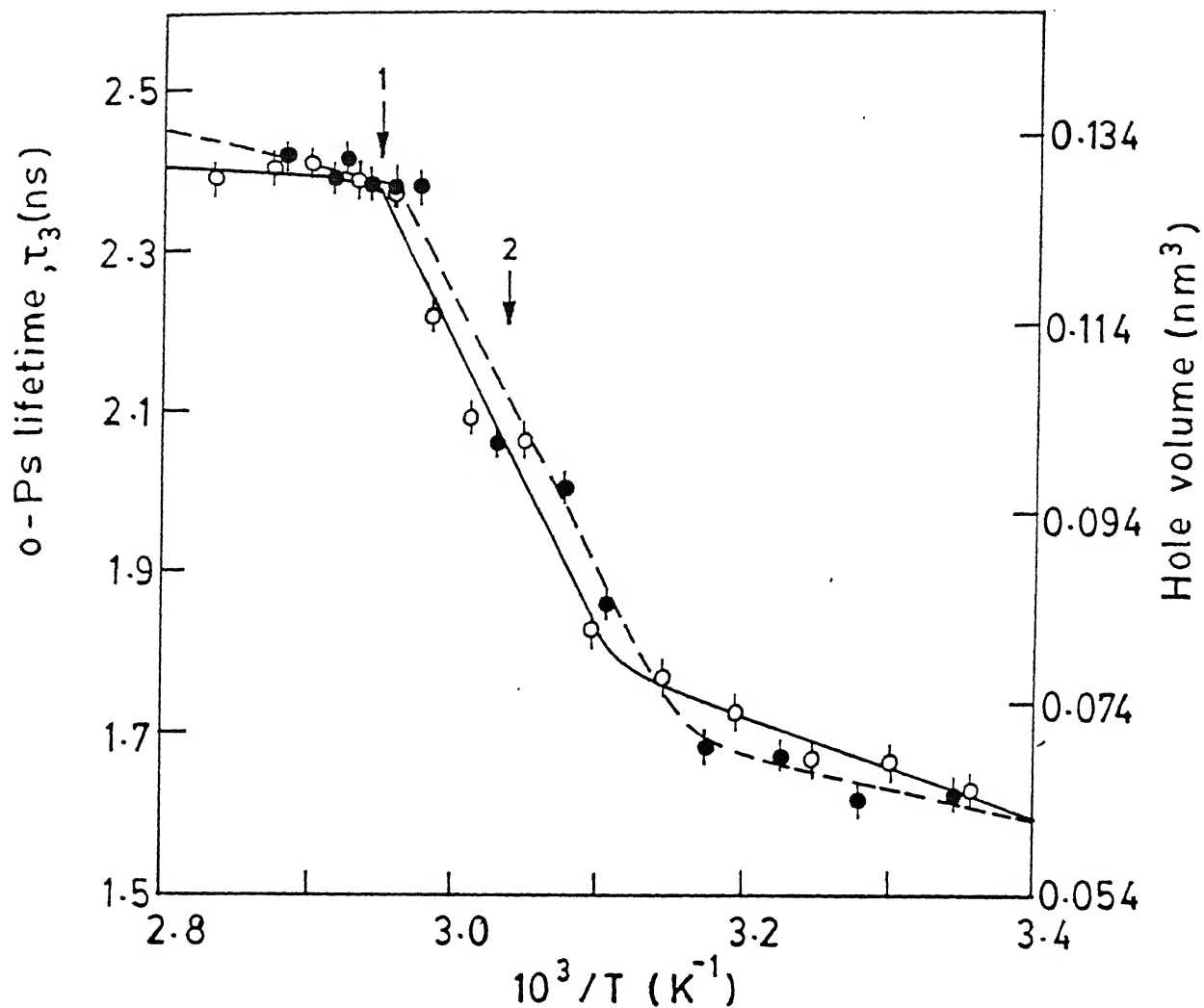


Fig. 4.7 Temperature dependence of o-Ps lifetime, τ_3 , in polyethylene oxide complexed with ammonium perchlorate ($\text{PEO:NH}_4\text{ClO}_4$) (80:20 wt %). Positions indicated by the arrows 1 and 2 correspond to the melting temperatures of uncomplexed PEO ($T_{m1} \sim 339 \text{ K}$) and crystalline complexed material ($T_{m2} \sim 239 \text{ K}$) [Ref. 21]. Open symbols describe the data for increasing temperature, while solid symbols describe the data for decreasing temperature.

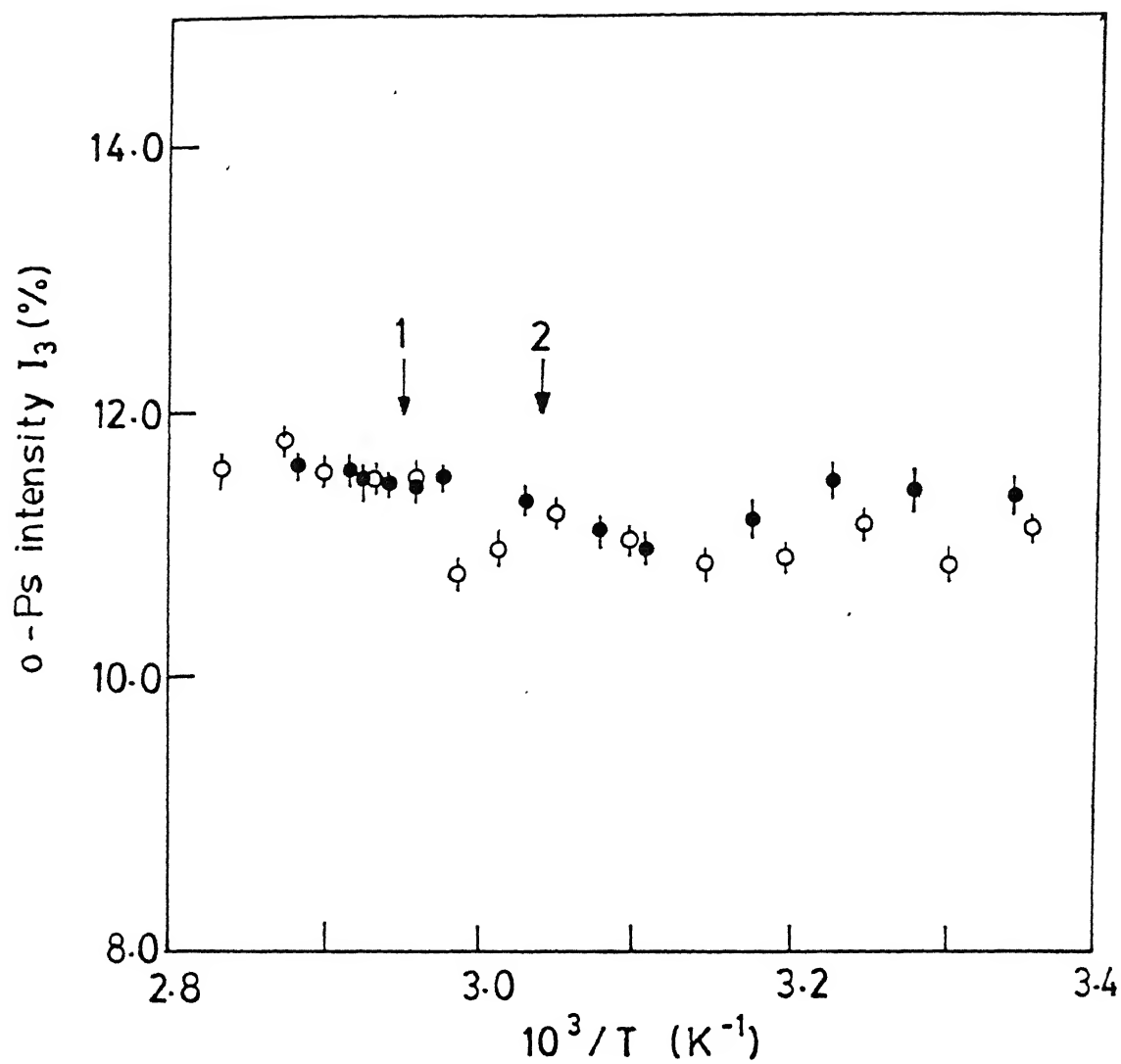


Fig. 4.8 Same as Fig. 4.7, but for the temperature dependence of o-Ps lifetime intensity, I_3 .

increase in τ_3 with temperature leading to an increase in the radius of the free-volume hole (in which o-Ps is annihilating) with temperature. However the variation in τ_3 is not linear with temperature. Initially the rate of increase in τ_3 with temperature is small in the range 298 to 320 K. This small increase in τ_3 (or the hole volume) is in accordance with the normal thermal expansion of the free volume holes [30]. Above 320 K, τ_3 increased at a much faster rate with further increase in the temperature. The change in the slope of τ_3 versus $1/T$ plot around 320 K is an indicative of the onset of a phase transformation. As mentioned earlier, the DTA spectrum [21] showed two endothermic peaks at $T_{m1} = 339$ K and $T_{m2} = 329$ K corresponding to the melting of the uncomplexed PEO and crystalline complexed material. In other words the change in the behaviour of the τ_3 versus $1/T$ plot over the temperature range 320 - 340 K corresponds to the gradual transformation of the material from semicrystalline to amorphous phase which resulted in the increase of free volume hole radius quite rapidly over this temperature range. This observed behaviour conforms to the known behaviour of free volume in the polymers [30]. Above 340 K the material actually softens and the value of τ_3 show a saturation. We also notice that τ_3 almost followed the same course during the heating and the cooling cycles, which further suggest that the whole process is almost reversible within the range of temperatures measured.

Although we have observed a large variation in τ_3 (or the free-volume hole size) with temperature (Fig. 4.7), the values of I_3 (Fig. 4.8) do not show any significant variation in

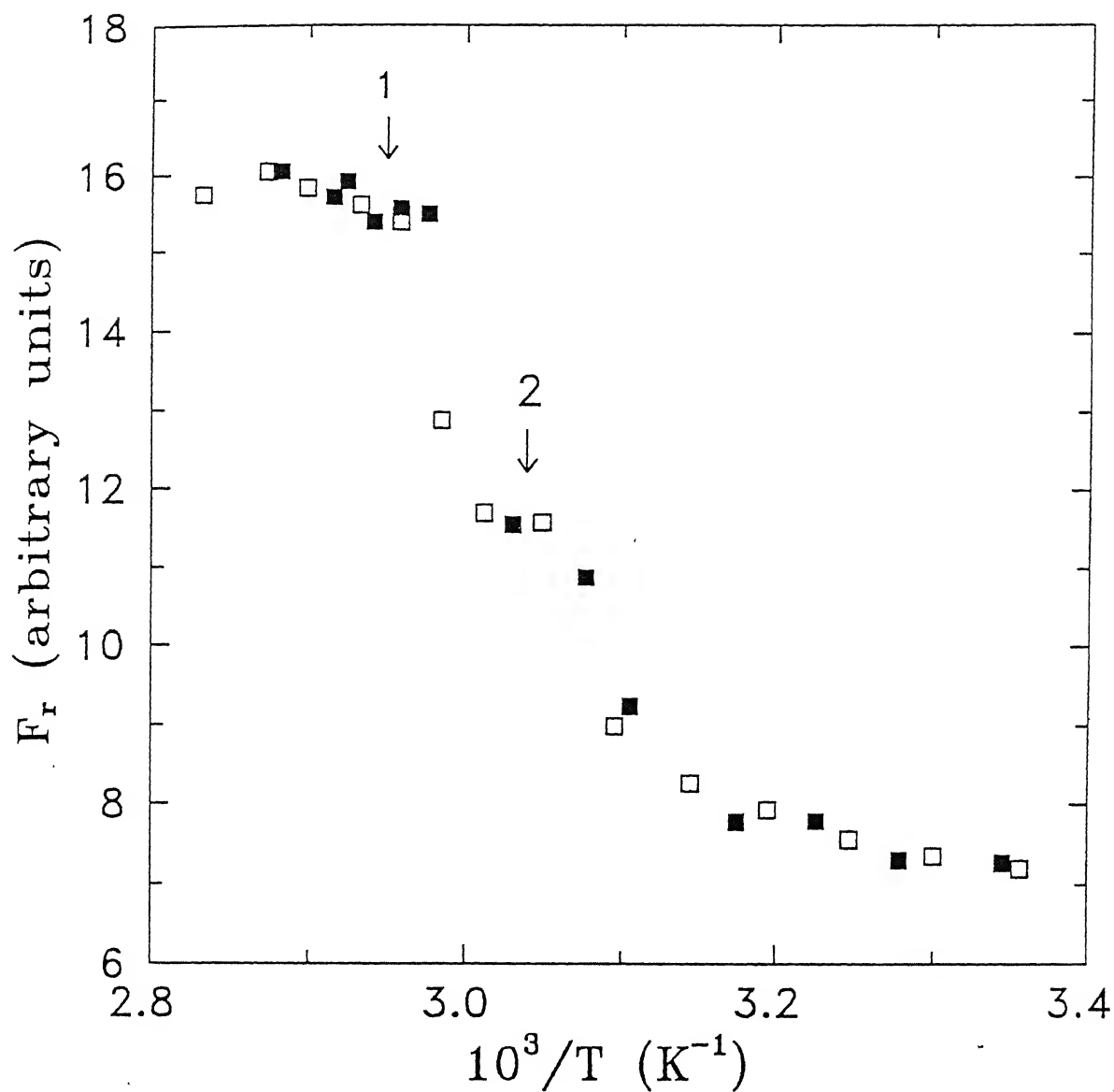
the entire temperature range of 298 to 353 K. This may suggest that the free-volume hole-density in the sample remained constant over the temperature range of 298 to 353 K for which I_3 is almost constant.

The total free volume available in a polymer is determined by the hole volume as well as the density (number of free-volume sites) of the holes although the dependence of these two factors is not separately understood. According to the Ps-hole theory the probability of o-Ps formation is related to the fraction of free-volume hole space, F_v , in a polymer [16,31]. A simple semiempirical equation has been proposed [16,31] for F_v ,

$$F_v = AI_3V_f \quad (4.2)$$

where I_3 is the o-Ps intensity and V_f is the hole volume and A is a parameter (for the particular material) to be determined. In the present case, I_3 is observed to be basically constant with temperature (Fig.4.8) and application of eq. (4.2) shows that F_v is almost proportional to V_f and hence should show a temperature dependence similar to that exhibited by V_f in Fig. 4.7. Moreover, in the present case we do not know the parameter A , and only a relative free volume fraction, F_r ($= I_3V_f$) [17] can be calculated by assuming $A=1$ and the temperature variation of F_r is shown in Fig. 4.9. The relative changes in the total free-volume fraction present in the sample should, therefore, be approximately represented by that of F_r .

On the other hand Ito et al. [33] have argued that both the chemical factor (e.g. electron affinities) and the physical factor



g. 4.9 Temperature dependence of relative fractional free volume F_r in PEO: NH_4ClO_4 (80:20 wt %). Positions indicated by 1 and 2 correspond to melting temperatures of uncomplexed PEO ($T_{m1} \sim 339$ K) and crystalline complexed material ($T_{m2} \sim 239$ K). Open symbols describe the data for increasing temperature, while solid symbols describe the data for decreasing temperature.

(e.g. hole size distribution) determine the o-Ps intensity or I_3 -values in polymers. In the present sample the chemical factor does not change and I_3 is observed to remain almost constant with temperature. The physical factor can control I_3 through the hole volume size and the hole density. The present results (Fig. 4.7) already indicate a variation of the hole volume size with temperature but no corresponding variation in I_3 with temperature. Unless the effects of hole volume size and hole density on I_3 cancel out, we can interpret the constancy of I_3 as well as the low Ps yield to mean that I_3 -values in the present case are determined by the chemical factor. If this is true then the present results for I_3 may not offer much information about the hole density. If it is assumed that hole density does not change with temperature, we can conclude that the observed increase in the hole size with temperature (Fig.4.7) will lead to proportional increase in total free volume. Similar conclusion based on the interpretation of eq. (4.2) was arrived in the last paragraph. It is interesting to note that Peng et al. [17] have interpreted their positron lifetime results for PEU-LiClO₄ above T_g by proposing that the increase in total free volume with temperature arises out of the growth in hole size rather than an increase in number of holes. Recently Jean [16] has reviewed our present understanding of the applications of positron annihilation spectroscopy to the study of hole size, content, distribution and anisotropic structure in polymers and has posed several questions that need to be answered before a more comprehensive understanding is reached.

By analyzing the measured positron lifetime spectra with the CONTIN program we have been able to determine of positron lifetime probability density function, $\lambda^2\alpha(\lambda)$, and our results for some representative temperatures are shown in Fig. 4.10 (a) and (b) during the increasing and decreasing temperatures respectively. Using the CONTIN results the mean positron lifetimes and intensities ($\bar{\tau}_i$ and \bar{I}_i , $i = 1 - 3$) have also been obtained with the help of the formulae [34]

$$\bar{\tau}_i = \int_{\tau_a}^{\tau_b} \alpha_i \lambda_i^2 \tau_i d\tau_i / \int_{\tau_a}^{\tau_b} \alpha_i \lambda_i^2 d\tau_i \quad (4.3)$$

and

$$\bar{I}_i = \int_{\tau_b}^{\tau_a} \alpha_i \lambda_i^2 d\tau_i \quad (4.4)$$

and their values are given in Table 4.2. We note that there is a good agreement between the peak positions of the three peaks resolved by the CONTIN program (Table 4.2) with those obtained by the PATFIT program (Table 4.1). The expanded profiles of the extreme right peaks (corresponding to τ_3) in Fig. 4.10 (a) and (b) are shown in Fig. 4.11 (a) and (b) to present the o-Ps lifetime distributions PEO:NH₄ClO₄ (80:20 wt. %) at different temperatures.

Following Jean and Deng [35] we have defined the free-volume hole-radius probability density function, $f(R)$; as probed by Ps,

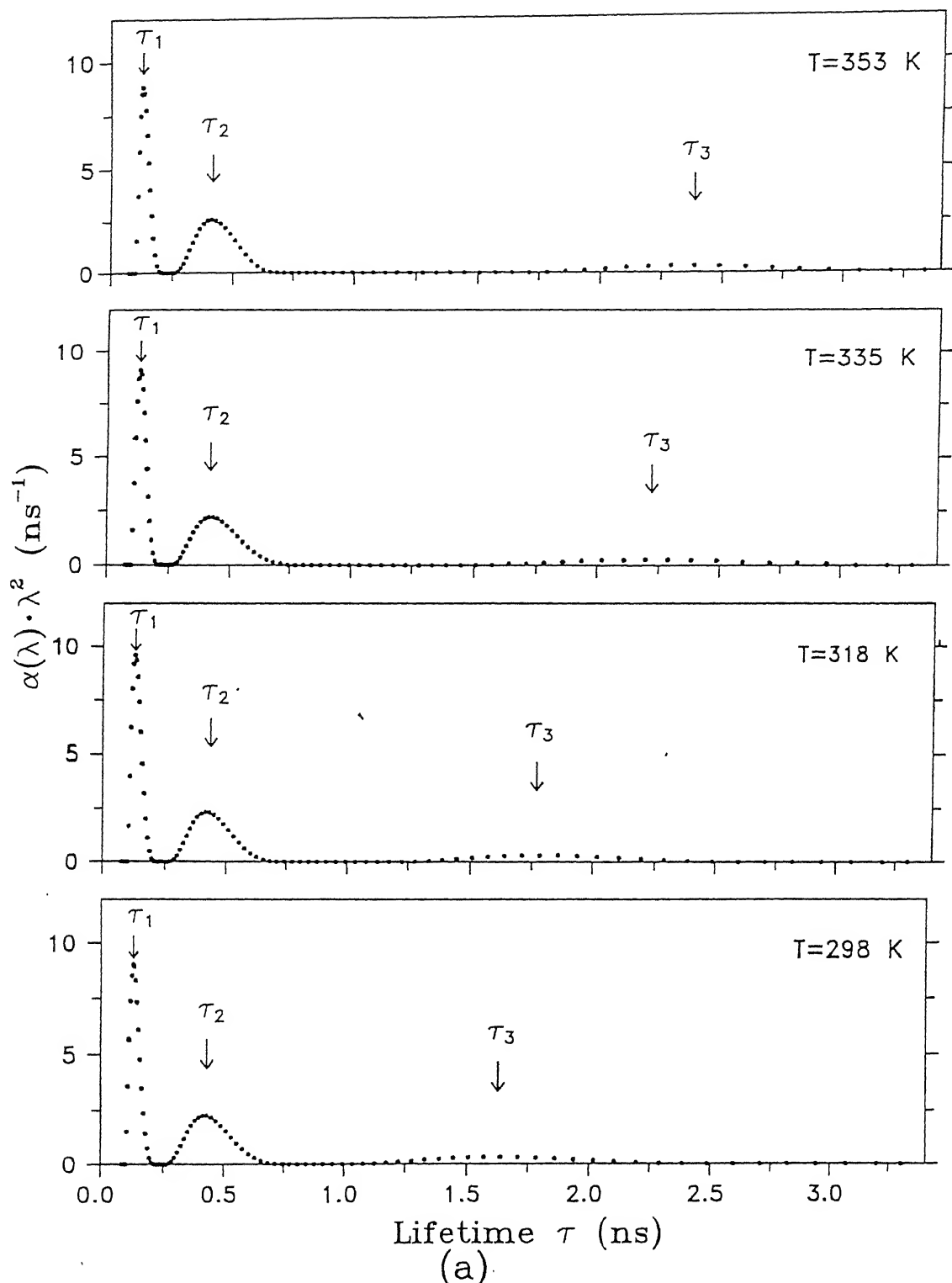
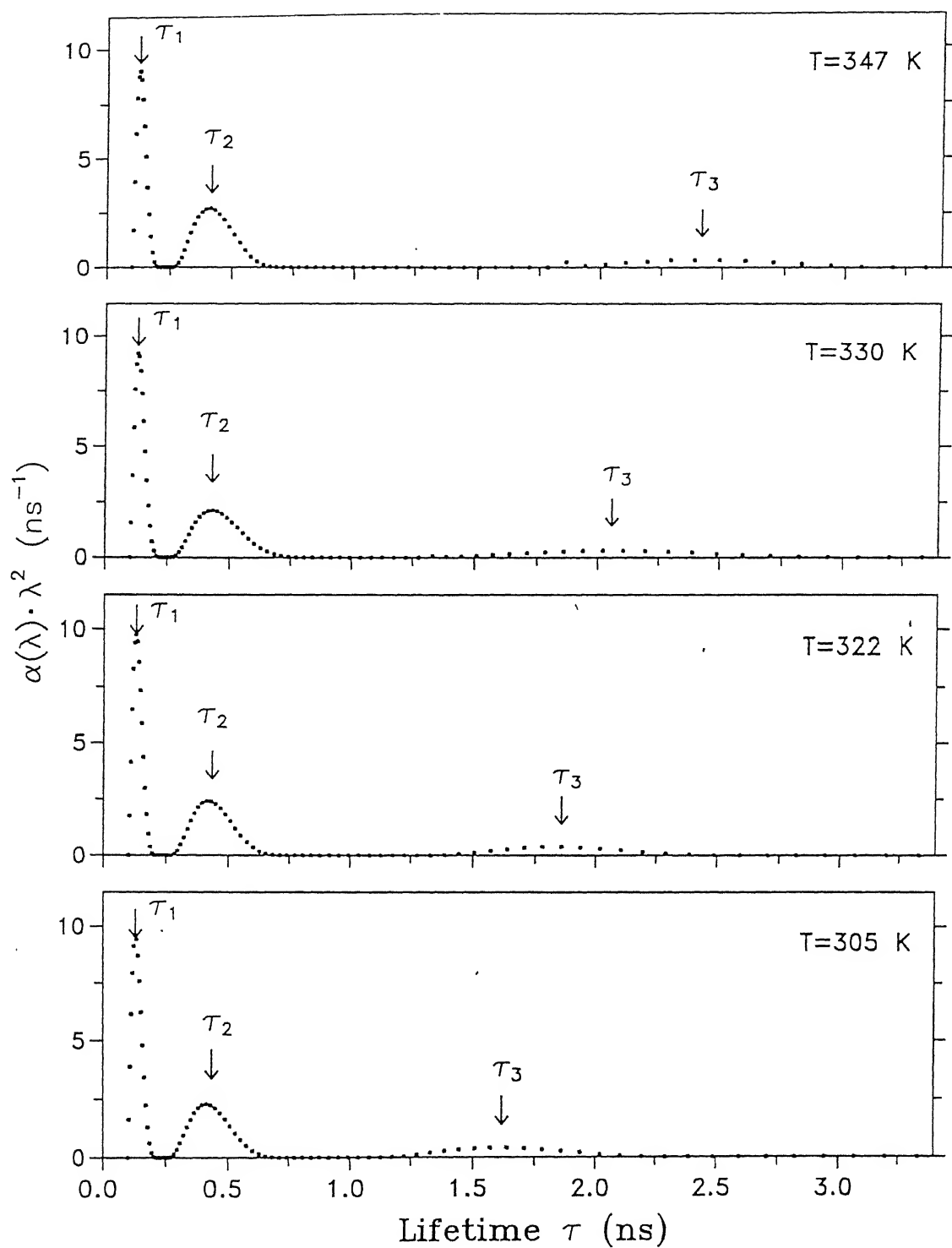


Fig. 4.10 Positron lifetime distribution functions in PEO: NH_4ClO_4 (80:20 wt %) at some representative temperatures during the (a) increasing and (b) decreasing temperature obtained from CONTIN analysis. The positions corresponding to the lifetime values τ_1 , τ_2 and τ_3 obtained from PATFIT analysis (Table 4.1) are shown by arrows.

(Continued on the next page)



(b)

Fig. 4.10 (Continued)

TABLE 4.2

Temperature dependence of mean positron lifetime parameters in polymer electrolyte PEO:NH₄ClO₄ (80:20 wt %) obtained from the **CONTIN** analysis.

Temperature T (K)	$\bar{\tau}_1$ (ns)	$\bar{\tau}_2$ (ns)	$\bar{\tau}_3$ (ns)	\bar{I}_1 (%)	\bar{I}_2 (%)	\bar{I}_3 (%)	\bar{R}^c (Å)
298±2 ^a	0.136	0.434	1.680	43.26	45.64	11.10	2.54
298±2 ^b	0.136	0.424	1.623	43.89	44.50	11.61	2.48
303±2 ^a	0.136	0.437	1.689	43.09	46.27	11.13	2.55
305±2 ^b	0.136	0.413	1.623	43.61	44.68	11.71	2.48
308±1 ^a	0.136	0.427	1.698	42.48	46.53	10.99	2.56
310±1 ^b	0.136	0.411	1.674	43.12	45.34	11.54	2.54
313±1 ^a	0.135	0.441	1.761	42.94	46.33	10.73	2.63
315±1 ^b	0.134	0.423	1.703	42.93	45.99	11.19	2.57
318±1 ^a	0.135	0.430	1.806	43.41	45.83	10.77	2.67
322±1 ^b	0.134	0.431	1.850	43.70	45.29	11.01	2.72
323±1 ^a	0.132	0.418	1.826	43.33	45.52	10.15	2.69
325±1 ^b	0.132	0.424	1.940	43.75	45.59	11.31	2.80
328±1 ^a	0.134	0.427	2.041	42.41	46.37	11.22	2.89
330±1 ^b	0.136	0.434	2.040	43.70	45.04	11.21	2.89
332±1 ^a	0.136	0.440	2.120	42.70	46.47	10.83	2.95
335±1 ^a	0.135	0.439	2.205	42.04	47.27	11.60	3.04
336±1 ^b	0.138	0.418	2.414	41.73	47.73	11.40	3.24
338±1 ^a	0.140	0.430	2.362	41.28	47.19	11.54	3.17
338±1 ^b	0.133	0.419	2.418	39.08	49.41	11.51	3.21
340±1 ^b	0.137	0.423	2.415	39.94	48.53	11.53	3.21
340±1 ^a	0.133	0.433	2.415	42.68	46.14	11.18	3.21
342±1 ^b	0.132	0.431	2.414	40.41	48.09	11.50	3.21
343±1 ^b	0.138	0.424	2.381	40.59	47.89	11.52	3.18
345±1 ^a	0.134	0.428	2.400	42.33	46.21	11.47	3.20
347±1 ^b	0.139	0.412	2.398	40.10	48.29	11.61	3.20
348±1 ^a	0.129	0.426	2.388	39.67	48.65	11.68	3.19
353±1 ^a	0.134	0.423	2.363	39.69	48.78	11.53	3.17

^a increasing temperature

^b decreasing temperature

^c \bar{R} are the mean free-volume hole radii obtained by using $\bar{\tau}_3$ and eq. (1.17).

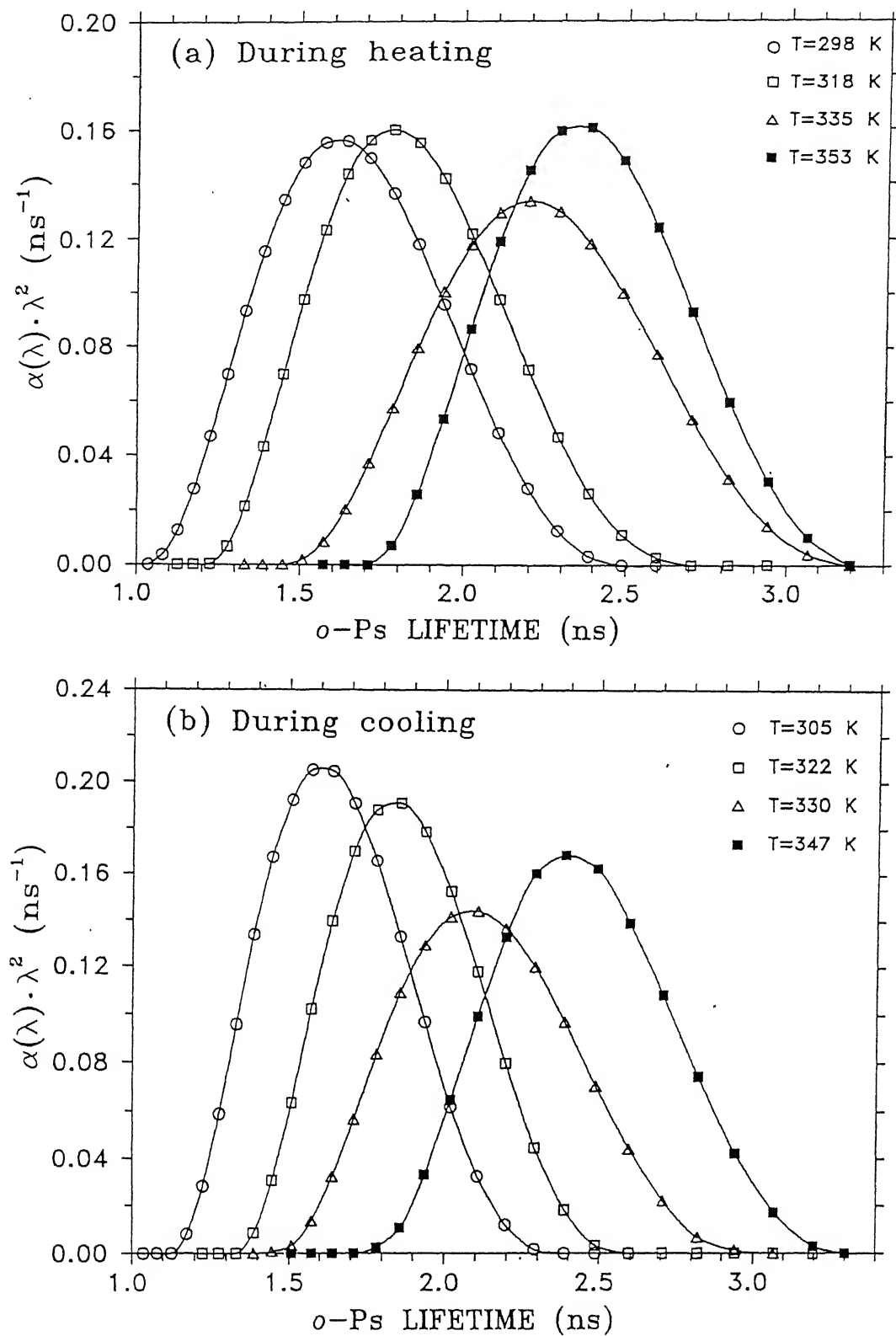


Fig. 4.11 o-Ps lifetime distribution functions in PEO:NH₄ClO₄ (80:20 wt %) at different temperatures for (a) increasing and (b) decreasing temperature. The data correspond to the right hand peaks in Fig. 4.10 (a) and (b) respectively.

to be

$$f(R) = -3.32 \left\{ \cos \left[\frac{2\pi R}{(R + 1.66)} \right] - 1 \right\} \frac{\alpha(\lambda)}{(R + 1.66)^2} \quad (4.5)$$

where we have not applied any correction factor for the Ps trapping [25,34]. The quantity, $f(R)dR$, then describes the fraction of free-volume holes having radii between R and $R + dR$. The present results for $f(R)$ corresponding to the o-Ps lifetime distributions shown in Fig. 4.11 (a) and (b) are plotted against R in Fig. 4.12(a) and (b) respectively and they show that as the temperature is changed from 298 to 353 K, the free-volume holes expand in size with their distribution function moving to higher radii while the mean radii changes from 2.5 Å to 3.20 Å. We further notice that the $f(R)$ functions (Fig. 4.12) appear fairly symmetric and can be approximately described by a Gaussian-type function whose FWHM changes from 0.8 to 0.6 Å. Jean and Dai [36] have pointed out that two major effects, the counting statistics and the instrument instability, contribute to a dispersion of lifetime distributions when CONTIN program is used to investigate free-volume hole distributions. In our studies we have tried to maintain good counting statistics and instrumental stability. The curves shown in Fig. 4.11 are raw results, not subjected to any deconvolution for natural broadening. The observed narrowing of the $f(R)$ distributions, if real, needs a suitable explanation. One possible explanation is that "Ps bubbles" are formed above the melting temperature and they might have a larger size and a narrower size distribution than the free volume holes present at

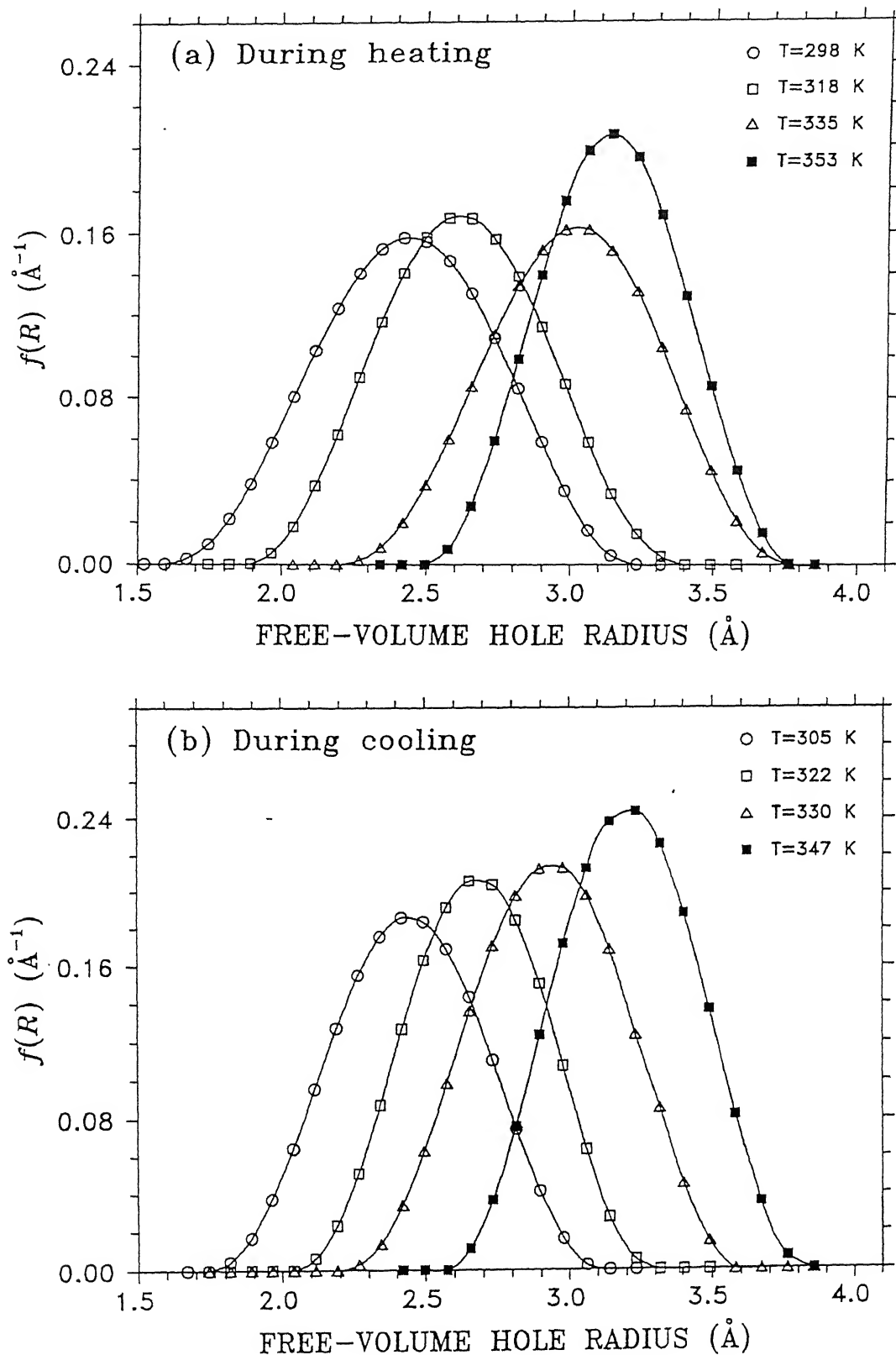


Fig. 4.12 Free-volume hole radius distribution functions $f(R)$ in PEO:NH₄ClO₄ (80:20 wt %) at different temperatures corresponding to the o-Ps lifetime distributions shown in Fig. 4.11 ((a) and (b)) for (a) increasing and (b) decreasing temperature.

lower temperature. A more systematic investigation is necessary to check these possibilities. In view of the uncertainties brought by the experimental factors [36], the distributions shown in Fig. 4.12 have to be interpreted qualitatively rather than quantitatively and they show only a certain trend. It is interesting to note that the present results for R lie in the range 2.5 - 3.0 Å which is consistent with the values obtained from molecular dynamics simulation. [37]

From the free-volume hole radius probability density function $f(R)$, one can also determine the probability density function for hole volumes, $g(V)$, by assuming a spherical hole and it can be expressed as

$$g(V) = \frac{f(R)}{4\pi R^2} \quad (4.6)$$

The fraction of the hole volume distribution as determined by o-Ps annihilation in holes with a volume between V and $V + dV$ is given by $g(V)dV$. The results of hole volume distribution, $g(V)$ obtained in this way are shown in Fig. 4.13(a) and (b). It is observed that the hole volume distribution, $g(V)$, are asymmetric with a skewing tendency towards larger volumes. The width of the peaks also become larger at higher temperature with the volume distribution varying from 20 to 200 Å³ in the temperature range 298 to 353 K. The above distribution of hole volumes should once again be taken as qualitative due to the limitations stated above together with the resolution of the measuring apparatus.

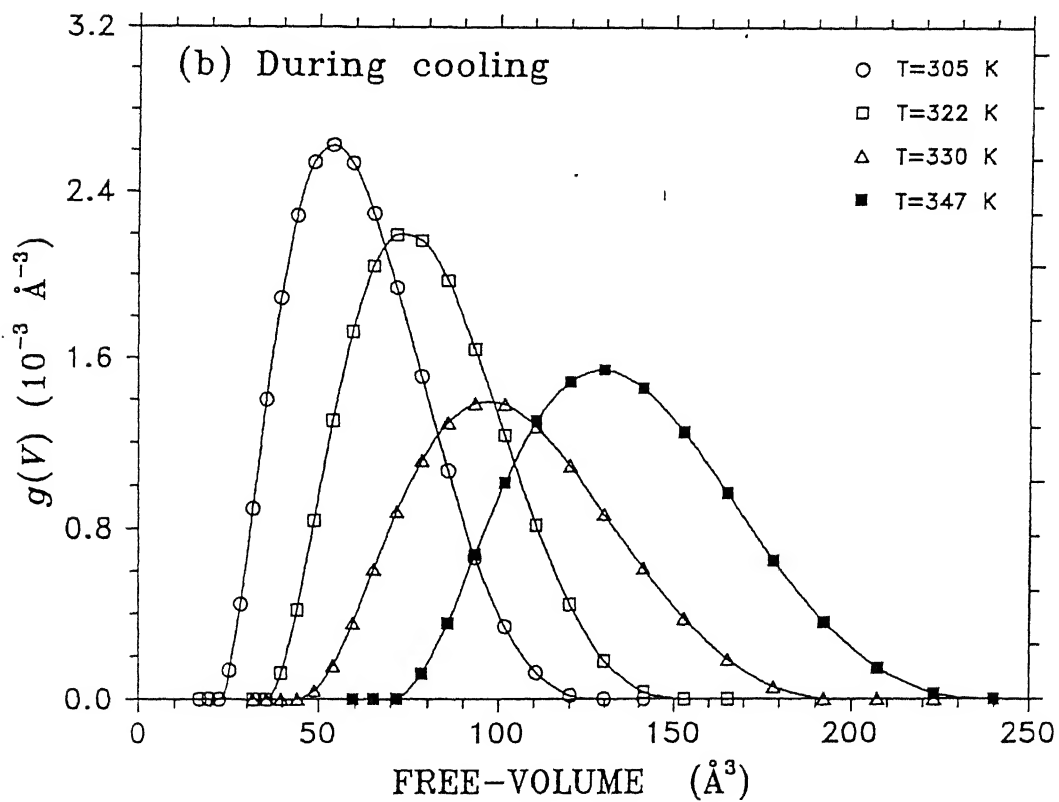
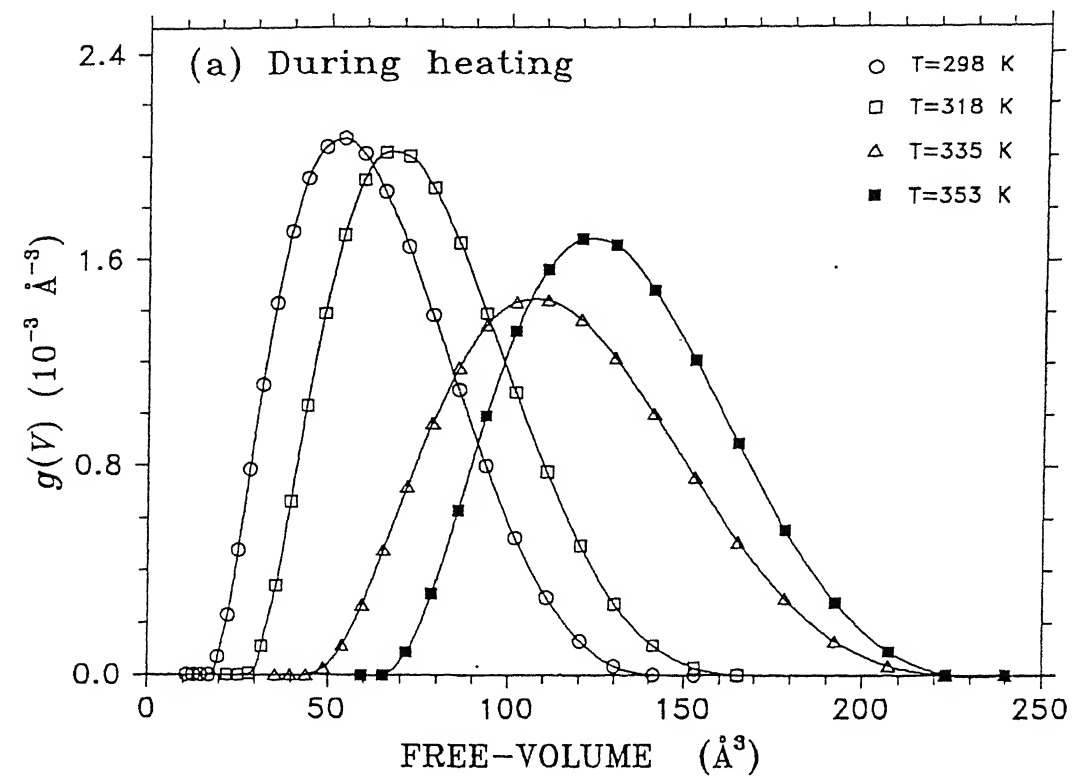


Fig. 4.13 Free-volume hole volume distribution functions $g(V)$ in PEO: NH_4ClO_4 (80:20 wt %) at different temperatures for (a) increasing and (b) decreasing temperature.

4.3.2 Conductivity, mobility, number of charge carriers and free volume

The results for the temperature dependence of conductivity (σ) and ionic (cationic and anionic) mobilities (μ^+ and μ^-) are shown in Fig. 4.14. These results show a change of slope in the σ versus $1/T$ plots of PEO:NH₄ClO₄ (80:20 wt %) at T_m and similar behaviour has been observed by many workers in other polymeric systems. The cationic and the anionic mobilities (Fig. 4.14), however, do not show significant change at the melting temperature, T_m . In general, the enhancement in the conductivity at T_m was earlier explained on the basis of an increase in the mobility values occurring during the crystalline-to-amorphous phase transition of the material.

As already discussed in the introduction, the approach used to explain the temperature dependence of the conductivity in polymers [2,38,39] is based either on the empirical Vogel-Tamman-Fulcher (VTF) relation (eq. 3.4) or the Williams-Landel-Ferry (WLF) empirical relation (eq. 3.5) for polymer relaxation processes. The possible relationships between these empirical relationships and various free-volume models have also been discussed in the literature [2,40]. Proponents of the applicability of the free-volume theory to the ionic transport in polymer electrolytes point out that conductivity as well as free volume increases with temperature and hence suggest that the ionic transport in these materials can be assumed to occur through the carrier ions assisted by the segmental motion of the polymeric chain which will increase with the increase in the free volume. In

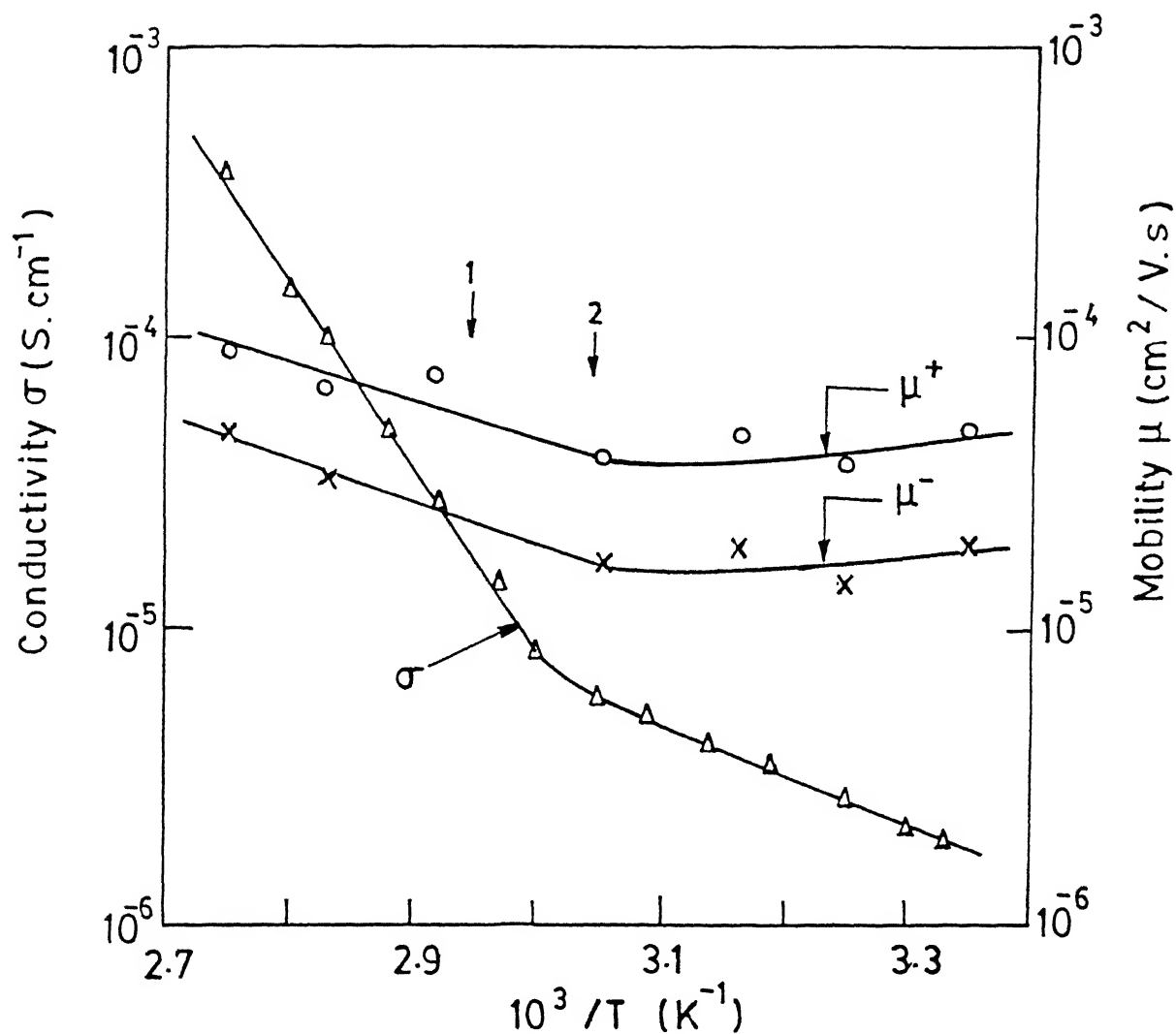


Fig. 4.14 Temperature dependence of cationic (μ^+) and anionic (μ^-) mobilities along with the conductivity (σ) for PEO: NH_4ClO_4 (80:20 wt %) at different temperatures. Positions indicated by 1 and 2 correspond to the melting temperatures of uncomplexed PEO ($Tm_1 \sim 339$ K) and crystalline complexed material ($Tm_2 \sim 239$ K).

this picture one, therefore, expects that with the increase in free volume with temperature the diffusive displacement (and hence the mobility) of the carrier ions should also increase. In other words, the pattern of increase in free volume should be reflected in the variation of mobility with temperature. The measurement of the temperature dependence of free volume (Fig. 4.9) and mobility (Fig. 4.14) in PEO:NH₄ClO₄ (80:20 wt %), however, does not yield such a similar pattern. These results indicate that an alternative explanation has to be sought.

We recall that $\sigma = ne\mu$ and hence the mobility is not the lone controlling factor which could explain the jump in the conductivity at T_m . We may ascribe the conductivity changes to a change in the number of charge carriers. The number of mobile charge carriers (cations and anions) can be calculated using the following equation

$$\frac{n^+}{n^-} = \left(\frac{t^+}{t^-} \right) \cdot \left(\frac{\mu^+}{\mu^-} \right) \quad (4.7)$$

where t^+ and t^- are the cationic and anionic transference numbers and they have already been determined for PEO:NH₄ClO₄ (80:20 wt %) from coulometric investigations [21].

Using eqs. (3.2) and (4.7), and the experimental data for $\sigma(T)$, $\mu(T)$, t^+ and t^- , the number of mobile cations (n^+) and anions (n^-) were calculated and their temperature dependence is shown in Fig. 4.15. It is interesting to note that the variation in the number of charge carriers is not linear and that it shows a somewhat steeper gradient near T_m as the temperature is raised

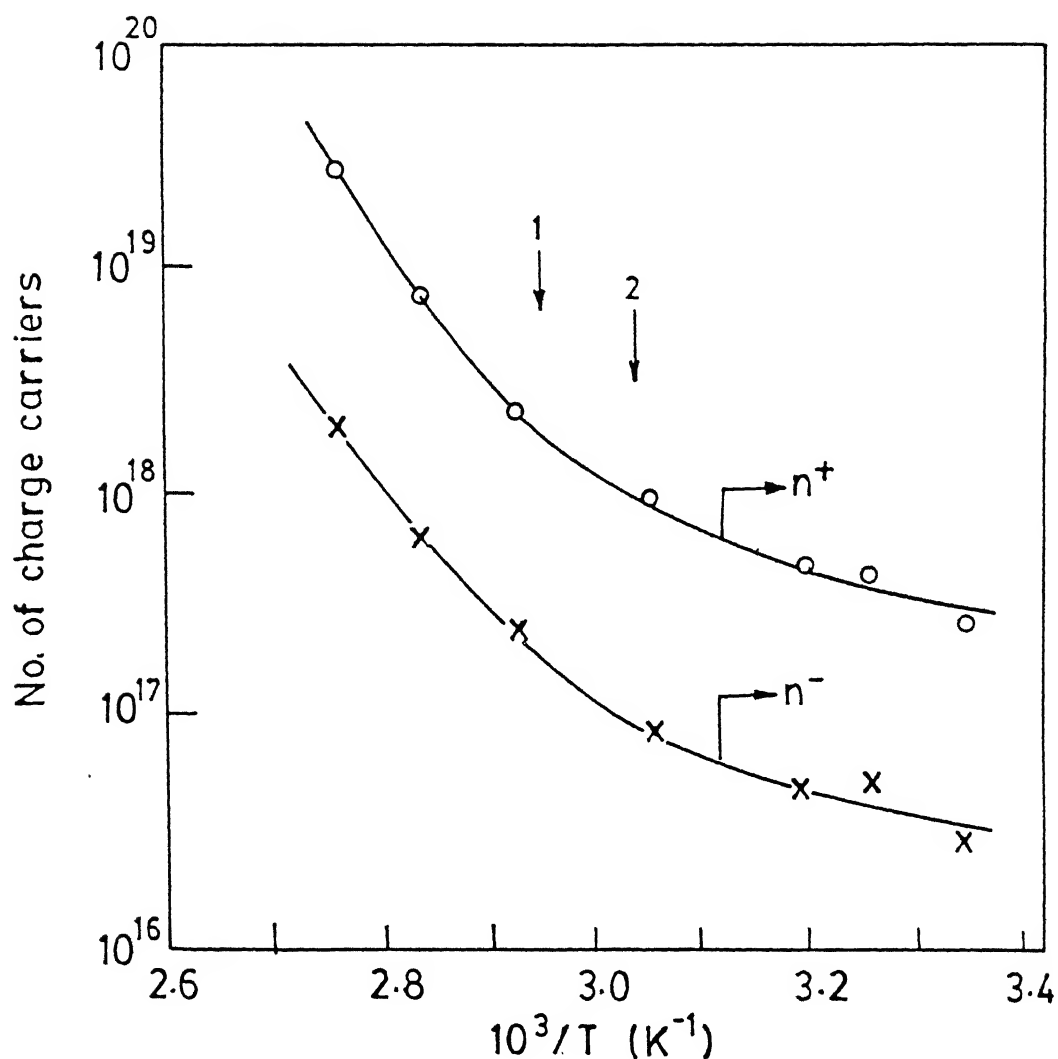


Fig. 4.15 Variation of number of mobile cations (n^+) and anions (n^-) with temperature for PEO: NH_4ClO_4 (80:20 wt %). Positions indicated by 1 and 2 correspond to the melting temperatures of uncomplexed PEO ($T_{m1} \sim 339 \text{ K}$) and crystalline complexed material ($T_{m2} \sim 239 \text{ K}$).

from room temperature. This indicates that the dissociation of complexed salts is increasing rather rapidly around T_m . On the basis of dissociation theory of electrolytes, the dissociation of ionic salts is determined by the dissociation energy 'U' and the effective dielectric constant (ϵ) of the medium. Barker and Thomas [41] gave the following expression for the number of dissociated ions, n,

$$n = n_o \exp \left[\frac{-U}{2\epsilon kT} \right] \quad (4.8)$$

or

$$\ln n = \ln n_o + \left[\frac{-U}{2\epsilon kT} \right] \quad (4.9)$$

where n_o is constant. This relation predicts a linear behaviour of $\ln n$ vs $1/\epsilon T$. A knowledge of ϵ is necessary if $\ln n$ is to be plotted against $1/\epsilon T$. Hence the dielectric constant of the sample was also measured at different temperatures and the results are shown in Fig. 4.16. We note that the dielectric constant increases more rapidly above T_m . The values of the dielectric constant were, therefore, used to plot $\ln n$ against $1/\epsilon T$. Such a plot of $\ln n$ versus $1/\epsilon T$ in fact gave a linear fit as shown in Fig. 4.17.

The value of the dissociation energy (U) in eq. (4.9) was obtained from the slopes of the straight lines (Fig. 4.17) to be 2.4 eV. Interestingly the value of U for the ammonium salts is nearly the same [21]. Therefore, the dissociation model of Barker and Thomas [41] appears to explain the increase in n observed in the present sample quite satisfactorily, with the dielectric

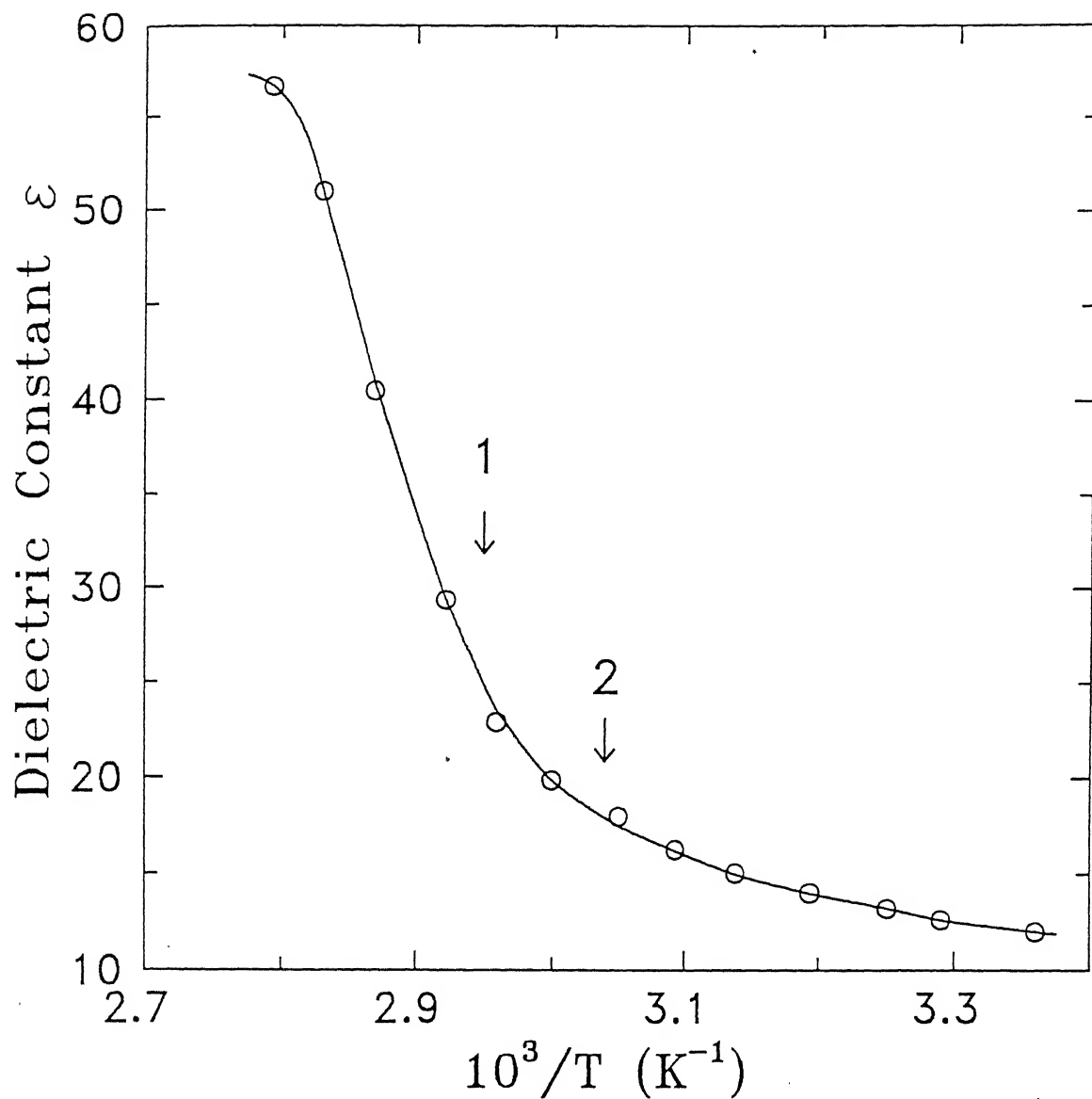


Fig. 4.16 The dielectric constant at different temperature for PEO: NH_4ClO_4 (80:20 wt %) . Positions indicated by 1 and 2 correspond to the melting temperatures of uncomplexed PEO ($T_{m1} \sim 339 \text{ K}$) and crystalline complexed material ($T_{m2} \sim 239 \text{ K}$).

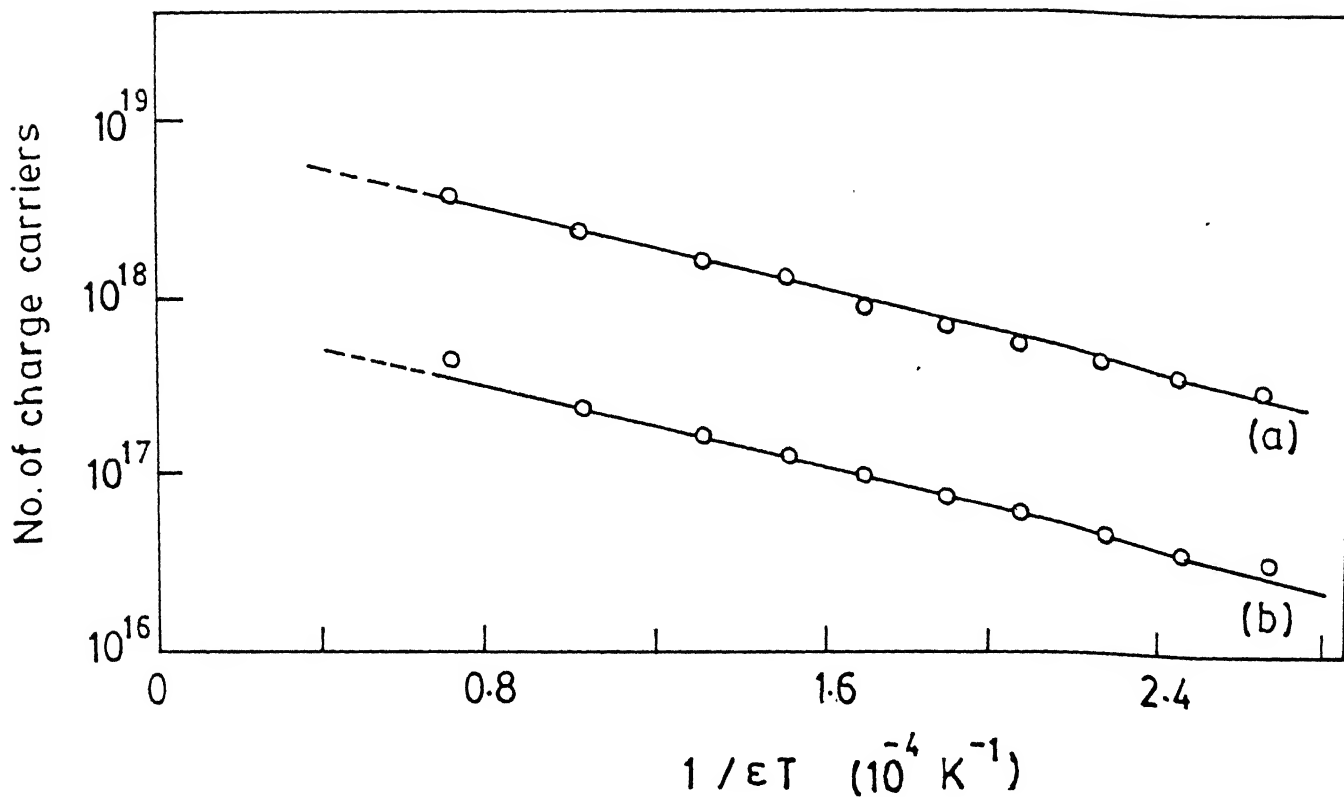


Fig. 4.17 Variation of number of mobile charge carriers (a) cations (n^+) and (b) anions (n^-) with $1/\epsilon T$ for PEO:NH₄ClO₄ (80:20 wt %) .

constant ϵ playing an important role. In brief, the sharp increase in the ionic conductivity σ around T_m in the sample $\text{PEO:NH}_4\text{ClO}_4$ is more related to the increase in the number of charge carrier rather than the increase in the free volume around T_m .

4.4 Conclusions

On the basis of positron lifetime, ionic transport and other studies described above, the following important conclusions can be drawn:

(i) The total free volume in $\text{PEO:NH}_4\text{ClO}_4$ increases with temperature, and the rate of increase changes its slope at T_m . The rate of increase in the free volume was higher around T_m .

(ii) The increase in total free volume is determined mainly by the enhancement in the hole-size rather than the increase in number of holes although chemical factors may be responsible for the low yield of o-Ps intensity and, therefore, may not corresponds to the actual free-volume hole density.

(iii) The pattern of increase in free volume with temperature is not reflected in the variation of μ with temperature as one should expect from the free volume theory. In particular, there is very little change in the value of mobility at T_m where free volume shows an increase.

(iv) The plot of conductivity σ versus $1/T$ shows a change of slope at T_m .

(v) The increase in conductivity at T_m is influenced more by the increase in the number of charge carriers (and not so much by the

mobility). This behaviour may be explained on the basis of a simple dissociation model in which the dielectric constant of the polymer electrolyte plays a role. The value of the dissociation energy has been determined using this model.

References

1. S.A.Hashmi, Ajay Kumar, K.K.Maurya and S. Chandra, J. Phys. D : Appl. Phys. 23, 1307 (1990).
2. "Polymer Electrolyte Reviews 1"; edited by J.R.MacCallum and C.A.Vincent (Elsevier Applied Science, London, 1987) ; "Polymer Electrolyte Reviews 2"; edited by J.R.MacCallum and C.A.Vincent (Elsevier Applied Science, London, 1989).
3. S.D.Druger, J. Chem. Phys. 100, 3979 (1994).
4. A. Nitzan and M.A.Ratner, J. Phys. Chem. 98, 1765 (1994).
5. G. Adams and J.H. Gibbs, J. Chem. Phys. 43, 139 (1965).
6. S.D.Druger, A. Nitzan and M.A.Ratner, J. Chem. Phys. 79, 3133 (1983).
7. A.K.Doolittle, J. Appl. Phys. 22, 1471 (1951).
8. Y.Abe, M.Kakizaki and T.Hideshima, Jpn. J. Appl. Phys., 24, 1074 (1985).
9. Y. Fu, K. Pathmanathan and J.R. Stevens, J. Chem. Phys. 94, 6323, (1991).
10. S.H. Chung, K.R. Jeffrey and J.R.Stevens, J. Chem. Phys. 94, 1803 (1991).
11. J.P. Donoso, T.J. Bonagamba, H.C. Panepucci, L.N. Oliveira, W. Gorecki, C. Berthier and M. Armand, J. Chem. Phys. 98, 10026 (1993).
12. A.E.Hamielec, M.Eldrup, O.Mogensen and P.Jansen, J. Macromol. Sci. Rev. Macromol. Chem. C9, 305 (1973).
13. "Positron and Positronium Chemistry", edited by D.M. Schrader and Y. C. Jean, (Elsevier, Amsterdam ,1988) ; "Positron and

- Positronium Chemistry", edited by Y.C.Jean (World Scientific, Singapore, 1990).
14. Y.C. Jean, Microchem. J. 42, 72 (1990).
 15. J.R. Stevens in "Probe and Label Techniques in Methods of Experimental Physics" edited by R.A. Fava (Academic Press, London, 1980), p. 371.
 16. Y.C. Jean, Mater. Sci. Forum 175-178, 59 (1995).
 17. Z.L.Peng, B.Wang, S.Q.Li, S.J.Wang, H.Liu and H.Q.Xie, Phys Lett. A 194, 228 (1994); Z.L.Peng, B.Wang, S.Q.Li and S.J.Wang, J. Appl. Phys. 77, 334 (1995).
 18. K.K.Maurya, S.A.Hashmi and S. Chandra, J. Phys. Soc. Jpn. 61, 1709 (1992).
 19. K.K.Maurya, B.Bhattacharya and S.Chandra, Phys. Stat. Sol. (a) 147, 347 (1995).
 20. K.K.Maurya, Neelam Srivastava, S.A.Hashmi and S.Chandra J. Mat. Sci. 27, 6357 (1992).
 21. K.K.Maurya, Ph.D. Thesis, Banaras Hindu University, Varanasi, India (1993), unpublished.
 22. Suresh Chandra (Private communication)
 23. "Impedance Spectroscopy : Emphasizing Solid Materials and Systems", edited by J. Ross Macdonald (John Wiley & Sons, New York, 1987).
 24. S.Chandra, "Superionic Solids : Principles and Applications", (North-Holland, Amsterdam, 1981).
 25. S.Chandra, S.K.Tolpadi and S.A.Hashmi, Solid State Ionics 28-30, 651 (1988).
 26. Q.Deng, F.Zandiehnadem and Y.C.Jean, Macromolecules 25, 1090

(1992).

27. S.J.Tao, J. Chem. Phys. 56, 5499 (1972).
28. M.Eldrup, D.Lightbody and J.N.Sherwood, Chem. Phys. 63, 51 (1981)
29. H.Nakanishi, S.J.Wang and Y.C.Jean, in "Positron Annihilation Studies of Fluids" edited by S.C.Sharma (World Scientific, Singapore, 1980),p. 292.
30. "The Physics of Glassy Polymers" edited by R.N.Haward (Applied Science Publishers Ltd, London, 1973).
31. H.Nakanishi, Y.C.Jean, E.G.Smith and T.C.Sandreczki, J. Polym. Sci. Polym. Phys. Ed. 27, 1419 (1989).
32. Y.C.Jean, T.C.Sandreczki and D.P.Adams J. Polym. Sci. Polym. Phys. Ed. 24, 1247 (1986).
33. Y. Ito, K.I.Okamoto and K. Tanaka, J. de Physique C4 3, 241 (1993); Y. Ito, Mater. Sci. Forum 175-178, 627 (1995).
34. Q.Deng and Y.C.Jean, Macromolecules 26, 30 (1993).
35. Y.C.Jean and Q.Deng , J. Polym. Sci. Polym. Phys. Ed. 30, 1359 (1992).
36. Y. C. Jean and G. H. Dai, Nucl. Instrum. Methods B 79, 356 (1993).
37. D.Rigby and R.J.Roe, Macromolecules 23, 5312 (1990).
38. M.Watanabe, M.Itoh, K.Sanui and N. Ogata, Macromolecules 20, 569 (1987).
39. S.H.Chung, K.Such, W.Weiczorek and J.R.Stevens J. Polym. Sci. Polym. Phys. Ed. 32, 2733 (1994).
40. M.H.Cohen and D.Turnbull, J. Chem. Phys. 31, 1164 (1959).
41. R.E.Barker Jr and C.R.Thomas, J. Appl. Phys. 35, 3203 (1964).

CHAPTER 5

POSITRON ANNIHILATION LIFETIME STUDIES OF FREE VOLUME IN A POLYMER ELECTROLYTE PEO COMPLEXED WITH NH_4I

5.1 Introduction

In the previous chapter we have already observed that the temperature dependence of ionic conductivity in $\text{PEO}:\text{NH}_4\text{ClO}_4$ is influenced more by the dissociation of salts rather than changes in the free volume. Positron lifetime studies played a key role in these investigations because they offered a direct measurement of free volume changes. This interesting observation led us to perform similar studies on another polymer electrolyte polyethylene oxide (PEO) complexed with another salt, viz. ammonium iodide (NH_4I), using positron lifetime technique. The polymer electrolyte PEO complexed with NH_4I ($\text{PEO}:\text{NH}_4\text{I}$) is another recently developed solvent-free polymer-salt complex [1] with high ionic conductivity ($\sigma = 10^{-5} \text{ S cm}^{-1}$) over the concentration range $\text{NH}^+/\text{EO} \approx 0.016 - 0.130$ and this was found to be greatly enhanced (by a factor of about 10^4) over the undoped PEO. The study of proton transport properties and characterization of various physical properties of this system was carried out by Maurya et al. [1] using experimental techniques such as X-ray diffraction, differential thermal analysis, infrared spectroscopy, complex impedance analysis for conductivity, σ vs $1/T$, transference number, mobility, etc. The charge transport in this polymer electrolyte was found to be predominantly protonic (or H^+) along

with I^- movement in the bulk. Further the temperature dependence of the electrical conductivity (σ vs $1/T$ plots) of the $PEO:NH_4I$ complex for the above-mentioned concentration range showed mainly two types of behaviour [1]. For lower concentration ($NH_4^+/EO \leq 0.076$) the σ vs $1/T$ plots follows the Arrhenius behaviour with two different activation energies one above and another below the melting point of crystalline PEO ($T_m = 328$ K). For higher concentrations ($NH_4^+/EO \approx 0.130$) σ vs $1/T$ follows the VTF pattern (eq. 3.5).

It has been observed that the variation in the ionic conductivity measured as a function of temperature usually depends on the experimental conditions, such as the presence of residual water [3], heating and cooling rates [4], and the thermal history of the electrolytes [5,6] etc. These conditions are in addition to the various other factors mentioned in the previous chapter (Sec 4.1) that govern the mechanism of ion-conduction in these polymer electrolytes. Lack of control over any of these parameters has resulted in contradictory and confusing data in the literature, which do not represent the intrinsic ionic conductivity properties of some polymer electrolyte system. In addition, the relative proportion of cationic and anionic mobilities must be properly characterized before an assumption about the ionic transport process can be made.

Although the results of our studies for the polymer electrolyte $PEO:NH_4ClO_4$ in the previous chapter indicated that the enhancement in the ionic conductivity with temperature is associated with the dissociation of the salt and not so much with

the observed free-volume changes, a thorough investigation in this direction for a wide range of compositions and in a variety of samples is needed before a more conclusive statement can be drawn.

The set of measurements involving methods like temperature dependence of conductivity, ionic mobility, dielectric constant, number charge carriers etc. and similar to the ones described in the previous chapter (for $\text{PEO:NH}_4\text{ClO}_4$) to investigate the mechanism of ionic conductivity could not be performed with the present sample $\text{PEO:NH}_4\text{I}$ due to some technical difficulties. However we have measured the temperature dependence of positron lifetime spectra in the sample $\text{PEO:NH}_4\text{I}$ for the composition ($\text{NH}_4/\text{EO} \approx 0.076$) in the temperature range 298-353 K following both the heating and the cooling cycle. The measured lifetime spectra were analyzed in terms of finite lifetimes as well as continuous lifetime distributions using the computer programs PATFIT and CONTIN respectively to obtain the temperature dependence of positron lifetime parameters and their distribution functions. Our positron lifetime analysis showed interesting results and these will be presented in the following sections.

5.2 Experimental

A sample of polyethylene oxide (PEO) complexed with ammonium iodide (NH_4I) under study was prepared in the laboratory of the Department of Physics, Banaras Hindu University, Varanasi, India [1] and various other characterizations and ion-transport studies

using the techniques of optical microscopy, X-ray diffraction, IR spectra, differential thermal analysis, temperature dependence of ionic conductivity by impedance spectroscopy etc. were also carried out in their laboratory and have been reported elsewhere [1]. A brief outline of the sample preparation is given below.

The sample PEO:NH₄I was prepared by solution-cast technique previously described in Sec. 3.2.4. The desired amount of PEO (obtained from Aldrich, U.S.A.) with MW $\sim 6 \times 10^5$ and NH₄I was dissolved in dehydrated methanol and stirred thoroughly at 313 K. The resulting solution of polymer-salt was poured into polypropylene dishes for casting the films by slow evaporation. Finally, the films were dried rigorously in a high vacuum to eliminate all traces of the solvent. Good thick films ($\sim 700\mu\text{m}$) of the polymer salt complex PEO:NH₄I (NH₄⁺/EO ≈ 0.076) were obtained after several trials.

The DTA spectrum for this sample was recorded by us using a computer controlled (Shimadzu DTA-50) differential thermal analyzer in the temperature range 300-373 K for a heating rate of 2 K/min.

Positron lifetime measurements were performed at 298 K using a conventional fast-fast coincidence spectrometer that has already been described in Chapter 2. A 15 μCi ²²Na positron source deposited on 2.5 μm thick Ni-foil was used. Polymer electrolyte films (NH₄⁺/EO ≈ 0.076) were stacked to prepare specimens of about 1.5mm thickness. The source of positrons was sandwiched between two such identical specimens of the sample. The time resolution of our lifetime apparatus was found to be 0.32 ns (FWHM) as measured

by the prompt spectrum from ^{60}Co source. For measuring the temperature dependence of the positron lifetime spectra for the present sample, the arrangement identical to that described in the previous chapter was used (Fig. 4.4). The spectra were taken in the temperature range 298 - 353 K in steps of about 5 K. The measurements were carried out both during the heating and the cooling cycle to look for any effect of hysteresis. A total of about 5×10^6 counts were recorded under each lifetime spectrum. As done in the previous case of $\text{PEO}+\text{NH}_4\text{ClO}_4$, the measured lifetime spectra were then analyzed in two different ways using the computer programs PATFIT and CONTIN. Our PATFIT analysis showed that best χ^2 (< 1.1) and most acceptable standard deviations were obtained when each spectrum was fitted in terms of three lifetime components. In the present analysis using the CONTIN program, we have used the reference spectrum arising from well-annealed and high-purity (99.99+ %) nickel with an annihilation rate $\lambda = 9.1 \text{ ns}^{-1}$. This reference spectrum was taken immediately before and after each measurement at a particular temperature was performed. A total of 85 grid points over the range $0.25 \text{ ns}^{-1} < \lambda < 13 \text{ ns}^{-1}$ were used to obtain the lifetime distributions.

5.3. Results and discussions

As mentioned earlier, the sample $\text{PEO}:\text{NH}_4\text{I}$ has already been characterized and studied in detail by Maurya et al. [1] for different percentage compositions of NH_4I . A tentative phase diagram based on the DTA studies was also proposed for these

samples [7] and it showed that apart from the presence of (PEO)_{crystalline} and (PEO)_{amorphous} phases, a phase related to the (PEO)_{crystalline} complex also exists in the sample at room temperature. Our DTA spectrum (Fig. 5.1) for the present sample ($\text{NH}_4^+/\text{EO} \approx 0.076$) showed an endothermic peak at $T_m = 329$ K. This value of T_m shows an excellent agreement with the value $T_m = 328$ K and it matches well with the one observed by Maurya et al. [1] in their DTA studies for the same composition. This endothermic peak at 329 K has been ascribed to the phase transition resulting from melting of the pure crystalline PEO [1,7].

5.3.1 Analysis of lifetime spectra using PATFIT program

We shall first discuss the results of our analysis for the measured positron lifetime spectra in terms of finite lifetime components obtained by using the PATFIT program. The positron lifetime spectra measured in the temperature range 298 -353 K for the sample PEO complexed with NH_4I ($\text{NH}_4^+/\text{EO} \approx 0.076$) showed the presence of three lifetime components whose values are in the range: $\tau_1 = 0.10\text{-}0.14$ ns, $\tau_2 = 0.35 - 0.37$ ns and $\tau_3 = 1.3 - 2.2$ ns. As discussed earlier in Chapter 1, these three lifetimes correspond to three states of positron and Ps in the sample [8]. The shortest lifetime $\tau_1 = 0.10 - 0.14\text{ns}$ can be attributed to the annihilation of singlet Ps (or p-Ps) while the intermediate lifetime $\tau_2 = 0.35 - 0.37$ ns arises from the free (or unbound) annihilation of positrons. The longest or the third lifetime $\tau_3 = 1.3 - 2.2$ ns is due to triplet Ps (o-Ps) annihilation. The relative intensities corresponding to the three lifetimes τ_1 , τ_2

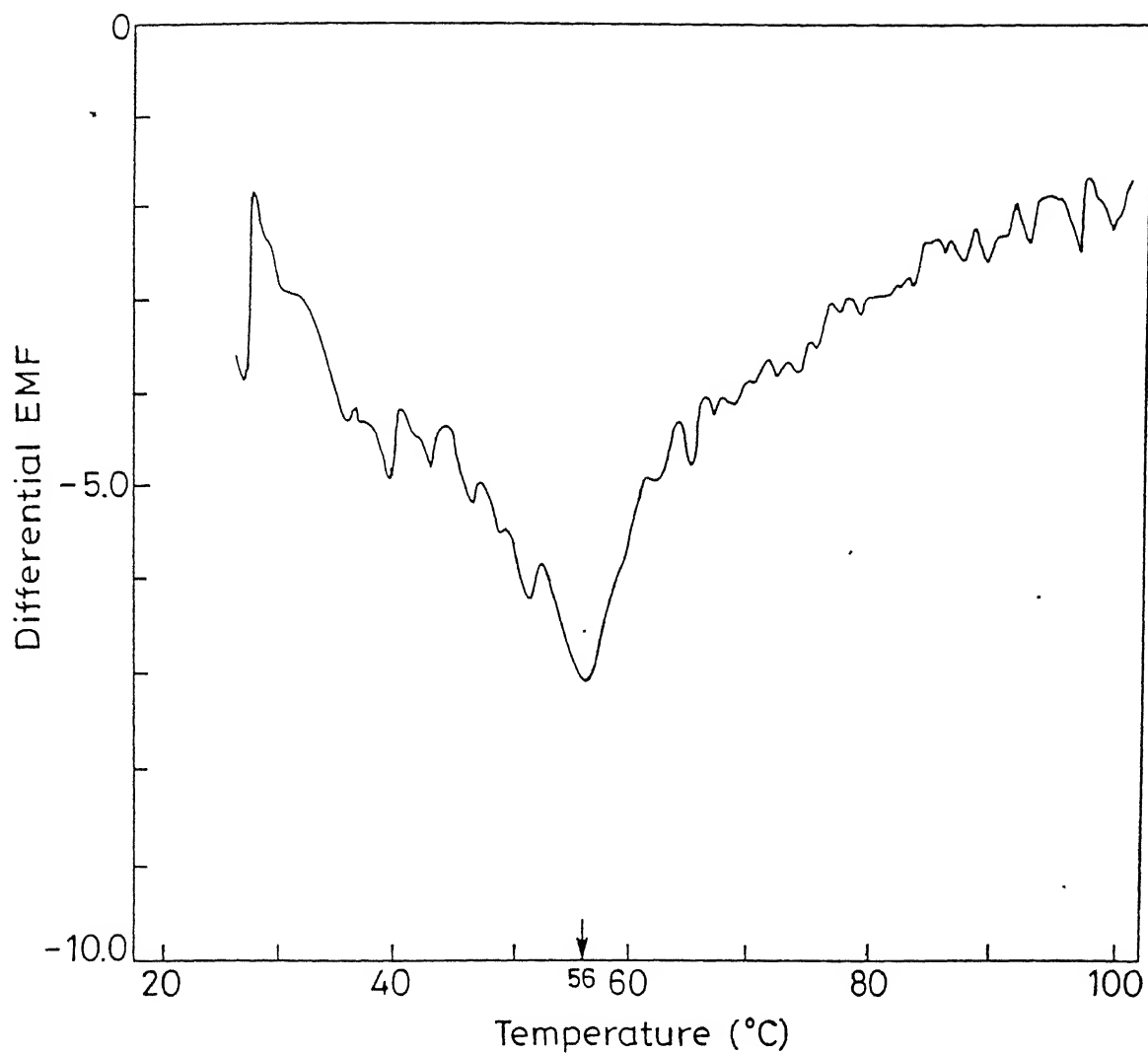


Fig. 5.1 DTA curve for the sample polyethylene oxide complexed with ammonium iodide NH_4I ($\text{PEO}:\text{NH}_4\text{I}$ with $\text{NH}_4^+/\text{EO} \approx 0.076$).

and τ_3 are given by I_1 , I_2 and I_3 respectively such that $I_1+I_2+I_3 = 100 \%$. The lifetime values and their intensities are given in Table 5.1.

As mentioned earlier in Chapter 1, the interaction between Ps and matter in polymers has been described in terms of free-volume theory [9,10] i.e. the rate of positron or Ps annihilation in the absence of any chemical reaction or spin conversion between Ps and matter, is a function of the effective free-volume in such materials. Annihilation rate of o-Ps trapped in the free-volume regions in polymers has been related to the size of the free volume sites.

As discussed in Sec 4.3.1, the total free volume available in a polymer is determined by the hole volume, as well as the density (number of free-volume sites) of the holes although the separate dependence of these two factors is not properly understood. Regarding the o-Ps intensity or the I_3 - values in polymers, Ito et al. [12,13] have argued that they are determined by both the chemical factor (e.g. electron affinity) and the physical factor (e.g. hole-size distribution). Recently Jean [11] has reviewed our present understanding of the applications of positron annihilation spectroscopy to the study of hole size, content, distribution and anisotropic structure in polymers and has posed several questions that need to be answered before a more comprehensive understanding is reached.

The semicrystalline polymers like polyarylether-ether- ketone (PEEK) or PEO and PEO-based polymer-salt complexes are partly crystalline and partly amorphous at room temperature [14,15]. For

TABLE 5.1

Temperature dependence of positron lifetime parameters in polymer electrolyte
PEO:NH₄I (NH₄⁺/EO \approx 0.076) obtained from **PATFIT** analysis.

Temp. (K)	τ_1 (ns)	τ_2 (ns)	τ_3 (ns)	I_1 (%)	I_2 (%)	I_3 (%)	R^c (Å)
298 ^a	0.136 \pm .006	0.360 \pm .003	1.682 \pm .014	23.50 \pm 1.15	68.58 \pm 1.08	7.92 \pm .12	2.54 \pm .01
298 ^b	0.108 \pm .008	0.362 \pm .002	1.339 \pm .020	21.74 \pm 0.71	71.99 \pm 0.61	6.27 \pm .20	2.15 \pm .01
308 ^a	0.118 \pm .004	0.359 \pm .002	1.787 \pm .016	22.08 \pm 0.63	69.99 \pm 0.57	7.94 \pm .11	2.65 \pm .01
306 ^b	0.105 \pm .008	0.359 \pm .002	1.329 \pm .012	21.22 \pm 0.69	72.32 \pm 0.58	5.46 \pm .18	2.14 \pm .01
313 ^a	0.128 \pm .006	0.357 \pm .003	1.838 \pm .017	21.52 \pm 1.15	70.00 \pm 1.09	8.48 \pm .12	2.70 \pm .01
310 ^b	0.118 \pm .005	0.359 \pm .002	1.375 \pm .007	21.66 \pm 0.35	71.65 \pm 0.29	5.69 \pm .13	2.19 \pm .01
318 ^a	0.109 \pm .005	0.355 \pm .003	1.942 \pm .016	22.11 \pm 0.76	68.93 \pm 0.70	8.96 \pm .10	2.80 \pm .01
316 ^b	0.106 \pm .004	0.362 \pm .002	1.447 \pm .021	20.81 \pm 0.30	72.87 \pm 0.26	5.32 \pm .14	2.28 \pm .01
323 ^a	0.131 \pm .005	0.363 \pm .003	1.984 \pm .016	23.82 \pm 1.07	67.31 \pm 1.01	8.87 \pm .10	2.84 \pm .01
321 ^b	0.118 \pm .006	0.361 \pm .003	1.463 \pm .028	21.26 \pm 0.77	72.30 \pm 0.94	5.44 \pm .17	2.30 \pm .01
328 ^a	0.116 \pm .004	0.358 \pm .003	2.003 \pm .016	22.16 \pm 0.82	69.03 \pm 0.77	8.81 \pm .10	2.86 \pm .01
326 ^b	0.117 \pm .007	0.356 \pm .002	1.474 \pm .022	21.36 \pm 0.37	72.99 \pm 0.33	5.65 \pm .16	2.31 \pm .01
333 ^a	0.109 \pm .005	0.351 \pm .002	2.092 \pm .015	20.50 \pm 0.68	69.92 \pm 0.64	9.59 \pm .09	2.94 \pm .01
331 ^b	0.109 \pm .006	0.361 \pm .001	1.647 \pm .020	20.93 \pm 0.34	73.16 \pm 0.30	5.90 \pm .09	2.51 \pm .01
338 ^a	0.109 \pm .005	0.351 \pm .003	2.069 \pm .014	21.06 \pm 0.73	69.21 \pm 0.69	9.73 \pm .09	2.92 \pm .01
335 ^b	0.109 \pm .007	0.363 \pm .002	1.672 \pm .022	21.25 \pm 0.46	72.64 \pm 0.41	6.11 \pm .11	2.53 \pm .02
243 ^a	0.123 \pm .006	0.360 \pm .003	2.021 \pm .017	22.25 \pm 1.04	68.36 \pm 0.98	9.39 \pm .11	2.87 \pm .01
341 ^b	0.120 \pm .008	0.363 \pm .002	1.677 \pm .020	21.65 \pm 0.58	71.52 \pm 0.51	6.84 \pm .11	2.54 \pm .01
348 ^a	0.117 \pm .005	0.358 \pm .003	1.996 \pm .015	21.03 \pm 0.81	69.87 \pm 0.76	9.09 \pm .10	2.85 \pm .01
346 ^b	0.125 \pm .009	0.367 \pm .003	1.838 \pm .018	21.85 \pm 0.88	69.95 \pm 0.82	8.18 \pm .11	2.70 \pm .01
353 ^a	0.116 \pm .005	0.359 \pm .003	1.897 \pm .016	21.72 \pm 0.86	69.76 \pm 0.77	8.51 \pm .10	2.76 \pm .01

^a During heating cycle

^b During cooling cycle

^c R are the free-volume hole radii obtained by using τ_3 and eq. (1.17).

I_1 and I_2 are shown in Fig. 5.2. The temperature dependence of τ_3 and I_3 are shown separately in Figs. 5.3 and 5.4 respectively. Since the values of τ_3 and I_3 are more related to the free-volume properties in polymers, our discussion will be confined to the variations of τ_3 and I_3 and we shall skip the temperature dependence of positron lifetimes τ_1 , τ_2 and their intensities from the subsequent discussion. Moreover the values of τ_1 , τ_2 and I_1 do not show any significant variation with temperature whereas the observed variations in I_2 during the heating and the cooling cycle is related to the variations in the values of I_3 due to the constraint $I_1 + I_2 + I_3 = 100\%$.

Once again, assuming that the o-Ps trapped in the free volume regions in the polymers resides in a spherical well of radius R_0 , we make use of the semiempirical relationship (eq. 1.17) to determine the free volume hole radius R from the values of τ_3 and the values of R determined in this way are also tabulated in Table 5.1. The values of R calculated from τ_3 are used to obtain the hole volume $V_f = 4\pi R^3/3$, and the variation in the value of V_f (see right axis) is also shown in Fig. 5.3.

Our results (Fig 5.3 and 5.4 and Table 5.1) show that the nature of variation of τ_3 and I_3 with temperature is rather complicated. It may be pointed out that the present positron lifetime measurements involved measurements (each run lasting for few hours) at several temperatures starting from room temperature ($T=298$ K) and then increasing the temperature in steps of about 5K upto the highest temperature ($T=353$ K) and thereafter returning to the room temperature. In view of this the heating and cooling was

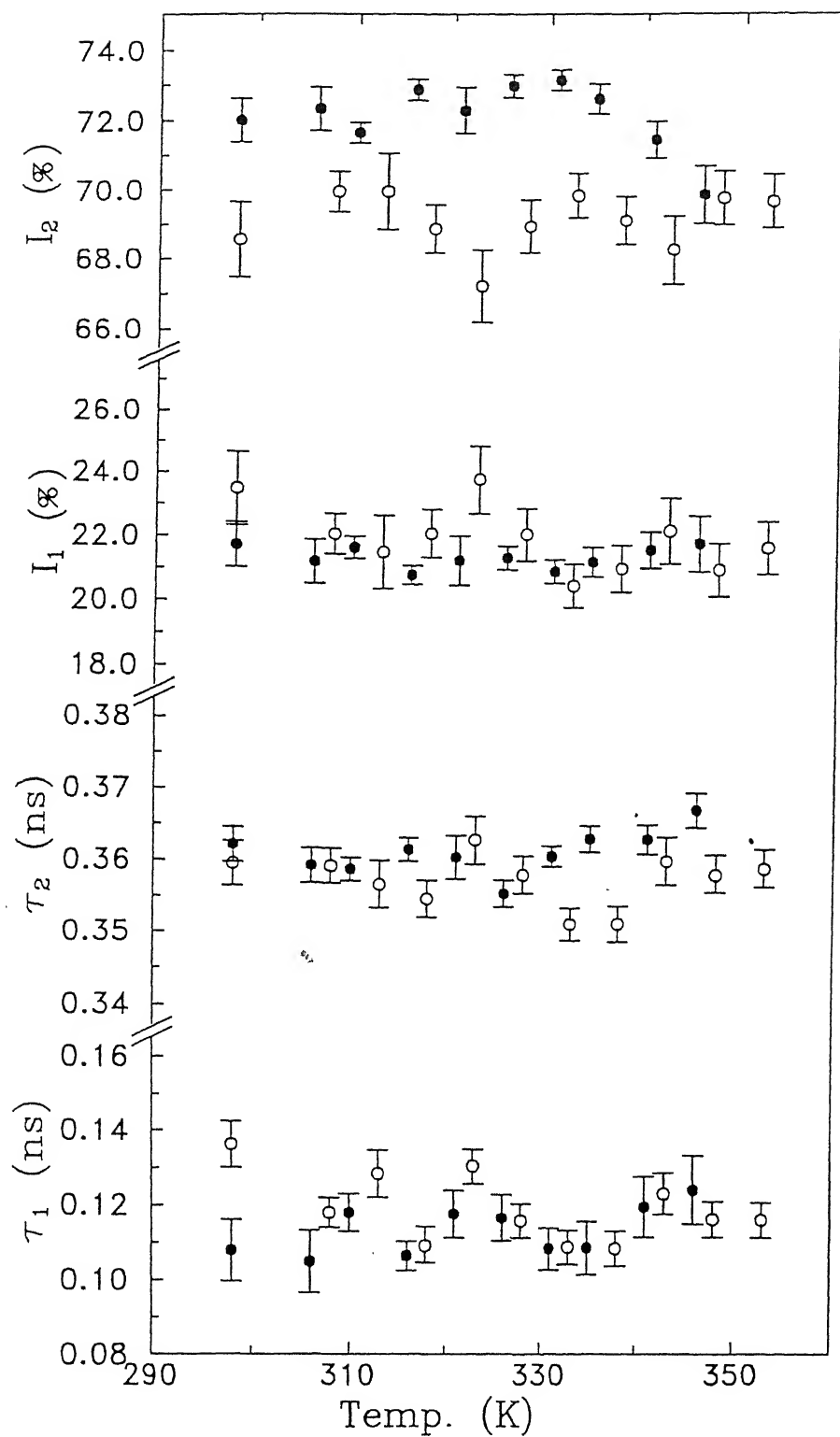


Fig. 5.2 Temperature variation of positron lifetime parameters τ_1 , τ_2 , I_1 and I_2 in PEO:NH₄I (NH₄⁺/EO \approx 0.076). Open symbols describe the data for increasing temperature, while solid symbols describe the data for decreasing temperature.

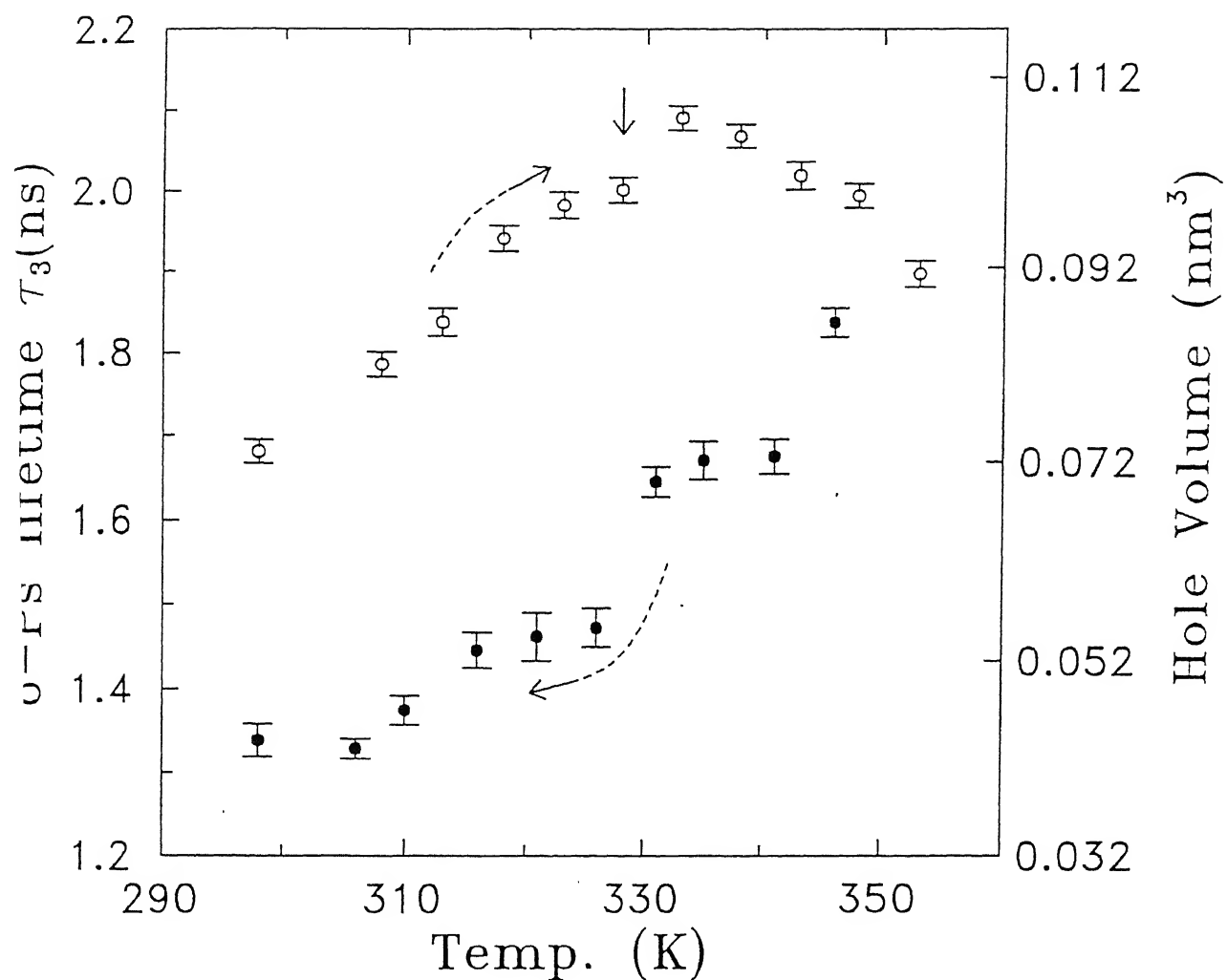


Fig. 5.3 Temperature dependence of o-Ps lifetime, τ_3 , in PEO:NH₄I(NH₄⁺/EO \approx 0.076). Positions indicated by the arrow corresponds to the melting temperature of uncomplexed PEO ($T_m \sim 29$ K) [Ref. 7]. Open symbols describe the data for increasing temperature, while solid symbols describe the data for decreasing temperature.

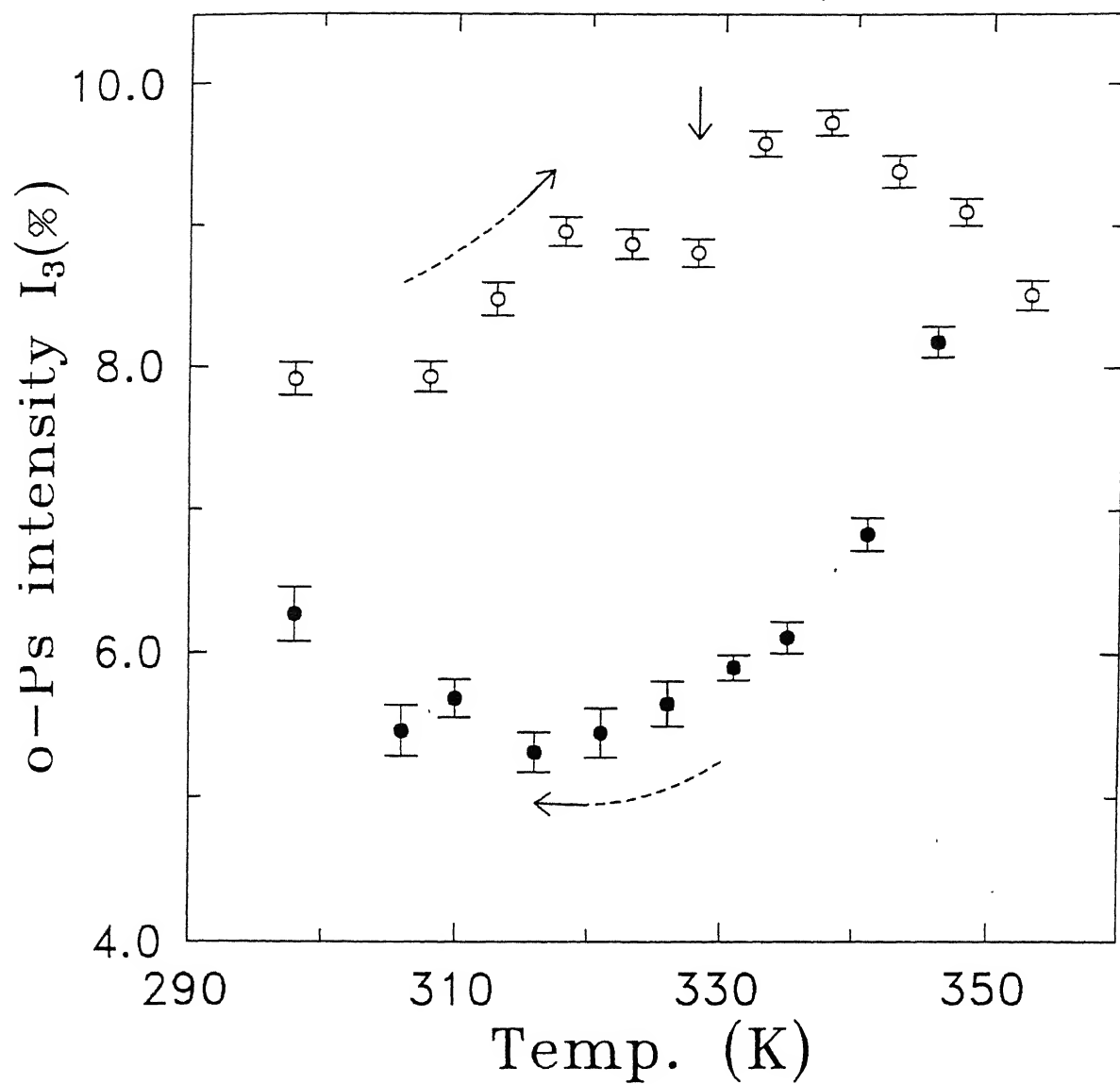


Fig. 5.4 Same as Fig. 5.3, but for the temperature dependence of o-Ps lifetime intensity, I_3 .

not rapid in our experiment. It is interesting to note that the temperature variation of τ_3 and I_3 during the heating and the cooling cycle do not follow the same course, thus suggesting that the o-Ps formation probability and the annihilation rate depends not only on the temperature but also on the thermal cycle used for this sample.

The present sample has substantial amount of crystallinity (~37%) at room temperature [7] in the form of pure crystalline and crystalline complex phases of PEO. This presence of crystalline phases in the material will also determine the observed values of o-Ps intensity I_3 as mentioned earlier. However, one can see from Table 5.1 that our o-Ps yield (I_3 values) at room temperature is rather low for the present sample and hence we suggest that both chemical as well as physical factors are responsible for such low yield of I_3 . Moreover our sample contains NH_4I in the form of complexes both in the amorphous and crystalline phases. Some of this NH_4I present in the amorphous phase may be dissociated thereby releasing iodine which can diffuse into the amorphous region of the polymer [19,20] and some of them may even be trapped in the free-volume holes themselves. Maurya et al. [1] have in fact found that a part of the ionic conductivity arises out from the I^- movements in the bulk.

It has already been established that in the case of polymers containing Cl, Br, I, CN, SCN etc, the electrons are scavenged to form the X^- - ions [20,21]. In such a case, Ps formation is either not possible or its formation is inhibited by the presence of electron scavenger (in the present case, I) resulting in low

yield of o-Ps formation and decay. The above process may be responsible for a low value of I_3 (7-8% in the present case, but 10-12% in the case of $\text{PEO:NH}_4\text{ClO}_4$) in the present case due to the presence of iodine in the form of NH_4I salt. Similar effect involving chlorine is less likely in the case of $\text{PEO:NH}_4\text{ClO}_4$ (Chapter 4) because chlorine exists in the sample as a part of ClO_4^- .

We shall first discuss the results for the heating cycle. As the temperature is raised above the room temperature (Fig. 5.3), the value of τ_3 started to increase upto $T = 328 \text{ K}$. Around $T=328 \text{ K}$, the τ_3 shows a small jump as the temperature is further raised to $T=333 \text{ K}$. As already mentioned above, the endothermic peak around $T = 329 \text{ K}$ ($= T_m$) observed in the DTA curve (Fig. 5.1), arises due to the melting of the pure crystalline PEO in our sample $\text{PEO+NH}_4\text{I}$ ($\text{NH}_4^+/\text{EO} \approx 0.076$). Therefore, the increase in the value of τ_3 (and in the corresponding hole volume in Fig.5.3) followed by the jump in τ_3 at $T=328 \text{ K}$ is attributed to the phase change occurring around $T \sim 328 \text{ K}$. Compared to the earlier case of $\text{PEO:NH}_4\text{ClO}_4$, the relative change in the value of τ_3 over the same temperature range was found to be smaller for the present sample.

Our results for the o-Ps intensity I_3 vs temperature (Fig.5.4) show a behaviour which is quite different from the one observed in the case of $\text{PEO:NH}_4\text{ClO}_4$ (Chapter 4) where the I_3 values remained relatively constant over the entire temperature range. In the present sample ($\text{PEO:NH}_4\text{I}$), increasing the temperature above the room temperature of 298 K led to an increase in the values of I_3 with a similar jump as that of τ_3 around 328

K. This increase in the value of I_3 may be explained in terms of decrease in the degree of crystallinity of the sample. On increasing the temperature, the crystalline PEO progressively melts into an elastomeric phase, resulting in an increase in the amount of amorphous phase and therefore an increase in the amount of free volume available in the sample. In other words we propose that the changes in I_3 in the range 298-328 K are caused by the structural (or physical) effects.

However with further increase ($T > T_m$) in the temperature, we find (Figs.5.3 and 5.4) that both τ_3 and I_3 started to decrease from about 335 to 353 K. This decrease in τ_3 and I_3 may have resulted from two simultaneous but [12,13] different effects. In the first effect the changes observed in τ_3 and I_3 may be due to the physical or morphological changes in the sample i.e. decrease in the amount of amorphous content in the material thereby reducing the amount of free volume in the sample. As observed by other workers [6,17,18], the degree of crystallinity of such complexes is determined by the thermal history of the samples. Hashmi [18] compared the degree of crystallinity of the as-prepared sample (of PEO + NH_4I with $\text{NH}_4^+/\text{EO} = 0.059$) with sample which was annealed and cooled slowly and with sample which was annealed and quenched and found that the the degree of crystallinity of these three samples was 31%, 35% and 64% respectively. These results indicate that the degree of crystallinity of PEO+ NH_4I should increase with thermal treatment and should thus lead to a reduction in free volume. In our case, a measurement of positron lifetime spectra involved several hours of

data acquisition at a particular temperature, which is equivalent to thermal annealing of the sample at that temperature. This may have resulted in an increased degree of crystallinity of the sample with an accompanying decrease in the free volume content in the sample.

The second effect could be chemical in nature and might cause the decrease in τ_3 and I_3 beyond 335 K. With increasing temperature, we believe that the amount of dissociation of NH_4I present in the complex may have increased resulting in the release of more iodine and I^- ions in the amorphous phase. Since iodine is known to be a good o-Ps quencher [20,21], an increase in the iodine content with temperature in the amorphous phase may bring about a progressive reduction in the values of τ_3 and I_3 . Moreover, some of the released iodine may have occupied the free-volume holes thereby reducing the values of τ_3 and I_3 further. However this second effect discussed above depends on the amount of dissociation of NH_4I salt present as complexes with PEO and this dissociation process is not completely understood yet. Therefore the observed variation in the o-Ps lifetime parameters in the range $335 < T < 353$ K may be due to any one or both of the effects (i.e. structural and chemical) discussed above.

During the cooling cycle, τ_3 and I_3 started to decrease rather sharply with decreasing temperature upto $T=325$ K. The rate of decrease in the value of τ_3 became slower when the temperature dropped below $T = 325$ K but did not regain the original value at 298 K. However at the end of the cooling cycle i.e. below 310 K, the I_3 values started to regain some (but not all) of its previous

value at room temperature. This complex behaviour of τ_3 and I_3 during the cooling cycle can be attributed to the recrystallization of the elastomeric phase upon cooling from above T_m to below T_m thereby reducing the amount of amorphous content in the sample which may vary with difference in the thermal treatment of the sample. The observation that τ_3 did not regain its value at 298 K at the end of the cooling cycle indicates that the free-volume hole radius has shrunk from 2.56 Å to 2.17 Å after the heat treatment (Table 5.1). However the observation that I_3 regained some of its initial value at room temperature could mean that the degree of amorphicity (or crystallinity) may have been regained to certain extent. However, other possibilities cannot be ruled out. The above explanation will, however, hold good if the chemical factors do not change during the process of heating and cooling of the sample. The presence of iodine in the sample may also dictate the nature of the temperature variation of τ_3 and I_3 and a more detailed and systematic (e.g. compositional dependence) study in this direction using positron annihilation and other characterization techniques is needed.

Another useful quantity related to the free volume in polymers is the total free-volume fraction F_v (eqn. 4.2) and it can be determined from the knowledge of τ_3 and I_3 . However an argument similar to the one given in the previous chapter does not hold in this case because in addition to the small values of I_3 , the I_3 itself changes in the present case with temperature. Moreover the chemical factors arising from possible release of free iodine or I^- ions in the amorphous phase may have changed

during the entire heating and the cooling cycle. Therefore the validity of the relation $F_v = AI_3V_f$ is questionable in the present case. Nevertheless, we have calculated the values of I_3V_f and plotted them against temperature in Fig. 5.5, purely with the purpose of bringing out the relative amount of change in this quantity before and after the thermal cycle. It is observed that the plot (Fig. 5.5) changes its behaviour at $T_m = 328$ K both during the heating and the cooling cycle. Further the values of I_3V_f at the beginning of the heating cycle, is not regained at the end of the cooling cycle.

It may be pointed out that the present measurements involved only one cycle of heating and cooling and involving only one sample. It is realized that several cycles and perhaps more than one sample with different percentage composition of NH_4I should have been studied to check the reproducibility of such effects of thermal history. However we were unable to study several cycles because of some technical problems in our laboratory, We suggest that any future experiments on $PEO:NH_4I$ should include such measurements.

5.3.2. Analysis of lifetime spectra using CONTIN program

The present results for the positron lifetime spectra measured at different temperatures were analyzed using the computer program CONTIN to obtain the positron lifetime probability distribution functions (PDF) $\alpha(\lambda).\lambda^2$. In Fig. 5.6 (a) and (b) we have presented the results of such analysis i.e. the distribution function $\alpha(\lambda).\lambda^2$ against the positron lifetime at

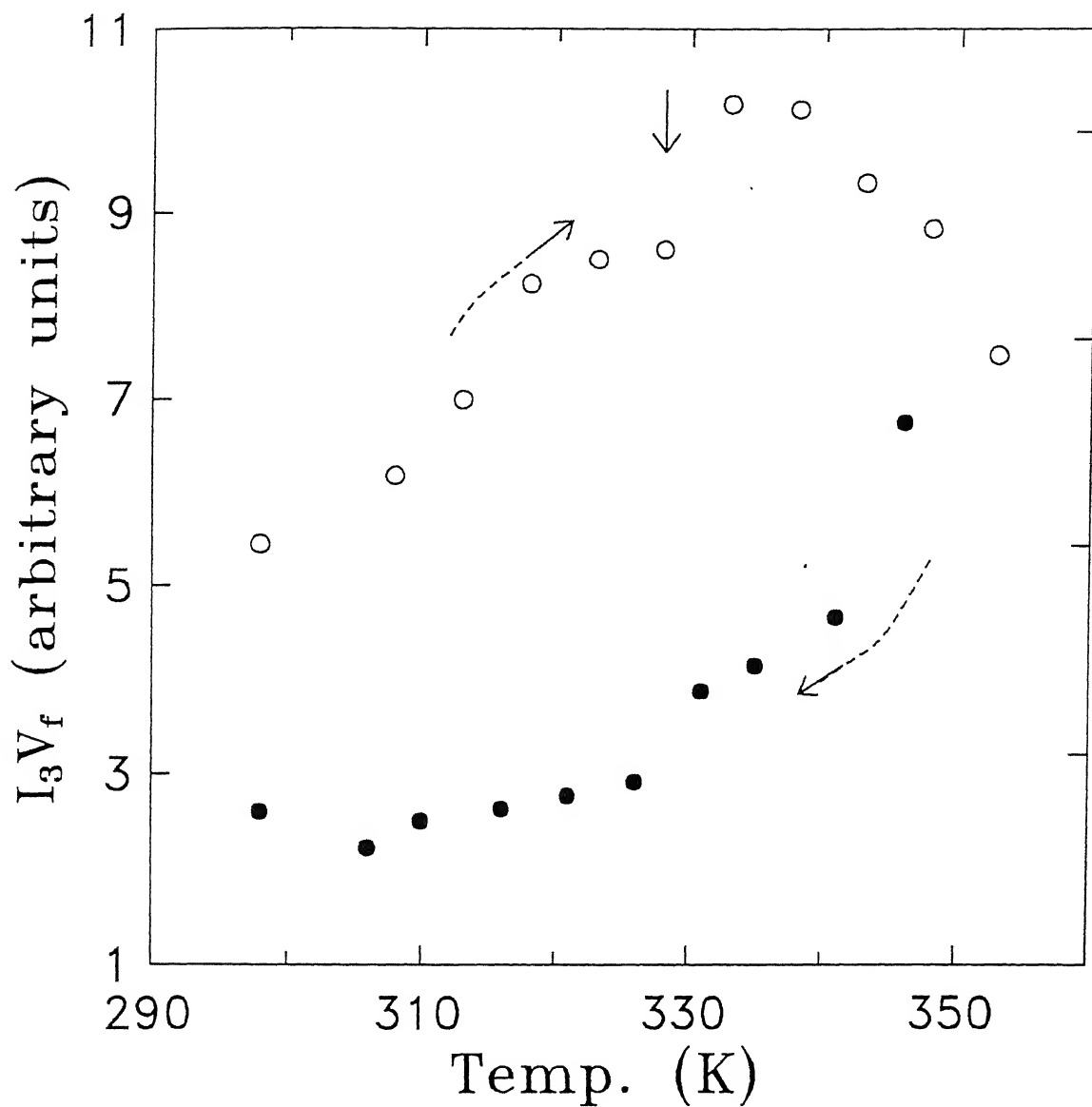


Fig. 5.5 Temperature dependence of I_3V_f in PEO: NH_4I ($\text{NH}_4^+/\text{EO} \approx 0.076$). Positions indicated by the arrow corresponds to the melting temperature of uncomplexed PEO ($T_m \sim 328$ K). Open symbols describe the data for increasing temperature, while solid symbols describe the data for decreasing temperature.

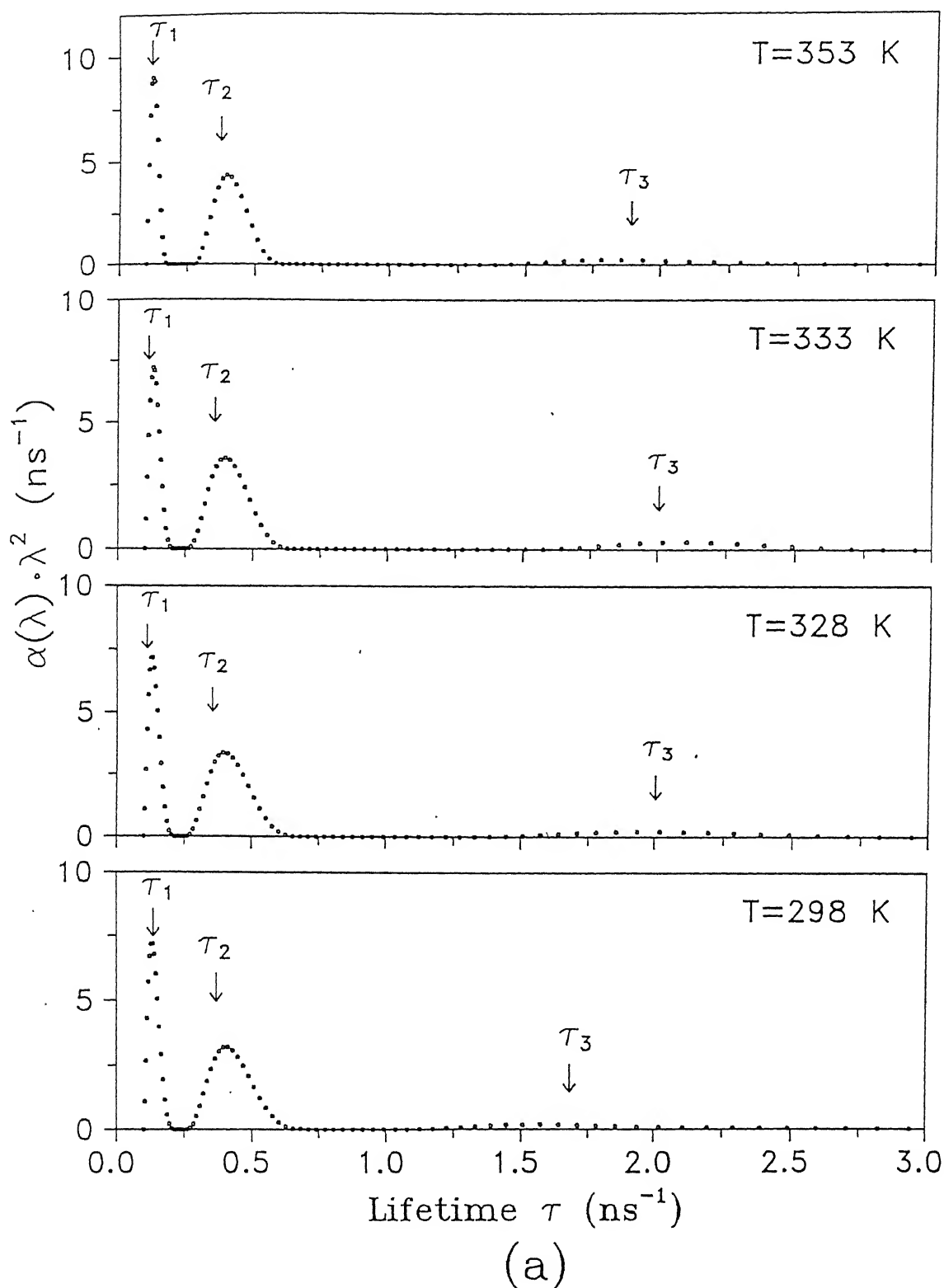


Fig. 5.6 Positron lifetime distributions in PEO:NH₄I (NH₄⁺/EO \approx 0.076) at some representative temperatures during the (a) heating and the (b) cooling cycle, obtained from CONTIN analysis. The positions corresponding to the lifetimes values τ_1 , τ_2 and τ_3 obtained from PATFIT analysis (Table 5.1) are shown by arrows.

(Continued on the next page)

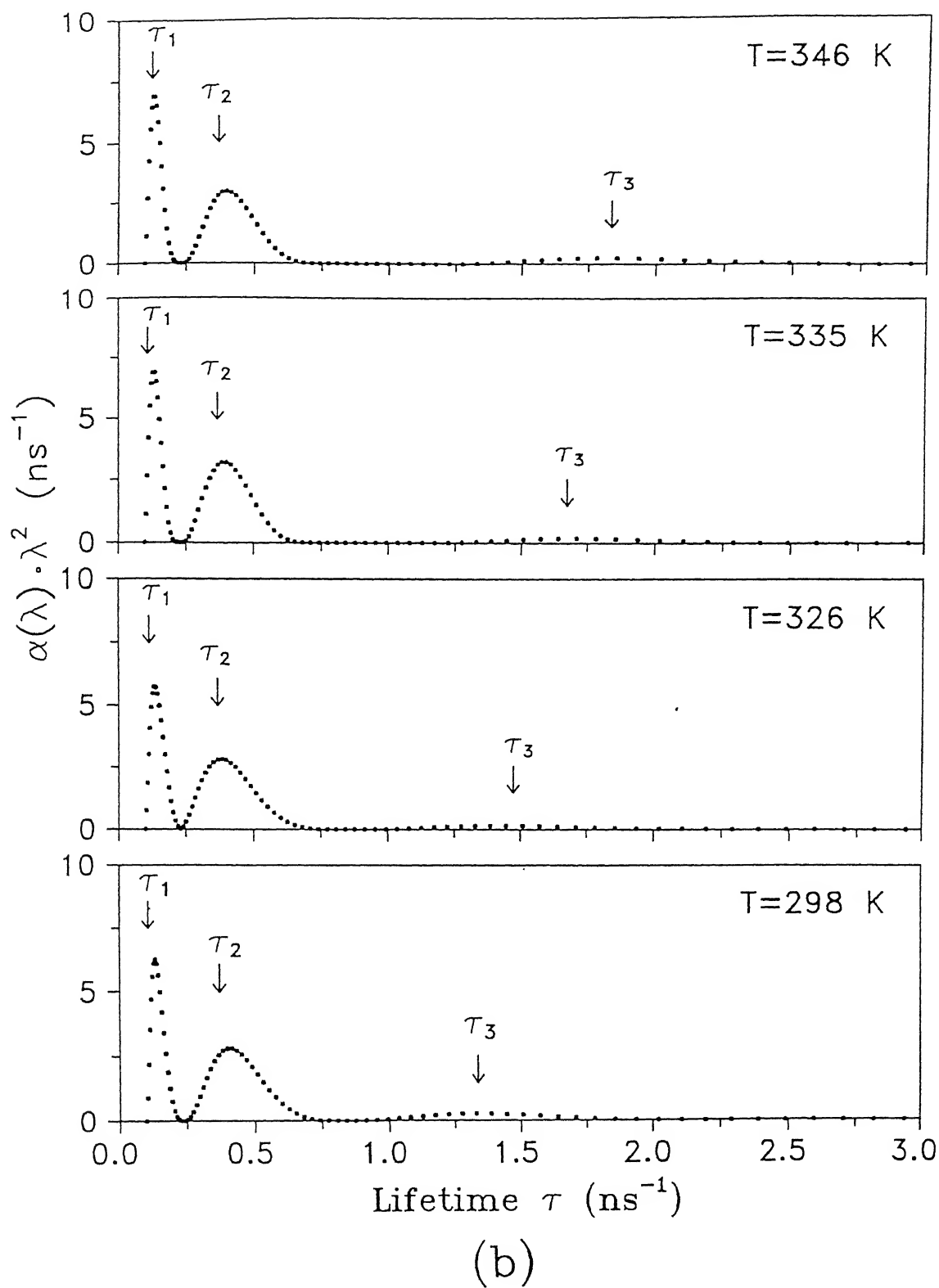


Fig. 5.6 (Continued)

some representative temperatures during the heating and the cooling cycle respectively. Each such lifetime distribution function showed presence of three distinct and well-resolved peaks. The mean positron lifetimes and intensities ($\bar{\tau}_i$ and \bar{I}_i , $i = 1-3$) obtained from CONTIN analysis have been obtained with the help of the eqs. (4.3) and (4.4) described in the previous chapter. The values of $\bar{\tau}_i$ and \bar{I}_i , ($i=1,2,3$) are listed in Table 5.2.

One can see that there is a fair amount of agreement between the peak positions of the three peaks (corresponding to τ_1 , τ_2 and τ_3) resolved by the CONTIN program (Table 5.2) and the values of τ_1 , τ_2 and τ_3 obtained by the PATFIT program (Table 5.1). However there are some minor discrepancies in the values of the intensities for the smaller two lifetimes (τ_1 and τ_2) and these are due to the difference in the deconvolution procedure used in the above two analysis to extract the lifetimes from the measured spectra which is always convoluted with the resolution function of the spectrometer. The expanded profiles of the extreme right peaks (corresponding to τ_3) in Figs 5.6 (a) and (b) are shown in Figs. 5.7 (a) and (b) during the heating and the cooling cycle respectively. It is observed that the peak position, width (FWHM), and asymmetry of each peak profile is different at different temperatures for heating and the cooling cycles.

At this point, we may like to indicate once again that although we have made attempts to maintain good counting statistics and instrumental stability during the time of lifetime measurements, the observed results for the lifetime and other

TABLE 5.2

Temperature dependence of mean positron lifetime parameters in polymer electrolyte PEO:NH₄I (NH₄⁺/EO \approx 0.076) obtained from **CONTIN** analysis.

Temp. (K)	$\bar{\tau}_1$ (ns)	$\bar{\tau}_2$ (ns)	$\bar{\tau}_3$ (ns)	\bar{I}_1 (%)	\bar{I}_2 (%)	\bar{I}_3 (%)	\bar{R}^c (Å)
298 \pm 2 ^a	0.14	0.41	1.65	31.3	61.8	7.0	2.51
298 \pm 2 ^b	0.11	0.40	1.37	28.6	65.1	6.3	2.18
308 \pm 2 ^a	0.14	0.40	1.82	31.0	62.0	7.0	2.68
306 \pm 2 ^b	0.12	0.41	1.35	27.7	66.3	6.0	2.17
313 \pm 1 ^a	0.13	0.42	1.92	31.4	61.4	7.2	2.78
310 \pm 1 ^b	0.14	0.39	1.30	27.0	67.3	5.7	2.11
318 \pm 1 ^a	0.13	0.42	2.01	30.5	61.5	8.0	2.86
316 \pm 1 ^b	0.12	0.40	1.41	26.9	67.4	5.7	2.24
323 \pm 1 ^a	0.14	0.39	2.06	30.7	61.5	7.8	2.91
321 \pm 1 ^b	0.13	0.43	1.44	27.0	68.4	5.0	2.28
328 \pm 1 ^a	0.12	0.42	2.07	29.7	62.2	8.1	2.92
326 \pm 1 ^b	0.14	0.40	1.50	27.0	67.8	5.2	2.34
333 \pm 1 ^a	0.11	0.39	2.11	28.8	62.4	8.8	2.95
331 \pm 1 ^b	0.11	0.38	1.75	26.2	68.5	5.3	2.62
338 \pm 1 ^a	0.12	0.40	2.11	28.8	62.3	8.9	2.96
335 \pm 1 ^b	0.12	0.41	1.73	26.6	67.6	5.8	2.59
343 \pm 1 ^a	0.13	0.42	2.04	28.9	62.5	8.6	2.89
341 \pm 1 ^b	0.14	0.40	1.70	25.8	67.4	6.8	2.56
348 \pm 1 ^a	0.10	0.39	1.85	27.5	64.1	8.4	2.86
346 \pm 1 ^b	0.11	0.41	2.42	25.9	65.9	8.2	2.71
353 \pm 1 ^a	0.10	0.43	1.90	28.0	64.2	7.8	2.76

^a during heating cycle

^b during cooling cycle

^c \bar{R} are the mean free-volume hole radii obtained by using $\bar{\tau}_3$ and eq. (1.17).

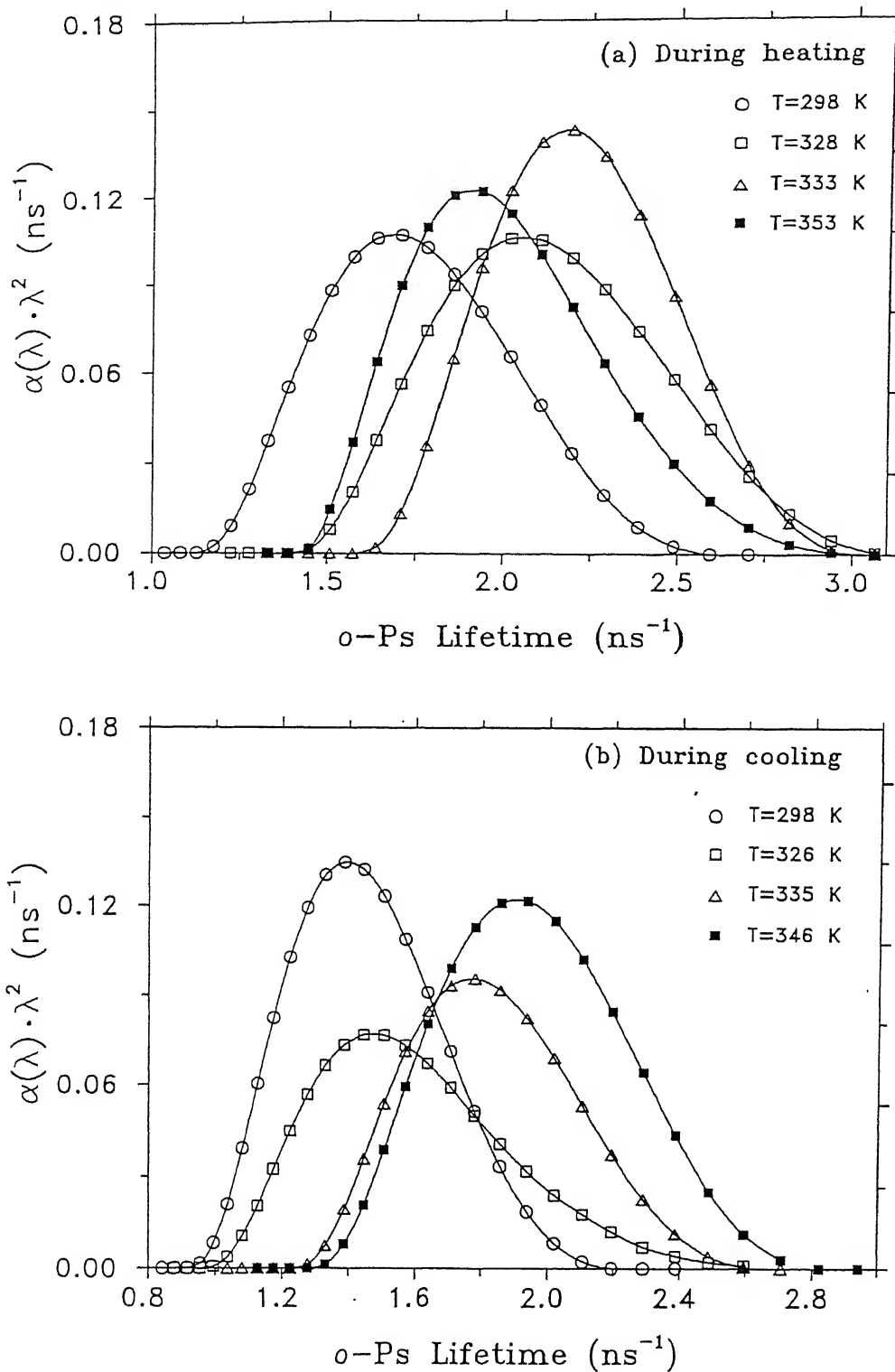


Fig. 5.7 o-Ps lifetime distribution in PEO:NH₄I ((NH₄⁺/EO ≈ 0.076) at different temperatures for the (a) heating and (b) cooling cycle. The data were taken from right hand peaks in Fig. 5.6 (a and b). The continuous lines are drawn through the data points for visual guidance.

related distributions should be accepted to provide a qualitative rather than a quantitative picture and that they represent a certain trend. Moreover the moderate resolution of our instrument may have a finite effect on these distributions.

From the observed o-Ps lifetime distributions, we have determined the free-volume hole-radius probability density function, $f(R)$, using eq. (4.5). Once again we have not applied any correction factor for the Ps trapping [22,23]. The present results for $f(R)$ are plotted against R for the heating and the cooling cycles in Figs. 5.8(a) and 5.8(b) respectively. The mean radius of the free volume hole in the interval R_1 to R_2 was determined by using the formula

$$\bar{R} = \frac{\int_{R_1}^{R_2} f(R) R dR}{\int_{R_1}^{R_2} f(R) dR} \quad (5.1)$$

where the $f(R)$ are the distribution functions discussed above. These values of the mean radii are also tabulated in Table 5.2. The behaviour of $f(R)$ as observed from these plots can be summarized as follows:

- (i) The $f(R)$ functions are fairly symmetric and can be approximated by Gaussian-type functions having FWHM of about 0.6-0.8 Å,
- (ii) The $f(R)$ functions corresponding to the melting ($T_m=328$ K) is the broadest,
- (iii) The effect of thermal history is reflected in the nature of distribution functions $f(R)$ during the heating and the cooling

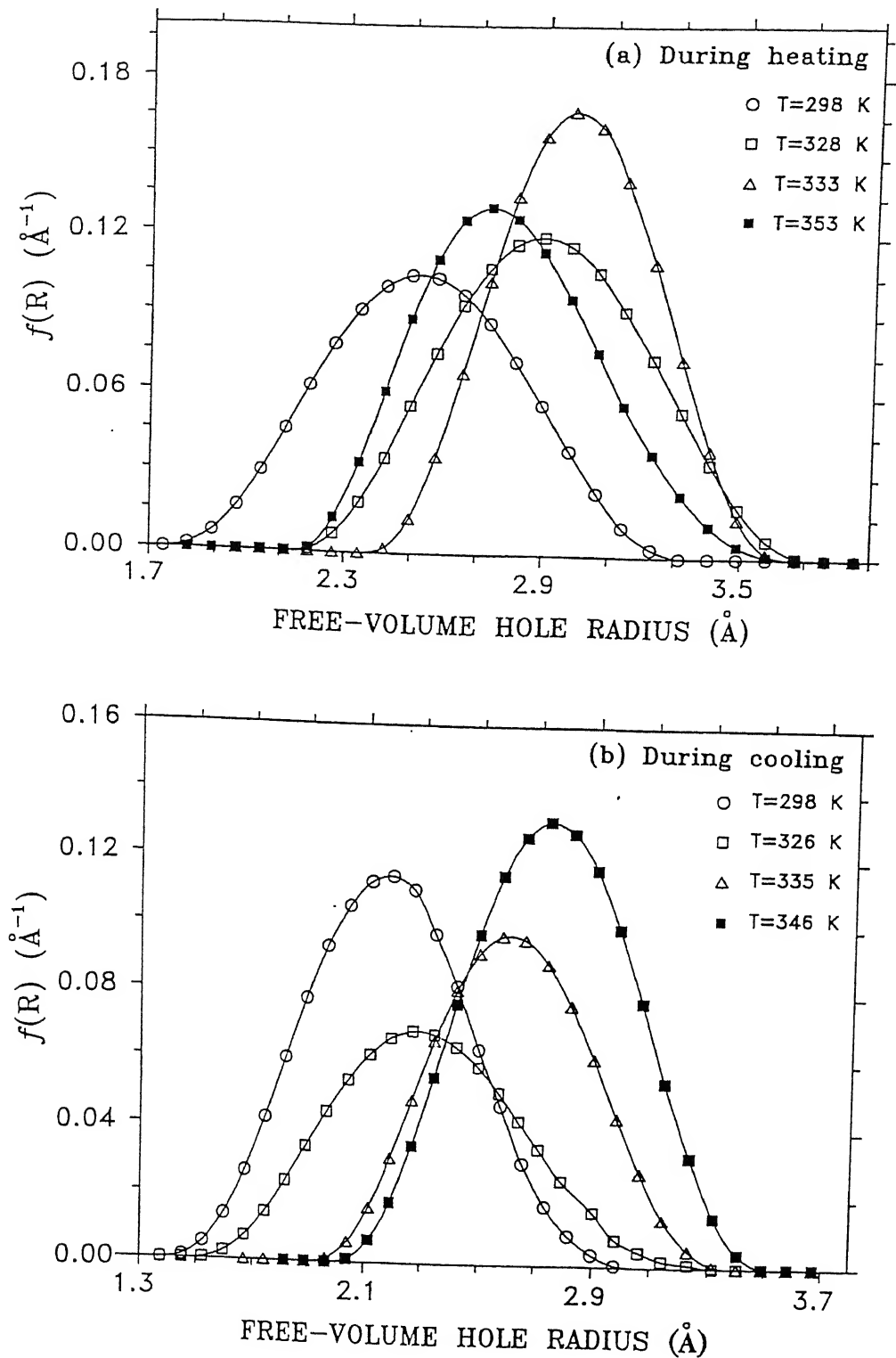


Fig. 5.8 Free-volume hole radius distribution functions $f(R)$ in $\text{PEO:NH}_4\text{I}$ ($\text{NH}_4^+/\text{EO} \approx 0.076$) at different temperatures corresponding to o-Ps lifetime distribution function in Fig. 5.7 (a) and (b) during the (a)heating and (b)cooling cycle. The continuous lines are drawn through the data points for visual guidance.

cycle.

Using the above distribution functions for $f(R)$ we have once again determined the probability density functions for the hole volume $g(V)$ using eq. (4.6). The results of hole volume distribution, $g(V)$, obtained in this way for the present sample corresponding to the hole radius distribution $f(R)$ in Figs. 5.8(a) and (b) are shown in Figs. 5.9(a) and (b). It is observed that the hole-volume distribution, $g(V)$, are asymmetric with a skewing tendency towards larger volume. The effect of thermal history is once again reflected in the temperature variation of $g(V)$ during the heating and the cooling cycle.

The present results (Figs. 5.8 ((a) and (b)) and Figs. 5.9 ((a) and (b)) for the distributions of hole radius and volume in the polymer electrolyte PEO: NH_4I ($\text{NH}_4^+/\text{EO} \approx 0.076$) obtained from the o-Ps lifetime distributions may provide useful information regarding the properties of free volume provided that the chemical factors like o-Ps quenching due to the presence of iodine are more completely understood for the present system do not interfere with these results.

5.4 Conclusions

The temperature dependence of the positron lifetime spectra in the sample of PEO complexed with NH_4I ($\text{NH}_4^+/\text{EO} \sim 0.076$) has been measured. The analysis of the present results qualitatively shows the temperature dependence of the free volume in PEO: NH_4I ($\text{NH}_4^+/\text{EO} \sim 0.076$) and indicates a hysteresis effect. It would be

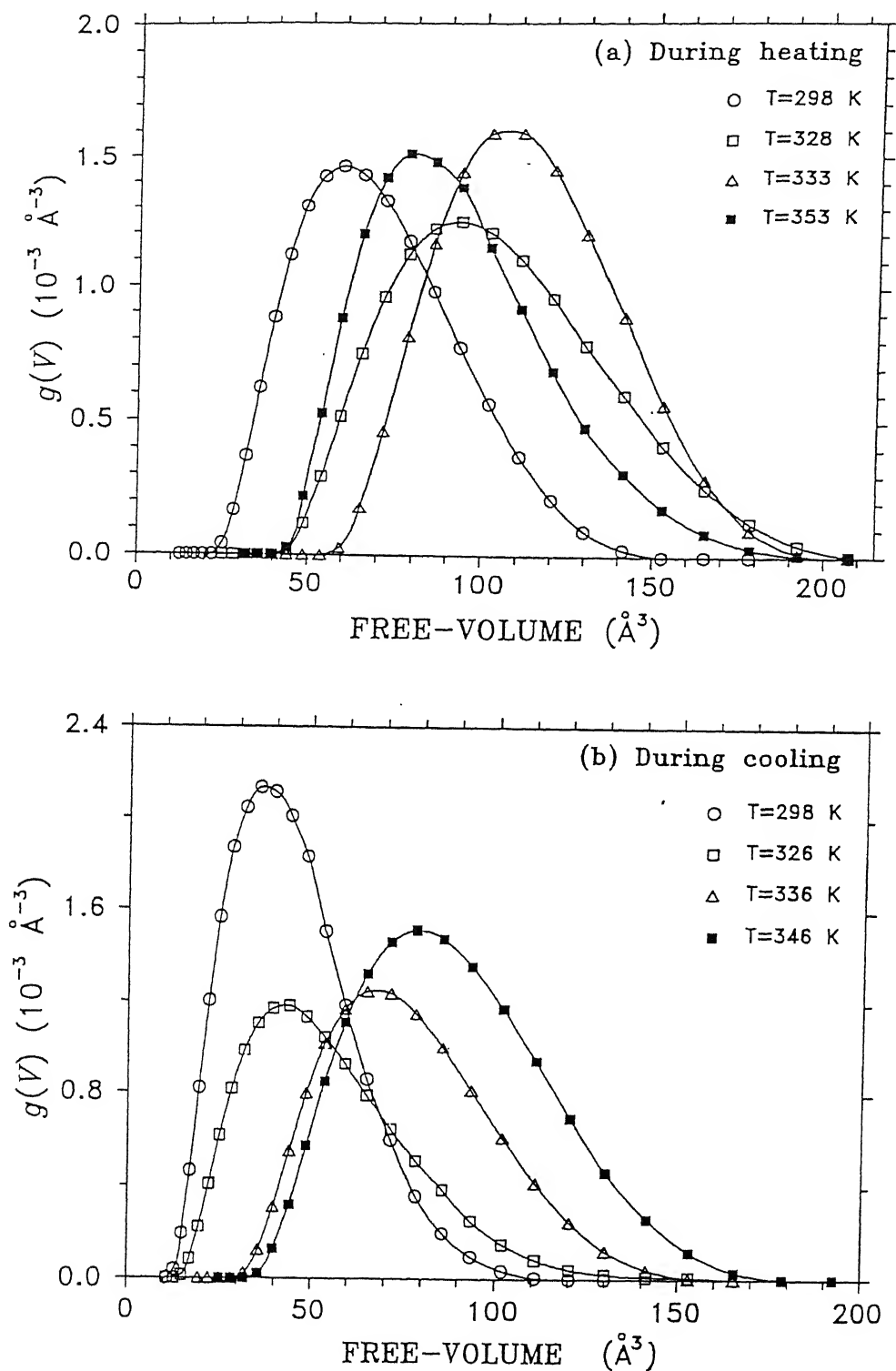


Fig. 5.9 Free-volume hole volume distribution functions $g(V)$ in PEO: NH_4I ($\text{NH}_4^+/\text{EO} \approx 0.076$) at different temperatures during the (a) heating and (b) cooling cycle. The continuous lines are drawn through the data points for visual guidance.

interesting to further investigate the effect of iodine and thermal hysteresis applying other characterization techniques to the present sample (PEO:NH₄I). Another interesting problem would be to systematically examine the effect of iodine by studying the composition dependence of positron lifetime parameters on the composition ratio (PEO:NH₄I) in this polymer salt-complex. Such studies involving positron annihilation lifetime studies are planned for the future.

References

1. K.K.Maurya, Neelam Srivastava, S.A.Hashmi and S.Chandra J. Mat. Sci. 27, 6357 (1992).
2. "Polymer Electrolyte Reviews 1" edited by J.R.MacCallum and C.A.Vincent (Elsevier Applied Science, London, 1987) ; "Polymer Electrolyte Reviews 2" edited by J.R.MacCallum and C.A.Vincent (Elsevier Applied Science, London, 1989);
3. E.A Reifman, M.L. Kaplan and R.J.Cava, Solid State Ionics 17, 67 (1985).
4. J.E. Weston and B.C.H. Steele, Solid State Ionics 2, 347 (1981).
5. S.M. Ansari, M. Brodwin, M. Stainer, S.D. Druger, M.A. Ratner and D.F. Shriver, Solid State Ionics 17, 101 (1985).
6. M.Minier, C.Berthier and W.Gorecki, Solid State Ionics 9/10, 1125 (1983).
7. K.K.Maurya, Ph.D. Thesis, Banaras Hindu University, Varanasi, India (1993), unpublished.
8. "Positron Solid State Physics" edited by W. Brandt and A. Dupasquier (North-Holland, Amsterdam, 1983).
9. S.J.Tao, J. Chem. Phys. 56, 5499 (1972).
10. "Positron and Positronium Chemistry", edited by D. M. Schrader and Y. C. Jean, (Elsevier, Amsterdam ,1988) ;
11. Y.C. Jean, Mater. Science Forum 175-178, 59 (1995).
12. Y. Ito, K.I.Okamoto and K. Tanaka, J. de Physique C4 3, 241 (1993).
13. Y. Ito, Mater. Science Forum 175-178, 627 (1995).

14. "The Physics of Glassy Polymers" edited by R.N. Haward
(Applied Science Publishers, London, 1973).
15. H. Nakanishi and Y.C. Jean, in "Positron and Positronium Chemistry", edited by Y.C.Jean, (World Scientific, Singapore, 1990), p. 95.
16. H.Nakanishi, Y.C.Jean, E.G.Smith and T.C.Sandreczki, J. Polym. Sci. Polym. Phys. Ed. 27, 1419 (1989).
17. M. Minier, C.Berthier and W.Gorecki, J. de Physique 45, 739 (1984).
18. S.A.Hashmi, J. Mater. Sci. Lett. 10, 1153 (1991).
19. R.H.Baughman, J.L. Bredas, R.R. Chance, R.L. Elsenbaumer and L.W. Shacklette, Chem. Rev. 82, 209 (1982).
20. V. Ravindrachary, H. R. Sreepad, A. Chandrashekara, C. Ranganathaiah, and S. Gopal, Phys. Rev. B 46, 11471 (1992).
21. O.E. Mogensen, Abstract of "Fourth International Workshop on Positron and Positronium Chemistry, Strasbourg, ,1993".
22. Q.Deng, F.Zandiehnam, and Y.C.Jean, Macromolecules 25, 1090 (1992).
23. Y.C.Jean and Q.Deng , J. Polym. Sci. Polym. Phys. Ed. 30, 1359 (1992).

CHAPTER 6

TEMPERATURE DEPENDENCE, PHYSICAL AGING AND MOISTURE ABSORPTION STUDIES IN CURED EPOXY AND POLYESTER RESIN POLYMERS USING POSITRON LIFETIME SPECTROSCOPY

6.1 Introduction

In the previous two chapters we have seen that positron lifetime spectroscopy can be a useful technique for studying polymer electrolytes and when combined with other characterization studies it can help us to understand the mechanism of ion-transport in the polymer electrolytes. The polymer electrolytes discussed so far belong to semicrystalline polymers and at room temperature the amorphous phase present in them lies above the glass transition temperature, T_g , ($T_g \sim 213$ K) for the amorphous phase which make these polymer electrolytes flexible. There are polymers whose glass transition temperatures lies above the room temperature and their physical properties are similar to that of the glasses i.e. having glassy type structure and thermodynamically at non-equilibrium state. Consequently these polymers in most of the cases are hard and tough at room temperature and this renders them suitable for applications requiring mechanical toughness. Such polymers are known as glassy polymers or polymer glasses [1]. All linear polymers are glasses at low temperatures and on increasing the temperature they change from a glassy to a rubbery state above T_g . Some of the glassy polymers include polyvinylacetate, polysulphonate, polyvinyl

formals, polyvinyl carbozoles, polycarbonate and the cross-linked polyester and epoxy resins. In the present work, we have also carried out some positron lifetime measurements on two such glassy polymers, i.e. polymers of epoxy and polyester resins, to study the free-volume properties in these polymers as a function of temperature, effect of physical aging and moisture absorption and these results will be presented later in this Chapter.

For the past several years there has been a growing interest in determining both equilibrium and non-equilibrium thermal properties of glassy polymers [2-4]. The thermal expansion of various polymers has been studied in the last several decades [5-9], and the results have been interpreted within the framework of different models. Thermal expansion of a material is one of the simple structural changes that a material undergoes without any mechanical and chemical intervention. For glassy polymers, several temperature dependent structural transitions can occur. Most notable is the glass transition temperature (see Chapter 3) at which the polymer undergoes a dramatic transformation as the degrees of freedom of the molecular chains and the resulting mobility change considerably. The glass transition process determines some of the major physical properties of the polymers, and a number of reviews on this subject have appeared in the literature[10-13]. There are still some difficulties in interpreting all the features of the glass transition phenomenon. Moreover the knowledge of the glass transition temperature is also essential for application of glassy polymers in many fields because above T_g , the mechanical properties of the polymer

deteriorate and the polymer loses its toughness. Considerable interest has been focussed on the structure and property changes that occur below and at glass transition temperature (T_g) and, therefore, understanding the nature of the glassy state and the glass transition has been one of the long-standing problems in materials science and physics.

The properties of glassy polymers are known to be strongly influenced by the density of molecular packing or free volume. The concept of free volume has long been used to explain the glass transition phenomenon and the behaviour of glassy materials. In Chapter 3, we have already noted that the free volume in glassy polymer reaches a critical value at the glass transition temperature, and below T_g there is insufficient room for molecular maneuver and therefore in the glassy state the free volume will be frozen in and will thus remain constant. Above T_g , there is usually a rapid increase in the free volume in the rubbery state till the temperature reaches the melting temperature of the solid.

In this way the concept of free volume has been very useful in explaining the overall behaviour of glassy polymers. In some cases, along with the knowledge of overall free volume, the knowledge of the size distribution of free volume and its variation with time, temperature and pressure is also necessary. These ideas have already received theoretical consideration [14-18]. Since amorphous polymers lack structural order, distribution of free volume may be the best way to characterize them. Experimental investigations of fractional free volume and related thermodynamic properties have been made by various

techniques [2-4,19]. Each technique has yielded certain information about the microstructural properties of free volume and the glassy state. In Chapter 1 we have already discussed the usefulness of positron annihilation spectroscopy (PAS) as a technique to determine the free-volume hole size and their distributions along with advantages that PAS offers over other techniques in determining the free-volume properties in polymers and polymeric materials.

Several positron lifetime studies have, therefore, been performed to investigate the free-volume properties in a variety of polymers including the glassy polymers, and such experimental studies of polymers measuring the variation in the free volume with temperature [5-9,20], pressure [21,22], physical aging and structural relaxation [5,6,23-25], stress-induced structural deformation [26,27] etc. have been reported in the literature. Among them, most of the studies are performed on the epoxy and polycarbonate polymers, specifically as a function of temperature, pressure, aging time, mechanical stresses etc. [6,7,9,20,21,23,24,27]. These studies provided us with some valuable information about the various phase transitions as well as the free-volume properties such as hole size, density and distributions and their dependence on temperature, pressure and time, and in some cases they have brought out a good comparison between thermal coefficient of free volume and the specific volume expansions. In this respect moisture and other solute absorption studies are relatively few [9,28]. Secondly, in some cases, the chemical factors involved during such absorption of solute can

complicate the interpretation of the results in terms of the free-volume properties [29].

One of the most important and serious problems in utilizing polymers as industrial materials is the degradation of their mechanical properties as a function of time. Such degradation can be caused by two possible processes. The first is the chemical degradation which involves chemical bond modification and/or rupture, and the other process is due to the physical change in the microstructure of the material with time. This second process arises because glassy polymers are thermodynamically at non-equilibrium state below T_g . This non-equilibrium nature of amorphous solids/glassy polymers was first pointed out by Simon [30] and others [31]. Such materials are regarded as solidified supercooled liquids whose volume, enthalpy and entropy are greater than they would be in the equilibrium state. This non-equilibrium state is quite unstable and they undergo slow processes which attempt to establish equilibrium, indicating that even below T_g molecular mobility is not quite zero. Volume-relaxation studies of glassy materials [32,33] have, in fact, confirmed this non-equilibrium process.

This gradual approach to equilibrium affects many properties of the material [31-36]. These properties change with time, and the material is said to undergo 'aging'. To distinguish this type of aging from the chemical aging (thermal decomposition, photo-oxidation, etc.) it has been called as the 'physical aging'. During the course of physical aging the enthalpy and volume [34,37], and by implication the free volume, decrease, and so do

its creep and stress-relaxation rates, dielectric constant, dielectric loss etc. and the material becomes stiffer and more brittle resulting in embrittlement [38] and decrease in gas permeability [39].

In view of all this the aging which is a time-dependent phenomenon, is just as important as other parameters such as temperature, stress-level, humidity etc. Moreover, a knowledge of the aging behaviour of a material is indispensable for the prediction of its long-term behaviour. In all glassy materials aging proceeds in a very similar way, and is independent of the chemical composition of the material. In most of its aspects, aging can be explained from the free-volume concept [4]. This is because the mobility of particles in a closely packed system is predominantly determined by the degree of packing of the system or the amount of free volume available. In the next section we shall briefly discuss the phenomenon of physical aging from free-volume concept.

6.1.1 Free volume and physical aging

In Chapter 3, we have already discussed the concept of free volume in amorphous polymers and solids. The phenomenon of physical aging originates to a large extent from the segmental mobility of the polymer chains and the free volume present in the material. Fig. 6.1 schematically shows how the free volume of an amorphous polymer decreases when it is cooled from a temperature T_0 above T_g to a temperature T_1 below its T_g , and thereafter is kept at that temperature T_1 . By doing so, the volume will decrease

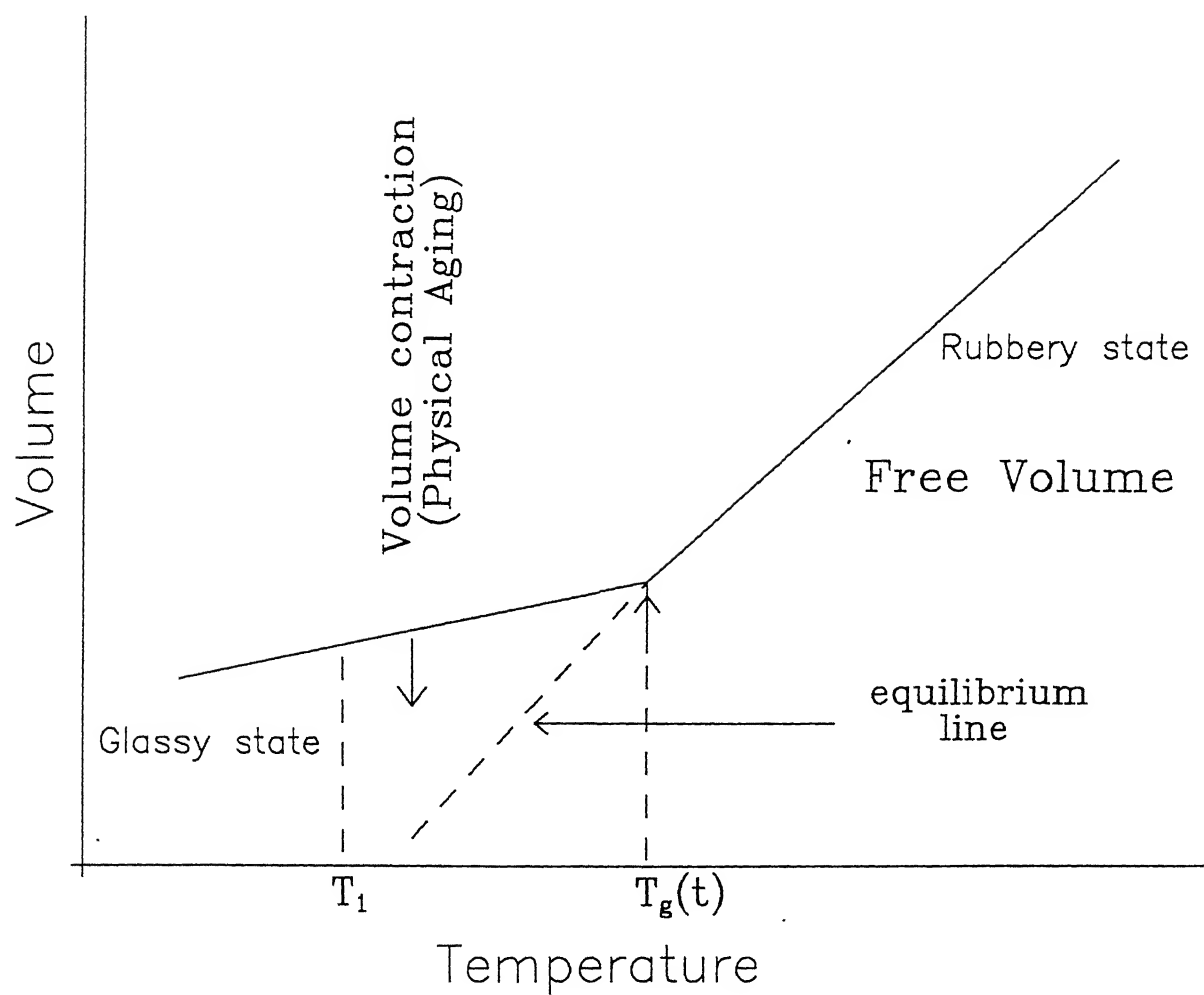


Fig. 6.1 Origin of physical aging from free volume concept. In the figure T_g is the glass transition temperature and T_1 is any temperature below T_g . Downward arrow represents the isothermal free-volume contraction.

continuously under the isothermal condition, tending at an ever decreasing rate towards the equilibrium volume, represented by the broken line. This volume contraction is accompanied by a progressive decrease in the free volume [31,33], and the segmental mobility of short molecular chains [36,40]. In other words, the change in the temperature will disturb the entire equilibrium distribution function for free-volume holes, existing T_0 before cooling has started, and a change in free-volume, V_f , is brought about by a redistribution of the free volume holes [14,41]. Moreover the relaxation processes found to be both non-exponential and non-linear in character and they are best represented by William-Watts relaxation type functions [42].

6.1.2 Effect of moisture on glassy polymers

Moisture is constantly present in almost every operational environment of these materials. Although the effect of moisture absorption on glassy polymers has been studied in detail in the past, its effect on the free volume has been only predicted and experimental studies are relatively few [9,12]. Moisture may be present in many forms and it can eventually penetrate all organic molecules by a diffusion-controlled process until a moisture equilibrium concentration is achieved. Application of heat can cause alterations in the microstructures of these materials that allow the water-holding capacity to increase. In general moisture causes a lowering of the mechanical properties of polymers. Once absorbed it is difficult to drive away all the moisture from the material. The moisture effectively plays the role

of a resin plasticizer which softens the polymer and thereby lowers the T_g . Recently, a great deal of attention has been focussed on the effect of moisture in epoxy resins because of their use in aerospace structural materials. In case of composites prepared by using polymers as matrix, moisture has a degrading effect in the mechanical performance of the composites. Free-volume theory predicts that the moisture or water absorbed in the process can readily diffuse through the material and occupy the free-volume sites available in the polymer. It is also believed that more the free volume larger will be the water-holding capacity.

Keeping some of these aspects in mind, we have performed positron lifetime studies on cured epoxy and polyester resin polymers with an aim of measuring not only the free volume available in these polymers but also to (i) monitor the changes in them as a result of temperature variation, (ii) study the effect of time on free-volume relaxation and (iii) study the changes in the free volume as a result of the moisture absorption at different temperatures. Moreover the polymers studied by us are technologically important as matrix materials in the preparation of composites and laminates. Hence studying the free volume and other physical properties are important to understand their mechanical behaviour. It may be pointed out that Jean et al. [20] have measured temperature dependence of positron lifetimes in epoxy samples earlier but the curing agent used by them was different. As for the polyester samples (to our knowledge) there are no positron lifetime results reported in the literature.

Details of the preparation, structure and the chemical and physical properties of various kinds of epoxy polymers are available in the literature [43-45]. Depending upon the choice of curing agent, resins can be made to cure, or harden, either slowly (several hours) or very quickly (less than a minute) at room temperature or at elevated temperatures. Epoxy resins with different chemical structures can be formulated to yield a variety of properties ranging from soft, flexible materials to hard, tough, chemically resistant products.

Epoxy resins possibly have the widest range of applications compared to other resins of similar types. Epoxy resins are used for potting and encapsulations (e.g. encapsulating welded modules, transformers, motors and IC's) to provide environmental protection against alkali, acid and humidity. Epoxy resins are also used to join many dissimilar materials because they provide the highest adhesive strength of any known polymeric material and can adhere to a wide variety of substrates. Epoxy resins are also used in tooling industries and to make moulded compounds with fillers and reinforcing agents. One of the most important use of epoxy resins is as a matrix material for manufacturing laminates and composites with various reinforcements such as glass, carbon, kevlar⁴⁷ etc. for structural parts in aircrafts, missiles and rockets, spacecrafts, and other industrial products such as used for printed circuit boards in electrical industries. In addition, composite storage tanks and pipes are used extensively in the chemical and petroleum industries. In general, epoxies are more expensive than other resins, but their superior performance makes

them more economical in the long run.

Polyester resins [47-49] have also attracted considerable attention because of the ease in their handling and fabrication and because of their superior mechanical properties. Unsaturated polyester resins are very versatile materials. At room temperature, the liquid resins are stable for months and even years, but can be triggered to cure in a few minutes simply by adding a peroxide catalyst which provides free radicals to start the chain reaction. Curing takes place by addition reaction that involves the conversion of double bonds into single bonds. Most peroxide catalysts decompose rather slowly when added to polyester resin. To get faster cure, accelerators (promoters) are used to speed up the reaction during curing. Styrene is by far the most commonly used diluents and it combines with the reactive double bonds of the polyester chains, linking them together to form a strong three-dimensional polymer network. The curing reaction is usually exothermic. Polyester resins are used in the manufacturing of a broad range of products, including boats, building panels, structural parts for automobile, aircraft and appliances like fishing rods and golf clubs etc.

6.2 Experimental

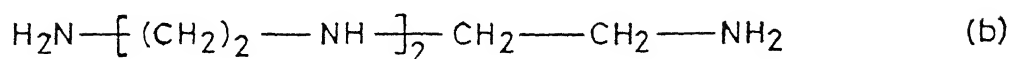
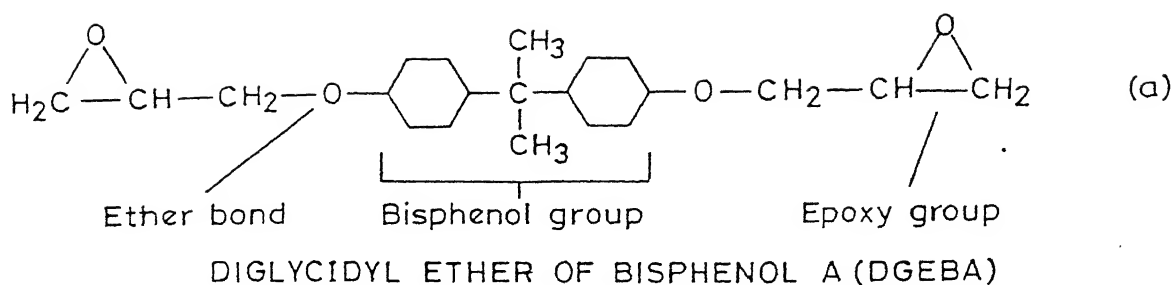
Both types of samples i.e. cured epoxy and unsaturated polyester resin polymers were prepared in our laboratory at Indian Institute of Technology Kanpur by cross-linking the liquid resins using appropriate curing agents.

Epoxy resin used in the present work to prepare the samples was diglycidyl ether of bisphenol A (DGEBA) commercially available as LY556 (Ciba-Geigy, India). The basic chemical structure of DGEBA is shown in Fig. 6.2 (a). The resin has got the following properties

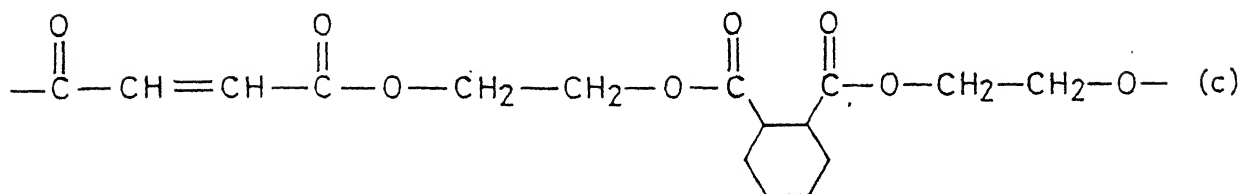
1. Viscosity at 298 K	9000 to 12000 MPa
2. Epoxy content	1.2 - 5.2 eq./Kg
3. Density at 298 K	1.1 to 1.2 gm/cm ³
4. Flash point	> 473 K

The epoxy resin was cured by 10 % (by weight) of the liquid aliphatic amine hardener (triethylene tetramine (TETA)) commercially available as HY951 (Ciba-Geigy, India). The chemical structure of the curing agent is also shown in Fig. 6.2(b). Curing of the epoxy resin involved an epoxide-amine addition polymerization. Desired amount of epoxy resin and hardener in the ratio 10:1 by wt. % were mixed and the resulting homogeneous mixture was poured in a cell covered with mylar sheets to cast laminates of epoxy polymers. The cell was then put in between two stainless-steel plates with spacers. Curing was performed at room temperature for 24 hours. Cured solid cross-linked epoxy was then cut into several pieces of 1cm x 1cm (each having thickness of 2 mm) using diamond cutter for further studies.

Polyester samples were prepared by curing unsaturated styrenated alkyds using 1 % by weight of methyl ethyl ketone peroxide (MEKP) as catalyst and 0.5 % by weight of cobalt octate as an active accelerator. The general chemical structure of unsaturated polyester resin is shown in Fig. 6.2(c). The resin



TRIETHYLENE TETRAMINE



UNSATURATED POLYESTER RESIN

Fig. 6.2 Chemical structure of resins and hardener used for sample preparation (a) Diglycidyl ether of Bisphenol A (DGEBA). (b) Triethylene tetramine and (c) Unsaturated polyester resin.

with catalyst and accelerator were mixed into a homogeneous mixture and then poured in a cell similar to the one used for preparing epoxy samples described above. Curing was performed at an elevated temperature of 343 K. For this purpose, the stainless steel plates were fitted with heaters whose temperature could be controlled by a temperature controller. Curing was done for 12h followed by post curing at 393 K for 4h and then at a temperature of 413 K for 2h respectively. Curing in this case was initiated by free-radical mechanism in the presence of the catalyst MEKP resulting in chain polymerization. Resulting sample is an extensive cross-linked solid. Cured polyester laminate of thickness 2mm was cut into several pieces of 1cm x 1cm using diamond cutter for further measurements.

DTA spectra were taken for both types of samples to observe the various transitions and determine their transition temperatures using a computer-controlled (Shimadzu DTA-50) differential thermal analyzer in the temperature range 300-473 K for a heating rate of 10 K/min. However our polyester sample failed to give any noticeable peak or dip over the entire temperature range of 300 to 473 K, which can be related to any transition even after repeated trials. DTA spectrum observed for the epoxy sample is shown in Fig. 6.3.

The positron lifetime measurements were performed at 298 K by using a conventional fast-fast coincidence spectrometer and a 15 μCi ^{22}Na as positron source. The source of positrons was sandwiched between two identical specimens of the sample. The time resolution of our lifetime apparatus was found to be 0.32 ns

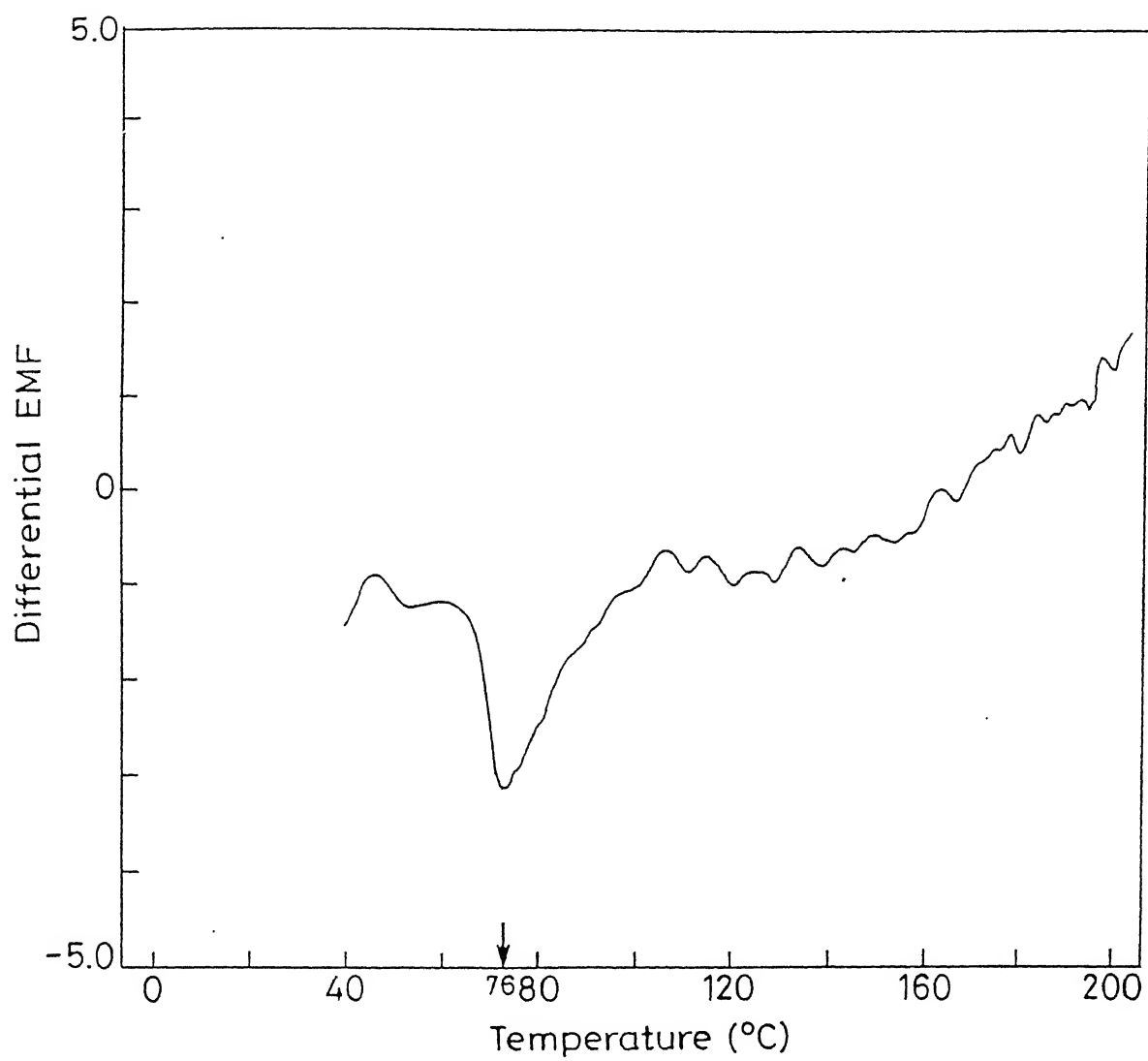


Fig. 6.3 DTA spectrum for the epoxy sample used in the present work.

(FWHM) as measured by the prompt spectrum from ^{60}Co source. For measuring the temperature dependence of the positron lifetime spectra for the present set of samples, the arrangements same as that described in Chapter 4 was used (Fig. 4.4). The positron lifetime spectra were taken in the temperature range 293 - 473 K in steps of about 10 K and 20 K for epoxy and polyester polymers respectively following both the heating and the cooling cycles. A total of about 5×10^6 counts were recorded under each lifetime spectrum. The measured lifetime spectra were then analyzed using the computer program PATFIT to extract the lifetime parameters for all the measured spectra. Once again our positron lifetime analysis showed that best χ^2 (< 1.1) and most acceptable standard deviations were obtained when each spectrum was fitted in terms of three lifetime components. For some spectra, we have also carried out continuous lifetime analysis using the CONTIN program where we have used the reference spectrum arising from well-annealed and high-purity (99.99+ %) nickel with an annihilation rate $\lambda = 9.1 \text{ ns}^{-1}$. This reference spectrum was taken immediately before and after each of the measurements at a particular temperature was performed. During the analysis by CONTIN, any relative time-zero shift between the reference and the sample spectrum was taken care in the input parameter file. A total of 85 grid points over the range $0.25 \text{ ns}^{-1} < \lambda < 13 \text{ ns}^{-1}$ were used to obtain the lifetime distributions.

For studying the effect of physical aging in our samples i.e. in epoxy and the polyester resin polymers, the samples were first aged at a temperature of 393 K for 100 hours in the case of epoxy

sample and 433 K for 100 hours for the cured polyester in vacuum. Annealed samples were thereafter cooled to the room temperature at various cooling rates which involved furnace cooling or water quenching or liquid nitrogen quenching of the samples. Quenched samples were thereafter used for positron lifetime measurements. Spectra were taken at regular time intervals to study the relaxation process or physical aging of the sample as a function of time at room temperature.

In addition, we have performed moisture and water absorption studies on our samples using positron lifetime measurements. For studying the moisture absorption, specially designed glass vessel having two arms with interconnection between them was used. In one of the arm the sample was put while in the other arm the water was kept. Both the arms were individually evacuated and then the valve connecting the two arms was kept open. Resulting saturation water vapor provided an atmosphere for the moisture absorption by the samples. Water absorption in our samples were performed by actually dipping the samples in water at 298 K and then at 370 K for different time periods. Positron lifetime spectra of the samples were recorded before and after the moisture/water was absorbed by the samples for 15 min, 30 min, 1 h, 2 h, 4 h and 16 h.

6.3 Results and discussions

We shall first discuss the results of our analysis for the temperature dependence of positron lifetime spectra in both epoxy and polyester. This will be followed by discussion on the effect

of physical aging and moisture absorption on positron lifetimes in our samples.

6.3.1 Temperature dependence of positron lifetime spectra in epoxy and polyester resin polymers

The positron lifetime spectra at two different temperatures (293 and 473 K) for the epoxy and the polyester are shown in Figs 6.4(a) and (b) respectively. It is readily observed from Fig. 6.4 that for each sample the positron lifetime spectrum shows significant changes in going from 293 to 473 K. At first we shall discuss the temperature dependence of positron lifetime parameters obtained for the epoxy sample when analysis was performed in terms of finite lifetime components using the PATFIT program. In epoxy samples, our analysis of the spectra measured in the temperature range 293-473 K showed the presence of three lifetime components whose values are in the range $\tau_1 = 0.11-0.14$ ns, $\tau_2 = 0.34-0.37$ ns and $\tau_3 = 1.8-2.4$ ns. The three lifetimes correspond to the three positron and Ps states in the sample [50]. The shortest lifetime is attributed to the singlet or p-Ps annihilation, while the intermediate lifetime τ_2 arises from the free (or unbound) annihilation of positrons. The longest or the third lifetime τ_3 is due to triplet Ps (o-Ps) annihilation. The relative intensities corresponding to the three lifetimes τ_1 , τ_2 and τ_3 are given by I_1 , I_2 and I_3 respectively such that $I_1 + I_2 + I_3 = 100$ %. The lifetime values and their intensities are given in Table 6.1(a) and (b) during the heating and cooling cycles respectively.

The temperature variation of τ_1 , τ_2 and their intensities I_1

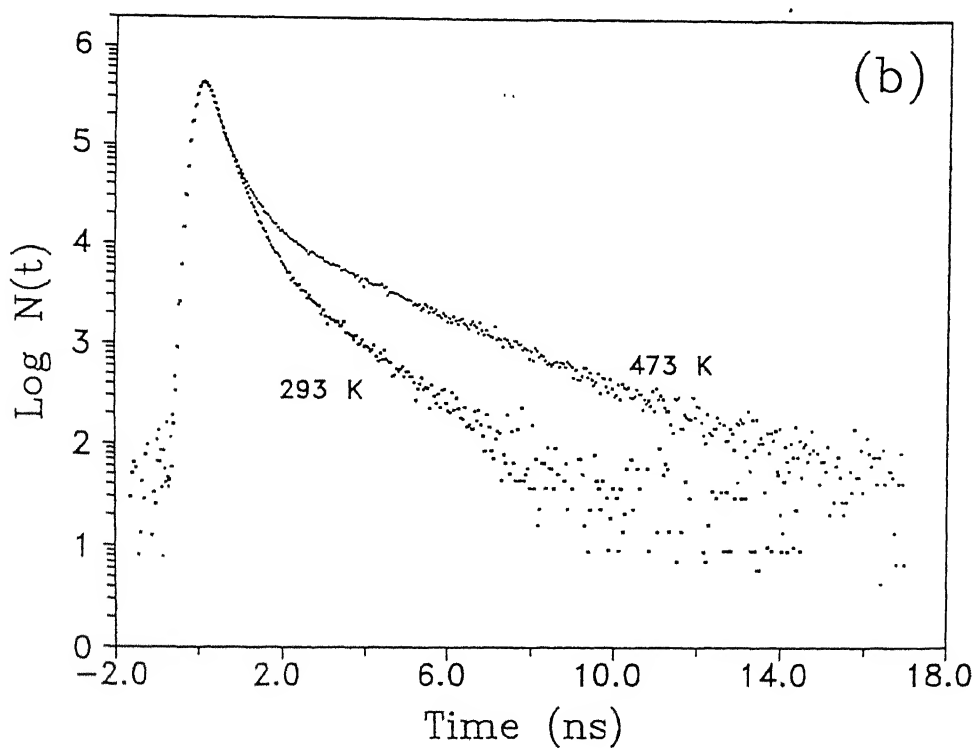
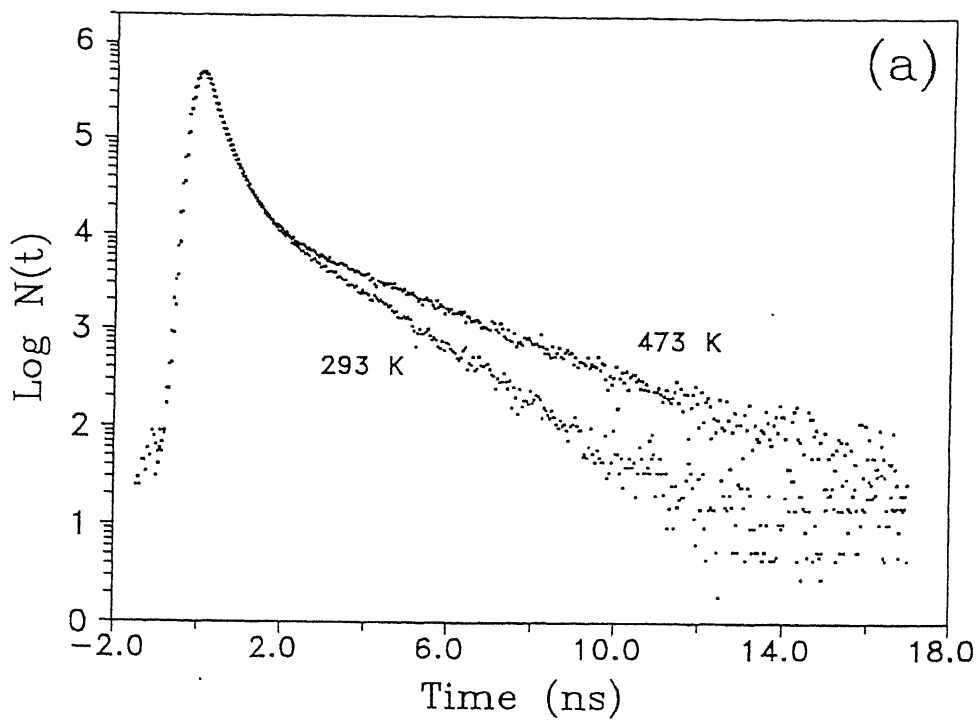


Fig. 6.4 Typical positron lifetime spectra at two different temperatures (293 K and 473 K) in (a) epoxy and (b) polyester samples used in the present work.

TABLE 6.1(a)

Temperature dependence of positron lifetime parameters in epoxy polymer (DGEBA:TETA) during the heating cycle obtained from PATFIT analysis.

Temp. (K)	τ_1 (ns)	τ_2 (ns)	τ_3 (ns)	I_1 (%)	I_2 (%)	I_3 (%)	R^a (Å)
293	0.124±.004	0.353±.004	1.618±.012	18.50±.96	62.27±.86	19.24±.17	2.48±.01
303	0.132±.004	0.348±.004	1.645±.012	18.73±.96	62.20±.96	19.08±.16	2.51±.01
313	0.129±.004	0.348±.004	1.662±.012	18.90±.93	62.86±.93	19.25±.16	2.52±.01
323	0.121±.003	0.355±.004	1.687±.014	19.09±.87	62.08±.78	18.88±.15	2.55±.01
333	0.127±.003	0.363±.003	1.776±.013	19.24±.88	62.08±.79	18.70±.15	2.64±.01
343	0.122±.003	0.359±.003	1.783±.013	19.48±.75	61.80±.87	18.71±.14	2.65±.01
353	0.137±.005	0.363±.004	1.878±.013	18.94±.95	62.04±.87	19.02±.13	2.74±.01
363	0.131±.004	0.353±.004	1.913±.014	18.81±.88	62.23±.99	18.87±.15	2.77±.01
373	0.137±.003	0.365±.004	1.963±.012	18.65±.95	61.84±.85	19.57±.12	2.82±.01
383	0.132±.004	0.367±.003	2.049±.013	18.87±.85	60.89±.88	19.24±.13	2.90±.01
393	0.132±.003	0.365±.003	2.088±.013	18.99±.75	61.68±.79	19.32±.11	2.94±.01
403	0.135±.003	0.365±.003	2.172±.012	18.48±.82	62.94±.78	18.57±.11	3.01±.01
413	0.133±.003	0.365±.003	2.231±.015	17.20±.99	63.16±.96	19.64±.12	3.06±.01
423	0.129±.003	0.364±.002	2.317±.013	17.19±.50	63.65±.45	19.15±.09	3.13±.01
433	0.129±.003	0.372±.003	2.377±.017	18.76±.71	63.53±.66	18.16±.09	3.82±.01
443	0.138±.003	0.370±.003	2.417±.014	17.15±.95	64.12±.90	18.72±.09	3.21±.02
458	0.126±.003	0.369±.003	2.421±.015	18.37±.73	63.36±.68	18.27±.09	3.22±.01
473	0.132±.003	0.368±.003	2.450±.016	18.49±.95	63.85±.98	18.65±.10	3.24±.01

^a R are the free volume hole radii obtained by using τ_3 and eq.(1.17).

TABLE 6.1(b)

Temperature dependence of positron lifetime parameters in epoxy polymer (DGEBA:TETA) during cooling cycle obtained from **PATFIT** analysis.

Temp. (K)	τ_1 (ns)	τ_2 (ns)	τ_3 (ns)	I_1 (%)	I_2 (%)	I_3 (%)	R^a (Å)
308	0.125±.003	0.358±.003	1.660±.012	19.33±.83	61.21±.62	19.45±.14	2.52±.01
318	0.132±.003	0.3459±.003	1.669±.012	19.82±.73	60.98±.73	19.20±.17	2.55±.01
328	0.119±.003	0.356±.003	1.699±.011	19.81±.97	61.30±.65	18.89±.13	2.56±.01
338	0.136±.004	0.368±.003	1.702±.014	19.35±.87	61.68±.89	18.97±.16	2.56±.01
348	0.121±.003	0.361±.003	1.745±.013	18.76±.63	61.78±.80	18.45±.15	2.61±.01
358	0.139±.003	0.379±.003	1.807±.013	19.36±.88	62.07±.52	18.57±.12	2.67±.01
368	0.134±.003	0.362±.003	1.886±.012	19.54±.88	61.98±.75	18.47±.13	2.75±.01
388	0.141±.004	0.377±.004	2.054±.012	18.79±.99	62.18±.90	19.05±.17	2.91±.01
398	0.112±.003	0.375±.004	2.110±.014	18.55±.83	61.91±.74	19.54±.13	2.95±.01
408	0.129±.003	0.377±.003	2.251±.013	18.32±.70	62.92±.62	18.75±.11	3.08±.01
418	0.113±.004	0.376±.003	2.301±.013	18.24±.95	62.75±.87	19.01±.13	3.12±.01
428	0.135±.003	0.378±.003	2.324±.014	17.87±.68	62.91±.60	19.21±.09	3.14±.01
438	0.120±.003	0.379±.003	2.385±.012	17.32±.85	63.91±.77	18.76±.09	3.19±.01
448	0.134±.004	0.379±.004	2.426±.014	18.46±.99	62.97±.89	18.76±.10	3.22±.01
465	0.129±.004	0.374±.004	2.416±.015	17.10±.95	64.57±.92	18.56±.12	3.22±.02

^a R are the free volume hole radii obtained by using τ_3 and eq. (1.17).

and I_2 for the heating and cooling cycles are shown in Fig. 6.5. Similarly the temperature dependence of τ_3 and I_3 are shown in Fig. 6.6 (a) and (b) respectively. Since the values of τ_3 and I_3 are more directly related to the free-volume properties in polymers, our discussion will be confined to the variations of τ_3 and I_3 and we shall omit the positron lifetimes τ_1 , τ_2 and their intensities from further discussion. Moreover the values of τ_1 , τ_2 and their intensities do not show any significant variation with temperature.

By assuming the free-volume holes to be spherical in shape, we make use of the semiempirical relationship given by eq. (1.17) to determine the free-volume hole radius R from the values of τ_3 and the values of R determined in this way are tabulated in Table 6.1 (a) and (b). The values of R calculated from τ_3 are used to obtain the hole volume $V_f = 4\pi R^3/3$, and the variation in the value of V_f (see right axis) is also shown in Fig. 6.6(a).

Positron lifetime studies have been previously reported in the literature for the resin DGEBA cured by using curing agents which are different from that used by us in the present work [20-22]. Despite a difference in the curing agent, the values of τ_3 and I_3 observed for our sample show a good agreement with those reported for the DGEBA samples [20-22]. It may be pointed out that epoxy polymers are completely amorphous at room temperature and they are also chemically very stable i.e. the chemical structure does not change in these polymers with temperature even upto a temperature as high as 470 K.

It is observed from Fig. 6.6(a), that the plot of o-Ps

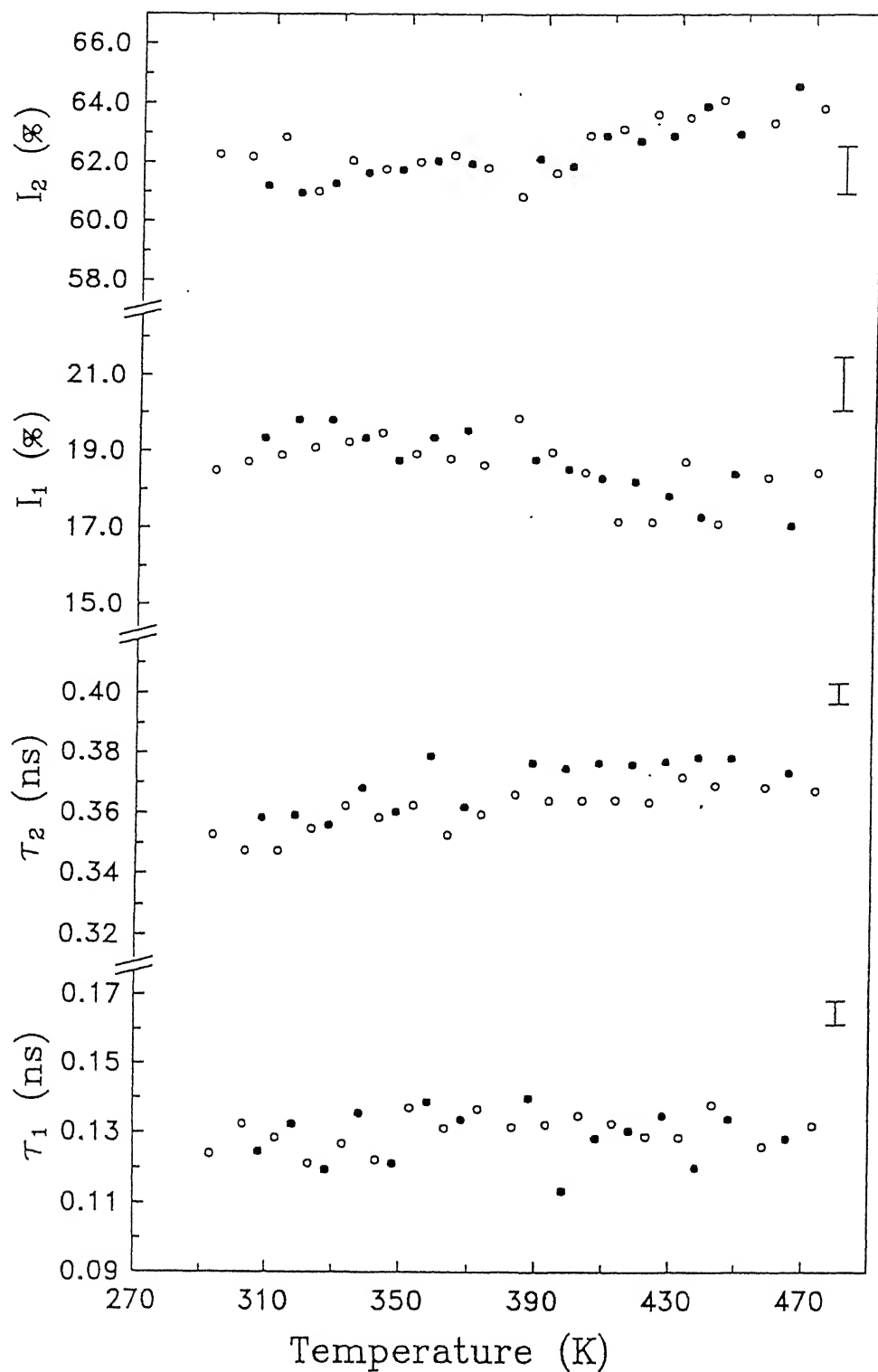


Fig. 6.5 Temperature variation of positron lifetime parameters τ_1 , τ_2 , I_1 and I_2 in epoxy polymer. Open symbols describe the data for the heating cycle, while solid symbols describe the data for the cooling cycle. Typical error associated with the data points are shown separately in each case by the vertical error bars.

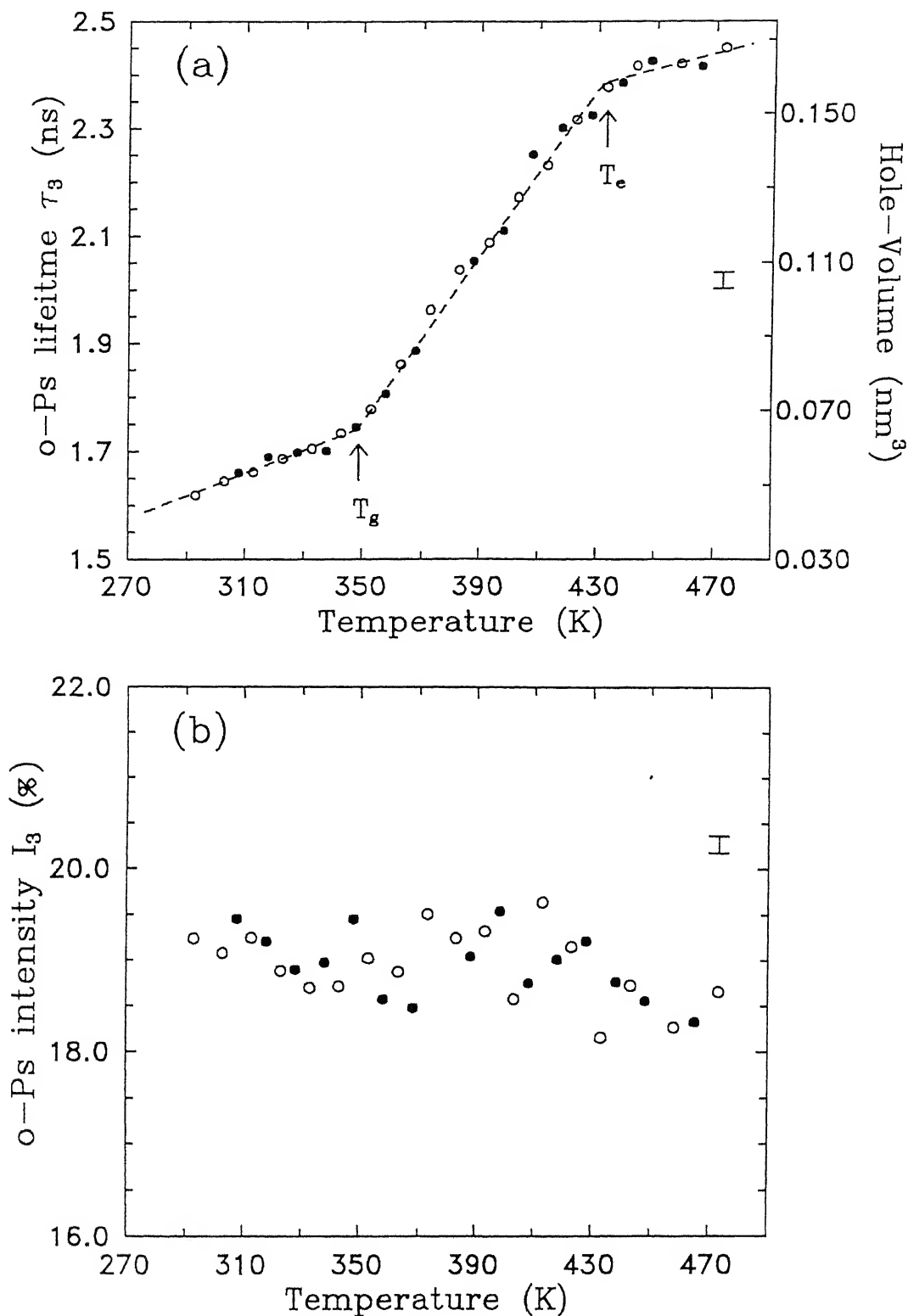


Fig. 6.6 Temperature dependence of (a) o-Ps lifetime, τ_3 , and (b) o-Ps intensity, I_3 in epoxy polymer. Open symbols describe the data for the heating cycle, while solid symbols describe the data for the cooling cycle. Positions corresponding to the various transitions are indicated by vertical arrows. Typical error associated with the data points are shown separately.

lifetime (τ_3) versus temperature (T) shows three distinct regions as far as the slope of the curve is concerned. In the region $293 < T < 350$ K, o-Ps lifetime increases with temperature. Around 350 K, the plot (Fig. 6.6(a)) shows a marked change in the slope of the curve and thus the temperature variation of τ_3 shows a steeper increase above 350 K. The DTA spectrum (Fig. 6.2) obtained by us for the epoxy resin in the temperature range of 300 - 473 K shows an endothermic peak around 350 K. This peak in the DTA curve is associated with the glass transition in our sample and the corresponding temperature was found to be $T_g = 349$ K (Fig 6.2). Therefore the observed change in the slope of the τ_3 vs T curve around $T=350$ K is attributed to the phase transition taking place around T_g . The value of the transition temperature obtained (temperature corresponding to the point of intersection between the two linear plots above and below the glass transition temperature) from Fig. 6.6 (a) was found to be $T_g = 350$ K, and this is in excellent agreement with the one obtained from the DTA analysis. As the temperature is further raised above T_g , the value of τ_3 (or the free-volume hole size) increased further and the slope of the curve almost remained constant in the temperature range 350 - 433 K. In Chapter 3, we have already mentioned that for glassy polymers, the free volume remains frozen below T_g . Above T_g , i.e. in the rubbery state, an increase in the temperature is accompanied by an increase in the total free volume in the material. This increase in the free volume may be due to a change either in the free-volume hole size or in the free-volume hole density (or both) in the material. Since τ_3 is related to the

free volume hole size by eq. (1.17), we find that the nature of variation in the free-volume hole size (see right hand axis in Fig. 6.6(a)) shows a behaviour which is similar to that observed in most of the glassy polymers (Fig. 3.5).

Around $T = 433$ K, the curve once more changes its slope and shows a plateau beyond $T = 433$ K. Similar appearance of a plateau has been previously observed [51,52] for positron annihilation lifetimes in glass-forming liquids. Jean et al. [20] have also observed a similar behaviour in their temperature dependence of o-Ps lifetime in epoxy sample (however cured with N,N'-dimethyl-1,6-diaminohexane and 1,4-diaminobutone) around a certain temperature called T_e (Fig. 6.6(a)). In general, in the epoxy samples the temperature T_e is well below the decomposition temperature. For the epoxy sample used by us the decomposition temperature was above 480 K. Previous dilatometric and EPR studies performed in the case of other polymers did not showed any such transition [53]. We also did not observe any transition at T_e during the DTA studies of our epoxy samples. This behaviour suggests that the saturation effect observed for τ_3 at T_e is linked to the positron lifetime technique only [20]. The transition at T_e , in some sense is similar to the melting of crystalline polymers although amorphous and cross-linked polymers do not undergo a true melting process.

During the cooling cycle, from $T = 473$ K down to the room temperature of 293 K, the value τ_3 vs T almost retraces the path previously followed during the heating cycle and this suggests that the whole process involving the heating and the cooling

cycles was almost reversible. Similarly the free-volume hole size derived from the τ_3 data (eq. 1.17) also comes back to the initial value after the temperature cycle.

Although τ_3 showed a large variation with temperature in the range 292 - 473 K, the values of I_3 remained almost constant over the entire temperature range of 293 - 474 K. In Sec. 4.3.1, we have already discussed the various factors that control the value of o-Ps intensity (or I_3). In the present sample i.e. epoxy polymer, the chemical factor does not change with temperature. Physical factors such as the change in the free-volume hole size (or τ_3) in the temperature range 293 - 473 K does not seem to have much effect on the value of I_3 .

We shall now discuss our results for the positron lifetimes in polyester resin (cured with MEKP as catalyst and cobalt octate as accelerator) and their temperature dependence. Positron lifetime spectra were acquired in the temperature range 293-473 K and the spectra were analyzed by using the PATFIT program. Our analysis once again showed that the best χ^2 (< 1.1) and most acceptable standard deviations were obtained for a 3-lifetime fit. The values of the lifetime components lie in the range $\tau_1 = 0.11$ - 0.14 ns, $\tau_2 = 0.35$ - 0.40 ns and $\tau_3 = 1.7$ - 2.5 ns. The relative intensities corresponding to the three lifetimes τ_1 , τ_2 and τ_3 are given by I_1 , I_2 and I_3 respectively such that $I_1 + I_2 + I_3 = 100$ %. The lifetime values and their intensities observed for the polyester as a function of temperature are given in Table 6.2.

The temperature variation of τ_1 , τ_2 and their intensities I_1 and I_2 in case of cured polyester are shown in Fig. 6.7. The

TABLE 6.2

Temperature dependence of positron lifetime parameters in an unsaturated polyester (cured by using MEKP and cobalt octate) obtained from PATFIT analysis.

Temp. (K)	τ_1 (ns)	τ_2 (ns)	τ_3 (ns)	I_1 (%)	I_2 (%)	I_3 (%)	R^c (Å)
293 ^a	0.121±.008	0.364±.003	1.711±.027	12.03±.91	82.26±.97	5.70±.14	2.57±.01
303 ^b	0.111±.007	0.359±.004	1.752±.020	11.88±.67	81.79±.61	6.44±.11	2.62±.01
313 ^a	0.121±.006	0.365±.002	1.743±.021	14.36±.94	79.17±.86	6.46±.12	2.61±.01
323 ^b	0.122±.006	0.368±.003	1.761±.021	14.30±.93	79.28±.86	6.39±.12	2.63±.01
333 ^a	0.123±.006	0.367±.003	1.762±.019	13.98±.86	78.94±.88	7.08±.12	2.63±.01
343 ^b	0.120±.006	0.368±.003	1.764±.018	15.44±.95	76.78±.87	7.86±.13	2.63±.01
353 ^a	0.119±.006	0.367±.003	1.834±.018	14.54±.89	77.37±.83	8.08±.12	2.70±.01
363 ^b	0.117±.005	0.380±.003	1.940±.018	18.74±.79	72.82±.73	8.44±.11	2.80±.01
373 ^a	0.121±.005	0.384±.003	2.001±.017	19.48±.83	71.00±.77	9.51±.11	2.86±.01
383 ^b	0.114±.005	0.379±.003	2.031±.016	19.40±.80	70.80±.74	11.02±.12	2.88±.01
393 ^a	0.126±.005	0.381±.003	2.116±.015	17.43±.90	70.75±.84	11.81±.11	2.96±.01
403 ^b	0.115±.004	0.394±.003	2.166±.014	20.83±.70	67.17±.65	12.00±.11	3.02±.01
413 ^a	0.123±.005	0.386±.003	2.214±.013	19.17±.79	67.66±.74	13.17±.10	3.04±.01
423 ^b	0.127±.004	0.389±.003	2.283±.011	19.54±.69	66.72±.65	13.73±.09	3.10±.01
433 ^a	0.132±.005	0.391±.004	2.233±.013	19.47±.89	66.11±.83	14.42±.11	3.42±.01
443 ^b	0.123±.005	0.387±.004	2.335±.013	19.23±.84	65.54±.79	15.23±.11	3.15±.02
453 ^a	0.123±.005	0.389±.004	2.383±.013	18.92±.83	65.05±.78	16.02±.11	3.18±.01
463 ^b	0.127±.005	0.389±.004	2.427±.012	18.91±.84	64.38±.79	16.70±.10	3.22±.01
473 ^a	0.124±.004	0.386±.004	2.414±.014	18.22±.49	63.97±.93	17.29±.12	3.21±.02

^a During heating cycle

^b During cooling cycle

^c R are the free volume hole radii obtained by using τ_3 and eq. (1.17).

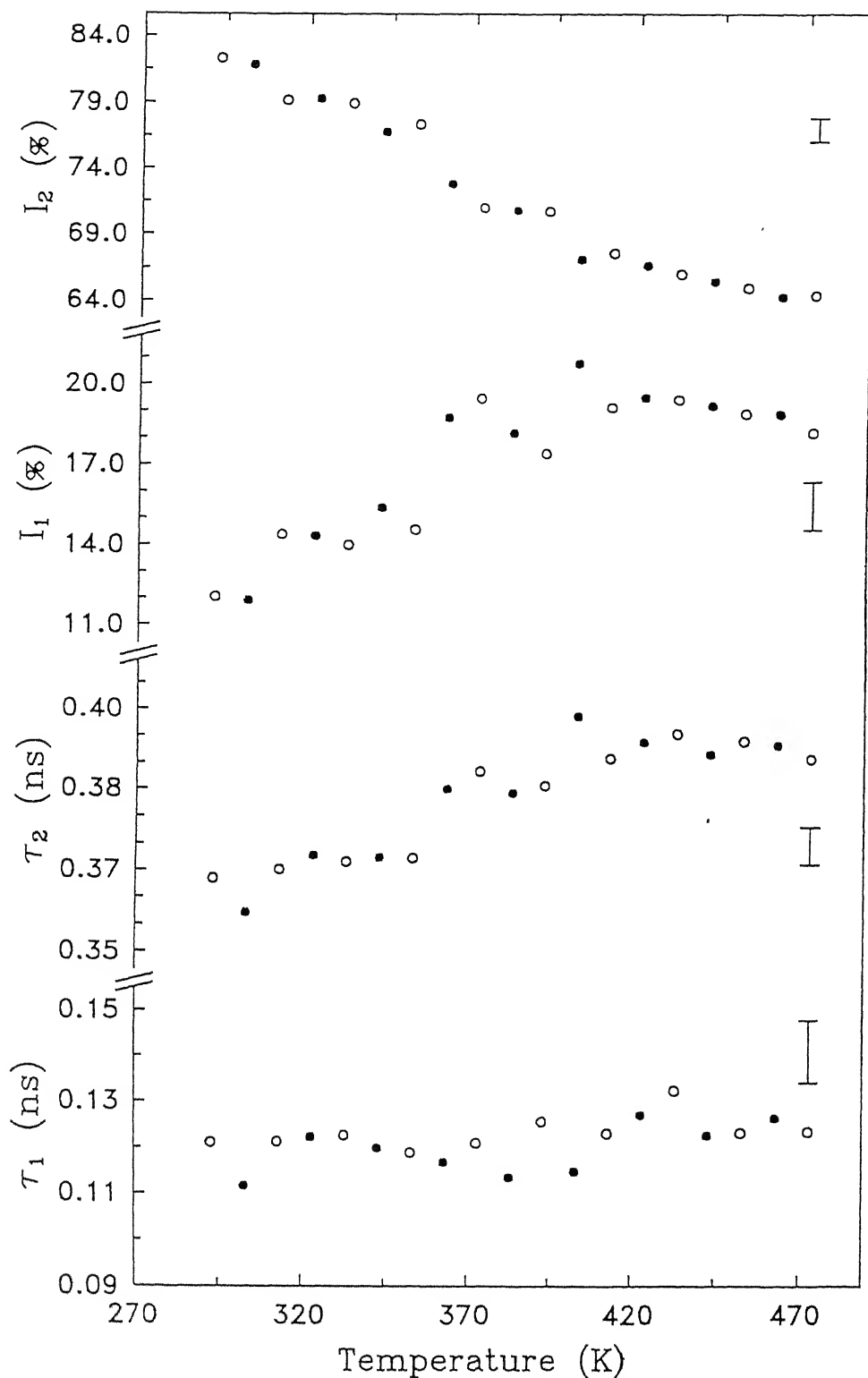


Fig. 6.7 Temperature variation of positron lifetime parameters τ_1 , τ_2 , I_1 and I_2 in polyester polymer. Open symbols describe the data for the heating cycle, while solid symbols describe the data for the cooling cycle. Typical error associated with the data points are shown separately in each case by the vertical error bars.

temperature dependence of τ_3 and I_3 are shown in Fig. 6.8 (a) and (b) respectively. If the present data for the epoxy and polyester samples are compared, one will notice a difference. This might be due to the difference in their physical structure - while epoxy is amorphous, polyester is microcrystalline. We shall confine our discussion to the variations of τ_3 and I_3 since they are more related to the free-volume properties in polymers, and we shall omit the temperature dependence of positron lifetimes τ_1 , τ_2 from further discussion. The values of free-volume hole radius R obtained from the observed values of τ_3 and eq. (1.17) are also given in Table 6.2 and the corresponding variation in the hole volume $V_f = 4\pi R^3/3$ is shown on the right hand axis in Fig. 6.8(a).

The temperature variation of τ_3 in this case was found to be quite similar to the one observed for the epoxy polymer (Fig. 6.6(a)) except that we do not observe a similar transition around T_g in this case which was earlier observed for the epoxy polymer. The change in the slope of τ_3 vs T curve around $T = 350$ K may be ascribed to a phase transition (such as the glass transition). However such a transition could not be confirmed independently by DTA analysis.

In the case of epoxy polymer, we observed $I_3 \approx 20\%$ but the polyester samples showed lower values of $I_3 \approx 7\%$ (both measured at room temperature). However with an increase in the temperature, the I_3 value for the polyester samples started to increase with temperature. The I_3 vs T plot shows a slow rise upto 350 K and beyond 350 K the plot shows a steeper rise upto the maximum temperature (473 K) used by us. It may be pointed out that the I_3

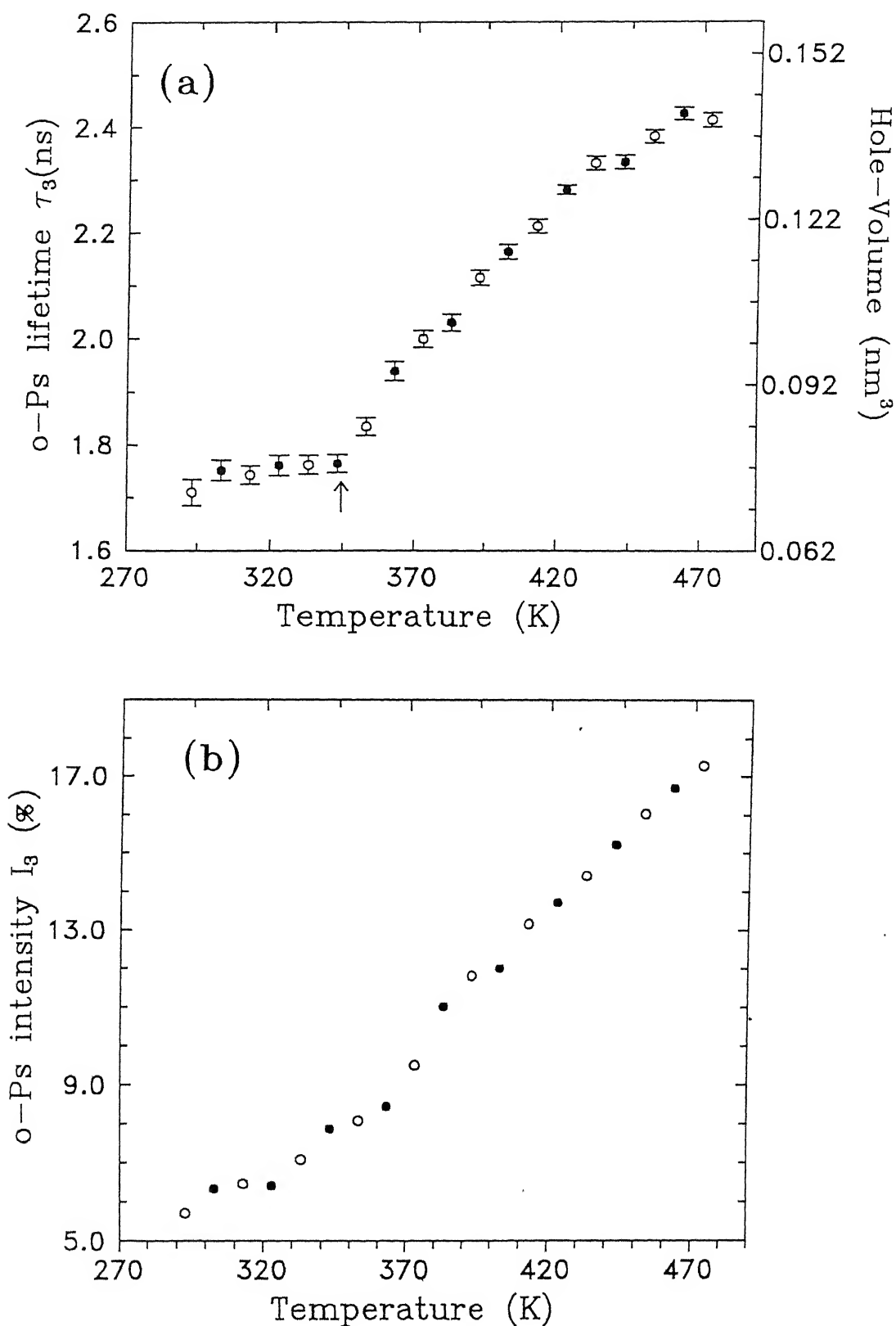


Fig. 6.8 Temperature dependence of (a) o-Ps lifetime, τ_3 , and (b) o-Ps intensity, I_3 in polyester polymer. Open symbols describe the data for the heating cycle, while solid symbols describe the data for the cooling cycle. Position indicated by the

vs T plot did not show such rise in the case of epoxy sample (Fig. 6.6 (b)). At 473 K, the value of I_3 for the polyester sample is about 17% and this is quite close to the value of I_3 obtained for the epoxy polymer. The observed behaviour of I_3 with temperature is quite interesting. Linear polyesters in some cases e.g. poly(ethylene terephthalate) (PET), nylon etc. [49] are either crystalline or may have microcrystalline domains with high degree of alignment of the polymer chains. In such cases the amount of intermolecular free space will be small. With increase in the temperature, disorder in their alignment may commence resulting in an increase in the intermolecular free space available within the polymer chains. At a sufficiently high temperature, the entire bulk of the material becomes totally disordered resulting in a larger fraction of free volume in the material. We believe that such a condition exists in our case. Since I_3 in some sense is related to the free-volume hole density, the increase in the disordering of oriented polymer chains with increasing temperature will increase the free-volume hole density and therefore the I_3 values. This mechanism discussed above may be responsible for the behaviour shown by I_3 with temperature. Moreover at room temperature there is a high degree of chain alignment and the amount of free volume is less at room temperature. This may explain the small I_3 value observed by us. It may be pointed out that polyester resin we have worked with is chemically very stable and its chemical structure does not change with temperature. Hence the possible change in I_3 can only come through the physical factors.

During the cooling cycle, both τ_3 and I_3 followed almost the same path as that taken during the heating cycle thereby suggesting that the process is almost reversible. It may be pointed out that present positron lifetime measurements involved measurement at each temperature lasting for several hours before going to the next temperature i.e. our measurements involved extremely slow heating and cooling rates.

As presented in the previous two cases of $\text{PEO:NH}_4\text{ClO}_4$ and NH_4I , we have plotted in Fig. 6.9 (a) and (b), the temperature variation of relative free volume fraction F_r ($= I_3 V_f$) for cured epoxy and the polyester with an argument similar to the one presented in Sec. 4.3.1. In case of polyester, although the value of I_3 changed in the entire range of temperature, the changes are only due to the change in the physical factor related to the structure of this polymer. Hence eq. (4.2) is likely to be valid in this case also. From Fig. 6.9, we find that the nature of variation of F_r for the epoxy polymer is similar to that of τ_3 , whereas in the polyester sample, the amount of variation in F_r is very large in the temperature range 350 - 473 K.

The positron lifetime spectra in the case of epoxy polymer (at some temperatures during the heating cycle) were also analyzed by using the CONTIN program to extract the positron lifetime distributions functions (PDF) $\alpha(\lambda) \cdot \lambda^2$. In Fig. 6.10 we have presented the results of such analysis i.e. the distribution function $\alpha(\lambda) \cdot \lambda^2$ against the positron lifetime at some representative temperatures for the epoxy polymer. All such lifetime distribution functions showed presence of three distinct

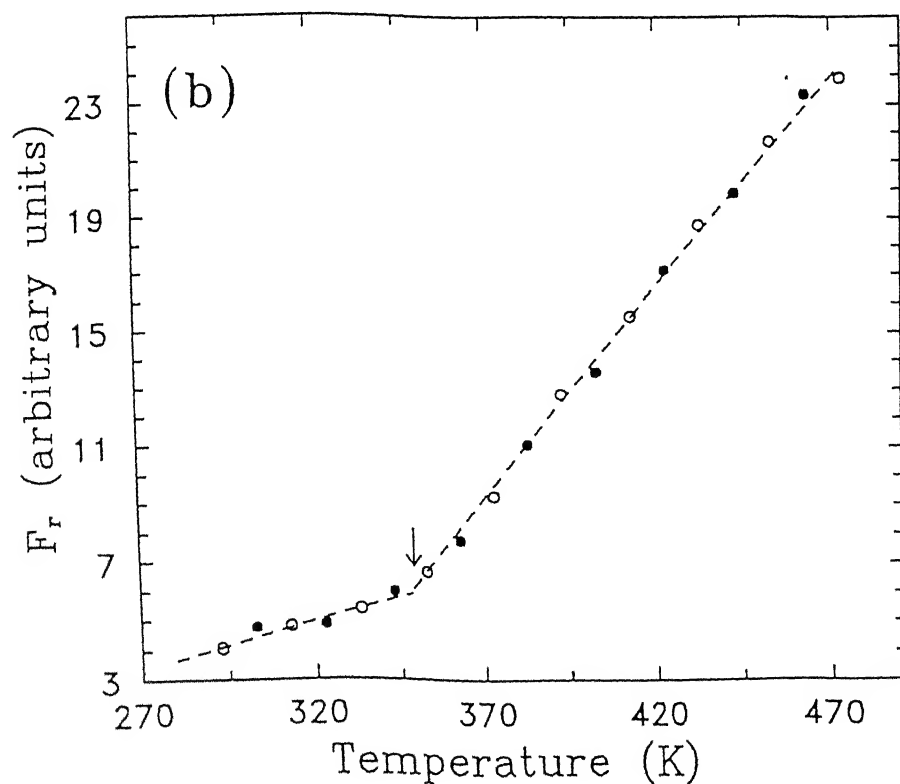
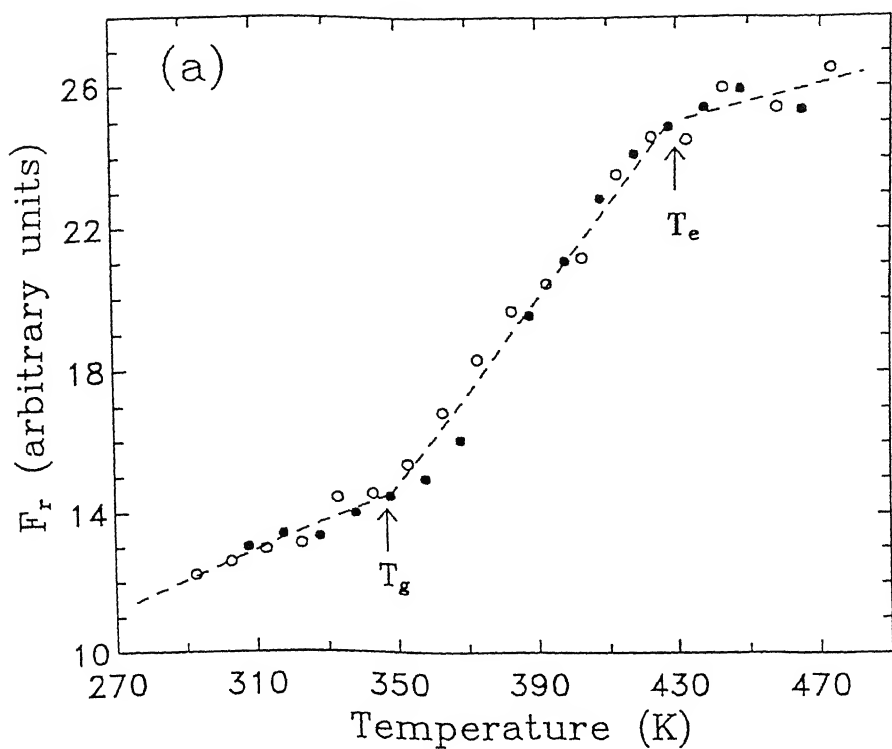


Fig. 6.9 Temperature dependence of relative free-volume fraction F_r ($=I_3 V_f$) in (a) epoxy and (b) polyester samples. Open symbols describe the data for the heating cycle, while solid symbols describe the data for the cooling cycle. Positions indicated by the arrows correspond to various transitions observed

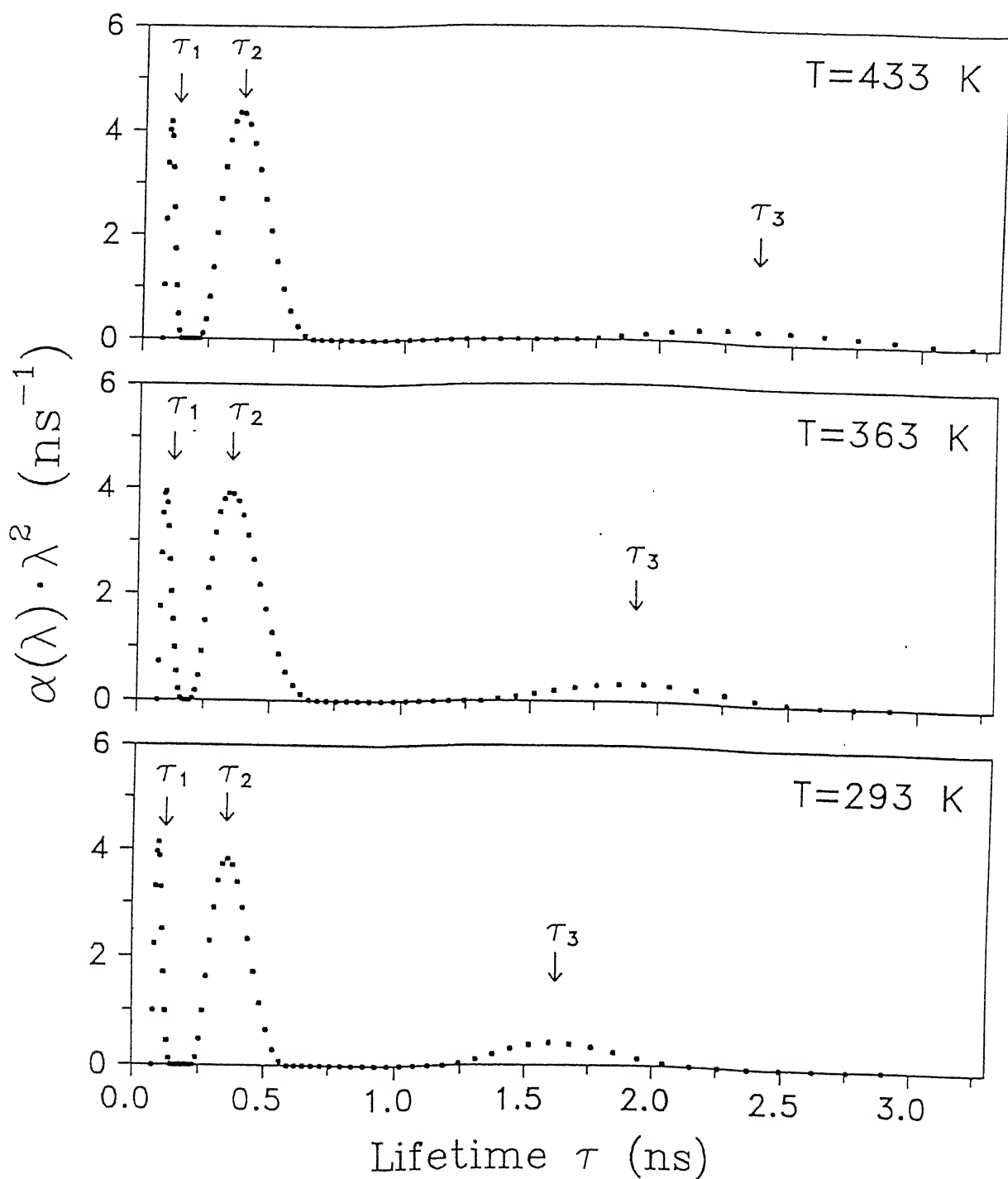


Fig. 6.10 Positron lifetime distributions in epoxy polymer at some representative temperatures during the heating cycle, obtained from CONTIN analysis. The positions corresponding to the lifetimes values τ_1 , τ_2 and τ_3 obtained from PATFIT (Table 6.1(a)) analysis are shown by arrows.

and well-resolved peaks. The mean positron lifetimes and their intensities ($\bar{\tau}_i$ and \bar{I}_i , $i = 1-3$) were obtained from the CONTIN results by using the eqs. (4.3) and (4.4) and they are listed in Table 6.3 for some of the lifetime spectra in epoxy polymer

One can see that there is a good agreement between the peak positions of the three peaks (corresponding to τ_1 , τ_2 and τ_3) resolved by the CONTIN program (Table 6.3) and the values of τ_1 , τ_2 and τ_3 obtained by the PATFIT program (Table 6.1). The expanded profiles of the extreme right peaks (corresponding to τ_3) in Fig. 6.10 are shown in Fig. 6.11. It is observed that the peak position, width (FWHM), and asymmetry of each peak profile is different at different temperatures. One can also see that higher the temperature, broader is the lifetime distribution.

As mentioned earlier, the lifetime and related distributions shown here are to be taken qualitatively and that they represent a certain trend. From the observed o-Ps lifetime distributions, we have determined the free-volume hole-radius probability density function, $f(R)$, using eq. (4.5) without any correction factor for the Ps trapping [7,21]. The present results for $f(R)$ corresponding to the o-Ps lifetime distribution shown in Fig. 6.11 are plotted against R in Fig. 6.12(a). The mean radius for each of the radius distributions obtained by us was determined by using the eq. (5.1). These values of the mean radii are also tabulated in Table 6.3. From Fig. 6.12 (a), we find that the $f(R)$ functions are fairly symmetric and exhibit a broader distribution at a higher temperature.

Using the above distribution functions for $f(R)$ we have also

TABLE 6.3

Temperature dependence of mean positron lifetime parameters in epoxy polymer (DGEBA:TETA) during heating cycle obtained from CONTIN analysis.

Temp. (K)	$\bar{\tau}_1$ (ns)	$\bar{\tau}_2$ (ns)	$\bar{\tau}_3$ (ns)	\bar{I}_1 (%)	\bar{I}_2 (%)	\bar{I}_3 (%)	\bar{R}^a (Å)
293	0.102	0.367	1.618	13.98	65.30	20.71	2.48
303	0.110	0.354	1.635	12.80	65.75	21.44	2.49
313	0.105	0.357	1.674	11.63	68.34	20.04	2.54
323	0.105	0.360	1.709	15.80	64.26	19.94	2.57
333	0.100	0.377	1.788	12.85	67.98	19.17	2.65
343	0.097	0.367	1.778	12.97	67.31	19.72	2.64
353	0.113	0.381	1.919	12.39	68.12	19.49	2.78
363	0.107	0.364	1.889	13.52	67.14	19.35	2.75
373	0.105	0.354	2.001	12.85	66.54	20.61	2.86
383	0.100	0.375	2.049	12.11	67.74	20.15	2.90
393	0.102	0.372	2.066	13.10	66.22	20.68	2.91
403	0.103	0.375	2.180	12.06	68.37	19.57	3.01
413	0.108	0.362	2.235	9.07	70.15	20.76	3.06
423	0.103	0.379	2.360	12.27	68.69	19.04	3.17
433	0.102	0.377	2.385	11.36	68.31	20.33	3.19
443	0.104	0.374	2.387	12.45	67.25	20.30	3.19
358	0.112	0.381	2.394	13.01	64.65	22.34	3.19
373	0.113	0.379	2.412	12.01	65.24	22.75	3.21

^a \bar{R} are the mean free volume hole radii obtained by using $\bar{\tau}_2$ and $\alpha = 1.17$.

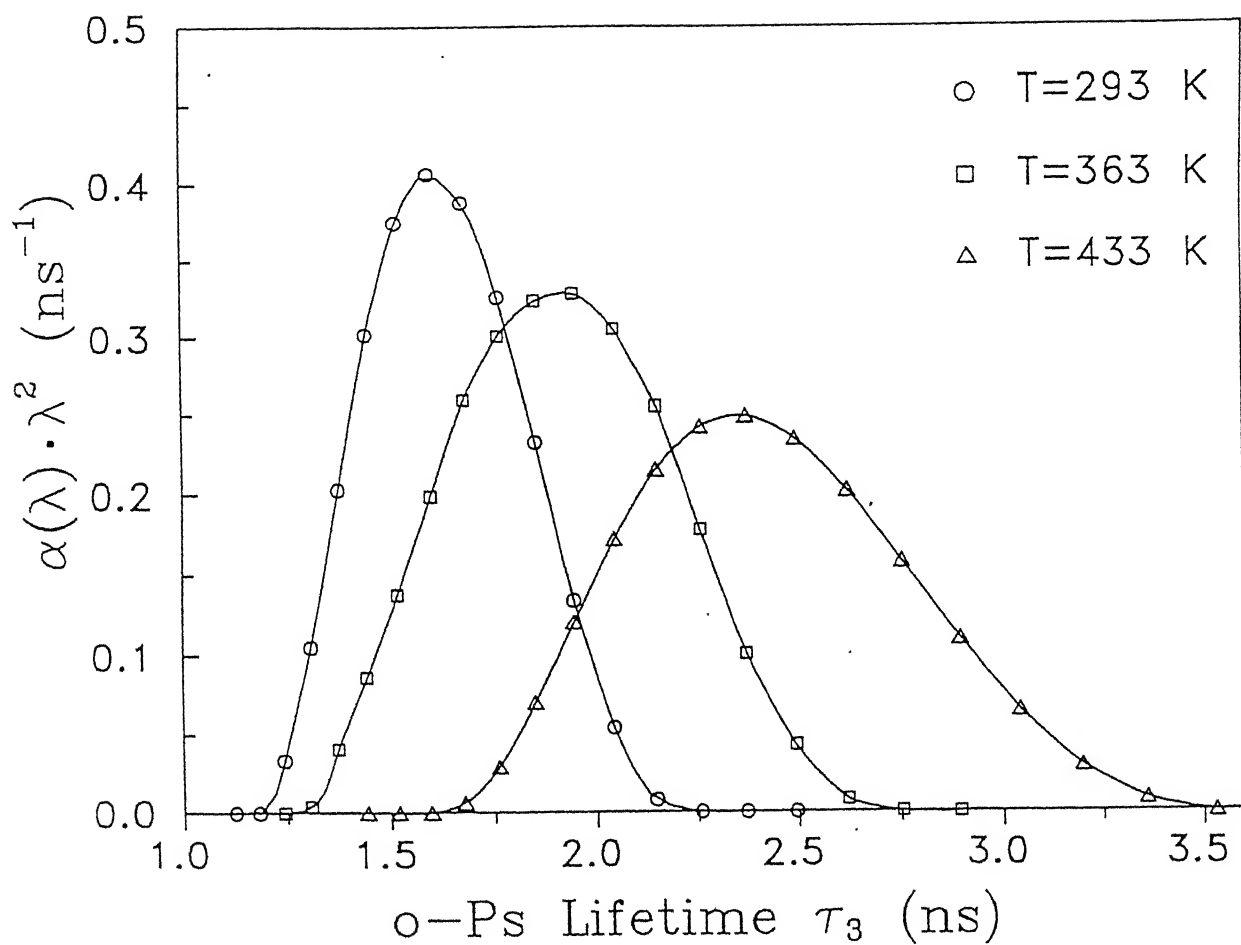


Fig. 6.11 o-Ps lifetime distribution in epoxy polymer at different temperatures during the heating cycle. The data were taken from right hand peaks in Fig. 6.10. The continuous lines are drawn through the data points for visual guidance.

determined the probability density functions for the hole volume $g(V)$ using eq. (4.6). The results of hole volume distribution, $g(V)$, obtained in this way for the epoxy sample corresponding to the hole radius distribution $f(R)$ in Figs. 6.12(a) are shown in Fig 6.12(b). The hole-volume distribution, $g(V)$, in Fig. 6.12(b) were observed to be asymmetric with a skewing tendency towards larger volume.

In the next section we shall discuss our results for the physical aging and moisture absorption studies on the epoxy and polyester using positron lifetime method.

6.3.2 Study of structural relaxation and physical aging

In order to study the structural relaxation and physical aging effects on the positron lifetime parameters, the sample of epoxy and polyester were annealed at a temperature above the respective glass transition temperatures for an extended time (~ 100 h) and then cooled to a temperature below their glass transition temperature. As mentioned earlier, the equilibrium free-volume distribution present before the cooling process will be disturbed as a result of cooling the sample below the glass transition temperature and the system will try to attain the new equilibrium distribution for the free-volume corresponding to the final temperature. This process is very slow because the segmental mobility of the polymer chains in the glassy state is very much retarded due to a smaller free volume available in the glassy state. Since o-Ps lifetime and the intensity are related to the free volume hole size and distribution, the above process of

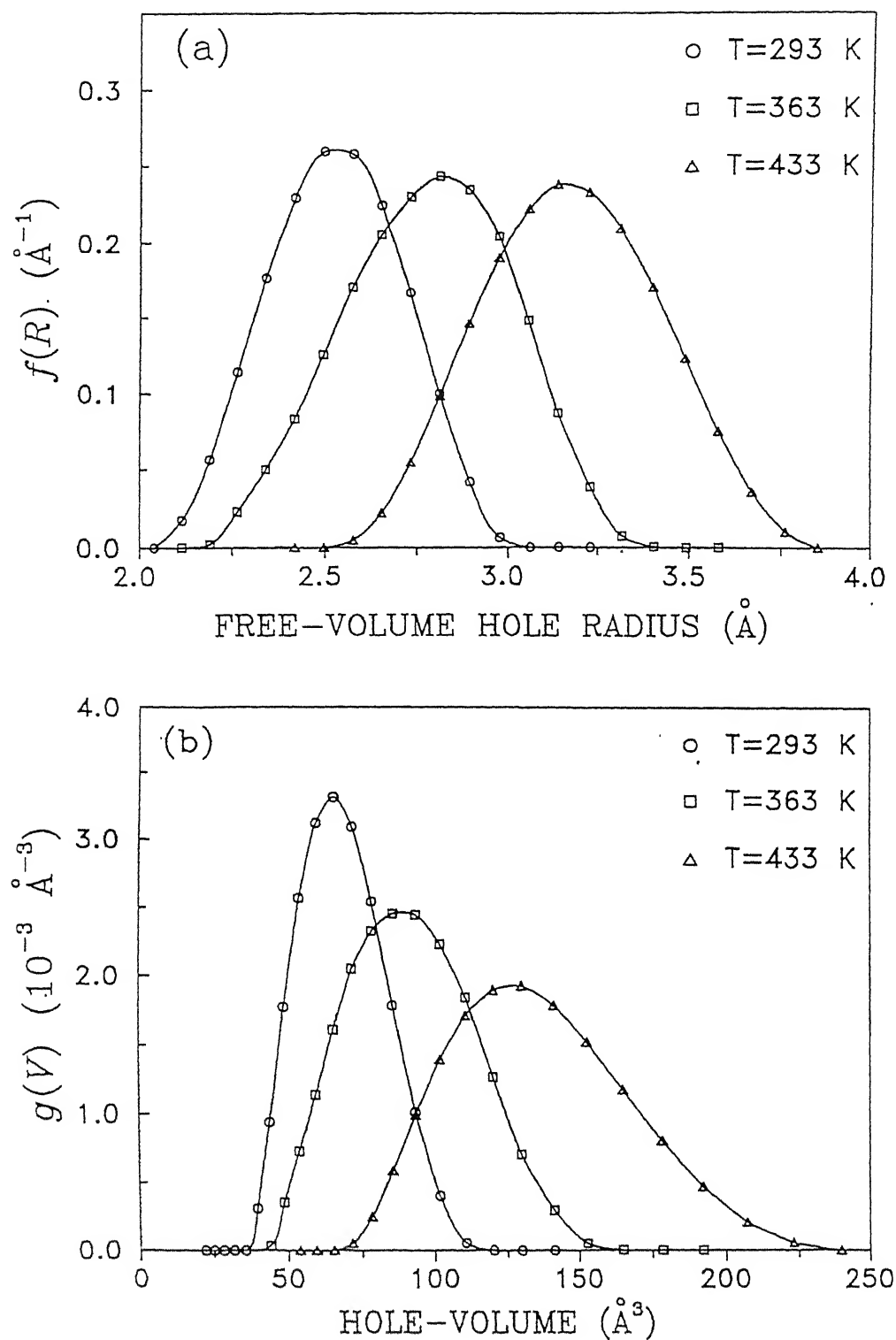


Fig. 6.12 The free-volume (a) hole radius distribution functions $f(R)$, and (b) volume distribution functions $g(V)$ in epoxy polymer at different temperatures corresponding to o-Ps lifetime distribution functions in Fig. 6.11 during the heating cycle. The continuous lines are drawn through the data points for visual guidance.

redistribution of the free volume is also expected to be observed in the variation of o-Ps lifetime parameters.

In Fig. 6.13(a) and (b) we have plotted the changes in τ_3 and I_3 respectively for the epoxy sample as a function of time for three different cooling rates described in the figure. Positron lifetime data were taken at room temperature for all the samples. It is observed from Fig. 6.13 that for epoxy samples the effect of physical aging on τ_3 and I_3 shows similar trends irrespective of the cooling rate used. In other words the aging process (in epoxy samples) was found to be independent of the quenching rates used. Physical aging appears to have a more marked effect on the intensity of o-Ps lifetime than the lifetimes themselves. Similar behaviour has been reported in the literature [5,23-25] for various other polymers. Keeping in view the correlation (Chapter 1) between the o-Ps lifetime (and intensity) and the free-volume hole size (and its distribution), we may conclude that during the aging process in epoxy polymer, the free-volume hole density changes with time whereas there is a little or no change in the hole size.

In the case of polyester resin, the physical aging process was studied using positron lifetime method for 3 sets of samples which were treated in exactly the same way as described for the epoxy polymer but for an annealing temperature of 423 K. In Figs. 6.14(a) and (b) we have plotted the values of τ_3 and I_3 respectively as a function of aging time for the samples cooled at different rates. In this case too, we find that the values of τ_3 are not much affected by the aging process whereas the values of

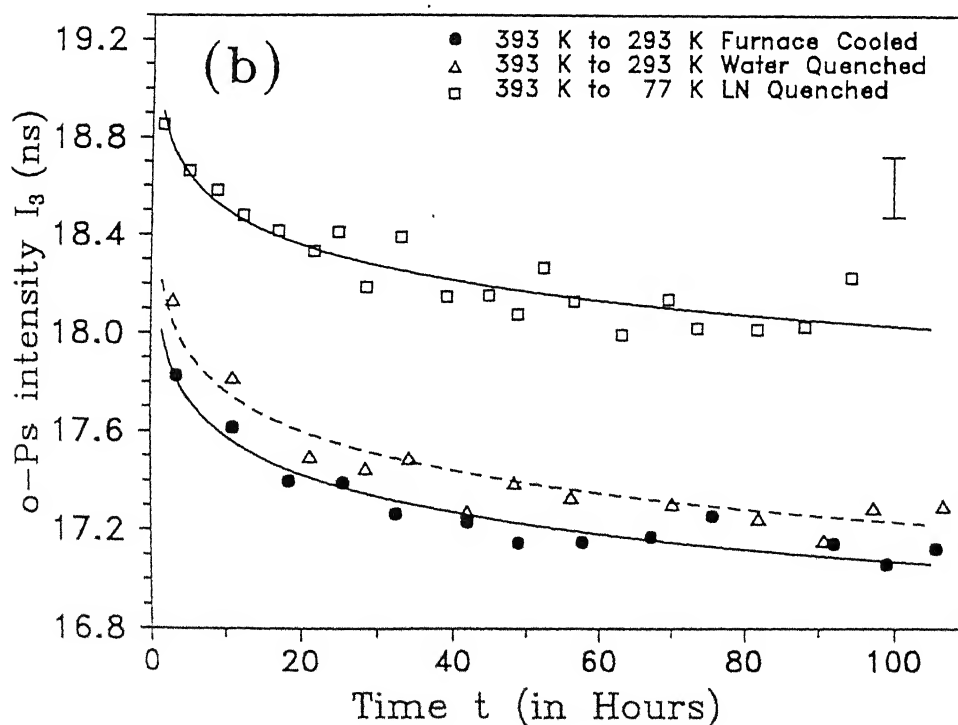
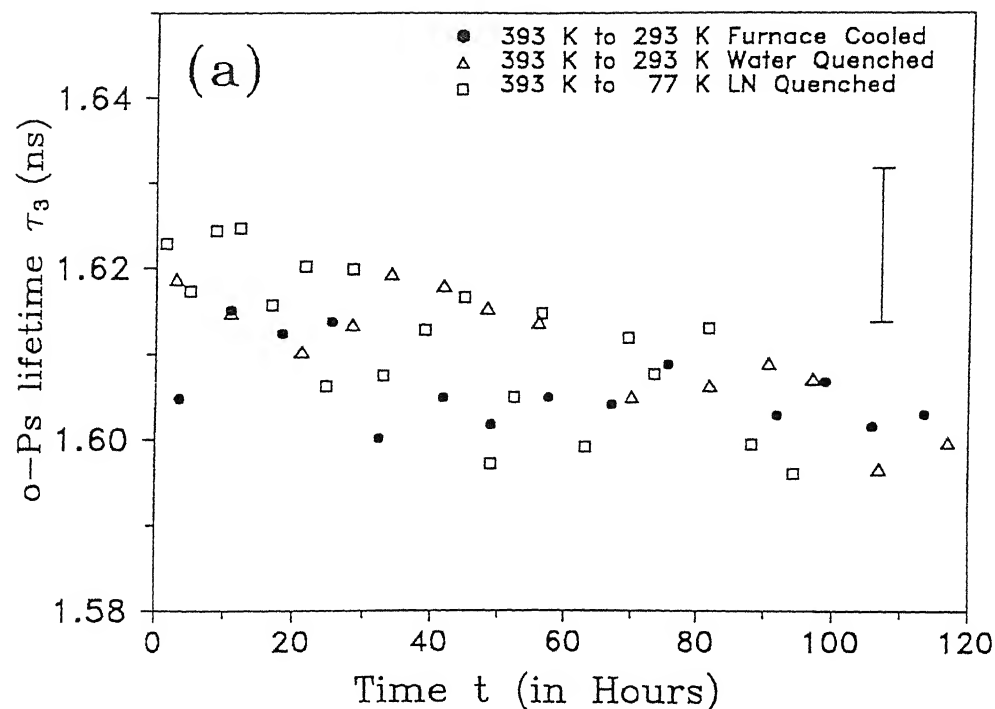


Fig. 6.13 Effect of physical aging on (a) τ_3 and (b) I_3 as a function of time for epoxy samples cooled at different rates. Typical error associated with the data points are shown separately by the vertical error bars.

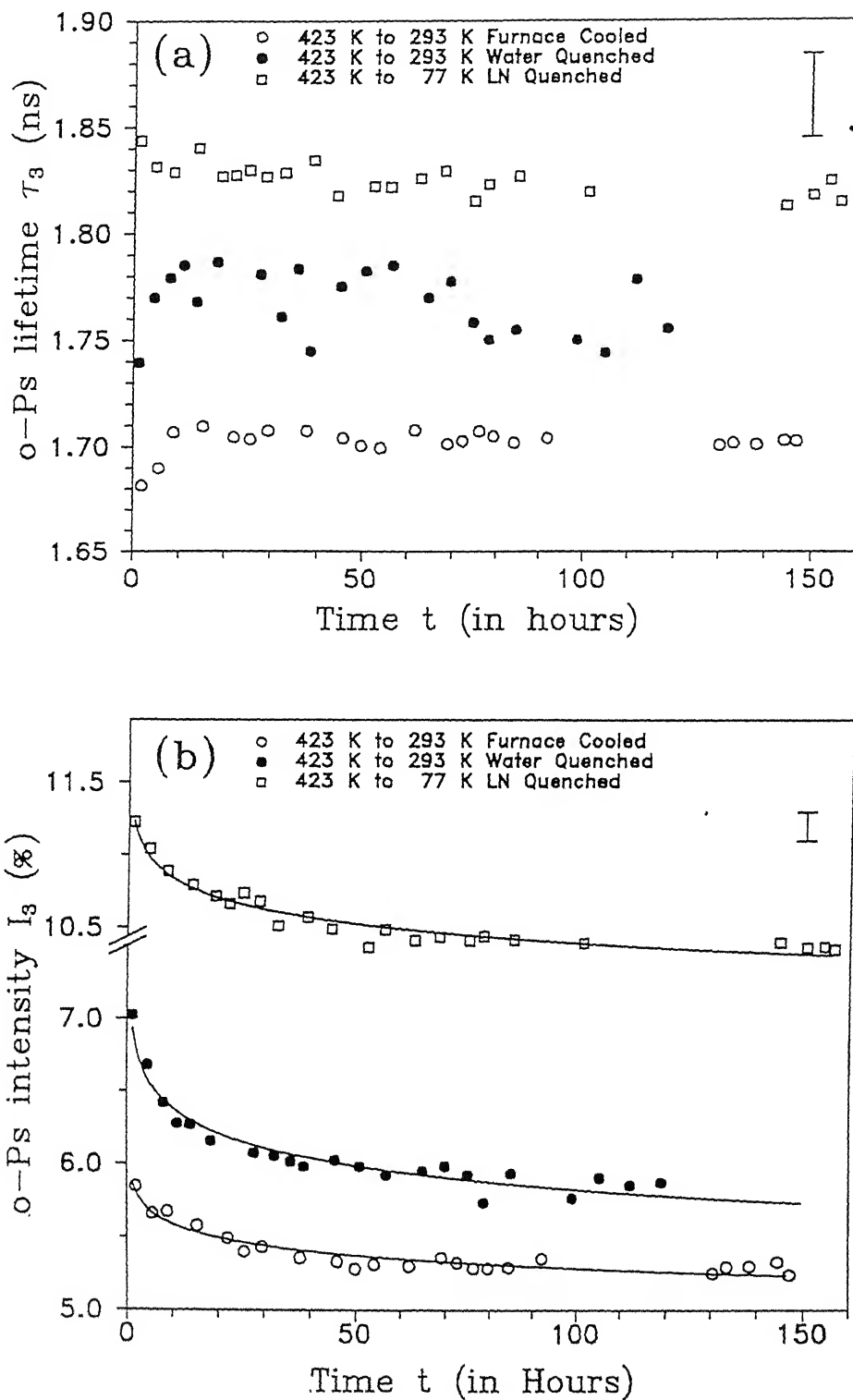


Fig. 6.14 Effect of physical aging on (a) τ_3 and (b) I_3 as a function of time for polyester samples cooled at different rates. Typical errors associated with the data points are shown separately by the vertical error bars.

I_3 changed at almost the same rate in all three cases. However in this case the individual values of τ_3 and I_3 were found to be dependent on the rate of quenching, the effect being more prominent for I_3 . From Figs. 6.14(a) and (b), we also find that faster the cooling rate, larger is the value of τ_3 and I_3 . One can explain this behaviour by considering the microstructure of our polyester sample. By rapid quenching the sample, the different polymer chains did not get enough time to reorient/realign themselves in a more closed packed structure, and are frozen in the state which existed before quenching. Therefore, faster rate of quenching, will lead to greater amount of disorder and larger amount of free volume. This may explain the observation that faster rate of quenching led to higher values of τ_3 and I_3 .

6.3.3 Water Absorption studies

The observed variation in the values of τ_3 and I_3 as a function of water absorption time is plotted in Fig. 6.15 and 6.16 for epoxy and polyester respectively. Each sample was subjected to three different absorption conditions described earlier in Sec. 6.2. The observed changes in the values of τ_3 and I_3 during the process of absorption are attributed to the trapping of water molecules at the intermolecular spaces (which arises out of the diffusion of water in the sample). It has already been found that absorption in polymers is a diffusion-controlled process that depends on the amount of free volume available in the polymer and the temperature at which the diffusion is taking place. Therefore for epoxy sample, which contains a larger free volume fraction as

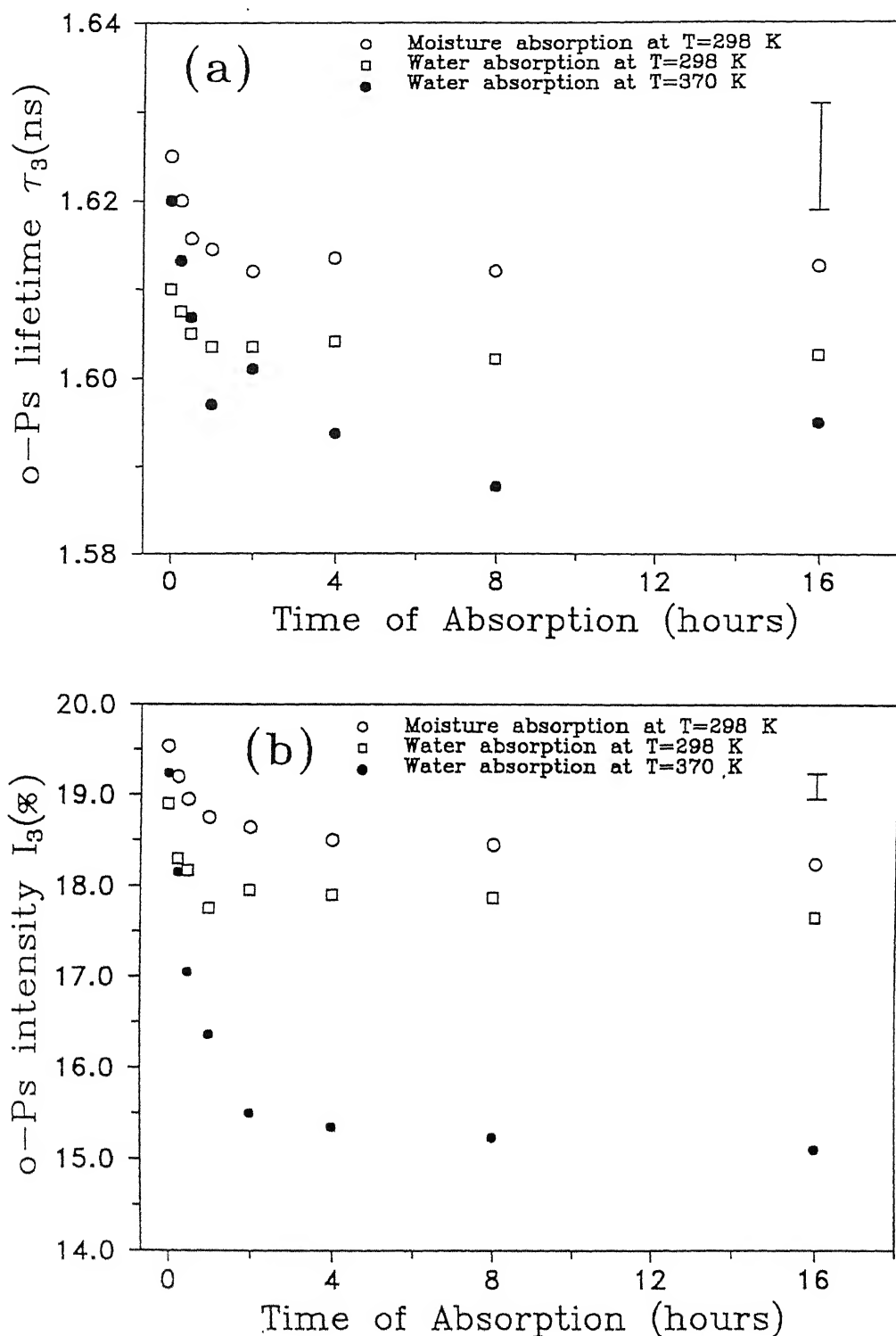


Fig. 6.15 Effect of moisture/water absorption on (a) τ_3 and (b) I_3 for various time of absorption in epoxy sample. Typical error associated with the data points are shown separately by the vertical error bars.

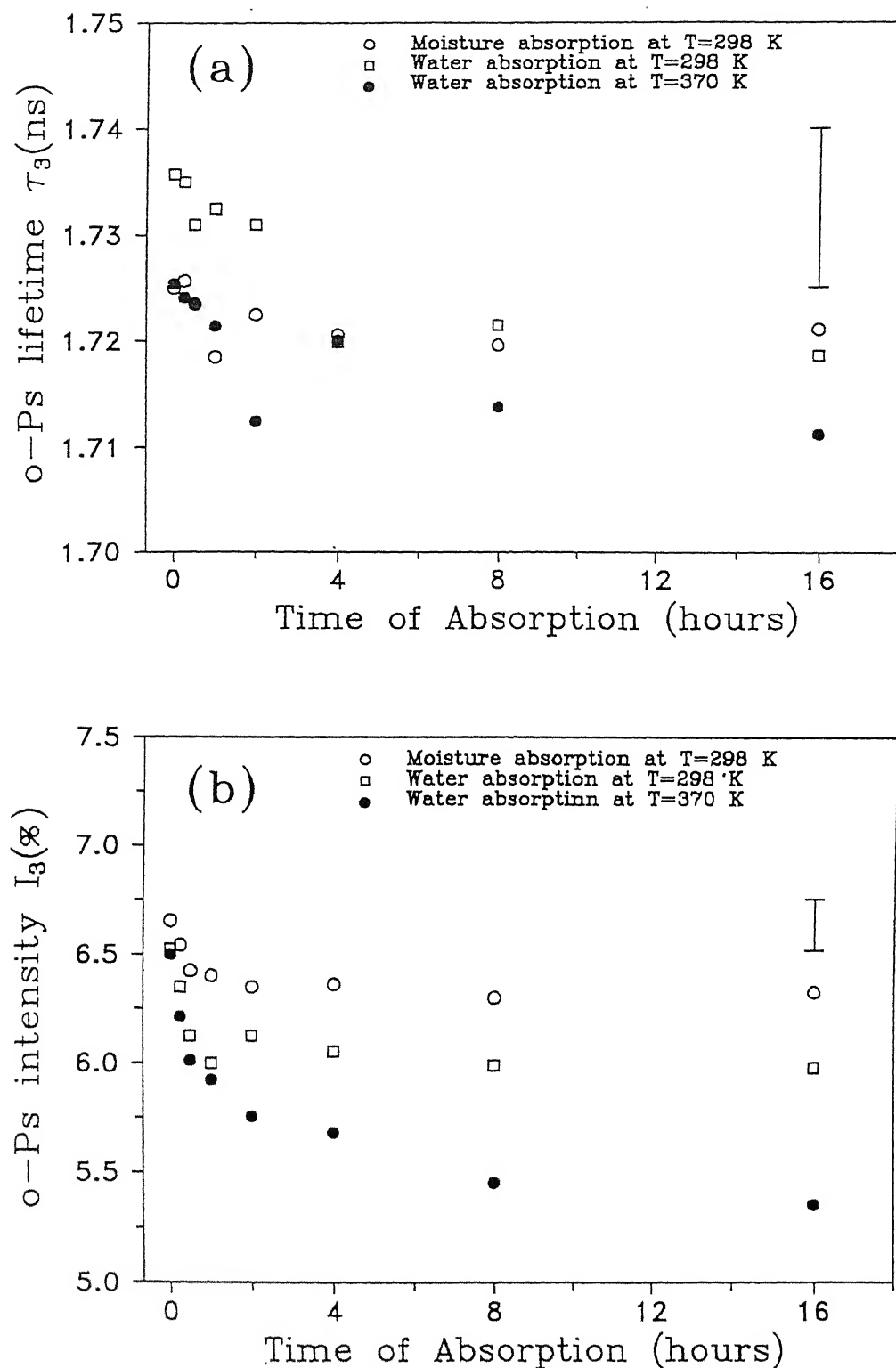


Fig. 6.16 Effect of moisture/water absorption on (a) τ_3 and (b) I_3 for various time for absorption in polyester sample. Typical error associated with the data points are shown separately by the vertical error bars.

compared to polyester sample, we expect to find larger changes in the values of τ_3 and I_3 than in polyester during the process of absorption under identical conditions. Our results (Fig. 6.15 and 6.16) indeed show such a behaviour. Our results are also in agreement with the results obtained by others [54,9]. The amount of change in the values of τ_3 and I_3 is more marked for water absorption at an elevated temperature of 370 K in both the samples. This observed behaviour can be explained in terms of diffusion coefficient which increases with temperature. At a higher temperature, the amount of free volume fraction is also expected to be more. Both the effects mentioned above are responsible for a larger change in the τ_3 and I_3 when water was absorbed at 370 K.

6.4 Summary and conclusions

Positron annihilation lifetime spectroscopy has been used to study free volume in epoxy and polyester polymers. While the epoxy samples were cured with triethylene tetramine (as hardener), the polyester samples were cured with MEKP (as catalyst) and cobalt octate (as accelerator). The temperature dependence of positron lifetime τ_3 in the epoxy and polyester samples were analyzed to obtain the variation of the free-volume hole size, V_f , in the temperature range 293 - 473 K using the PATFIT program. The increase of V_f with temperature shows a steeper rise at $T = T_g$ (glass transition temperature) for both the samples. However in the case of the epoxy sample the plot of τ_3 vs T shows a

saturation behaviour beyond $T = T_e$ (the so-called onset temperature). Attempt has been made to discuss this behaviour. The positron lifetime spectra in the epoxy sample have also been analyzed using the CONTIN program to obtain the distribution of o-Ps lifetimes, free-volume hole radii and hole-volumes at different temperatures.

Positron annihilation lifetimes in the samples of epoxy and polyester have been monitored during their aging over a time period ranging from 1h to 150h, and for different cooling rates. The o-Ps lifetimes τ_3 did not show significant changes with time t . The o-Ps intensity I_3 showed systematic changes whose trend did not depend on the rate of cooling used, although the actual values of I_3 did depend on the rate of cooling. These results have been discussed.

Finally the effect of water absorption on the o-Ps lifetime and intensity in the samples of epoxy and polyester have been studied as a function of absorption time at 298 K and 370 K. It was observed that the changes in τ_3 and I_3 were more marked for water absorption at an elevated temperature of 370 K. An explanation for this behaviour is proposed.

The present study has provided useful information about the effect of temperature, physical aging and water absorption on the positron lifetime parameters and free volumes in the epoxy and polyester polymers.

References

1. "The Physics of Glassy Polymers" edited by R.N. Haward (Applied Science Publishers, London, 1973).
2. M. Goldstein and R. Simha, "The Glass Transition and the Nature of the Glassy State" (NY Academy of Science, NY, 1976).
3. "Polymer Materials : Relationship between structure and Mechanical Behaviour", edited by E. Baer and S.V. Radcliffe (American Society for Metals, Metal Park, OH, 1975).
4. R.E. Robertson, R. Simha and J.G. Curro, *Macromolecules*, 17, 911 (1984).
5. Y. Kobayashi, W. Zheng, E.F. Meyer, J.D. MacGervey, A.M. Jamieson and R. Shima, *Macromolecules*, 22, 2302 (1989).
6. A. J. Hill, I.K. Katz and P.L. Jones, *Polym. Engg. Sci.* 30, 782 (1990).
7. Q. Deng, F. Zandiehnam and Y.C. Jean, *Macromolecules*, 25, 1090 (1992).
8. J.E. Kluin, Z. Yu, S. Vleeshauvers, J.D. MacGervey, A.M. Jamieson, R. Shima and K. Sommer, *Macromolecules*, 26, 1853 (1993).
9. T. Suzuki, Y. Oki, M. Namajiri, T. Miura, K. Kondo, Y. Shiomi and Y. Ito, *J. Appl. Polymer Sci.* 49, 1921 (1993)
10. M.C. Shen and A. Eisenberg, "Progress in Solid State Chemistry" (Paragamon Press, Oxford, 1966), Vol. 3, p. 407.
11. M. Goldstein in "Modern Aspects of the Vitreous State" edited by J.D. Mackenzie (Butterworth, London, Vol. 3, p. 30.
12. N.G. McCrum, B.E. Read and G. Williams, "Anelastic and

dielectric Effects in Polymers Solids" (John Wiley and Sons Inc. London, 1967).

13. R.E. Boyler, Poly. Engg. Sci. 8, 161 (1968).
14. M.H. Cohen and D. Turnbull, J. Chem. Phys. 31, 1164 (1959).
15. J.G. Curro, R.R. Lagasse and R. Simha, Macromolecules 15, 1522 (1982).
16. S.C. Jain and R. Simha, Macromolecules, 15, 1522 (1982).
17. S.Vleeshauvers, J.E. Kluin, J.D. MacGervey, A.M. Jamieson and R. Simha, J. Polym. Sci. Polym. Phys. Ed. 30, 1429 (1982).
18. R. Simha and J.G. Curro, J. Polym. Sci. Polym. Phys. Ed. 32, 2645, (1994).
19. J.J. Aklonis and A.J. Kovacs, in "Contemporary Topics in Polymer Science", edited by M.Shen, (Plenum, NY, 1979) V.3, p-267.
20. Y.C. Jean, T.C. Sandreczki and D.P. Adem, J. Polym. Sci. B. Polym. Phy. 24, 1247 (1986).
21. Q. Deng and Y.C. Jean, Macromolecules, 26, 30 (1993).
22. Y.C. Jean and Q. Deng, J. Polym. Sci. Polym. Phys. 30, 1359 (1992).
23. A.J.Hill, P.L.Jones, J.H. Lind and G.W.Pearsall, J. Polym. Sci. A Polym. Chem. 26, 1541 (1988).
24. K. J. Heater and P.L.Jones, Nucl. Instrum. Meth. B 56/57, 610 (1991).
25. A.J.Hill, K. J. Heater and C.M.Agarwal, J. Polym. Sci. Polym. Phys. Ed. 28, 387 (1990).
26. C.L.Wang, B. Wang, S.Q.Li and S.J.Wang, J. Cond. Matter 5, 7515 (1993).

27. L Xie, D.W. Gidley, H.A. Hristov and A.F.Yee, J. Polym. Sci. Polym. Phys. 33, 77 (1995).
28. Y. Ito, V. Sanchez, R. Lopez, L.A. Fucugauchi, K. Tanaka, and K. Okamoto, Bull. Chem. Soc. Jap. 66, 727 (1993).
29. Y. Ito, K.I. Okamoto and K. Tanaka, J, de Physique C4 3, 241 (1993); Y. Ito, Mater. Sci. Forum 175-178, 627 (1995).
30. F. Simon, Z. Anorg. Allgem. Chem 203, 219 (1931).
31. A.J. Kovacs, Adv. Polym. Sci. 3, 394 (1963).
32. L.C.E. Struik, Rheol. Acta 5, 303 (1966).
33. A.J. Kovacs, R.A. Stratton and J.D. Ferry, J. Phys. Chem. 67, 152 (1963).
34. S.E.B. Petrie, J. Polym. Sci. A2 10, 1255 (1972).
35. C. Klason and J. Kubat, J. Appl. Polym. Sci. 19, 831 (1975).
36. L.C.E. Struik, "Physical Aging in Amorphous Polymers and other Materials" (Elsevier, Amsterdam, 1978).
37. J.M.G. Cowie and R. Ferguson, Macromolecules, 22, 2307 (1989).
38. S.E.B. Petrie, " Physical structure of the Amorphous State", edited by G. Allen and S.E.B. Petrie (Marcel Dekker, New York, 1976), p. 225.
39. G. Levita and T.L.Smith, Polym Engg. Sci. 21, 936 (1981).
40. L.C.E. Struik, Polym. Eng. Sci. 17, 165 (1977).
41. D. Turnbull and M.H. Cohen, J. Chem. Phys. 34, 120 (1961).
42. G.William and D.C. Watts, Trans. Faraday Soc. 66, 80 (1970).
43. H. Lee and K. Neville, " Epoxy Resin - Their Applications and Technology", (McGraw-Hill, New York, 1957).
44. H. Lee and K. Neville, "Handbook of Epoxy Resin" (McGraw-Hill, New York, 1967).

45. "Handbook of Composites", edited by George Lubin (Van Nostrand Reinhold Company Inc., New York, 1982).
46. A.M. Clayton, "Epoxy Resin Chemistry and Technology" (Marcel Dekker, New York, 1988).
47. J. R. Lawrence, "Polyester Resins" (Reinhold Publishing Company, New York, 1962).
48. H.V. Boenig, "Unsaturated Polyester: structure and Properties" (Elsevier Publishing Company, Amsterdam, 1964).
59. "Solid-State behaviour of linear polyester and polyimides" edited by J.M. Schultz and S. Fakiro (Prentice-Hall, New Jersey, 1990)
50. "Positron Solid State Physics" edited by W. Brandt and A. Dupasquier (North-Holland, Amsterdam, 1983).
51. W. Brandt and I Sprin, Phys. Rev. 142, 231 (1966).
52. B.D. Malhotra and R.A.Pethrick, J. Chem. Soc. Faraday Trans. 2 78, 297 (1982).
53. R.A.Pethrick, F.M. Jacobsen, O.E. Mogensen and M. Eldrup, J. Chem. Soc. Faraday Trans. 2 76, 225 (1980).
54. V.B.Gupter, L.T. Drazal and M.J.Rich, J. Appl. Polym. Sci. 30, 4467 (1985).

CHAPTER 7

POSITRON ANNIHILATION LIFETIME STUDY OF HYDROGEN-CHARGED Al-Al₂O₃ COMPOSITES

7.1 Introduction

Metal matrix composites (MMC) are a new class of materials that have attracted considerable attention in the recent past because of their excellent mechanical properties. This is due to the presence of a tough, ductile and environment-resistant metallic matrix and a strong, light and thermally stable reinforcement. Composite materials are in general produced by blending two or more materials (either metallic or non-metallic) to obtain unique combinations of physical and mechanical properties which cannot be obtained in a single material.

A wide variety of novel composite materials with metals, ceramics and intermetallics as reinforcement have been developed. This has led to the availability of several low-cost, discontinuous ceramic reinforcements. Recently much research attention has focussed on the Al-based MMC's. They have been identified as candidate materials for automobiles engine components because of their amenability to common metal-forming operations like forging, extrusion and rolling [1]. In addition, the Al-based MMC's have other useful properties like adequate mechanical properties, light weight, resistance to environmental attacks etc. Composites based on Al-alloys and having graphite

reinforcements have also been considered for marine and nava applications [2-4].

Hydrogen embrittlement (HE) is one of the important forms of environmental degradation of materials. Hydrogen may enter the metal from hydrogen-bearing atmosphere during corrosion, cathodic polarization, electroplating, heat treatments, welding or other manufacturing processes. Because of the small size, hydrogen can readily migrate through the crystal structure of most metals and alloys and get dissolved in the crystal lattice. This dissolved hydrogen can drastically affect the mechanical strength and ductility in these metals and alloys. It is also understood that the dissolved hydrogen gets trapped at various metallurgical inhomogeneities/defects or similar trap sites [5] and the hydrogen trapping behaviour of these traps determine the susceptibility to HE. These traps sites may act as a reversible or irreversible traps for hydrogen [6]. It is believed that the hydrogen atom which are reversibly trapped in the materials are mostly responsible for causing hydrogen embrittlements.

Earlier investigation carried out on the hydrogen embrittlement of cast Al-Al₂O₃ particulate composites at our Institute [7] have revealed that the degree of hydrogen embrittlement was lower in composites compared to the base metal. Moreover, the susceptibility to HE was least for the 2% Al₂O₃ composites. In fact, the tensile ductility of hydrogen charged Al-2% Al₂O₃ was found to be greater than the uncharged condition. An explanation for the embrittlement behaviour of these composites was proposed by considering the microstructural effects on

properties and the trapping tendency of hydrogen at various traps sites in the materials [7].

During sample preparation, Mg was added [7] to the Al for improving the wettability between the Al and the Al_2O_3 particles. From a structural point of view, the presence of Mg in the Al alloy led to the transformation of Al_2O_3 to MgAl_2O_4 thereby cracking the particles due to the stress generated during the transformation (Fig. 7.1). The degree of conversion (and hence the degree of cracking) was lower for the composites containing higher Al_2O_3 reinforcement fraction. Moreover, at higher volume fractions of Al_2O_3 , the converted zone only forms a MgAl_2O_4 layer on the Al_2O_3 particles (Fig. 7.1) which has been shown by micro X-ray diffraction [7] and transmission electron microscopy [8].

Therefore, an interesting problem that arose during the investigations on the hydrogen embrittlement of these materials was to find out the trapping behaviour of hydrogen in these materials as they all contained different types and amounts of interfaces. While analyzing the anomalous mechanical behaviour of the Al-2% Al_2O_3 composites after hydrogen charging, and the general reduced susceptibility to the HE for the composites, it was hypothesised [7] that the cracks in the particle in addition to the reinforcement-matrix interface would trap hydrogen. Although the exact nature of these traps is still in doubt, the literature cites that these locations should irreversibly trap hydrogen and hence contribute positively by lowering the amount of hydrogen to cause embrittlement.

Recently the technique of positron annihilation spectroscopy

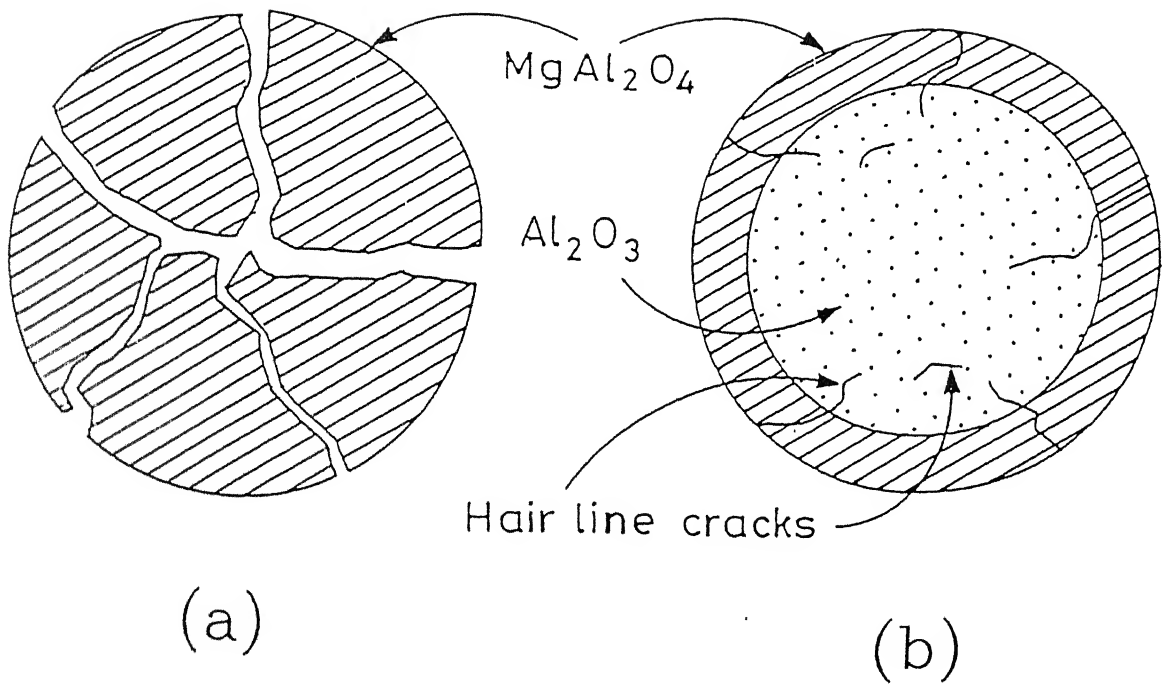


Fig. 7.1 Schematic representation of particle cracking in (a) Al-2% Al_2O_3 and (b) Al-8% Al_2O_3 [taken from Ref. 7].

has emerged as an effective method for characterisation and investigation of hydrogen in metals [9,10]. These applications arise from the sensitivity of positrons to defects. Although positron annihilation spectroscopy has been applied to study different light gas impurities in metals, no such study in MMC has been reported. We, therefore, thought it interesting to study the trapping behaviour of hydrogen in the aluminium-alumina composites by measuring positron annihilation lifetimes.

7.2 Experimental

Samples of Al-Al₂O₃ composites having 0, 2, 4 and 8 weight % Al₂O₃ particulates were prepared by the vortex casting methods [4] using commercially pure aluminium. Magnesium was added to the melt for improving the wetability between Al and Al₂O₃ particles and this resulted in residual Mg concentration of 4% by weight. Preheated acicular Al₂O₃ particles of 10-15 μ m size were dispersed into the molten melt using a mechanical stirrer whose speed was gradually increased to 450 rpm. Samples were then cast in permanent metallic molds. Details of the sample preparations are described elsewhere [7]. Metallographic specimens made from the cast ingot were then studied under a scanning electron microscope (JEOL, JSM 840 A) and optical microscope to observe the distribution of the reinforcing second phase. Mechanical properties and their characterisations in these materials under different conditions are discussed by Gopinath et. al. [7].

Circular disc specimens of 8mm diameter and 1 mm thickness

were then prepared from the cast ingot. Both the surfaces were polished down to 600 grit level. They were de-greased and cleaned with acetone before charging them with hydrogen. The hydrogen was charged electrolytically in an electrochemical cell with 0.5 mol/l H_2SO_4 as electrolyte, a stainless steel strip as anode and the specimen as cathode. The specimens were individually hydrogen charged at a constant current density of 50 mA/cm^2 for 12 hours. A few drops of sodium arsenite which serves as a hydrogen recombinant poison was added to the solution. Its role is to inhibit the formation of molecular hydrogen thereby accelerating the entry of hydrogen into the material.

Positron lifetime measurements were performed at 298 K using a conventional fast-fast coincidence spectrometer described in Chapter 2, with a time resolution of 310 ps and a sandwich geometry for the ^{22}Na source-specimen assembly. Positron lifetime spectra were recorded for samples containing 0%, 2%, 4% and 8% Al_2O_3 particles by weight. For each weight composition of the sample, positron lifetime spectra were measured for three different conditions : (i) as prepared (as cast) sample, (ii) sample charged with hydrogen for 12 hours, and (iii) sample annealed (after hydrogen charging) in vacuum at 573 K. After applying the source correction etc., the measured lifetime spectra were analyzed into 3 lifetime components (τ_1 , τ_2 and τ_3 having intensities I_1 , I_2 and I_3 with $I_1+I_2+I_3 = 100$) using the computer program POSITRONFIT [11].

7.3 Results and discussions

The results of our measurement for the three positron lifetimes are presented in Table 7.1. The values of the lifetimes, obtained for the different percentage composition of Al_2O_3 particles measured under different conditions lie in the range $\tau_1=139-176$ ps with intensity $I_1=64-75\%$, $\tau_2=285-365$ ps with $I_2=24-35\%$ and $\tau_3=1.5-2.2$ ns with intensity $0.6-1.3\%$. Here we shall like to point out that the longest lifetime τ_3 (1.5-2.2 ns) having very weak intensities (0.6-1.3%) are ascribed to the annihilation of the positrons on the surface of the samples [12]. In our work we have not been able to control the character of the surface of the samples nor have we been able to use any depth-selection technique involving positron annihilation and hence we will not discuss our results of τ_3 and I_3 any more.

In Fig. 7.2 ((a) - (d)), we have plotted the variation of τ_1, τ_2 and their intensities I_1 and I_2 respectively with the weight percentage of Al_2O_3 particulates in the matrix for (A) as prepared (as-cast) samples, (B) samples charged with hydrogen, and (C) annealed (after hydrogen charging) at 573 K for 1h. The shortest lifetime τ_1 , which provided the major contribution to the lifetime spectra of all the samples, was ascribed to positron annihilation in pure Al in the bulk [13,14]. The second lifetime τ_2 and its intensity are associated with the interaction of positrons with the imperfections in solids, including point defects (vacancy, impurities) and their aggregates, various types of dislocations, stacking faults, grain boundaries etc. [13,14]. The mean lifetime

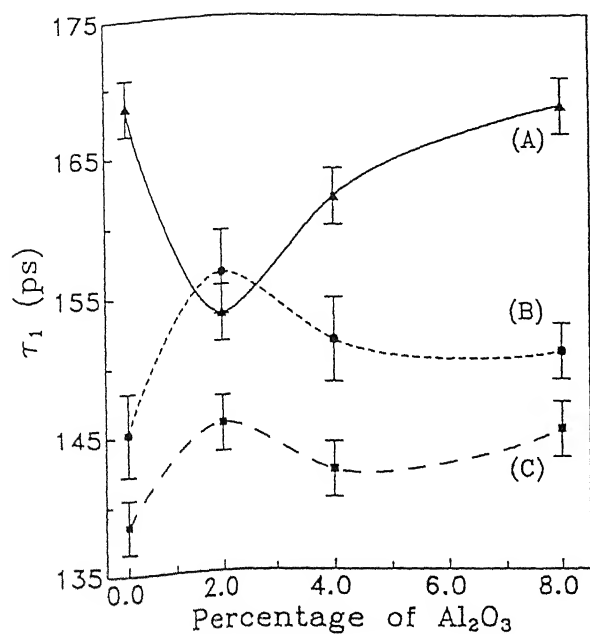
TABLE 7.1

Positron lifetime parameters in Al-Al₂O₃ composites containing different weight percentage of Al₂O₃ particles in the matrix.

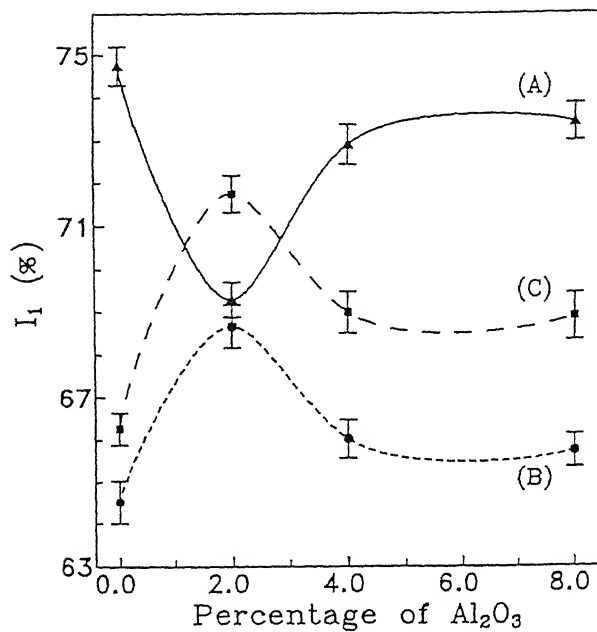
Sample (see text)	% *	τ_1 (ps)	I_1 (%)	τ_2 (ps)	I_2 (%)	τ_3 (ns)	I_3 (%)	τ_m^a (ps)
As-cast	0	168±2	74.75±.45	362±7	24.15±.45	2.26±.06	1.11±.06	216±3
	2	154±2	69.30±.41	333±6	29.87±.40	2.18±.08	0.83±.06	208±3
	4	162±2	72.91±.47	352±6	26.48±.45	2.36±.10	0.61±.07	212±3
	8	168±2	73.42±.44	354±7	25.61±.42	2.14±.07	0.97±.07	216±3
Charged with hydrogen	0	145±3	64.53±.52	295±7	34.06±.48	2.05±.08	1.22±.08	197±4
	2	157±3	68.67±.50	315±9	30.11±.48	2.04±.08	1.22±.08	205±4
	4	152±3	66.03±.39	311±8	32.77±.43	1.97±.05	1.20±.05	205±4
	8	151±2	65.75±.39	303±7	33.02±.38	2.07±.09	1.04±.04	200±4
Annealed at 73 K/1h	0	139±2	66.27±.38	286±5	32.71±.36	1.61±.05	1.02±.06	187±3
	2	145±2	71.75±.43	313±5	27.31±.40	1.92±.05	0.96±.05	192±3
	4	142±2	69.00±.48	300±4	30.05±.45	1.75±.05	0.96±.06	190±2
	8	145±2	68.89±.55	297±5	30.23±.52	1.71±.06	0.88±.07	192±3

Percentage composition of Al₂O₃ (see text)

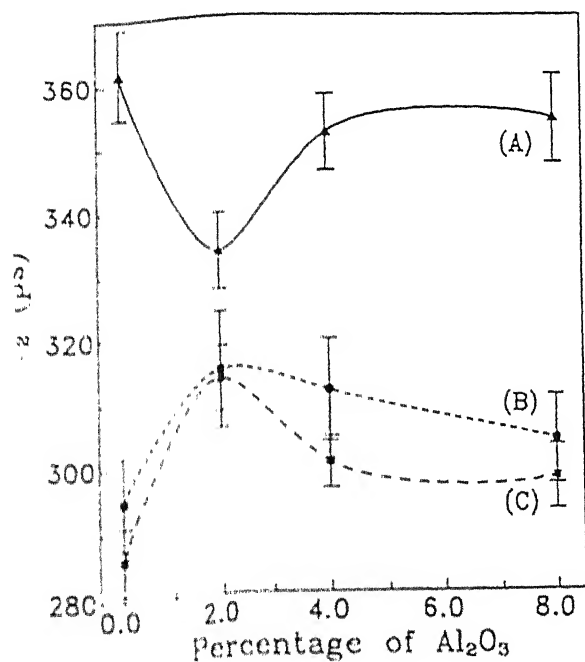
$$\text{Mean positron lifetime } \tau_m = \frac{\tau_1 I_1 + \tau_2 I_2}{I_1 + I_2}$$



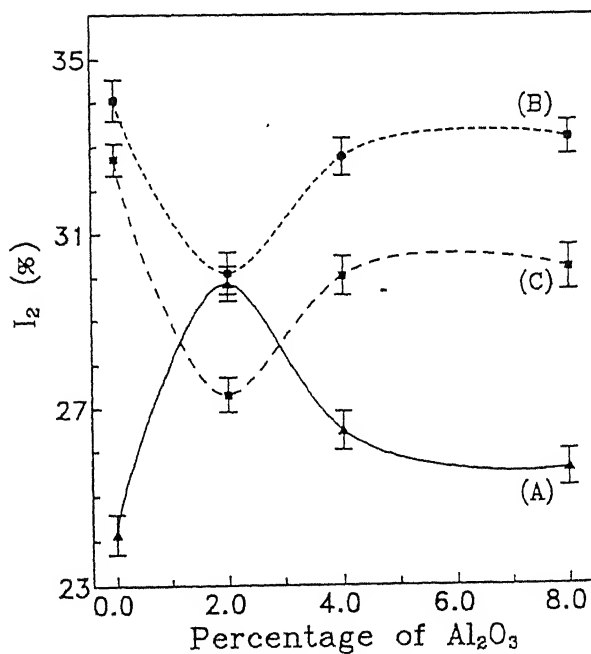
(a)



(b)



(c)



(d)

Fig. 7.2 Variation of positron lifetime parameters with percentage composition of Al_2O_3 , (a) τ_1 , (b) I_1 , (c) τ_2 , and (d) I_2 . (A) as-prepared (as-cast) samples, (B) charged with hydrogen for 12h and (C) annealed (after hydrogen charging) at 573 K for 1h. Lines are drawn through the data points for visual guidance.

τ_m ($\tau_m = (\tau_1 I_1 + \tau_2 I_2) / (I_1 + I_2)$) [15] calculated from τ_1 and τ_2 are also plotted in Fig. 7.3 against percentage composition of Al_2O_3 particles for different sample treatments. Following common practice [15] we shall concentrate on τ_m , rather than individual lifetimes and their intensities, to analyze the present results.

We first discuss the results for the samples without any Al_2O_3 (or "pure" Al). The value of τ_m observed for the as-cast sample of Al + 0% Al_2O_3 is 216 ps which is higher than the values $\tau_m = 163$ ps for the perfect lattice of Al [13]. This might be due to the presence of about 4 % Mg in the sample [7]. The reported value for the positron lifetime in the lattice of Mg is 238 ps [13] and it is also expected that the relative affinities of positron for Al and Mg would be different [16]. The present results show that the charging of the pure sample of Al with hydrogen leads to a decrease in τ_m to 197 ps (Fig. 7.3). This behaviour is in agreement with the results for the positron lifetimes in hydrogen charged Al reported by Cao et al. [17]. Previous experimental [18,19] and theoretical [20] studies have suggested that charging a metal sample with hydrogen gives rise to two processes which have opposite effect on the positron lifetimes. In the first place, hydrogen-induced defects try to increase the lifetime. On the other hand, hydrogen charging leads to trapping of protons in the defects and these protons reduce the attractive potential between the positrons and the defects. As pointed out by Jena et al. [20] the positron lifetimes in vacancy-hydrogen complex is reduced because of the simultaneous decrease in the number of electrons, and decrease in the number of

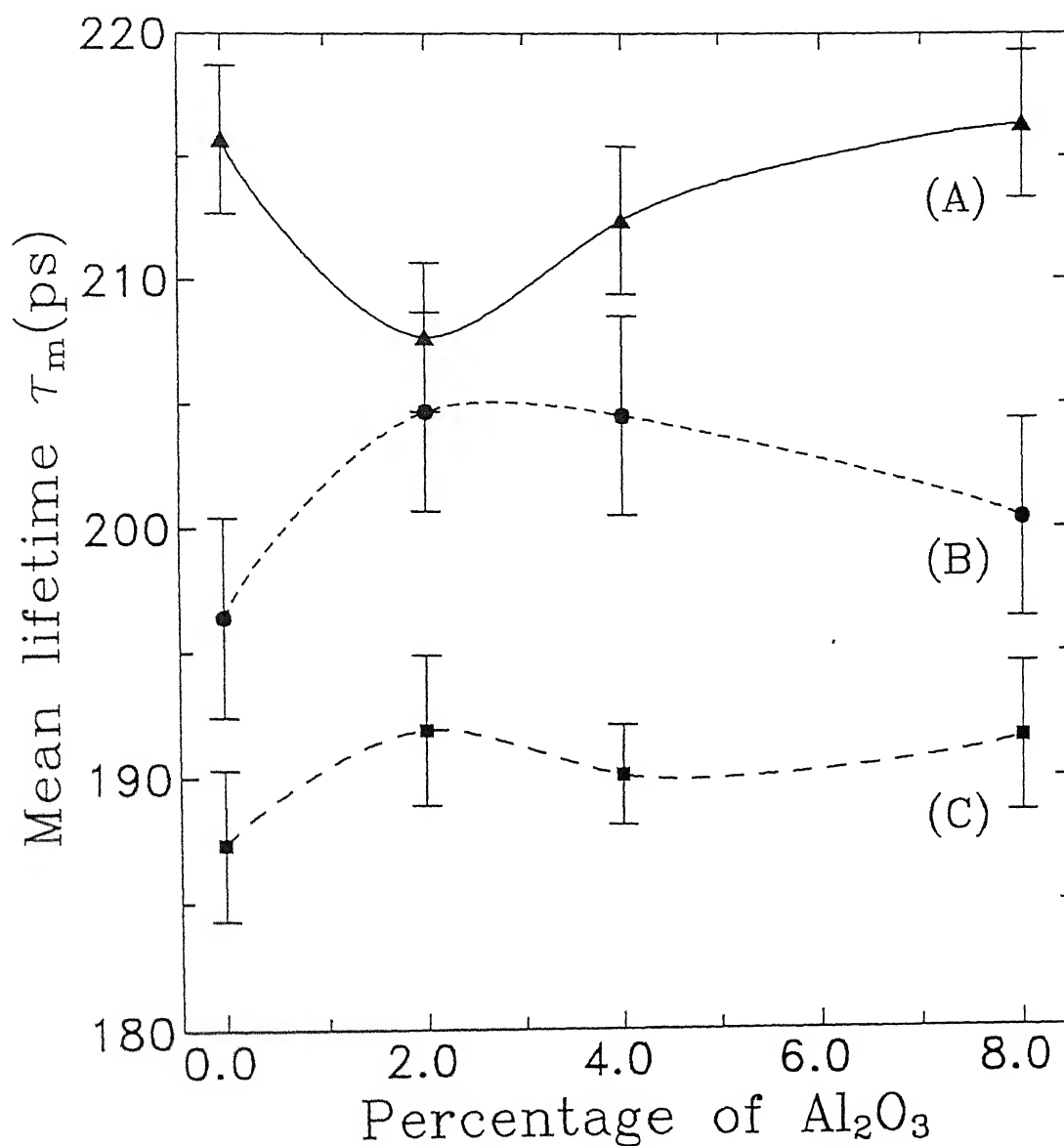


Fig. 7.3 Variation in mean lifetime τ_m with different percentage composition of Al_2O_3 particulates for (A) as-cast samples, (B) samples charged with hydrogen for 12h and (C) annealed (after hydrogen charging) at 573 K for 1h. Lines are drawn through the data points for visual guidance.

positrons inside the Wigner-Seitz sphere of the vacancy-hydrogen complex. The latter type of process is more effective and as a consequence the net effect of hydrogen charging is the lowering of τ_m . Our observations support this view. We have further observed that the τ_m for pure Al sample decreases to 187 ps upon annealing (Fig. 7.3). This decrease is understood because annealing treatment for 1 h at 300 °C is expected to reduce the hydrogen as well as the defect concentration.

As the percentage of Al_2O_3 is increased from 0% to 8%, the τ_m values display a variation with the 2% sample showing anomalous behaviour (Fig. 7.3). As reported earlier [7], the 2% sample showed the poorest mechanical properties in the uncharged condition. This behaviour was attributed to the formation of MgAl_2O_4 , with the interaction between Al_2O_3 particles and Mg (present in the matrix) being maximum for 2 % sample. Our results for the as-cast samples show that τ_m slightly decreases from 216 ps for 0% to 208 ps for the 2 % sample (curve A in Fig. 7.3). This small decrease is attributed to the loss of Mg which has gone to form the compound MgAl_2O_4 . As the percentage of Al_2O_3 is increased from 2% to 8% the degree of conversion to MgAl_2O_4 becomes lower [7] and the τ_m values increased from 208 ps for 2% Al_2O_3 to 216 ps for 8% Al_2O_3 samples (curve A in Fig. 7.3).

In the case of hydrogen-charged samples, slight increase in τ_m in going from 0% to 2% Al_2O_3 (Fig. 7.3) could be ascribed to the trapping of hydrogen in the cracks in Al_2O_3 particles. This has resulted in a reduced hydrogen concentration in the bulk of the Al-matrix. As already been discussed [7], a large number of

particles cracked in the case of Al- 2% Al_2O_3 composites whereas particles are essentially crack-free in composites containing higher Al_2O_3 fractions. Therefore, the amount of hydrogen trapped in the cracks is maximum for 2% Al_2O_3 and least for 8% Al_2O_3 composite. In other words, the amount of hydrogen available in the bulk of the host matrix increases as the percentage Al_2O_3 increases in the composites. This has resulted in a maximum drop in mean lifetime τ_m for the 8% case and a very little change for 2% Al_2O_3 composite upon charging with hydrogen (curve B in Fig. 7.3).

In the case of annealed samples, τ_m values further go down (curve C in Fig. 7.3) in all the four cases (0%, 2%, 4% and 8% Al_2O_3) from the hydrogen-charged condition. Also τ_m values do not show significant variation with the percentage of Al_2O_3 in this case. This behaviour suggest that most of the defects and hydrogen have annealed out from the sample and hence we are observing the same annihilation rate in all the four samples.

7.4 Conclusions

It may be concluded that present positron annihilation lifetime measurements can provide us useful information about the trapping behaviour of hydrogen in the aluminium-alumina composites. Moreover, the present positron results are in agreement with the trapping behaviour of hydrogen proposed by Gopinath et al. [7] in these composites. In other words positron annihilation technique can be a useful tool to monitor the changes in metal matrix composites upon hydrogen charging and subsequent

annealing. Positron annihilation technique, which has been used to characterise other different materials, can be used to characterise metal matrix composites.

References

1. M. Taya and R. J. Aresnault, " Metal Matrix Composites - Thermo-mechanical behaviour", (Pergamon Press, New York, 1989), p. 2.
2. D. M. Aylor and P. J. Moron, J. Electrochem. Soc. 132, 1277 (1985).
3. M. Saxena, B. K. Prasad and T. K. Dan, J. Mater. Sci. 27, 4805 (1994).
4. B. C. Pai, S. Ray, K. V. Prabhakar and P. K. Rohatgi, Mat. Sci. Engg. 24, 31 (1976).
5. D.A.Jones, " Principles and Prevention of Corrosion", (Maxwell Macmillan International Publishing group, New York, 1992), p. 336.
6. G.M. Pressouyre and I.M. Bernstein, Acta Metall. 27, 89 (1979)
7. K. Gopinath, R. Balasubramaniam and V. S. R. Murthy, Z. Metallkd. 85, 880 (1994).
8. D.L. Lloyd, I. Jin and G.C. Weatherly, Scripta Metall. Mater. 31, 393 (1994).
9. M. Eldrup, Mater. Sci. Forum 105-110, 229 (1992), and references cited therein.
10. K. P. Gopinathan and R. Rajaraman, Mater. Sci. Forum 175-178, 261 (1995), and references cited therein.
11. P. Kirkegaard, M. Eldrup, O.E. Mogensen, and N.J. Pedersen, Comput. Phys. Commun. 23, 307 (1981).
12. W. Deng, L. Y. Xiong, C. W. Lung, S. H. Wang and J. T. Guo, Mater. Sci. Forum 175-178, 339 (1995).

13. M. Doyama and R. M. J. Cotterill, in "Positron Annihilation", edited by R.R.Hasiguti and K. Fujiwara (The Japan Institute of Metals, Sendai, 1979), p. 89.
14. R.M. J. Cotterill, K. Peterson, G. Trumpy and J. Traff, J. Physics F 2, 459 (1972).
15. A. Vehanen and K. Rytölä, in " Positron Solid State Physics", edited by W. Brandt and A. Dupasquier (North-Holland, Amsterdam, 1983), p. 659.
16. M. J. Stott, A. T. Stewart and P. Kubica, Appl. Phys. 4, 213 (1974).
17. B. Cao, N. Gao, D. Wang and L. Zhang, Mater. Sci. Forum 175-178, 311 (1995).
18. F. Alex, T. D. Hadnagy, K. G. Lynn and J. G. Byrne, "International Conference on the Effect of Hydrogen on Behaviour of Materials", (The Metallurgical Society of AIME, 1975), p. 642.
19. Po-We Kao, R. W. Ure, Jr. and J. G. Byrne, Philos. Mag. A 39 517 (1979).
20. P. Jena, M. J. Ponnambalam and M. Manninen, Phys. Rev. B 24, 2884 (1981).

12.034

A 125 834

This book is to be returned on the date last stamped.

[illegible]

* 1945-1946: 1st year, 1946-1947: 2nd year, 1947-1948: 3rd year, 1948-1949: 4th year